Biocompatible polysaccharide-based hydrogels for attracting and trapping invasive glioma cells

Paraskevi Kasapidou

A thesis submitted in partial fulfillment of the requirements of the University of Kent and the University of Greenwich for the degree of Doctor of Philosophy

October 2018

Declaration

″ I certify that this work has not been accepted in substance for any degree, and is not concurrently being submitted for any degree other than that of Doctor of Philosophy being studied at the Universities of Kent and Greenwich. I also declare that this work is the result of my own investigations except where otherwise identified by references and that I have not plagiarised the work of others ″.

Signed:  (Student)

Miss Paraskevi Kasapidou

Signed:  (Supervisor)

Dr Vladimir Gubala

Date: 1/10/2018

Acknowledgements

First of all, I would like to thank my first supervisor Dr Vladimir Gubala for his continuous support, motivation and the trust received in order to complete this project. His patience and guidance helped me a lot in all the time of my PhD. My sincere thanks and appreciation also go to Dr Helene Castel as external supervisor who provided me an opportunity to join her research team as intern in INSERM U1239 at the University of Rouen in France. This internship was an invaluable experience for me as I was introduced in the world of cancer cell biology. Without the significant continuous guidance and support from her and the team there, it would not be possible to conduct this research. I would like to thank Dr Andrew Hall as second internal supervisor for his insightful comments and the opportunity to widen my research from different research perspectives.

In addition, I would like to thank my fellow PhD students Colin Moore, Giorgia Giovannini, Filip Kunc, Sam Hobbs, Ouafa Benlaouer, Svetlana Sakhnevych, Rebecca Lilley and Kevin Cunningham for working together, the stimulating and long discussions and undoubtedly, for having fun all these three years. In addition, I am really grateful to Dr Dimitrios Lamprou for his helpful comments and advice whenever I needed it. My sincere thanks to Dr Jennifer Hiscock and Andrew Hurt for their invaluable help and training on rheology and scanning electron microscopy respectively. I would like to thank all the SRP and Nuffield students that I have supervised all these three years, for their contribution to my project and help to improve and develop my teaching skills. I am also thankful to Kristyna Kupcova as visitor researcher in our group for her assistance whenever I needed it.

Most importantly, all these three years in UK I made real friendships that will last for years. I would like to thank Carmen Piras and Rob Sparrow for the introduction to the ″ Medway Research Crew″, their helpful advice and the fun that we had all these years in UK. In addition, I would like to thank my good friend in the office, Cris Pissinato thank you so much for the support. It was also a pleasure to meet Mervat Shafik and be a real friend, thank you so much for everything.

A special thank you should also be reserved for Stratos Sitsanidis. Thank you so much for your help, support and advice all these years. Agnie Arapopoulou was one of the people that I was so lucky to meet during my time in UK, she taught me how to see always the bright side of things, enjoy every moment and fight for my life. She left so early from this world but she will be always remembered. Last but not least, I would like to thank my mum, my uncle, my sister and my brother for their unconditional support and motivation throughout the writing of this thesis and my entire life. I dedicate this thesis to my dad who left so early and suddenly. Dad, I know that you are my angel and you follow me in each step of my life.

Abstract

Glioblastoma multiforme (GBM) is the most common deadly and aggressive malignant brain tumour of the central nervous system in humans. The relentless progression of this disease is due to the infiltration of the cells from the primary tumour site into distant regions of the brain, which renders complete resection of the tumour impossible leading to tumour recurrence. Current methods of treatment including surgical removal, chemotherapy combined to radiotherapy are mainly unsuccessful because of the highly invading and resistant nature of these glial tumours. Therefore, there is an urgent need to develop new methods and understand the complex behaviour and microenvironment of glioblastoma tumours. The key challenge in successful glioblastoma treatment lies in destroying the cancer cells that invade the brain tissue and exist in the brain parenchyma after the removal of the primary tumour bed.

To date, strategies that have been used, suffer from several disadvantages, including the absence of molecules that naturally exist in the brain extracellular matrix and most importantly they lack from effective chemoattractants. Consequently, residual invasive tumour cells remain in the margins of the resection cavity, leading to inevitable tumour recurrence. Therefore, this thesis aims to shed light on and tackle the majority of different limitations of the conventional methods of GBM treatment. In order to address these challenges, we here investigated the use of 3D scaffolds such as hydrogels for attracting and trapping glioma cells. Particular attention was given to those based on polysaccharides such as hyaluronic acid (HA) and methylcellulose (MC). HA is one of the main components of the brain extracellular matrix and is implicated in tumour cell behavior, creating a microenvironment favourable for migration, proliferation and invasiveness of malignant cells. HA-based hydrogels were prepared by chemical crosslinking of HA with Adipic Acid Dihydrazide (ADH) or Bovine Serum Albumin (BSA) as crosslinkers using EDC/sulfo-NHS chemistry. In this work, the fabricated hydrogels were loaded with a chemokine at a concentration gradient in order to achieve the migration of glioma cells to the hydrogel matrix and with a chemotherapeutic drug in order to induce cell death. The chemokine that was used is the vasoactive peptide urotensin II (UII) which at a gradient concentration has demonstrated chemoattracting migratory effects on glioma cells. Herein, the chemoattraction was tested on hydrogels loaded with this chemokine peptide.

Moreover, the physicochemical and mechanical properties of the fabricated hydrogels were mainly characterised by swelling studies, Scanning Electron Microscopy, enzymatic degradation experiments, Differential Scanning Calorimetry, Infrared Spectroscopy and oscillatory rheology. In overall, hydrogels presented favourable physicochemical features and mechanical properties that can mimic those of the native brain tissue. Preliminary biological results showed that glioma cells could invade and migrate in response to the loaded chemoattractant UII in the matrix.

Table of Contents

List of Figures

List of Tables

List of Abbreviations

AA	Antibiotic/Antimicotic
ADH	Adipic Acid Dihydrazide
APNG	Alkylpurine-DNA-N-glycosylase
BBB	Blood-Brain Barrier
BBTB	Blood-Brain Tumour Barrier
BCNU	Bis-chloroethylnitrosourea (Carmustine)
BER	Base Excision Repair
BSA	Bovine Serum Albumin
BS3	Bis (sulfosuccinimidyl) suberate
CCNU	1-(2-chloroethyl)-3-cyclohexyl-1-nitrosourea (Lomustine)
CDA	Cytosine Deaminase
CD44	Cluster determinant adhesion molecule
CED	Convection Enhanced Delivery
CNS	Central Nervous System
CSF	Cerebrospinal fluid
CT	Computed Tomography
DAPI	4′,6-Diamidino-2-phenylindole
DMA	Dimethacrylate
DMEM	Dulbecco's Modified Eagle Medium
DNA	Deoxyribonucleic acid
DOX	Doxorubicin
DPBS	Dulbecco's phosphate buffered saline
DSG	Disuccinimidyl glutarate
DSC	Differential Scanning Calorimetry
DSS	Disuccinimidyl suberate
EBE	2,2′-(Ethylenedioxy) bis(ethylamine)
ECM	Extracellular Matrix
EDC	1-Ethyl-3-(3-dimethylaminopropyl) carbodiimide
EGF	Epidermal Growth Factor
EGFR	Epidermal Growth Factor Receptor
ELISA	Enzyme-Linked Immunosorbent Assay
FBS	Fetal Bovine Serum
FDA	Food and Drug Administration
FEG-SEM	Field Emission Gun Scanning Electron Microscopy
FITC	Fluorescein isothiocyanate
FT-IR	Fourier Transform Infrared Spectroscopy
FU	Fluorouracil
FUS	Focused Ultrasound
GAGs	Glycosaminoglycans
GBM	Glioblastoma Multiforme
GCV	Ganciclovir
$GemC_{12}$	Gemcitabine
GPCRs	G-protein coupled receptors
HA	Hyaluronic Acid
HPMA	2-Hydroxypropylmethacrylate
HSP	Heat Shock Protein
HSV-TK	Herpes Simplex Virus Thymidine Kinase
IDH	Isocitrate Dehydrogenase
IL	Interleukin
IPNs	Inter-penetrating networks

LMWGs	Low Molecular Gelators
LNC	Lipid Nanocapsule
LVR	Linear Viscoelastic Regime
MA	Methacrylate
MBs	Microbubbles
MC	Methylcellulose
ME	Metformin
MGMT	Methylguanine methyl transferase
MMP	Metalloproteinase
MMR	Mismatch Repair Protein
MRI	Magnetic Resonance Imaging
MTIC	(5E)-5-(methylaminohydrazinylidene)imidazole-4-carboxamide
NADH	Nicotinamide adenine dinucleotide
NADPH	Nicotinamide adenine dinucleotide phosphate
NDS	Normal Donkey Serum
NICE	National Institute for Health and Clinical Excellence
NPs	Nanoparticles
PBCA	Poly (butyl cyanoacrylate)
PBS	Phosphate Buffered Saline
PCL	Polycaprolactone
PCCP	1,3-bis-(p-carboxyphenoxy) propane
PEG	Polyethylene glycol
PEI	Polyethylenimine
PFA	Paraformaldehyde
PGA	Polyglycolic acid
PGs	Proteoglycans
pHA	p-hydroxybenzoic acid
PLA	Polylactic acid
PLGA	Poly (lactic-co-glycolic acid)
PMMA	Poly (methyl methacrylate)
PVA	Poly (vinyl alcohol)
RGD	Arginylglycylaspartic acid
RHAMM	Receptor for Hyaluronan Mediated Motility
SA	Sebacid acid
SD	Swelling Degree
SEM	Scanning Electron Microscopy
SiPCL	Silane-polycaprolactone
Sulfo-NHS	Sulfo-N-Hydroxysuccinimide
TMZ	Temozolomide
TTfields	Tumour Treating Fields
UII	Urotensin II
US	Ultrasound
UT	Urantide
UV	Ultraviolet
VEGF	Vascular Endothelial Growth Factor
XG	Xanthan Gum
WHO	World Health Organization

Chapter 1: Introduction

1.1 Background

Over the past two decades the number of people diagnosed with cancer worldwide has increased dramatically. In many countries, cancer ranks the second most common cause of death following cardiovascular diseases and it remains as a major health problem around the world [1], [2]. There are different types of cancer, the most common types include lung, breast, prostate, colorectal, bladder cancer, melanoma and leukaemia. Brain tumours are less common, but there is evidence that the incidence of these tumours has been rising since the last years. Approximately 19 in 0.1 million individuals are diagnosed with central nervous system (CNS) tumours and primary brain tumours every year worldwide [2]. Indeed, brain cancer treatment presents several challenges due to the unique sanctuary situation of the brain and there is an urgent need for the development of new therapeutic strategies. Chemotherapy is the most efficient standard treatment for cancer in general, and can be also used in brain cancer treatment combined with radiotherapy. However, conventional methods of treatment are mainly unsuccessful, giving rise to alternative strategies that potentially overcome the limitations of the traditional ones and they will be further discussed below.

1.2 Brain tumours

A brain tumour is an intracranial mass produced by the uncontrolled growth of cells either normally found in the brain or spread from primary tumours located in other tissues of the body. Brain tumours are considered one of the worst diseases as they have a direct impact on patient's life from a psychological, physical and neurological aspect [3].

These tumours can be classified by the biological behaviour as benign or malignant. In both cases, there is an abnormal aggregation and proliferation of cells. Benign tumours originate from cells within or surrounding the brain and are less likely to spread to other parts of the brain. On the other hand, malignant tumours are the most aggressive type of brain tumours, tending to invade the surrounding brain tissue and are considered to be life threatening. Brain tumours can be classified by the location of origin as primary or secondary tumours. Primary tumours arise in the brain, rather than spreading from another part of the body while secondary spread to the brain through a metastatic process. Metastasis is the most common cause of brain cancer while tumours originating in situ from nerve cells are less common [4]. There are more than 100 types of primary CNS tumours [5]. Figure 1.1 summarises the different types of brain tumours and their location. The most common types are gliomas and meningiomas. Acoustic neuroma, lymphoma, medulloblastoma and hemangioblastoma are rarer types of brain tumours.

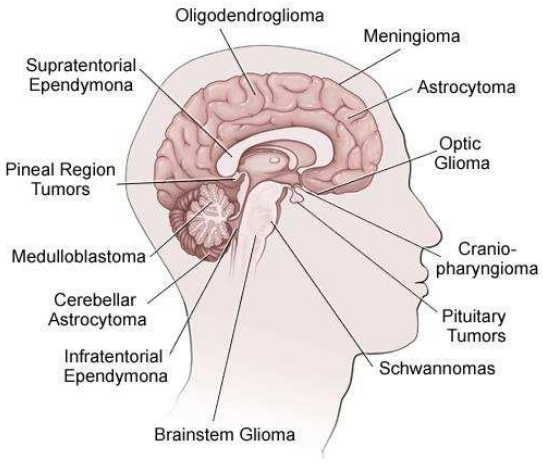

Figure 1.1: Illustration of the most common locations of different types of brain tumours in adults. Adapted from reference [5].

CNS tumours are the 9th most common cancers in the United Kingdom and are accounting for approximately 2 % of all cancer cases in adults [6]. In adults, the majority of brain tumours are supratentorial with high-grade gliomas and meningiomas to predominate. Brain tumours can develop at any age but are most common in people aged between 50 and 70. The period 2013-2015, on average each year approximately 24 % of new cases observed in people aged 75 and over and the incidence rates were similar between both genders. Figure 1.2 presents the average number of brain cancer cases per year in the United Kingdom and the different rates between both genders. It can be concluded that the highest incidence is observed at the age of 70 for male and female population and there is an increasing number of patients diagnosed with brain tumours per year.

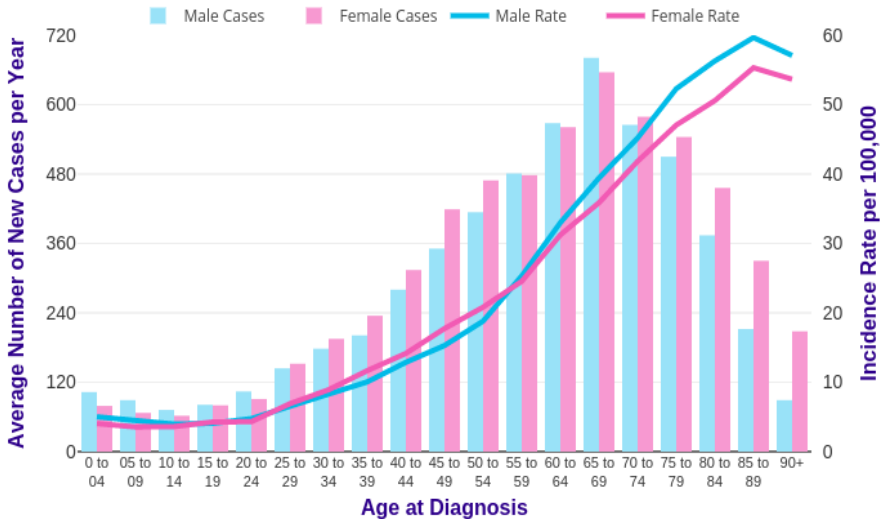

Figure 1.2: Average number of new cases diagnosed with brain cancer per year in the United Kingdom and age incidence rates. Adapted from Cancer Research UK [6].

On the other hand, brain tumours are the second most common cancer in children, accounting for almost 26 % of all childhood cancers [7]. In the United Kingdom approximately 400 children are

diagnosed with brain tumour each year and boys are affected slightly more than girls as demonstrated in Figure 1.3. These brain cancer pediatric patients generally have a better outcome than adults but they are frequently unwell for months prior to diagnosis and a prolonged period between the appearance of symptoms and diagnosis is associated with increased morbidity [8]. In addition, treatments in children would potentially impact normal brain development [9].

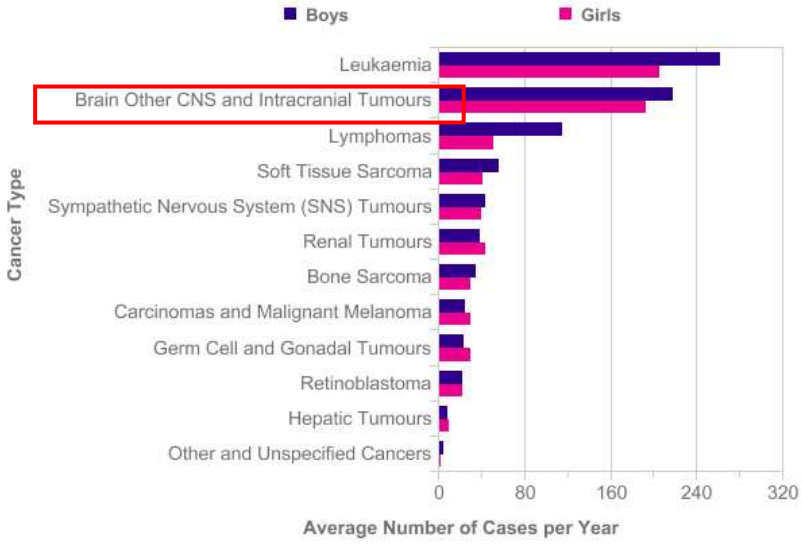

Figure 1.3: Average number of new cases diagnosed with cancer per year, children (0-14 years old) in the United Kingdom. Adapted from Cancer Research UK [10].

1.3 Classification of brain tumours

The German pathologist Rudolf Virchow was the first in 1860 to introduce the term ″glioma″, distinguishing this class of tumours from other brain primary tumours. With the progression of cytological and histological techniques, a more refined classification was published by the WHO in 1979, and revised by the same organisation in 1993, 2000 and 2007 [11] and more recently in 2016 [12]. Malignant or high-grade gliomas are the most common type of primary brain tumours that arise from glial cells, accounting for 80 % of patients and an annual incidence of 5.81 per 100.000 population [13]. There are several types of gliomas including brain stem gliomas, optic nerve gliomas, astrocytomas, oligodendrogliomas, ependydomas or glioblastomas as shown in Figure 1.1. Based on histological criteria, WHO 2007 has identified more specifically the growing malignancy of astrocytoma into 4 grades (I-IV) and of oligodendroglioma in 2 grades (II-III). Among malignant gliomas, grade IV astrocytomas or glioblastomas are the most common and deadly primary brain tumours. Grade I or pilocytic astrocytoma is delimited, benign and is most often treated by resection. Malignant grade II glioma or diffuse astrocytoma, exhibits a high degree of differentiation and moderate cell density, and is classically called ″low grade glioma″ but can be infiltrative often progressing to higher grades [14]. The anaplastic astrocytoma or grade III consists of undifferentiated grouped cells having nuclear atypia and already considered as ″high grade glioma″. Finally, the grade

IV or glioblastoma multiforme (GBM) is a very aggressive tumour that can be developed de novo (primary GBM) or evolve from lower grades (secondary GBM) [15].

1.4 Glioblastoma multiforme

1.4.1 General information

The most common type of gliomas is GBM and it is the most aggressive malignant primary brain tumour, accounting for approximately 50 % of all brain tumours as shown in Figure 1.4 [16], [17]. The most frequent anatomic location of GBMs is the cerebral hemispheres, with 95 % of these tumours arise in supratentorial region, whereas only few of them occur in the cerebellum, brainstem and spinal cord [18]. GBM is characterised by high infiltration along white matter tracts [19] and blood vessels [20], high heterogeneity [21], significant mitotic activity, high tortuous vascularisation, necrotic areas, chemoresistance and high recurrence rates [22]. The average survival period is around 15 months following standard Stupp protocol e.g. radio and chemotherapy [23]. According to the histomolecular classification published by WHO 2016 three major diagnostic subtypes of GBM based on the status of Isocitrate Dehydrogenase (IDH) are individualised in 3 groups: (i) IDH mutant, (ii) IDH-wildtype and (iii) IDH not otherwise specified. This classification would facilitate clinical, experimental and epidemiological studies dedicated to improvements in the development of diagnosis and therapeutic options.

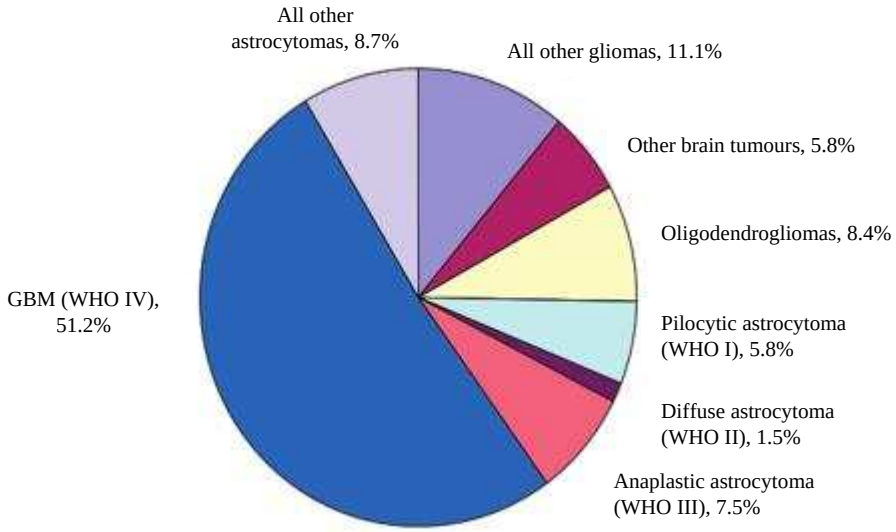

Figure 1.4: Distribution of all primary central nervous system gliomas. Astrocytomas account for 75 % of all gliomas. Adapted from Central Brain Tumor Registry of the United States [16].

1.4.2 Incidence of GBM

GBM typically affects adult population ranging in age from 50 to 70 years and is mainly located in the cerebral hemispheres. It has an incidence of 2 to 3 per 100.000 adults per year and they tend to affect more men than women [24]. While GBMs are primarily an adult-age tumour, pediatric GBMs are also classified as high-grade gliomas. Pediatric GBMs account for 3 % of childhood primary brain tumours and are rarely diagnosed among children and adolescents. The incidence of these tumours is 4.84 cases per 100.000 children per year. Anatomically, the majority of these tumours are located in the brain stem [25].

1.4.3 Risk factors

For the majority of gliomas, no underlying carcinogenetic causes have been identified, however, scientists have found that mutations in the genes of different chromosomes might play role in the development of these tumours. There is convincing evidence that specific inherited genes can significantly affect the risk of developing brain tumours in 5-10 % of glioma cases [26]. More specifically, some gliomas can be associated with genetically inherited syndromes, such as Neuro-fibromatosis [27], Li-Fraumeni [28], Von Hippel-Lindau, Turcot and Tuberous Sclerosis [29]. Furthermore, exposure to therapeutic radiation may be responsible for the onset of GBM [30]. Specifically, several studies have demonstrated that children who received prophylactic CNS irradiation, a cumulative dose of 2.500 cGy for acute lymphnoblastic leukaemia, were susceptible to be diagnosed with brain tumours [31]. Other environmental risk factors include exposure to smoking, pesticides, petroleum refining and employment in synthetic rubber manufacturing [30]. Additional factors such as severe head injury, dietary habits, exposure to electromagnetic fields and diagnostic irradiation are suspected to lead to GBM but it is not confirmed [32].

1.4.4 Clinical presentation, diagnosis and prognosis

Depending on the localisation and the increasing intracranial pressure, as a result of the clinical stage of the disease, the most common symptoms of GBM include headaches, seizures, memory loss and changes in mental status [33]. More specifically, for patients who present hearing and visual problems, it is indicated that the tumour is located in the temporal lobe region. In contrast, 20-40 % of the patients diagnosed with impairing cognitive functions, the location of the tumour is in the frontal lobe [34]. Gadolinium-enhanced magnetic resonance imaging (MRI) and computed tomography (CT) are routinely used to visualise brain tumours as shown in Figure 1.5 [35].

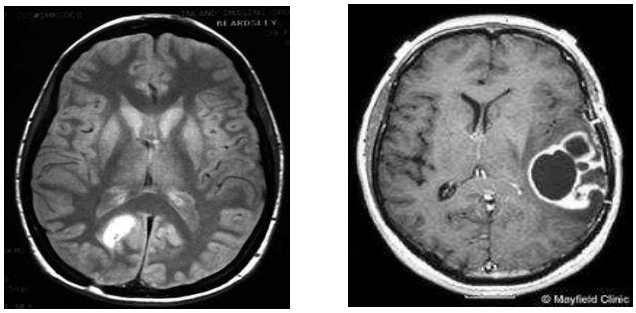

Figure 1.5: MRI and CT imaging are commonly used in the detection of brain tumours. To the left is MRI of a brain tumour, to the right is a CT scan of a brain tumour. Adapted from Nelson et al [35].

MRI plays a crucial role in the detection of the location of the tumour and diagnosis of GBM. In addition, a definite diagnosis of GBM on MRI or CT requires a stereotactic biopsy for tumours localised in essential functional zones, or craniotomy with tumour resection for histological and molecular characterisations. A meta-analysis published in 2016 in which the Stupp protocol (fractional radiotherapy combined with chemotherapy with temolozomide and then chemotherapy alone) indicated that the overall survival of 1 year and 2 years of follow-up was significantly improved in the case of ″complete″ excision [36]. Currently, the prognosis of patients with GBM remains poor as the median survival rate is 12-15 months from the time of diagnosis rendering this disease incurable [37]. The poor prognosis is mainly related to the tumour location, the high heterogeneity of GBM and infiltration of glioma cells in the health brain parenchyma, likely leading to recurrence.

1.5 Challenges in the treatment of GBM

Generally, gliomas show a high proliferation rate, phenotypic variations, variability in tumour histopathology and diffusely infiltrate adjacent brain tissue [38], rending GBM a very challenging cancer to treat. Several features unique to GBM limit the assessment of tumour response and the reliable delivery of cytotoxic agents to the tumour, are highlighted in Figure 1.6. GBM cells widely diffuse into the brain parenchyma and cannot be detected by conventional brain imaging techniques. Moreover, it has been reported that i) GBM invasion occurs through white matter tracts and blood vessels responsible for incomplete surgical resection, increasing tumour recurrence, ii) GBMs were found to be highly angiogenic, crucial step to their growth and resistance to therapy [39], iii) the anatomic location of GBM in the brain usually hinders a complete surgical removal of the tumour without damaging the surrounding functional tissue close to the vicinity of the tumour [40], iv) the presence of the blood-brain barrier (BBB) limits the number of cytotoxic drugs that can effectively reach the tumour site at therapeutic concentrations [41] and v) the unique brain microenvironment drives GBM progression indicating craving for the brain microenvironment [42]. In overall, despite therapeutics strategies, GBM still remains as one of the most deadly cancers.

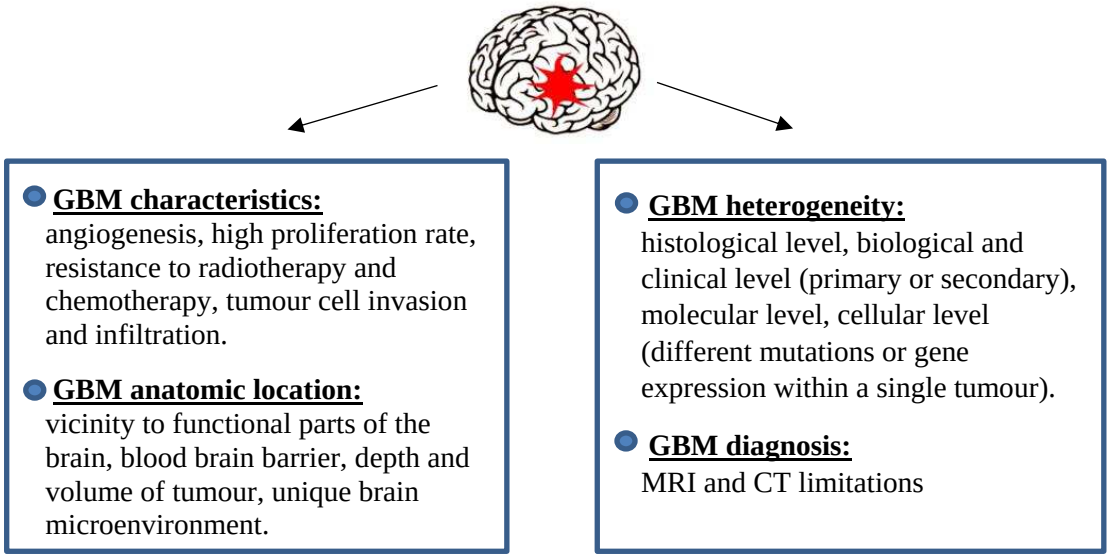

Figure 1.6: Features unique to GBM that provide a challenge for the current treatment options and contribute to its fatal outcome.

One of the recognised challenges for the current GBM treatment strategies, is the ability to penetrate the BBB and at the same time, to minimise the systemic toxicity in order to overcome the tumour resistance. Furthermore, one of the hallmarks of GBM is its heterogeneity at all levels, from the histological to molecular and clinical level [43], [44]. GBMs display a highly phenotypic heterogeneity because they are composed of cells that express markers of differentiated and undifferentiated cells [45]. Patel et al studied the intratumoural heterogeneity in primary GBMs and they demonstrated that spheroids and differentiated clusters represent two morphologically distinct types of cells within a single tumour [46]. In addition, this intratumoural heterogeneity in GBM contributes to variability in responses and resistance to conventional methods of treatment [47]. Moreover, a subpopulation of GBM cells has been found to demonstrate stem like properties such as expression of stem cell markers or long-term self-renewal which can be responsible for the resistance to chemotherapy or radiotherapy. Imaging plays a central role in diagnosis, MRI and CT consist the conventional diagnostic methods to visualise brain tumours, but these techniques suffer from significant limitations. Firstly, conventional MRI hardly distinguishes low grade from high grade gliomas requiring histological analysis and biopsies for a secure diagnosis [48]. Secondly, high grade tumours, intracranial metastasis and inflammation induce disruptions in BBB leading to contrast enhancement on MRI. Finally, the extent of GBM and the margins of the malignant tumour are not always detectable by the conventional neuroimaging techniques as tumour cells can be only detected in close proximity to the tumour bed.

1.6 Brain microenvironment and blood-brain barrier

The brain microenvironment is a critical regulator of the cancer progression in primary and metastatic brain tumours [49]. GBM cells interact with their microenvironment for invasion, as these cells have the ability to move along the myelinated axons in white matter, spreading into healthy brain regions [50]. It is widely accepted that the BBB is the most important factor in GBM recurrence as it prevents the effective systemic administration of the chemotherapeutic drugs to the tumour site. The BBB is a highly selective semipermeable membrane which separates the blood vessels in the brain and the spinal cord by monitoring the circulation of blood and extracellular fluid in the CNS [51]. It is mainly comprised of cellular and molecular factors, endothelial cells, pericytes, astrocytes and extracellular matrix (ECM) as shown in Figure 1.7. The main role of BBB is to block the passage of toxic molecules from the systemic blood circulation to the brain and this can be achieved by the specific defense mechanisms (transport barrier, immunologic and enzymatic barrier) [52]. In addition, another important role of BBB is to transport nutrients and other necessary molecules to the brain tissues, however, only small hydrophobic molecules can cross the unique morphology of BBB [53]. The barrier's function is mainly endorsed by the endothelial cells and is highly impenetrable to hydrophobic molecules larger than 200 kDa including the majority of the common chemotherapeutic agents. On the other hand, only lipophilic molecules with molecular weight lower than 400-500 Da can effectively cross the BBB which are used for the treatment of neurological diseases such as epilepsy, chronic pain and depression [54].

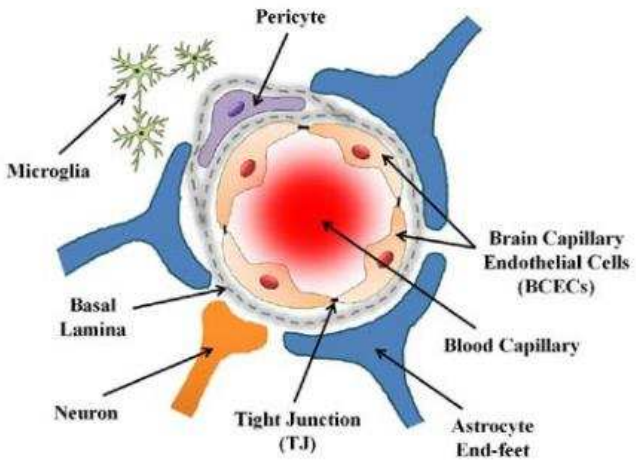

Figure 1.7: Structure of the blood-brain barrier. It is a complex network which is impermeable to large macromolecules, excessive CNS fluids and other blood components. Adapted from Sarkar et al [55].

Furthermore, the structure and function of the BBB can be affected from the intensity of the tumour growth which results in the formation of the blood brain tumour barrier (BBTB). This barrier is formed by disruption of the tumour membrane, albeit it resembles the intact structure of the BBB. The abnormalities caused by the vascularisation of GBM decrease the permeability of the brain barrier, thus acting as an obstacle for the effective delivery of the majority of the antitumour agents.

1.7 Conventional methods of treatment

1.7.1 Surgical resection

The treatment of GBM currently presents several challenges due its location, aggressiveness and highly infiltrative nature. GBM remains an incurable cancer despite the intense clinical research including improvements in surgery, use of combined chemoradiation and the advent of novel methods of treatment. The surgical resection and the extent of the excision are critical factors for the determination of tumour diagnosis and patient prognosis. Current technologies used for glioma resection include laser interstitial thermal therapy, awake craniotomy, fluorescence guided surgery and intraoperative mass spectrometry [56]. In addition, it has been observed that longer survival rates occur in patients who have undertaken aggressive resection surgery, almost 98 % of tumour volume resected with a mean initial tumour volume being 33-39 cm^3 without causing neurologic deficits [57], [58]. The current scheme of treatment for newly diagnosed GBM patients consists of maximum tumour resection plus daily administration of temozolomide (TMZ) at a dose of 75 mg/m^2 and 60 Gy of radiotherapy (2 Gy daily) for 4-6 weeks, followed by a TMZ maintenance dose of 150-200 mg/m^2 for 5 days every 28 days for 6 cycles [59]. Although, extensive and ″complete″ surgical resection of GBM represents the most effective way to increase survival rates of GBM patients, it is difficult due to the location and infiltration of the tumours. Broadening the resection area could lead to neurological deficit and loss of the functional brain tissue. Particularly, most of the tumours are located in sensitive areas of the brain, including areas that control the speech, motor function and senses [60]. The high degree of invasiveness renders radical removal of the primary tumour challenging as the infiltrating tumour cells remain within the surrounding brain, leading to recurrence of the tumour [61]. To conclude, surgery suffers from critical limitations that contribute to recurrences. Residual cancer cells that have not been removed and remain in the periphery of the tumour site and the existence of brain tumour initiating cells can increase the risk for tumour recurrence. In addition, the natural wound healing process initiated at the surgical site with the presence of growth factors can enhance the proliferation or migration of tumour cells [62].

1.7.2 Chemotherapy

Chemotherapy also plays a significant role in the treatment of the disease and is commonly administered to patients. Several chemotherapeutic agents have been tested for their effectiveness in the treatment of GBM in order to improve the survival rates of patients, are summarised in Figure 1.8. Among them, alkylating agents such as carmustine (BCNU), lomustine (CCNU) and temozolomide (TMZ) have indicated some advantages and been used in clinical trials for the treatment of GBM [63]. However, it has been reported that BCNU and CCNU result in early development of resistance and their use is associated with many side effects such as nausea, myelosuppression and pulmonary fibrosis [64]. Doxorubicin (DOX) is not commonly used in gliomas due to its low bioavailability in the brain, however, new delivery strategies focus on low

doses of this drug, especially as part of a drug cocktail [65]. Currently, TMZ is the preferred FDA approved chemotherapeutic drug in the treatment of GBM due to its lipophilic nature which enables it to penetrate the BBB and is currently used in combination with radiotherapy as recommended by the Stupp protocol. More specifically, TMZ acts by methylating adenine and guanine residues to form the methylated bases N^3-methyladenine, N^7-methylguanine and O^6-methylguanine which causes the cytotoxicity of TMZ. However, TMZ is administered at high doses and its prolonged systemic administration has been associated with several side effects such as nausea, headaches, vomiting [66] and bone marrow suppression. In addition, at least 50 % of TMZ treated patients do not respond to the treatment. This resistance mainly arises from the overexpression of O^6-methylguanine methyltransferase (MGMT) which is an enzyme involved in DNA repair processes [67]. Several ongoing studies focus on the identification of the factors including the expression level of DNA alkylating proteins, DNA repair enzymes and gene mutations which contribute to TMZ resistance will be discussed in Chapter 4.

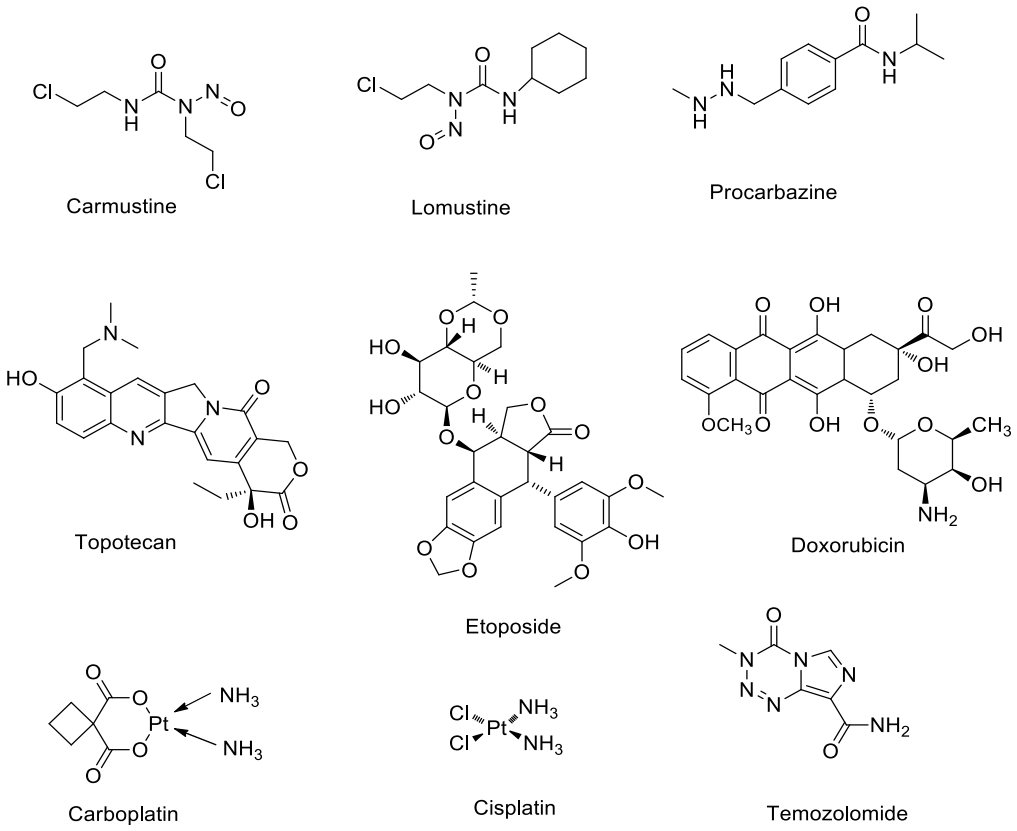

Figure 1.8: Chemical structures of traditional chemotherapeutic agents used in the treatment of GBM.

The use of chemotherapeutic agents in the treatment of GBM presents several important limitations. Firstly, systemic delivery of the drugs at the site of the tumour is ineffective due to the presence of BBB and the repeated administration of high doses of the drugs is necessary which leads in severe side effects. Secondly, malignant gliomas are often resistant to alkylating agents and this results in the formation of recurrences close to the resection borders, rendering GBM treatment challenging

[68]. For the aforementioned limitations of the current chemotherapeutic approach, there is an urgent need to develop more efficient local drug delivery strategies that will enable the targeted drug release to the tumour site over a sustained period of time.

1.7.3 Radiotherapy

Surgical treatment is followed by radiotherapy in order to kill the remaining tumour cells and it aims to improve the life expectancy of the patients diagnosed with high grade glioma [69]. Since 1940s, clinicians have routinely incorporated radiotherapy into the treatment of brain tumours. Walker et al investigated a dose-effect correlation in radiotherapy and the response of GBM [70]. They found that doses of 50-60 Gy were associated with improved survival rates and patients who were subjected to this dose of radiation, demonstrated 2.3 times longer survival compared with those with no radiotherapy. Currently, the radiotherapy scheme consists of administration of approximately 60 Gy of radiation in 1.8 to 2.0 Gy daily doses 5 times per week for 6 weeks and it is delivered to the surrounding area of the original tumour. The extent of the treatment is controversial since it is difficult to define the margins of the tumour with the conventional imaging techniques such as MRI and CT. Alternative advances of radiotherapy include intensity-modulated radiotherapy, image-guided radiotherapy, image-guided radiotherapy and use of radiation sensitisers [71]. The efficacy of radiation regimen can be improved by using radiosensitisers, which are mainly chemotherapeutic agents. Despite the efforts to provide higher local doses of radiation and improve the efficacy of radiotherapy, GBM recurrences occur. Moreover, increasing the intensity of radiation could lead to adverse side effects including radionecrosis, radiation-induced oedema and damage to healthy surrounding brain tissue. Another limitation of this treatment regimen is that tumour margins cannot be accurately detected and identified by MRI, rendering difficult to be reached by radiation. Radiation oncology should focus on the development and improvement of delivery and dose of radiotherapy in order to minimise the toxicity associated with this treatment.

Over the past decades, scientific community has made a lot of efforts to prolong patients' life expectancy and increase the long-term benefits of GBM treatment. However, conventional methods of treatment including surgical resection, radiotherapy and concomitant chemotherapy suffer from crucial limitations highlighted in Figure 1.9. Alternative therapeutic strategies should be developed for the treatment of GBM in order to overcome the several obstacles.

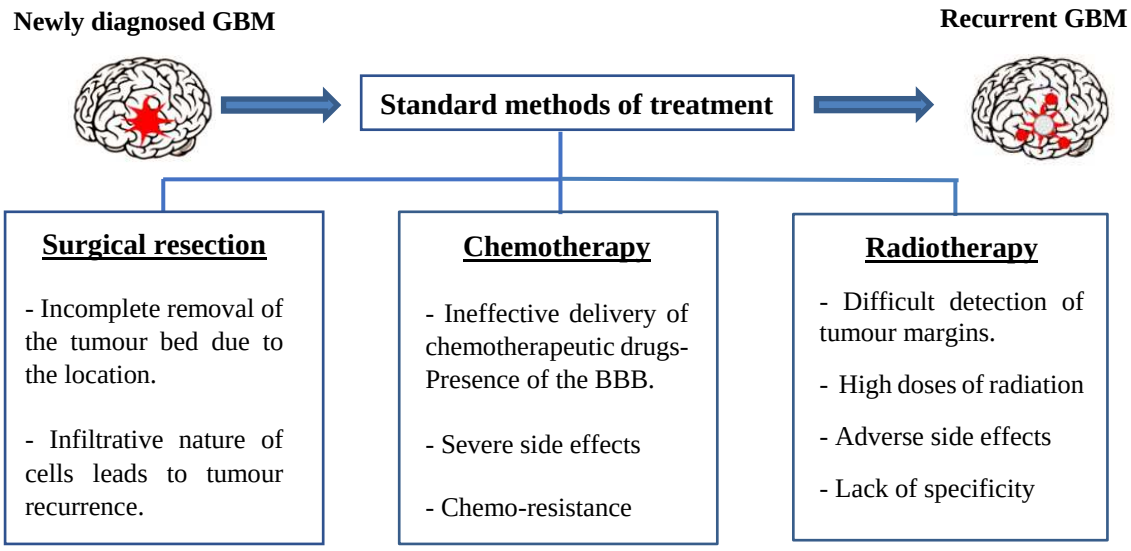

Figure 1.9: Schematic representation of critical limitations of conventional methods of GBM treatment.

1.8 New strategies for GBM treatment

1.8.1 Targeted delivery of genetic therapeutics to the brain

Standard treatment of GBM includes surgical resection of the tumour mass followed by radiation in the vicinity of the resection cavity and concomitant administration of TMZ. Despite this multi-therapeutic approach, tumour recurrence occurs. The majority of gliomas, almost 95 % reoccur in close proximity (1-2 cm) to the initial tumour bed within 5 to 8 months after the treatment [72]. Most of the current local delivery systems depend on drug diffusion into brain parenchyma which only covers few millimeters around the delivery site. Unfortunately, the clinical end point for GBM is restricted to stabilise the disease, to slightly prolong patient's life and to improve the quality of life during the last stages of the disease. Therefore, the development of effective therapeutic treatment for GBM is necessary and requires multidisciplinary approaches that can overcome the complexity of these malignant tumours. During the last decades, great efforts have been made to develop innovative methods of GBM treatment including BBB opening or effux pump inhibition, convection-enhanced delivery (CED), immunotherapy strategies including use of monoclonal antibodies and vaccines, pharmaceutical formulations for local drug delivery such as wafers, liposomes, nanoparticles and hydrogels as shown in Figure 1.10.

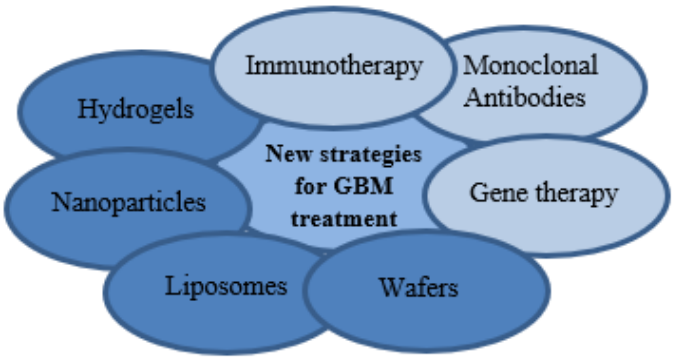

Figure 1.10: Schematic representation of novel strategies for the treatment of GBM. Strategies of targeted delivery of therapeutics are represented in light blue background, while strategies for local delivery of chemotherapeutics are depicted in dark blue background.

1.8.2 Immunotherapy strategies and targeted therapies

Recently, immunotherapy seems to be a novel promising approach for GBM treatment and brings new hopes for GBM patients [73], [74]. The principal targets of immunotherapy include the improvement of the immune response and the targeting of specific antigens. The brain hosts several immune cells such as microglia which are concentrated in brain's gray matter and migrate to inflammatory sites in the CNS, secreting cytokines and chemokines [75]. Interestingly, brain was considered to be an immune privileged site due to the presence of the BBB and the absence of a usual lymphatic system. However, there are significant limitations of this treatment strategy and GBM patients demonstrate low immune responses. Firstly, immune cells can migrate into the brain parenchyma by chemotaxis, where interferons and integrins play an important role in GBM cell migration and invasion. Secondly, in the microenvironment of GBM, hypoxia triggers the secretion of immunosuppressive factors that inhibits the cytotoxic T cell activity [76]. A high level of vascular endothelial growth factor (VEGF) expression can contribute to increased permeability of BBB, enhancing the interaction between tumour cells and the immune system. Therefore, current approaches to immunotherapy focus on targeted therapies such as the use of monoclonal antibodies and vaccines.

Over recent years, several studies investigated the administration of immune cells or antibodies targeted against tumour antigens to patients. It is well known that GBM cells are highly vascularised and they enhance the secretion of proangiogenic factors such as VEGF, which role is critical in angiogenesis and the vascular permeability of the BBB. These proangiogenic factors bind with their corresponding receptors which contributes to the development of angiogenesis, lymphangiogenesis and increased vascular permeability of the BBB. In 2009, FDA approved the use of the monoclonal antibody bevacizumab for the treatment of adult patients diagnosed with GBM [77]. More specifically, bevacizumab selectively binds to the different forms of the VEGF and prevents the interaction of VEGF with target receptors VEGFR-1 and VEFGR-2 on the surface of endothelial cells [78]. The role of bevacizumab by neutralising the biological activity of VEGF contributes to

the reduction of tumour angiogenesis and inhibition of the tumour growth. Despite many clinical trials for the treatment of GBM, recent studies to evaluate the use of bevacizumab combined with the standard therapy, demonstrated no increase of GBM survival rates and patients did not present benefits from the bevacizumab treatment. On the other hand, severe side effects were reported such as hemorrhage, deep vein thrombosis and gastrointestinal problems [79]. To date, there is lack of information on the optimal conditions of using bevacizumab for the treatment of GBM in terms of dosage, the duration of the treatment and lack of biomarkers to identify the benefits from this targeted therapy.

Moreover, the rapid development of immune targeted therapeutic strategies contributed to the investigation of anticancer vaccines. Advantages of the vaccination strategy involve the targeted delivery of tumour associated antigens directly to the tumour site [80]. Currently, vaccine therapies for GBM have been successfully investigated in clinical trials, with promising results so far highlighting their potential for future therapeutic integration. There are different types of vaccines for GBM treatment including peptide vaccines, heat shock protein (HSP) and dendritic cell vaccines [81]. Among the immunotherapies studied for the treatment of GBM, there are several therapeutic vaccines including the peptide vaccine, Rindopepimut [82]. The main component is a peptide corresponding to a mutated form of EGFR, EGFRVIII (expressed solely by 20 to 30 % of GBM). Initial results from a randomised trial presented no improvement in median overall survival and progression-free survival in EGFRVIII-expressing GBM patients who received + TMZ + vaccine compared to patients who received only TMZ (ACT IV trial) [83].

Main limitations of these type of vaccines include the alteration of second- or third-line therapeutic approach in case of tumour recurrence and the restriction of targeting specific antigens, while GBM cells are highly heterogeneous and this results in inadequate tumour control. Furthermore, immunotherapy is usually combined with chemoradiation which causes adverse side effects and it renders immunotherapy regimen challenging and sometimes difficult to be integrated into the GBM treatment.

1.8.3 Gene delivery

Strategies for gene therapy of gliomas have been in development for the last 2 decades focusing on the delivery of genetic therapeutics with the aim to induce apoptosis of tumour cells or activating the immune response against them. More specifically, the gene therapeutic strategies for the treatment of GBM include the delivery of cytokine genes or suicide genes to trigger immune cells and convert prodrugs into active cytotoxic compounds in the tumour site leading to apoptosis. In addition, gene treatment involves the delivery of specific viruses in order to induce intracellular toxicity to the tumour cells or destroy them during the replication process [84]. In 1991, Ezzedine et al studied the selectivity and efficacy of the Herpes simplex virus thymidine kinase (HSV-TK) on the apoptosis of

glioma cells upon the administration of the prodrug ganciclovir (GCV) [85]. The enzymatic process induced by the GCV leads to death of the tumour cells that express the HSV-TK enzyme. Another widely studied gene is the bacterial enzyme Cytosine Deaminase (CDA), which converts the prodrug 5-fluorocytosine to the toxic compound 5-fluorouracil (5-FU). Combination of CDA with radiotherapy has shown significant results by killing tumour cells and delaying tumour growth in xenograft models of glioma [86]. Moreover, latest studies focus on the viral delivery of p53 gene which is one of the most frequently mutated genes in glioma cells in order to prevent the tumour growth [87]. However, gene therapy still faces considerable challenges for successful long-term therapeutic benefits for GBM patients. Firstly, poor rate of delivery and diffusion of genes to the tumour cells renders GBM treatment challenging. Secondly, lack of clinical effectiveness which can be mainly assigned to the poor distribution of the genes into the tumour. Interestingly, in a recent clinical study using retrovirus-producing cells to deliver HSV-TK gene therapy in GBM patients, researchers did not observe any improvements in the overall survival [88]. Moreover, gene infected cells could present potential resistance to the prodrugs, requiring combination of gene therapy with the conventional chemoradiotherapy regimen in order to overcome this obstacle.

1.8.4 Alternative magnetic field treatment

A treatment based on the application of very low intensity alternating fields, named TTfields (Tumour Treating Fields) is currently being studied using the NovoTTF-100A and involves wearing a helmet consisting of 4 electrodes on the patient's skull, producing a magnetic field treatment [89]. This device should be worn as long as possible per day, every day. In vitro, these fields lead to tumour apoptosis at the time of cell division and inhibition of cell migration. The Optune device has recently been approved for patients with newly diagnosed GBM. Despite progress and knowledge, and the multiplicity of avenues and therapeutic options, the improvements in terms of survival for the patient remain insignificant and suggest to propose innovative strategies for local delivery of chemotherapeutics.

1.9 Local delivery of chemotherapeutics

Current conventional methods of treatment for GBM are mainly insufficient followed by inevitable tumour recurrence due to the drug delivery challenges in the brain as illustrated in Figure 1.11. A major reason for this failure is the unique brain microenvironment and the presence of the BBB which prevents the effective delivery of cytotoxic drugs at the tumour site. In fact, over 95 % of tumour recurrence cases occur within 1-2 cm from the margins of the resection cavity [90]. Therefore, the application of local drug delivery systems that will enable therapeutic concentration of the drugs to reach the tumour site avoiding adverse side effects, seems a hopeful alternative to overcome the barriers to effective brain tumour treatment. Current developments in the local drug delivery to the brain involve direct injection, CED and implantation of pharmaceutical formulations.

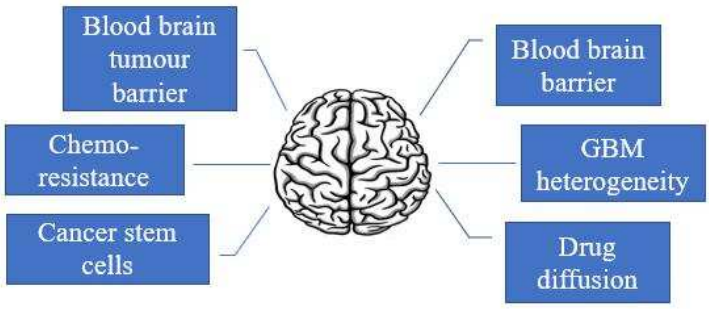

Figure 1.11: Illustration summarising the drug delivery challenges encountered in the treatment of GBM.

Direct injection of chemotherapeutics via a repeated needle-based injection is the earliest method used for GBM local drug delivery targeting the injection of chemotherapeutic agents into the resection cavity or the brain parenchyma. In 2003, Prados et al evaluated the efficacy of direct injection of HSV-TK gene vector producer cells followed by intravenous GSV administration on 30 patients and observed severe effects in 16 patients, confirming that gene expression was only present few millimeters from the resection cavity [91]. Despite being a simple and easy method to apply for local drug delivery, there are several limitations to this injection strategy. More specifically, repeated surgical operations are required thus increase the risk of local side effects such as infection and intracranial hemorrhage. Additionally, the drug distribution into the tumour and the surrounding brain parenchyma is poor due to the limited depth of diffusion and high concentrations of the drug can be found mainly around the injection point [92].

Therefore, another approach was developed to facilitate local drug distribution to the brain and overcome the inadequacy of the direct injection method. CED relies on the direct continuous diffusion of the chemotherapeutic agent in the brain parenchyma using a micro-catheter connected to a motor-driven pumping device which allows wider distribution of the drug in the brain tissue [93]. Bruce et al in 2011 performed a Phase I trial evaluating the safety profile of CED of topotecan in 16 patients with recurrent malignant gliomas and they observed early response in 4 patients (25 %), pseudoprogression in 2 (44 %), progressive disease in 5 (31 %) and dose limiting toxicities in 2 (13 %) [94]. However, disadvantages of this method involve the continuous refilling of the reservoir, dependence of the drug distribution on the features of the device, drug properties and infusion parameters (rate, volume and duration) and potential neurotoxicity.

1.9.1 Liposomes for the treatment of GBM

Liposomes have been studied extensively as drug carriers since several decades and their use for the treatment of GBM was investigated due to several features of these systems. Firstly, they can cross the BBB through the inter-endothelial gaps of the blood brain tumour barrier in case of high-grade gliomas. Secondly, the relatively simple and cost-effective preparation procedure, long-term stability in plasma and biocompatibility are key factors for the effective application of these systems.

Moreover, liposomes have the ability to efficiently encapsulate high concentrations of hydrophilic or amphiphilic anticancer agents and should decrease the systemic toxicity of anti-neoplastic agents [95].

The potential of liposomes for the delivery of anticancer drugs has been investigated extensively in different types of cancer. Liposomes are constituted of a double lipid membrane, some can be surface linked with polyethylene glycol (PEG-coated) and/or can be functionalised by means of antibody or peptide-coated membrane to bind more specifically transporters expressed by the BBB or receptors expressed by glioma cells. Commercially available liposomes (Caelyx®) loaded with DOX have been approved for clinical trials in several types of cancer and they are under investigation for the treatment of GBM [96]. Recently, Lu et al developed a multifunctional liposomal glioma-targeted drug delivery system modified with cyclic RGD (c(RGDyK)) and p-hydroxybenzoic acid (pHA) in which c(RGDyK) could target integrin αvβ3 overexpressed on the BBTB and glioma cells [97]. Moreover, Yu et al presented an effective method to improve the drug delivery to brain tumour. Particularly, as shown in Figure 1.12, they conjugated the iNGR peptide to liposomes to enable them to specifically recognise and penetrate across the tumour blood vessels, thereby increasing the drug concentration on tumour tissue [98]. Thus, their simple and large-scale production, easily tunable composition, their ability to penetrate the BBB and the preferential accumulation within the tumour tissue renders them very promising drug delivery systems for the treatment of GBM.

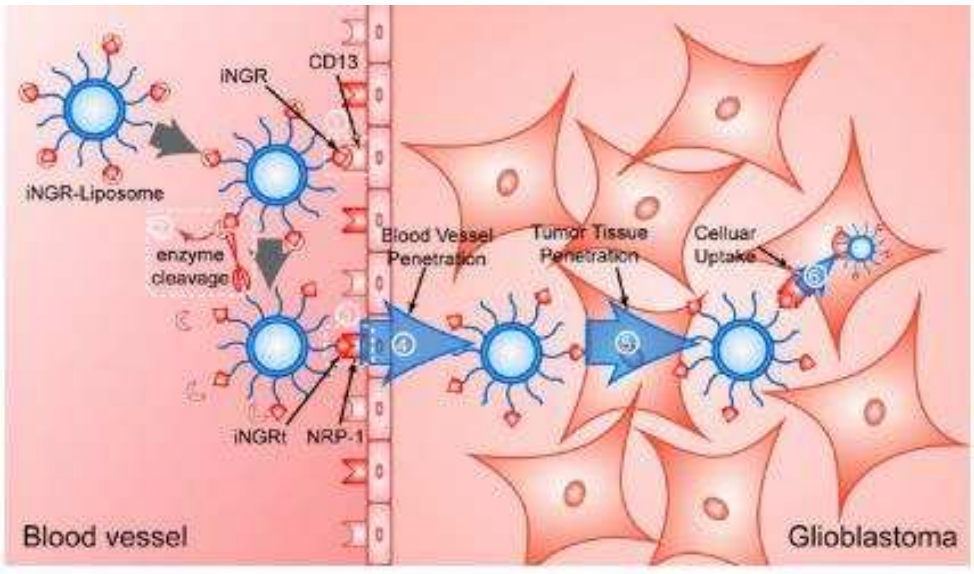

Figure 1.12: Tumour vessel recognising and tumor penetrating system is developed by modifying the iNGR peptide to the surface of liposomes (iNGRSSL/DOX). The iNGR-SSL/DOX first binds to tumour blood vessel by the interaction of iNGR and CD13 receptor. Then iNGR is proteolytically cleaved to iNGRt, which specifically binds to NRP-1 overexpressed on tumour blood vessel. The iNGRt mediates the liposome penetration through tumour neovascularisation and tumour tissue, and finally the cellular uptake by glioblastoma cells. Adapted from Zhou et al [98].

Despite the advantages from the application of liposomes for the treatment of GBM, this method suffers from several limitations. To date, there is insufficient knowledge on clinical studies of these therapeutic systems for the treatment of GBM. The majority of the studies are restricted to in vitro and in vivo conditions and no clinical trials are ongoing.

1.9.2 Nanomedicine for the treatment of GBM

The development of new technologies based on nanoparticles (NPs) for cancer treatment has been extensively investigated in the past two decades [99]. Particularly, integration of nanomedicine into conventional chemotherapy has provided significant advantages in terms of solubility, stability and side effects of the conventional chemotherapeutic drugs. NPs have attracted much interest in the targeted drug delivery due to their physical properties. More specifically, their small size, their tunable degree of surface coating, the drug loading capacity and the controllable release profile are essential elements for their successful application in drug delivery. In addition, these materials can improve the plasma circulation half-life of the drug molecules, rendering them promising drug carriers for local delivery. Particularly, NPs for brain drug delivery should be nontoxic, nonimmunogenic, biocompatible and biodegradable, protecting the encapsulated drug from any means of degradation [100]. Additionally, encapsulation of chemotherapeutic drugs into NPs facilitates the penetration of the BBB or BBTB in the brain [101].

Intravenous administration of NPs has been emerged as promising strategy for GBM treatment due to their versatility in surface modification [102]. Interestingly, Steiniger et al investigated the use of poly (butyl cyanoacrylate) (PBCA) nanoparticles loaded with DOX, with or without surface coating of PS80 as targeting moiety against intracranial 101/8 GBM tumour model in rats [103]. Animals treated with DOX loaded NPs demonstrated prolonged survival time and histological analysis confirmed slight reduction in the size of the tumour. Gao et al developed PEG-poly(caprolactone) (PEG-PCL) NPs with surface coating of interleukin-13 (IL-13) peptide, which preferentially binds with the IL-13Rα2 receptor overexpressed in gliomas [104]. Highest cellular uptake and better targeted delivery was observed with the coated NPs. It is well known that PEGylated NPs, such as Doxil® with encapsulated DOX allow surface functionalisation to penetrate the BBB and was shown to stabilise malignant glioma patients [105]. In another study, magnetic iron oxide NPs were modified through the PEGylation, conjugation by chlorotoxin and cyclodexterin, loaded with fluorescein and paclitaxel. These formulations led to increased uptake of NPs by GBM cells, thus paclitaxel could act more efficiently in suppressing GBM and malignant drug resistant cells [106].

The local delivery of drugs through NPs system is a major challenge and consequently several methods have been developed to achieve the highest localised drug delivery due to the contribution of ultrasounds (US). For example, Hall et al investigated the development of ultrasound sensitive microbubbles (MBs) that were consisted of silica-based materials, presenting significant stability and

potential to be used for localised drug delivery [107]. Additionally, in another study from the same group, the impact of US as potential trigger for the release of drugs encapsulated in silane-polycaprolactone (SiPCL) MBs was investigated [108]. SiPCL MBs were loaded with docetaxel and the release was further studied in either with the effect of ultrasound as trigger or not. The cytotoxicity of the released docetaxel on C4-2B cells was evaluated and increased cytotoxicity was observed, concluding that US as trigger, enhances the local delivery of the drug.

It is generally believed that the delivery of drugs to the brain is extremely challenging due to the low permeability of the BBB as discussed in section 1.6. It has been demonstrated that the combination of focused ultrasound (FUS) and NPs or MBs can reach brain tissues with minimally invasive methods [109]. The MBs interact strongly with low-intensity US, producing mechanical forces on the endothelium that result in transient disassembly of tight junctions. Safe disruption or loosening of the BBB is significantly important to deliver chemotherapeutic agents and overcome the limitations arise from the tight junctions of the barrier. Successful delivery of the drugs can be achieved through BBB disruption using focused US as illustrated in Figure 1.13.

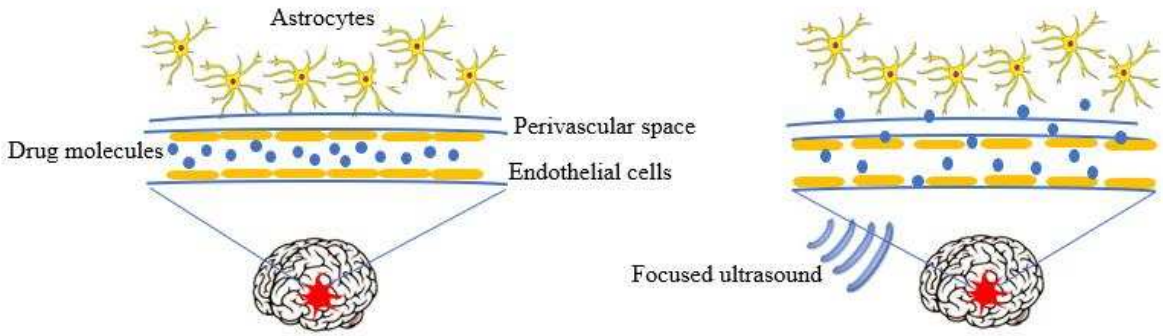

Figure 1.13: Illustration of the application of FUS for disruption of the BBB. The BBB is impermeable to many drugs. FUS can reversibly loosen this barrier, allowing drugs to penetrate.

Recently, Aryal et al developed a FUS-based strategy to improve the delivery of liposomal DOX in a rat glioma model. They tested the impact of three weekly sessions of FUS and liposomal DOX on 9L rat glioma tumours. Treated animals with combination of FUS and liposomal DOX demonstrated significant increase in survival time compared to animals received only FUS or DOX or no treatment [110]. Moreover, transcranial FUS has been demonstrated to disrupt the BBB in a focal and reversible manner and its potential application to brain tumour treatment has been recently demonstrated in rat models [111], [112]. Rutka et al have demonstrated the use of Magnetic Resonance-Guided FUS in order to induce disruption of the BBB in rats and allow the targeted delivery of cisplatin loaded gold NPs to the tumour margins [113].

According to the promising results gathered from in vitro and in vivo experiments at the preclinical stage of NPs based therapy, further clinical studies are required for the successful application of these systems on the treatment of devastating GBM.

1.9.3 Implantable drug polymers

Another drug delivery approach in the treatment of GBM is the use of implantable drug loaded polymers. Polymers present several advantages in the local drug delivery. Firstly, they allow sustained release of the drug through degradation of the polymer matrix. Secondly, polymers can be easily manipulated during their implantation in the resection cavity avoiding invasive surgical manners.

FDA and the National Institute for Health and Clinical Excellence (NICE) have only approved the use of polymeric wafers Gliadel® loaded with BCNU for local chemotherapy in the treatment of malignant glioma [114]. Particularly, this type of wafers, mainly consists of a biodegradable copolymer formed of 1,3-bis-(p-carboxyphenoxy)propane (pCPP) and sebacic acid (SA), are implanted along the margins of the tumour resection cavity as shown in Figure 1.14 and release BCNU in a controlled manner into the surrounding brain tissue over 2-3 weeks.

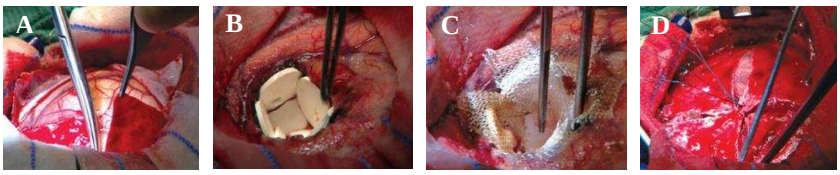

Figure 1.14: Stages of wafer implantation in the resection cavity, **A.** Surgical resection of GBM, **B.** Administration of Gliadel® wafers along the wall of the resection cavity of a patient at the time of the surgery. Up to 8 wafers can be placed to cover as much as of the resection cavity, **C.** Surgicel® may be placed over the wafers to secure them against the cavity surface, **D.** Close and ensure cavity integrity. Adapted from reference [115].

The recommended dose of BCNU is 61.6 mg, represented by 8 wafers (7.7 mg BCNU each) that are implanted intracranially to fill the resection cavity. Multiple clinical trials have reported the prolonged survival time for patients treated with Gliadel®. Particularly, Valtonen et al investigated the effects of BCNU wafers or placebo on patients with newly diagnosed malignant gliomas and they observed significantly longer survival for the group of patients treated with wafers compared with the placebo group [116]. Therapeutic strategies using Gliadel wafers have demonstrated prolongation of survival in GBM patients, albeit, tumour recurrence cases have been reported in the majority of treated groups. Additionally, there are several concerns about the use of wafers for the treatment of brain tumours. Adverse side effects have been associated with their use including seizures, intracranial hypertension, impaired neurosurgical wound healing, brain oedema, meningitis and wafer migration [117]. In addition, rapid release of carmustine within the first 5-7 days of implantation instead of sustained release within 3 weeks in vivo studies in mammalian models has been reported [118]. The short half-life of BCNU, approximately 20-30 minutes and the solid nature

of these wafers does not allow homogeneous distribution of the drug. Therefore, several groups focused on the administration of implantable polymers with other chemotherapeutic agents in the resection cavity. For example, Manome et al developed a PLGA implant loaded with DOX which was exposed to the glioma induced significant inhibition of the tumour growth. Khang et al tested BCNU-loaded PLGA wafers on 9L gliosarcoma cells and on a solid tumour model of 9L gliosarcoma and they also observed substantial regression of the tumour [119], [120]. Finally, it is of paramount importance to develop new strategies that will overcome some of the limitations of implantable polymers. Hydrogels used as targeted chemotherapy systems own a promising role in the treatment of GBM.

1.9.4 Hydrogels for the treatment of GBM

During the last decades, many therapeutic approaches have been developed to treat GBMs, among them the local delivery of chemotherapeutic drugs in the resection cavity has gained a lot of attention. Many researchers have focused on different drug delivery systems. Among them, injectable drug-loaded hydrogels have shown promising results. Hydrogels are three-dimensional, hydrophilic crosslinked networks capable of absorbing large amounts of water or biological fluids. They are used for many applications in the medical and pharmaceutical field such as for cell culture and as drug delivery systems [121], [122]. Their unique physical properties, particularly their biocompatibility, tunable mechanical properties, hydrophilic nature and the structural resemblance to the extracellular matrix of living tissues rendering them attractive in a variety of biomedical applications.

Particularly, the in situ gelation is one of the key elements in the success of hydrogels in the biomedical field and it will be further discussed in Chapter 2. In recent years, the injection of gel forming solutions has been considered a promising method to deliver drugs at targeted areas. Injectable hydrogels possess several advantages over the conventional approaches for drug delivery systems [123]. Firstly, their initial liquid formulation can flow easily and turn into gel, thus filling any cavity shape. Secondly, the hydrogel can be loaded with a variety of therapeutic agents including hydrophobic drugs, growth factors or cells. Thirdly, the polymer formulation can be stored at room temperature or at lower temperature before the administration and turn into gel at physiological conditions. Above all, there is no requirement for an invasive surgical procedure for implantation. The therapeutic agent can be delivered directly into the targeted site by a simple injection of a liquid formulation, which undergoes thermal gelation at body temperature.

Interestingly, hydrogels have been used in several studies for the investigation of GBM treatment and they are summarised in Table 1.1. They have been involved in the fabrication of complex microenvironment models to study the mechanobiology and migration behaviour of glioma cells [124], [125]. They have also been used in the development of a three-dimensional culture system in order to assess the response of malignant gliomas to radiation and chemotherapeutic drugs [126]. To

date, hydrogels have extensively been studied as anticancer drug delivery systems for the treatment of malignant brain tumours. These systems can be administered in the brain after craniotomy in the resection cavity via intracerebroventricular injection or intracerebral implantation. Albeit, few studies have been focused on the administration of hydrogels in the resection cavity and very little is described in the literature.

Table 1.1: Examples of hydrogels developed for intracranial implantation for local treatment of GBM.

Hydrogel matrix	Active agent	Type of study	Reference
PEG-based hydrogel	CRGDS and a MMP-cleavable peptide	In vitro tumour model	124
Collagen-HA hydrogel	-	GBM behaviour in 3D matrix	125
Extracell^{TM}	TMZ, BCNU, cisplatin	Ex vivo culture of GBM	126
OncoGel^{TM}	TMZ	Intracranial GBM model	127, 128
GemC12-LNC hydrogel	Lauroyl-gemcitabine	Human xenograft GBM model	129, 130
PEG-based hydrogel	TMZ	Human GBM model	131
Chitosan-based hydrogel	TMZ/ ^{131}I	In vivo study in nude mice	132
Collagen-based hydrogel	Cyclopamine	Human xenograft GBM model	133
Alginate-based hydrogel	PTX-loaded PLGA microspheres	Xenograft GBM model	134, 135

Recently, Tyler et al investigated the use of OncoGel^{TM} in an intracranial 9L GBM model alone or in combination with TMZ and radiotherapy [127], [128]. OncoGel ^{TM} consists of ReGel ^{TM} which is a copolymer of PLGA and PEG that forms a biocompatible gel at body temperature. It can be injected in the proximity of the tumour and provide controlled release of paclitaxel for 6 weeks with dose-limiting toxicities. Interestingly, Bastiancich et al proposed the use of a novel hydrogel formed of lipid nanocapsules (LNC) and Lauroyl-gemcitabine ($GemC_{12}$) for the local treatment of GBM [129]. The $GemC_{12}$-LNC hydrogel was well tolerated in mouse brain after 2 and 6 months of exposure and the researchers proceeded with the intratumoural administration of the hydrogel in an orthotopic human xenograft GBM model for further investigation. They reported the antitumour efficacy of the nanomedicine hydrogel after injection in the resection cavity of an orthotopic human xenograft model and the significant increase in survival in mice treated groups [130] as demonstrated in Figure 1.15. Although, further studies in other animal models are required to ensure the efficacy of this system in comparison with other chemotherapeutic drugs or radiotherapy.

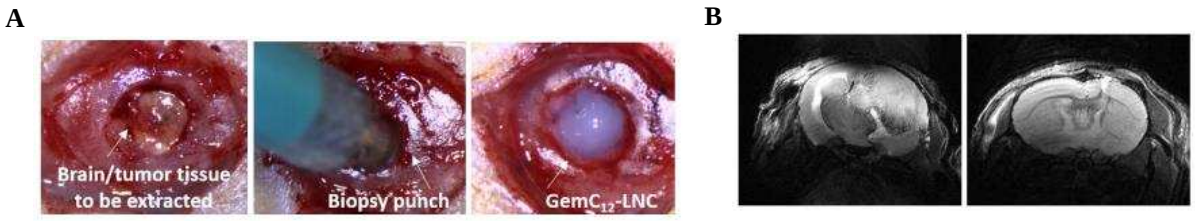

Figure 1.15: A. Images taken from the intratumoural administration of the $GemC_{12}$-LNC hydrogel: tumour tissue visible within the 2x2 mm cranial window (left), biopsy punch twisting (middle) followed by aspiration. $GemC_{12}$-LNC hydrogel (5μL) injected into the resection cavity (right), **B.** Axial (T2-weighted) images of mouse brain following resection: untreated (day 31 post-resection, left) and treated with $GemC_{12}$-LNC (day 61 post-resection, right), demonstrating the antitumour efficacy of the specific hydrogel. Adapted from Bastiancich et al [130].

In the field of photopolymerisable hydrogels, Danhier et al described the development of an injectable hydrogel for the local delivery of TMZ in the resection borders of the tumour cavity. This injectable hydrogel consisted of a mixture of PEG dimethacrylate and water at a ratio of 75:25 and 0.5 % of Lucirin-TPO® was used as photoinitiator. The antitumour effect of this hydrogel was evaluated in nude mice on a subcutaneous human GBM model, which showed that the tumour growth of mice treated with the photopolymerised TMZ hydrogel significantly decreased compared with control (untreated animals) [131]. In another study, Puente et al investigated the use of a biodegradable injectable chitosan-based hydrogel for the local chemoradiotherapy treatment of GBM. The hydrogels were loaded with TMZ or radioactive isotopes agents (iodine, ^{131}I) in nude mice and their efficacy on tumour growth was evaluated. Tumour growth was significantly delayed and the survival was improved in treated groups compared with the control group [132].

Despite the growing number of research studies in the field of injectable hydrogels, up to now, just few focused on the development of systems for trapping glioma cells. As mentioned in section 1.3, malignant glioma cells intend to invade and migrate along white matter tracts and blood vessels. Recently, Bellamkonda et al exploiting this characteristic of glioma cells, by means of engineered aligned or smooth PCL-based nanofibers in order to mimic the structure of white matter tracts and blood vessels. These nanofibers allowed tumour cells to invade and then guide them from the primary tumour site to a collagen-based hydrogel loaded with cyclopamine as cytotoxic drug [133]. More specifically, they inserted the nanofibers in a conduit which was placed in the margins of an intracortical human glioblastoma U87MG xenograft model as shown in Figure 1.16. They observed that a considerable number of human GBM cells managed to invade and migrate along the aligned PCL-based nanofibers network and underwent apoptosis in the drug loaded hydrogel.

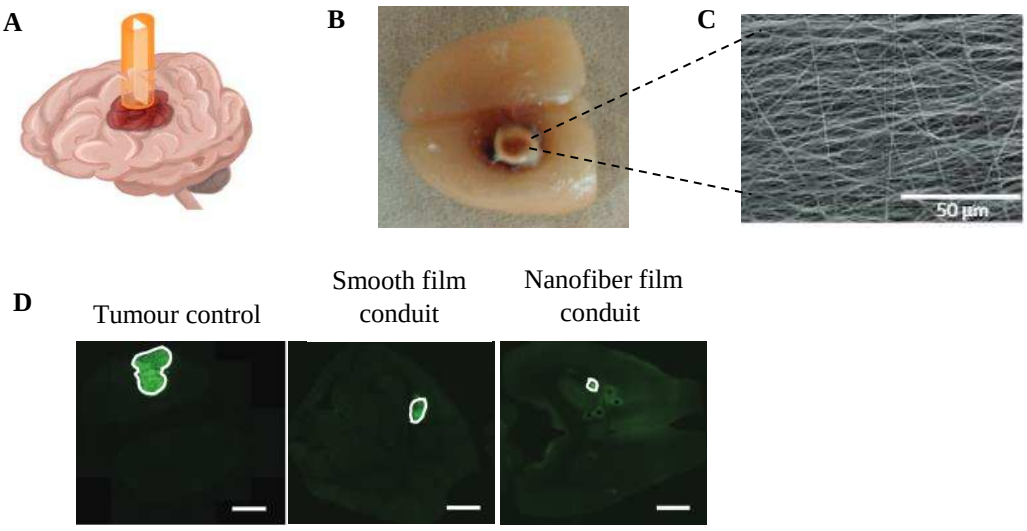

Figure 1.16: A. Schematic illustration of the conduit inserted into the rat brain with GBM from an angled view**. B.** Digital image of fixed extracted brain containing a conduit from the top view, **C.** Scanning electron microscopy image of the aligned polycaprolactone-based nanofiber film, **D.** Fluorescence images showing the tumour core in the brain in the tumour control condition, the smooth film conduit and the nanofiber film conduit condition. The tumours are outlined with green colour. Scale bars: 3.75 mm. Adapted from Puente et al [133].

In the context of non-CNS tumours, Williams et al developed a medical device that was implanted into a tumour site and studied the tumour microenvironment. This device consisted of a transparent hydrogel that was loaded with growth factors to be released into the tumour site forming a gradient. The hydrogel was formed by 20 % of polyethylene glycol diacrylate, 7 % methoxy polyethylene glycol monoacrylate and Irgacure 2959 as photoinitiator. The aim of their study was the evaluation of migration of the invasive cells towards the gradient concentration of the released growth factors from the tumour site to the device. The sustained release of the chemoattractants such as epidermal growth factor (EGF) efficiently contributed to the migration of adenocarcinoma cells [136]. However, considering the very well-known knowledge about the stimulating impact of EGF on tumour growth, it would be particularly dangerous to apply this strategy to cure cancer patients.

To date, the majority of the research studies has focused on the local delivery of anticancer drugs in the resection cavity by using injectable hydrogels as delivery systems. However, the aforementioned strategies suffer from several disadvantages, including the absence of molecules that naturally exist in the brain extracellular matrix and most importantly, they lack from effective chemoattractants. Consequently, residual invasive tumour cells remain in the margins of the resection cavity, or even at distance from this, leading to inevitable tumour recurrence.

1.10 Thesis objectives and overview

After decades of intense clinical research, there is not an efficient treatment for GBM. Therefore, there is an urgent need to develop new methods and understand the complex behaviour and microenvironment of GBM tumours. The key challenge in successful GBM treatment lies in destroying the cancer cells that invade the brain tissue and already exist in the brain parenchyma at the time of the removal of the primary tumour bed by neurosurgeon.

This thesis aims to shed light on and tackle the majority of different limitations of the conventional methods of GBM treatment outlined in sections 1.7 and 1.8. In order to address these challenges, we here investigated the use of 3D matrices such as hydrogels for attracting and trapping glioma cells. Particular attention was given to those based on Hyaluronic Acid (HA). HA is a naturally occurring polysaccharide and it is the main component of the extracellular matrix of the brain tissue [137]. Recently, HA hydrogels have been involved in studies to explore glioma cell behaviour and migration [138], [139]. In this work, hydrogels were loaded with a small peptidic chemokine at a concentration gradient in order to achieve the migration of glioma cells to the hydrogel matrix and with a chemotherapeutic drug in order to induce apoptosis of the cells as illustrated in Figure 1.17.

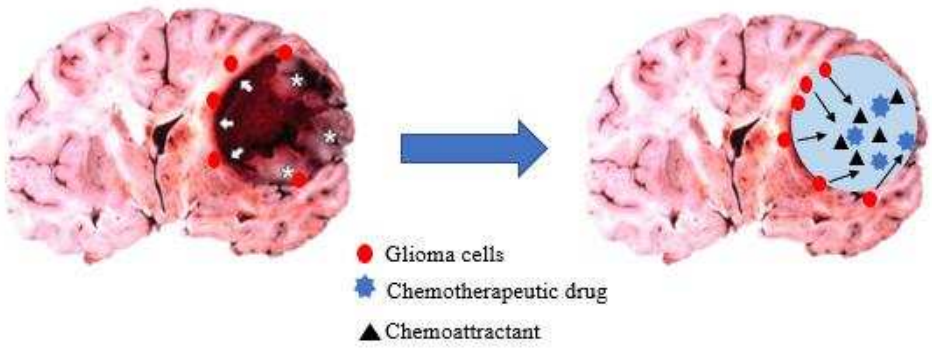

Figure 1.17: Illustration of hydrogel loaded with a chemoattractant at a concentration gradient and with a chemotherapeutic drug for attracting and inducing apoptosis of migrated glioma cells.

The chemokine that was used is the vasoactive peptide urotensin II (UII). Recently, it has been established that glioma cells express this peptide and its receptor UT which are involved in glioma cell migration and adhesion. UII used at gradient concentrations demonstrated chemoattracting migratory effects on glioma cells [140]. Hence, the proposed system for attracting and trapping brain cancer cells is safer and more effective than the currently available methods. The specific aims of this PhD thesis are as follows:

1. Preparation of biocompatible polymeric hydrogels based on FDA approved materials and optimisation of their physical and mechanical properties for cell adhesion.
2. Formulation of the material in order to achieve the transition from the liquid phase to gel phase and optimisation of the injectability of the system (e.g. responsive hydrogel).

3. Characterisation of the physicochemical and mechanical properties of the fabricated hydrogels.
4. Formulation of the matrix to deliver the chemoattractant in a concentration gradient and allow controlled release of the loaded chemotherapeutic drugs.
5. Evaluation of the biological response of glioma cells in the formulated hydrogels.

In addition, an overview of the thesis structure is presented below:

Chapter 1: Introduction

This chapter aims to provide a brief overview of the challenges encountered in the treatment of GBM and the limitations of the conventional methods of treatment, highlighting the urgent need for alternative and more efficient therapeutic strategies.

Chapter 2: Preparation of injectable polysaccharide-based hydrogels

This chapter proposes the use of 3D scaffolds such as hydrogels in order to address the challenges of GBM treatment. In particular, this work focuses on the preparation of hydrogels based on polysaccharides including mainly hyaluronic acid, methylcellulose and xanthan gum. The crosslinking methods used and the protocols to fabricate these scaffolds are described.

Chapter 3: Physicochemical and mechanical characterisation of hydrogels

The physicochemical and mechanical properties are of paramount importance in determining if a material is suitable for a specific application. This section focuses on the characterisation methods to study the physicochemical and mechanical properties of the fabricated hydrogels. More specifically, hydrogels were mainly characterised by swelling studies, Scanning Electron Microscopy, enzymatic degradation experiments, Differential Scanning Calorimetry, Infrared Spectroscopy and Oscillatory Rheology.

Chapter 4: In vitro evaluation of glioma cells response on polysaccharide-based hydrogels

Glioma cells were seeded on the fabricated hydrogels and their biocompatibility was mainly evaluated using MTS assay and Live/Dead staining. In addition, the chemoattraction of the hydrogels loaded with the chemokine was investigated.

Chapter 5: Conclusion

The general conclusion remarks of this PhD thesis are presented and a personal reflection on the development of hydrogels and their implications in the treatment of GBM is stated.

References

[1] Ma X., Yu H., Global Burden of Cancer, Yale J. Biol. Med., 2006, 79, 85-94.

[2] Phillips J.L., Currow D.C., Cancer as a chronic disease, Collegian, 2010, 17, 47-50.

[3] Omuro A., DeAngelis L.M., Glioblastoma and other malignant gliomas: a clinical review, JAMA, 2013, 310, 1842-1850.

[4] https://www.cancer.gov/types/metastatic-cancer (accessed 03/2018).

[5] http://www.nyhq.org/diw/content.asp?pageid=P02627 (accessed 03/2018).

[6] Cancer Research UK, http://www.cancerresearchuk.org/health-professional/cancer-statistics/statistics-by-cancer-type/brain-other-cns-and-intracranial-tumours/incidence#heading-One, (accessed 03/2018).

[7] National Registry of Childhood Tumours/Childhood Cancer Research Group, http://www.ccrg.ox.ac.uk/datasets/registrations.shtml (accessed 03/2018).

[8] Wilne S., Koller K., Collier J., Kennedy C., Grundy R., Walker D., The diagnosis of brain tumours in children: a guideline to assist healthcare professionals in the assessment of children who may have a brain tumour, Arch. Dis. Child., 2010, 95, 534-539.

[9] Packer R.J., Childhood Brain Tumours: Accomplishments and Ongoing Challenges, J. Child. Neurol., 2008, 23, 1122-1127.

[10] Cancer Research UK, http://www.cancerresearchuk.org/health-professional/cancer-statistics/childrens-cancers/incidence#heading-Three (accessed 03/2018).

[11] Louis D.N., Ohgaki H., Wiestler O.D., Cavenee W.K., Burger P.C., Jouvet A., Scheithauer B.W., Kleihues P., The 2007 WHO Classification of Tumours of the Central Nervous System, Acta Neuropathol., 2007, 114, 97-109.

[12] Louis D.N., Perry A., Reifenbergen G., Deimling A., Figarella-Branger D., Cavenee K.W., Ohgaki H., Wiestler D.O., Kleihues P., Ellison W.D., The 2016 WHO classification of tumours of the central nervous system: a summary, Acta Neuropathol., 2016, 131, 803-820.

[13] Ostrom Q.T., Gittleman H., Liao P., Vecchione-Koval T., Wolinsky Y., Kruchko C., CBTRUS statistical report: primary brain and central nervous system tumours diagnosed in the United States in 2010-2014, Neuro Oncology, 2017, 19, 1-88.

[14] Mandonnet E., Delattre J.Y., Tanguy M.L., Swanson K.R., Carpentier A.F., Duffau H., Cornu P., Van Effenterre R., Alvord E.C., Capelle L., Continuous growth of mean tumour diameter in a subset of grade II gliomas, Ann. Neurol., 2003, 53, 524-528.

[15] Maher E.A., Brennan C., Wen P.Y., Durso L., Ligon K.L., Richardson A., Khatry D., Feng B., Sinha R., Louis D.N., Quackenbush J., Black P.M., Chin L., DePinho R.A., Marked genomic differences characterise primary and secondary glioblastoma subtypes and identify two distinct molecular and clinical secondary glioblastoma entities, Cancer Res., 2006, 66, 11502-11513.

[16] CBTRUS Statistical report: primary brain tumours in the United States, 2000-2004. Chicago: Central Brain Tumour Registry of the United States, 2008.

[17] De Robles P., Fiest K.M., Frolkis A.D., Pringsheim T., Atta C., St Germaine-Smith C., Day L., Lam D., Jette N., The worldwide incidence and prevalence of primary brain tumours: A systematic review and meta-analysis, Neuro Oncology, 2015, 17, 776-783.

[18] Nakada M., Kita D., Watanabe T. et al, Aberrant signaling pathways in glioma, Cancers, 2011, 3, 3242-3278.

[19] Bellail A.C., Hunter S.B., Brat D.J., Tan C., Van Meir E.G., Microregional extracellular matrix heterogeneity in brain modulates glioma cell invasion, Int. J. Biochem. Cell Biol., 2004, 36, 1046-1069.

[20] Bernstein J.J., Woodard C.A., Glioblastoma cells do not intravasate into blood vessels, Neuro-surgery, 1995, 36, 124-132.

[21] Vartanian A., Singh S.K., Agnihotri S., Jalali S., Burrell K., Aldape K.D., Zadeh G., GBM's multifaceted landscape: highlighting regional and microenvironmental heterogeneity, Neuro Oncology, 2014, 16, 1167-1175.

[22] Holland E.C., Glioblastoma multiforme: the terminator, Proceedings of the National Academy of Sciences of the United States of America, 2000, 97, 6242-6244.

[23] Stupp R., Hegi M.E., Mason W.P., Van den Bent M.J., Taphoorn M.J.B., Janzer R.C., Ludwin S.K., Allgeier A., Fisher B., Belanger K. et al, Effects of radiotherapy with concomitant and adjuvant temozolomide versus radiotherapy alone on survival in glioblastoma in a randomised phase III study: 5-year analysis of the EORTC-NCIC trial, Lancet Oncol., 2009, 10, 459-466.

[24] Brandes A.A., Tosoni A., Franceschi E., Reni M., Gatta G., Vecht C., Glioblastoma in adults, Crit. Rev. Oncol. Hemat., 2008, 67, 139-152.

[25] Jones C., Pediatric high-grade glioma: biologically and clinically in need of new thinking, Neuro Oncology, 2017, 19, 153-161.

[26] Fisher J.L., Schwartzbaum J.A., Wrensch M., Wiemels J.L., Epidemiology of brain tumours, Neurol. Clin., 2007, 25, 867-890.

[27] Friedman J.M., Gutmann D.H., MacCollin M., Riccardi V.M., Neurofibromatosis: Phenotype, Natural History and Pathogenesis, 3rd edition., Johns Hopkins University Press, 1999, 380.

[28] Malkin D., p53 and the Li-Fraumeni syndrome, Biochim. Biophys. Acta, 1994, 1198, 197-213.

[29] Hamilton S.R., Liu B., Parsons R.E., Papadopoulos N., Jen J., Powell S.M., The molecular basis of Turcot's syndrome, N. Engl. J. Med., 1995, 332, 839-847.

[30] Wrensch M., Minn Y., Chew T., Bondy M., Berger M.S., Epidemiology of primary brain tumours: current concepts and review of the literature, Neuro Oncology, 2002, 4, 278-299.

[31] Relling M.V., Rubnitz J.E., Rivera G.K., Boyett J.M., Hancock M.L., Felix C.A., Kun L.E., Walter A.W., Evans W.E., Pui C.H., High incidence of secondary brain tumours after radiotherapy and antimetabolites, Lancet, 1999, 354, 34-39.

[32] Alifieris C., Trafalis D.T., Glioblastoma multiforme: Pathogenesis and Treatment, Pharmacol. Therapeut., 2015, 152, 63-82.

[33] Grossman S.A., Batara J.F., Current management of glioblastoma multiforme, Semin. Oncol., 2004, 31, 635-644.

[34] Salah Uddin A.B.M., Jarmi T., Neurologic manifestations of glioblastoma multiforme clinical presentation (available online), 2015, http://emedicine.medscape.com/article/1156220-clinical.

[35] Nelson S.J., Cha S., Imaging glioblastoma multiforme, Cancer J., 2003, 9, 134-145.

[36] Brown T.J., Brennan M.C., Li M., Church E.W., Brandmeir N.J., Rakszawski K.L., Rizk E.B., Suki D., Sawaya R., Glantz M., Association of the Extent of Resection With Survival in Glioblastoma: A Systematic Review and Meta-analysis, JAMA Oncol., 2016, 2, 1460-1469.

[37] Furnari F.B., Fenton T., Bachoo R.M., Mukasa A., Stommel J.M., Stegh A., Hahn W.C., Ligon K.C., Louis D.N., Brennan C., Chin L., DePinho R.A., Cavenee W.K., Malignant astrocytic glioma: genetics, biology and paths to treatment, Genes, 2007, 21, 2683-2710.

[38] Bernardi A., Braganhol E., Jager E., Figueiro F., Edelweiss M.I., Pohlmann A.R., Guterres S.S., Battastini A.M., Indomethacin-loaded nanocapsules treatment reduces in vivo glioblastoma growth in a rat glioma model, Cancer Lett., 2009, 281, 53-63.

[39] Fischer I., Gagner J., Law M., Newcomb E., Zagzag D., Angiogenesis in gliomas: biology and molecular pathophysiology, Brain Pathol., 2005, 15, 297-310.

[40] Bastiancich C., Danhier P., Preat V., Danhier F., Anticancer drug-loaded hydrogels as drug delivery systems for the local treatment of glioblastoma, J. Control. Release, 2016, 243, 29-42.

[41] Sminia P., Westerman B.A., Blood-brain barrier crossing and breakthroughs in glioblastoma therapy, Br. J. Clin. Pharmacol., 2016, 81, 1018-1020.

[42] Xiao W., Sohrabi A., Seidlits S., Integrating the glioblastoma microenvironment into engineered experimental models, Future Sci. OA, 2017, 3, 189-213.

[43] Soeda A., Hara A., Kunisada T., Yoshimura S., Iwama T., Park D.M., The Evidence of Glioblastoma Heterogeneity, Sci. Rep., 2015, 5, 7979-7984.

[44] Jue T.R., McDonald K.L., The challenges associated with molecular targeted therapies for glioblastoma, Neuro Oncology, 2016, 127, 427-434.

[45] Kleihues P., Louis D.N., Scheithauer B.W., Rorke L.B., Reifenberger G., Burger P.C., Cavenee W.K., The WHO classification of tumours of the nervous system, J. Neuropath. Exp. Neur., 2002, 61, 215-225.

[46] Patel A.P., Tirosh I., Trombetta J.J., Shalek A.K., Gillespie S.M., Wakimoto H., Cahill D.P., Nahed B.V., Curry W.T., Martuza R.L., Louis D.N., Rozenblatt-Rosen O., Suvà M.L., Regev A., Bernstein B.E., Single-cell RNA-seq highlights intratumoral heterogeneity in primary glioblastoma, Science, 2014, 344, 1396-1401.

[47] Parker N.R., Hudson A.L., Khong P., Parkinson J.F., Dwight T., Ikin R.J., Zhu Y., Cheng Z.J., Vafaee F., Chen J., Wheeler H.R., Howell V.M., Intratumoral heterogeneity identified at the epigenetic, genetic and transcriptional level in glioblastoma, Sci. Rep., 2016, 6, 22477-22486.

[48] Treister D., Kingston S., Hoque K.E., Law M., Shiroishi M.S., Multimodal magnetic resonance imaging evaluation of primary brain tumours, Semin. Oncol., 2014, 41, 478-495.

[49] Quail D.F., Joyce J.A., The microenvironmental landscape of brain tumours, Cancer Cell, 2017, 31, 326-341.

[50] Vehlow A., Cordes N., Invasion as target for therapy of glioblastoma multiforme, Biochim. Biophys. Acta, 2013, 1836, 236-244.

[51] Daneman R., Prat A., The blood-brain barrier, CSH. Perspect. Biol., 2015, 7, 1-21.

[52] Wilhelm I., Fazakas C., Krizbai I.A., In vitro models of the blood-brain barrier, Acta Neurobiol. Exp., 2011, 71, 113-128.

[53] Karim R., Palazzo C., Evrard B., Piel G., Nanocarriers for the treatment of glioblastoma multiforme: Current state-of-the-art, J. Control. Release, 2016, 227, 23-37.

[54] Aryal M., Arvanitis C.D., Alexander P.M., Mc Dannold N., Ultrasound-mediated blood brain barrier disruption for targeted drug delivery in the central nervous system, Adv. Drug Deliv. Rev., 2014, 72, 94-109.

[55] Sarkar A., Fatima I., Jamal Q.M.S., Sayeed U., Khan M.K.A., Akhtar S., Kamal M.A., Farooqui A., Siddiqui M.H., Nanoparticles as a Carrier System for Drug Delivery Across Blood Brain Barrier, Curr. Drug Metab., 2017, 18, 129-137.

[56] Lara-Velazquez M., Al-Kharboosh R., Jeanneret S.,Vazquez-Ramos C., Mahato D., Tavanaiepour D., Rahmathulla G., Quinones-Hinojosa A., Advances in brain tumour surgery for glioblastoma in adults, Brain Sci., 2017, 7, 166-181.

[57] Chaichana K.L., Jusue-Torres I., Navarro-Ramirez R. et al, Establishing percent resection and residual volume thresholds affecting survival and recurrence for patients with newly diagnosed intracranial glioblastoma, Neuro Oncology, 2014, 16, 113-122.

[58] Kuhnt D., Becker A., Ganslandt O., Bauer M., Buchfelder M., Nimsky C., Correlation of the extent of tumour volume resection and patient survival in surgery of glioblastoma multiforme with high-field intraoperative MRI guidance, Neuro Oncology, 2011, 13, 1339-1348.

[59] Stupp R., Mason W.P., van den Bent M.J., Weller M., Fisher B., Taphoorn M.J., Belanger K., Brandes A.A., Marosi C., Bogdahn U. et al, Radiotherapy plus concomitant and adjuvant temozolomide for glioblastoma, N. Engl. J. Med., 2005, 352, 987-996.

[60] Paolillo M., Boselli C., Schinelli S., Gioblastoma under Siege: An overview of current therapeutic strategies, Brain Sci., 2018, 8, 1-15.

[61] Wilson T.A., Karajannis M.A., Harter D.H., Glioblastoma multiforme: State of the art and future therapeutics, Surg. Neurol., 2014, 5, 64-62.

[62] Glas M., Rath B.H., Simon M., Reinartz R., Schramme A., Trageser D. et al, Residual Tumour Cells Are Unique Cellular Targets in Glioblastoma, Ann. Neurol., 2010, 68, 264-269.

[63] Iacob G., Dinca E.B., Current data and strategy in glioblastoma multiforme, J. Med. Life, 2009, 2, 386-393.

[64] Hanif F., Muzaffar K., Perveen K., Malhi S.M., Simjee S.U., Glioblastoma Multiforme: A Review of its Epidemiology and Pathogenesis through Clinical Presentation and Treatment, Asian Pac. J. Cancer Prev., 2017, 18, 3-9.

[65] Villodre S.E., Kipper F.C., Silva A.O., Lenz G., da Costa Lopez P.L., Low Dose of Doxorubicin Potentiates the Effect of Temozolomide in Glioblastoma Cells, Mol. Neurobiol., 2017, 55, 4185-4194.

[66] Zhang H., Gao S., Temozolomide/PLGA microparticles and antitumour activity against glioma C6 cancer cells in vitro, Int. J. Pharm., 2007, 329, 122-128.

[67] Lee S.Y., Temozolomide resistance in glioblastoma multiforme, Genes and Diseases, 2016, 3, 198-210.

[68] Weller M., Stupp R., Reifenberger G., Brandes A.A., van den Bent M.J., Wick W., Hegi M.E., MGMT promoter methylation in malignant gliomas: ready for personalised medicine?, Nat. Rev. Neurol., 2010, 6, 39-51.

[69] Scott J., Tsai Y.Y., Chinnaiyan P., Yu H.H., Effectiveness of radiotherapy for elderly patients with glioblastoma, Int. J. Radiat. Oncol. Biol. Phys., 2011, 81, 206-210.

[70] Walker M.D., Strike T.A., Sheline G.E., An analysis of dose-effect relationship in the radiotherapy of malignant gliomas, Int. J. Radiat. Oncol. Biol. Phys., 1979, 5, 1725-1731.

[71] Gzell C., Back M., Wheeler H., Bailey D., Foote M., Radiotherapy in Glioblastoma: the past, the present and the future, Clin. Oncol., 2017, 29, 15-25.

[72] Chaichana K.L., Pinheiro L., Brem H., Delivery of local therapeutics to the brain: working toward advancing treatment for malignant gliomas, Ther. Deliv., 2015, 6, 353-369.

[73] Razavi S.M., Lee K.E., Jin B.E., Aujla P.S., Gholamin S., Li G., Immune evasion strategies of glioblastoma, Front Surg., 2016, 3, 11-19.

[74] Finocchiaro G., Pellegatta S., Novel mechanisms and approaches in immunotherapy for brain tumours, Discov. Med., 2015, 20, 7-15.

[75] Sehgal A., Berger M.S., Basic concepts of immunology and neuroimmunology, Neurosurg. Focus, 2000, 9, 1-6.

[76] McGranahan T., Li G., Nagpal S., History and current state of immunotherapy in glioma and brain metastasis, Ther. Adv. Med. Oncol., 2017, 9, 347-368.

[77] Diaz R.J., Ali S., Gull Qadir M., De La Fuente M.I., Ivan M.E., Komotar R.J., The role of bevacizumab in the treatment of glioblastoma, Neuro Oncology, 2017, 133, 455-467.

[78] Gil-Gil M.J., Mesia C., Rey M., Bruna J., Bevacizumab for the Treatment of Glioblastoma, Clin. Med. Insights Oncol., 2013, 7, 123-135.

[79] Hernández-Pedro N.Y., Rangel-López E., Vargas Félix G., Pineda B., Sotelo J. An update in the use of antibodies to treat glioblastoma multiforme, Autoimmune Dis., 2013, 2013, 1-14.

[80] Tanaka S., Louis D.N., Curry W.T., Batchelor T.T., Dietrich J., Diagnostic and therapeutic avenues for glioblastoma: no longer a dead end? Nat. Rev. Clin. Oncol., 2013, 10, 14-26.

[81] Oh T., Sayegh E.T., Fakurnejad S., Oyon D., Balquiedra Lamano J., DiDomenico J.D., Bloch O., Parsa A.T., Vaccine Therapies in Malignant Glioma, Curr. Neurol. Neurosci. Rep., 2015, 15, 508-518.

[82] Del Vecchio C.A., Wong A.J., Rindopepimut, a 14-mer injectable peptide vaccine against EGFRvIII for the potential treatment of glioblastoma multiforme, Curr. Opin. Mol. Ther., 2010, 12, 741-754.

[83] Weller M., Butowski N., Tran D.D., Recht L.D., Lim M., Hirte H., Ashby L., Mechtler L., Goldlust S.A., Iwamoto F., Rindopepimut with temozolomide for patients with newly diagnosed, EGFRvIII-expressing glioblastoma (ACT IV): a randomised, double-blind, international phase 3 trial, Lancet Oncol., 2017, 18, 1373-1385.

[84] Kwiatkowska A., Nandhu M.S., Behera P., Chiocca E.A., Viapiano M.S., Strategies in Gene Therapy for Glioblastoma, Cancers, 2013, 5, 1271-1305.

[85] Ezzeddine Z.D., Martuza R.L., Platika D., Short M.P., Malick A., Choi B., Breakefield X.O., Selective killing of glioma cells in culture and in vivo by retrovirus transfer of the herpes simplex virus thymidine kinase gene, New Biol., 1991, 3, 608-614.

[86] Kaliberov S.A., Market J.M., Gillespie G.Y., Krendelchtchikova V., Della Manna D., Sellers J.C., Kaliberova L.N., Black M.E., Buchsbaum D.J., Mutation of Escherichia coli cytosine deaminase significantly enhances molecular chemotherapy of human glioma, Gene Ther., 2007, 14, 1111-1119.

[87] Lang F.F., Yung W.K., Sawaya R., Tofilon P.J., Adenovirus-mediated p53 gene therapy for human gliomas, Neurosurgery, 1999, 45, 1093-1104.

[88] Rainov N.G., A phase III clinical evaluation of herpes simplex virus type 1 thymidine kinase and ganciclovir gene therapy as an adjuvant to surgical resection and radiation in adults with previously untreated glioblastoma multiforme, Hum. Gene Ther., 2000, 11, 2389-2401.

[89] Hottinger A.F., Pacheco P., Stupp R., Tumour treating fields: a novel treatment modality and its use in brain tumours, Neuro Oncology, 2016, 18, 1338-1349.

[90] Roy S., Lahiri D., Maji T., Biswas J., Recurrent Glioblastoma: Where we stand, South Asian J. Cancer, 2015, 4, 163-173.

[91] Prados M.D., McDermott M., Chang S.M. et al., Treatment of progressive or recurrent glioblastoma multiforme in adults with herpes simplex virus thymidine kinase gene vector-producer cells followed by intravenous ganciclovir administration: a phase I/II multi-institutional trial, Neuro Oncology, 2003, 65, 269-278.

[92] Torres L.A., Coca M.A., Batista J.F., Casaco A., Lopez G., García I., Perera A., Peña Y., Hernández A., Sanchez Y., Romero S., Leyva R., Prats A., Fernandez R., Biodistribution and internal dosimetry of the 188Re-labelled humanised monoclonal antibody anti-epidemal growth factor receptor, nimotuzumab, in the locoregional treatment of malignant gliomas, Nucl. Med. Commun., 2008, 29, 66-75.

[93] Zhou J., Atsina K.B., Himes B.T., Strohbehn G.W., Saltzman W.M., Novel Delivery Strategies for Glioblastoma, Cancer, 2012, 18, 89-99.

[94] Bruce J.N., Fine R.L., Canoll P. et al, Regression of recurrent malignant gliomas with convection-enhanced delivery of topotecan, Neurosurgery, 2011, 69, 1272-1280.

[95] Karim R., Palazzo C., Evrard B., Piel G., Nanocarriers for the treatment of glioblastoma multiforme: Current state-of-the-art, J. Control. Release, 2016, 227, 23-37.

[96] Chua S.L., Rosenthal M.A., Wong S.S, Ashley D.M., Woods A.M., Dowling A., Cher L.M., Phase 2 study of temozolomide and Caelyx in patients with recurrent glioblastoma multiforme, Neuro Oncology, 2004, 6, 38-43.

[97] Belhadj Z., Zhan C., Ying M., Wei X., Xie C., Yan Z., Lu W., Multifunctional targeted liposomal drug delivery for efficient glioblastoma treatment, Oncotarget, 2017, 8, 66889-66900.

[98] Zhou J., Yu J., Gao L., Sun L., Peng T., Wang J., Zhu J., Lu W., Zhang L., Yan Z., Yu L., iNGR-Modified Liposomes for Tumour Vascular Targeting and Tumour Tissue Penetrating Delivery in the Treatment of Glioblastoma, Mol. Pharmaceut., 2017, 14, 1811-1820.

[99] Liu Y., Lu W., Recent advances in brain tumour-targeted nano-drug delivery systems, Expert Opin. Drug Deliv., 2012, 9, 671-686.

[100] Lee Koo Y.E., Reddy R., Bhojani M., Schneider R., Philbert M.A., Rehemtulla A., Brian Ross B.D., Kopelman R., Brain cancer diagnosis and therapy with nanoplatforms, Adv. Drug Deliv. Rev., 2006, 58, 1556-1577.

[101] Saraiva C., Praça C., Ferreira R., Santos T., Ferreira L., Bernardino L., Nanoparticle-mediated brain drug delivery: Overcoming blood-brain barrier to treat neurodegenerative diseases, J. Control. Release, 2016, 235, 34-47.

[102] Sun C., Fang C., Stephen Z., Veiseh O., Hansen S., Lee D., Ellenbogen R.G., Olson J., Zhang M., Tumour-targeted drug delivery and MRI contrast enhancement by chlorotoxin-conjugated iron oxide nanoparticles, Nanomedicine, 2008, 3, 495-505.

[103] Steiniger S.C., Kreuter J., Khalansky A.S., Skidan I.N., Bobruskin A.I., Smirnova Z.S., Severin S.E., Uhl R., Kock M., Geiger K.D., Gelperina S.E., Chemotherapy of glioblastoma in rats using doxorubicin-loaded nanoparticles, Int. J. Cancer, 2004, 109, 759-767.

[104] Gao H., Yang Z., Zhang S., Cao S., Shen S., Pang Z., Jiang X., Ligand modified nanoparticles increases cell uptake, alters endocytosis and elevates glioma distribution and internalisation, Sci. Rep., 2013, 3, 2534-2541.

[105] Fabel K., Dietrich J., Hau P., Wismeth C., Winner B., Przywara S., Steinbrecher A., Ullrich W., Bogdahn U., Long-term stabilisation in patients with malignant glioma after treatment with liposomal doxorubicin, Cancer, 2001, 92, 1936-1942.

[106] Pourgholi F., Hajivalili M., Farhad J.N., Kafil H.S., Yousefi M., Nanoparticles: Novel vehicles in treatment of Glioblastoma, Biomed. Pharmacother., 2016, 77, 98-107.

[107] Lin P.L., Eckersley R.J., Hall A.H.E., Ultrabubble: A Laminated Ultrasound Contrast Agent with Narrow Size Range, Adv. Mater., 2009, 21, 3949-3952.

[108] Tsao N.H., Hall A.H.E., A model for microcapsule drug release with ultrasound activated enhancement, Langmuir, 2017, 33, 12960-12972.

[109] McDannold N., Arvanitis C.D., Vykhodtseva N., Livingstone M.S., Temporary disruption of the blood-brain barrier by use of ultrasound and microbubbles: safety and efficacy evaluation in rhesus macaques, Cancer Res., 2012, 72, 3652-3663.

[110] Aryal M., Vykhodtseva N., Zhang Y.Z., Park J., McDannold N., Multiple treatments with liposomal doxorubicin and ultrasound-induced disruption of blood-tumour and blood-brain barriers improve outcomes in a rat glioma model, J. Control. Release, 2013, 169, 103-111.

[111] Treat L.H., McDannold N., Zhang Y., Vykhodtseva N., Hynynen K., Improved anti-tumour effect of liposomal doxorubicin after targeted blood-brain barrier disruption by MRI-guided focused ultrasound in rat glioma, Ultrasound Med. Biol., 2012, 38, 1716-1725.

[112] Wei K.C., Chu P.C., Wang H.Y., Focused ultrasound-induced blood-brain barrier opening to enhance temozolomide delivery for glioblastoma treatment: a preclinical study, PLoS One, 2013, 8, e58995.

[113] Coluccia D., Figueiredo C.A., Wu M.Y., Riemenschneider A.N., Diaz R., Luck A., Smith C., Das S., Ackerley C., O'Reilly M., Hynynen K., Rutka J.T., Enhancing glioblastoma treatment using cisplatin-gold-nanoparticle conjugates and targeted delivery with magnetic resonance-guided focused ultrasound, Nanomedicine, 2018, 14, 1137-1148.

[114] Westphal M., Ram Z., Riddle V., Hilt V., Bortey E., Gliadel® wafer in initial surgery for malignant glioma: long-term follow-up of a multicenter controlled trial, Acta Neurochir., 2006, 148, 269-275.

[115] http://gliadel.com/hcp/implantation-guidelines.php, (accessed 05/2018).

[116] Valtonen S., Timonen U., Toivanen P. et al., Interstitial chemotherapy with carmustine-loaded polymers for high-grade gliomas: a randomised double-blind study, Neurosurgery, 1997, 41, 44-48.

[117] Perry J., Chambers A., Spithoff K., Laperriere N., Gliadel wafers in the treatment of malignant glioma: a systematic review, Curr. Oncol., 2007, 14, 189-194.

[118] Bota D.A., Desjardins A., Quinn J.A., Affronti M.L., Friedman H.S., Interstitial chemotherapy with biodegradable BCNU (Gliadel®) wafers in the treatment of malignant gliomas, Ther. Clin. Risk Manag., 2007, 3, 707-715.

[119] Manome Y., Kobayashi T., Mori M., Suzuki R., Funamizu N., Akiyama N., Inoue S., Tabata Y., Watanabe M., Local delivery of doxorubicin for malignant glioma by a biodegradable PLGA polymer sheet, Anticancer Res., 2006, 26, 3317-3326.

[120] Lee J.S., Ana T.K., Chae G.S., Jeong J.K., Cho S.H., Lee H.B., Khang G., Evaluation of in vitro and in vivo antitumour activity of BCNU-loaded PLGA wafer against 9L gliosarcoma, Eur. J. Pharm. Biopharm., 2005, 59, 169-175.

[121] Peppas N.A., Bures P., Leobandung W., Ichikawa H., Hydrogels in pharmaceutical formulations, Eur. J. Pharm. Biopharm., 2000, 50, 27-46.

[122] Caló E., Khutoryanskiy V.V., Biomedical applications of hydrogels: A review of patents and commercial products, Eur. Polym. J., 2015, 65, 252-267.

[123] Kim S., Nishimoto S.K., Bumgardner J.D., Haggard W.O., Gaber MW., Yang Y., A chitosan/b-glycerophosphate thermo-sensitive gel for the delivery of ellagic acid for the treatment of brain cancer, Biomaterials, 2010, 31, 4157-4166.

[124] Wang C., Tong X., Yang F., Bioengineered 3D brain tumour model to elucidate the effects of matrix stiffness on glioblastoma cell behaviour using PEG-based hydrogels, Mol. Pharm., 2014, 11, 2115-2125.

[125] Rao S.S., Dejesus J., Short A.R., Otero J.J., Sarkar A., Winter J.O., Glioblastoma Behaviours in Three-Dimensional Collagen-Hyaluronan Composite Hydrogels, ACS Appl. Mater. Interfaces, 2013, 5, 9276-9284.

[126] Jiguet Jiglaire C., Baeza-Kallee N., Denicolaï E., Barets D., Metellus P., Padovani L., Chinot O., Figarella-Branger D., Fernandez C., Ex vivo cultures of glioblastoma in three-dimensional

hydrogel maintain the original tumour growth behaviour and are suitable for preclinical drug and radiation sensitivity screening, Exp. Cell Res., 2014, 321, 99-108.

[127] Vellimana A.K., Recinos V.R., Hwang L., Fowers K.D., Li K.W., Zhang Y., Okonma S., Eberhart C.G., Brem H., Tyler B.M., Combination of Paclitaxel thermal gel depot with temozolomide and radiotherapy significantly prolongs survival in an experimental rodent glioma model, Neuro Oncology, 2013, 111, 229-236.

[128] Tyler B., Fowers K.D., Li K.W., Recinos V.R., Caplan J.M., Hdeib A., Grossman R., Basaldella L., Bekelis K., Pradilla G., Legnani F., Brem H., A thermal gel depot for local delivery of paclitaxel to treat experimental brain tumours in rats, Neurosurgery, 2010, 113, 210-217.

[129] Bastiancich C., Vanvarenberg K., Ucakar B., Pitorre M., Bastiat G., Lagarce F., Preat V., Danhier F., Lauroyl-gemcitabine-loaded lipid nanocapsule hydrogel for the treatment of glioblastoma, J. Control. Release, 2016, 225, 283-293.

[130] Bastiancich C., Bianco J., Vanvarenberg K., Ucakar B., Joudiou N., Gallez B., Bastiat G., Lagarce F., Préat V., Danhier F., Injectable nanomedicine hydrogel for local chemotherapy of glioblastoma after surgical resection, J. Control. Release, 2017, 264, 45-54.

[131] Fourniols T., Randolph L.C, Staub A., Vanvarenberg K., Leprince J.G., Preat V., des Rieux A., Danhier F., Temozolomide-loaded photopolymerisable PEG-DMA-based hydrogel for the treatment of glioblastoma, J. Control. Release, 2015, 210, 95-104.

[132] Jain A., Betancur M., Patel G.D., Valmikinathan C.M., Mukhatyar V.J., Vakharia A., Pai S.B., Brahma B., MacDonald T.J., Bellamkonda R.V., Guiding intracortical brain tumour cells to an extracortical cytotoxic hydrogel using aligned polymeric nanofibers, Nat. Mater., 2014, 13, 308-316.

[133] Puente P., Fettig N., Luderer M.J., Jin A., Shah S., Muz B., Kapoor V., Goddu S.M., Salama N.N., Tsien C., Thotala D., Shoghi K., Rogers B., Azab A.K., Injectable Hydrogels for Localised Chemotherapy and Radiotherapy in Brain Tumours, J. Pharm. Sci., 2018, 107, 922-933.

[134] Ranganath S.H., Kee I., Krantz W.B., Chow P.K., Wang C.H., Hydrogel matrix entrapping PLGA-paclitaxel microspheres: drug delivery with near zero-order release and implantability advantages for malignant brain tumour chemotherapy, Pharmaceut. Res., 2009, 26, 2101-2114.

[135] Ranganath S.H., Fu Y., Arifin D.Y., Kee I., Zheng L., Lee H.S., Chow P.K., Wang C.H., The use of submicron/nanoscale PLGA implants to deliver paclitaxel with enhanced pharmacokinetics and therapeutic efficacy in intracranial glioblastoma in mice, Biomaterials, 2010, 31, 5199-5207.

[136] Williams J.K., Padgen M.R., Wang Y., Entenberg D., Gertler F., Condeelis J.S., Castracane J., Probing the tumour microenvironment: collection and induction, Proc. of SPIE, 2012, 8251, 1-7.

[137] Laurent T.C., Fraser J.R.E, Hyaluronan, FASEB, 1992, 6, 2397-2404.

[138] Ananthanarayanan B., Kim Y., Kumar S., Elucidating the mechanobiology of malignant brain tumours using a brain matrix-mimetic hyaluronic acid hydrogel platform, Biomaterials, 2011, 32, 7913-7923.

[139] Jin S.G., Jeong Y.I., Jung S., Ryu H.H., Jin Y.H., Kim I.Y., The Effect of Hyaluronic Acid on the Invasiveness of Malignant Glioma Cells: Comparison of Invasion Potential at Hyaluronic Acid Hydrogel and Matrigel, J. Korean Neurosurg. S., 2009, 46, 472-478.

[140] Lecointre C., Desrues L., Joubert J.E., Perzo N., Guichet PO., Le Joncour V., Brulé C., Chabbert M., Leduc R., Prézeau L., Laquerrière A., Proust F., Gandolfo P., Morin F., Castel H., Signaling switch of the urotensin II vasosactive peptide GPCR: prototypic chemotaxic mechanism in glioma, Oncogene, 2015, 34, 1-15.

Chapter 2: Preparation of injectable polysaccharide-based hydrogels

2.1 Introduction

Current therapeutic strategies for the treatment of GBM, suffer from several limitations, including the absence of molecules that naturally exist in the brain ECM and scaffolds that can mimic its structure and mechanical properties. To date, the majority of the developed implantable 3D scaffolds such as hydrogels have focused on the delivery of anticancer drugs close to the tumour site as discussed in Chapter 1. These matrices mainly lack of effective chemoattractants, thus the majority of the residual invasive tumour cells remain in the margins of the resection cavity, leading to inevitable tumour recurrence. The first section of this chapter will present a literature review on hydrogels used for biomedical applications and the following experimental section will focus on the preparation of injectable hydrogels based on polysaccharides. Particular attention will be given to HA-based hydrogels as they have been studied during this PhD thesis. The second half of this chapter will discuss the attempts to obtain injectable hydrogels based on methylcellulose which is another known polysaccharide. Subsequently, the fabricated hydrogels will be loaded with the chemoattractant and the response of glioma cells will be investigated in the following chapters.

2.1.1 Hydrogels

Hydrogels are 3D hydrophilic crosslinked polymer networks which are characterised by their ability to absorb significant amount of water or biological fluids and they have been extensively studied over the last decades as biocompatible materials. Another definition of hydrogels has been proposed by Hoffman and defines hydrogel as a permanent or chemical gel stabilised by covalently crosslinked networks [1]. The high hydrophilicity of hydrogels is mainly attributed to the presence of hydrophilic moieties such as carboxyl, amide, amino, and hydroxyl groups distributed along the backbone of polymeric chains. The soft consistency, elasticity and structural resemblance to body tissues are unique characteristics of hydrogels. Consequently, these crosslinked polymeric materials presenting great potential in a wide range of applications including tissue engineering [2], wound dressing [3], sensors [4], contact lenses [5] and drug delivery systems [6]. More than 30.000 scientific papers focused on hydrogels, published in the last 50 years, demonstrate the significance of this type of materials.

2.1.2 Classification of hydrogels

Numerous classifications of hydrogels have been proposed in the literature [7]. They are commonly classified according to their origin, method of crosslinking, degradability, response to different stimuli, ionic charge as summarised in Figure 2.1. Hydrogels can be classified into natural, synthetic or hybrid according to their origin. Naturally derived hydrogels are used in drug delivery, tissue engineering, regenerative medicine due to their inherent biocompatibility, low toxicity, and susceptibility to enzymatic degradation [8], [9].

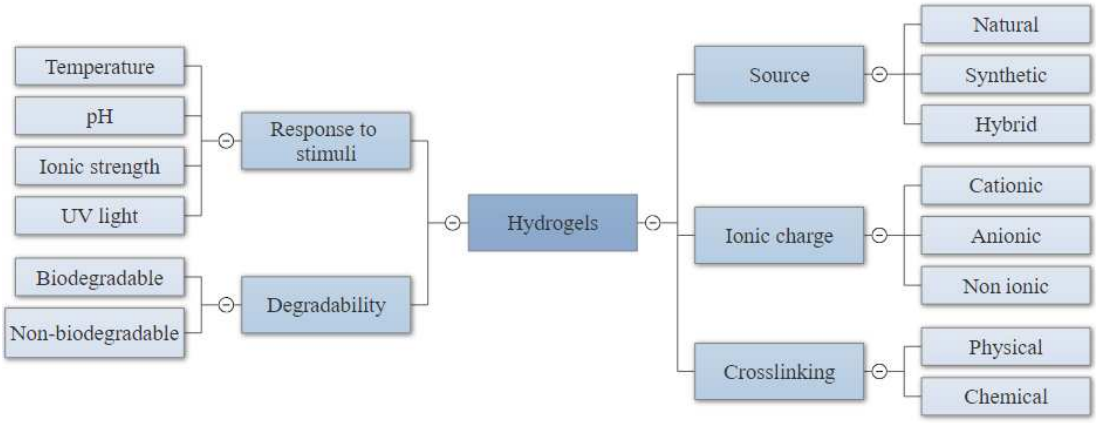

Figure 2.1: Schematic diagram summarising the main classification of hydrogels according to their source, method of crosslinking, degradability, response to stimuli and ionic charge.

They are mainly produced from polysaccharides or natural fibrous proteins such as collagen, fibrin, alginate and hyaluronic acid, resembling the structure of the native ECM [10]. Polysaccharides are innately biodegradable and they are usually modified in order to form hydrogels allowing cell adhesion. On the other hand, synthetic polymers are more appealing because their physical and chemical properties are more tunable and controllable than those of natural polymers. Furthermore, they can be reproducibly prepared with specific block structures, molecular weights and degradable linkages, providing better control of chemical composition and matrix architecture. Representative examples of synthetic polymers are poly (vinyl alcohol) (PVA), poly (ethylene glycol) (PEG), poly-lactic-glycolic acid (PLGA), poly (methyl methacrylate) (PMMA) and poly- (NIPAAM) [8]. More complex hydrogels can be derived either from copolymers, where multiple backbone groups are crosslinked together or inter-penetrating networks (IPNs), where a polymer mesh is constructed from the binding of oligomer chains within an already assembled polymeric scaffold [11], [12]. However, these polymers lack of inherent biological functionality, therefore they are usually conjugated to proteins or polysaccharides in order to increase the cellular interactions and achieve desirable responses in vivo.

Hydrogels can also be classified into physical or chemical depending on the method of crosslinking. In physically crosslinked hydrogels, physical reversible interactions exist between the polymer chains, whereas in chemically crosslinked hydrogels, covalent bonds are present between the polymer chains. An increasing interest in physically crosslinked hydrogels is assigned to the absence of crosslinkers for their preparation. Common methods of physical crosslinking include hydrogen bonding, self-assembly interactions, crosslinking by crystallisation and ionic interactions [10]. Chemically crosslinked hydrogels typically present better mechanical resistance than the physically crosslinked networks and are characterised by their tunable elasticity. Focusing on polysaccharide-based systems, several strategies have been exploited to form chemical hydrogels through covalent bonds. Common chemical crosslinking methods include free radical polymerisation, addition or

condensation chemical reactions and crosslinking using enzymes [13]. The well-known Michael's addition is also another interesting approach for the formation of chemical hydrogels. Recently, thiolated hyaluronic acid has been used for a Michael addition with a methacrylated triblock copolymer leading to an injectable hydrogel [14].

Unsurprisingly, stimuli responsive hydrogels represent a broad class of materials that can undergo reversible gelation in the presence of physical or chemical stimuli such as pH, temperature, UV light and changes in ionic strength [15], [16]. pH-responsive hydrogels consist a group of stimuli-responsive systems capable of responding to changes in the environmental pH. The pH responsive behaviour of the hydrogels is due to the presence of ionisable side functional groups in the polymer backbone [17]. For example, natural polymers such as alginate, chitosan, gelatin and albumin are known for their pH responsive behaviour [18]-[21]. Polysaccharides including alginate and chitosan undergo swelling as a result of the ionisation of groups along the polysaccharide chain, whereas in the case of proteins such as albumin and gelatin, they will form helices stabilised by hydrogen bonding at specific pH and temperature conditions. When the pH of the solution is either lower or higher than the isoelectric point, electrostatic repulsions are developed that result in the swelling of the network. The process of swelling is reversible; thus, pH responsive hydrogels can be applied to controlled release of encapsulated drugs. For instance, Na et al fabricated doxorubicin loaded nanogels composed by hydrophobic pullulan – N-alpha-Boc-L-histidine conjugates and they studied their response to tumour extracellular pH [22]. The anticancer efficiency against breast cancer cell lines (MCF-7) was evaluated and the results showed that the nanogels can potentially be applied as antitumour drug carriers.

Thermoresponsive hydrogels are vastly attractive due to their spontaneous gelation without the presence of any other chemical trigger. For temperature responsive hydrogels, a small variation in temperature induces phase transition as shown in Figure 2.2. It is well known that the phase transition is governed by the equilibrium of hydrophilic and hydrophobic moieties on the polymer chain and on the Gibbs free energy of mixing [23]. According to the second law of thermodynamics ($\Delta G = \Delta H - T\Delta S$) as the temperature increases, it favours the polymer chain association. Many natural polymers have demonstrated gelation upon temperature change. Recently, Stabenfeldt et al developed a thermosensitive hydrogel system based on methylcellulose [24]. They functionalised methylcellulose with the protein laminin in order to fabricate a bioactive scaffold for neural tissue engineering and they concluded that the concentration of methylcellulose could affect the temperature at which gelation occurs. Bhattarai et al reported the development of a biodegradable and thermoreversible hydrogel that consisted of chitosan functionalised with monofunctional methoxy poly (ethylene glycol) without the use of crosslinking agents. They observed that the presence of PEG improved the solubility of chitosan in water and the system was able to undergo thermoreversible transition from solution at low temperatures to gel at body temperature [25]. Gelatin

is another biopolymer with thermoreversible properties. Ohya and Matsuda grafted gelatin with NiPAAm in order to create a thermoresponsive extracellular matrix analogue. Interestingly, they observed that when the weight ratio of NiPAAm to gelatin chains was greater than 5.8, aqueous solutions showed a sol-gel transition at physiological temperature [26].

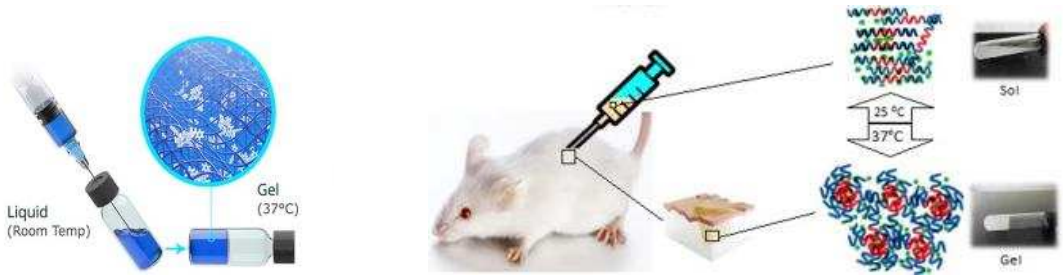

Figure 2.2: Illustration of thermoresponsive hydrogels which undergo gelation at body temperature. Adapted from Shaker et al [27].

In the case of ionic triggered gelation, the formation of the hydrogel occurs upon treatment of an ionic polysaccharide with multivalent counterions. Several examples of ionic gelation exist of which alginate crosslinked with calcium is the most well-known [28]. The divalent cation of calcium electrostatically interacts with the anionic carboxylic groups of alginate to form a crosslinked network. Other representative examples of ionic crosslinked hydrogels include chitosan-polylysine, chitosan-glycerol phosphate salt and chitosan-alginate hydrogels [29]-[31]. Despite their easy preparation under mild conditions, these groups of hydrogels are not ideal candidates for tissue engineering due to their uncontrollable degradation.

Moreover, photoresponsive hydrogels have attracted a lot of attention due to their mild gelation conditions. The most commonly used method to prepare this group of hydrogels involves photopolymerisation induced by UV or visible light and enables in situ gelation at physiological pH and temperature [32], [33]. Among the photopolymerisable groups, acrylate or methacrylate moieties are most commonly used. Leach et al investigated the conjugation of photopolymerisable methacrylate groups to hyaluronic acid and the photopolymerisation of these conjugates in order to form hydrogels for tissue engineering applications [34]. Photopolymerised systems provide the advantage of controllable gelation process and injectability which contribute to their successful application in tissue engineering.

2.1.3 Injectable hydrogels as biomaterials

Significant interest has been recently paid on injectable hydrogels formed in situ. Historically, hydrogels used to be preformed and implanted afterwards using highly invasive surgical manipulations. However, improvements in synthetic chemistry and materials science demonstrated

that hydrogels precursors can be injected locally through a standard syringe and crosslinked in situ avoiding invasive surgical techniques.

Injectable hydrogels can be formed in situ either by physical or chemical crosslinking as illustrated in Figure 2.3. As discussed earlier, many methods have been employed for their preparation including thermal gelation, pH-triggered gelation, ionic interaction, physical self-assembly, photopolymerisation or chemical crosslinking with agents such as genipin, glutaraldehyde and adipic acid dihydrazide [35], [36].

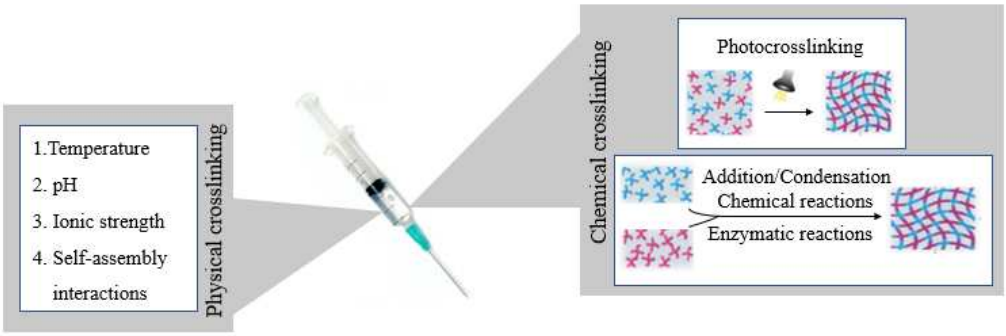

Figure 2.3: Injectable hydrogels can be delivered as liquid precursors which are either physically or chemically crosslinked into stable hydrogels at the site of injection. Common chemical crosslinking methods include free radical polymerisation, addition or condensation chemical reactions and crosslinking using enzymes.

To date, several reviews have been focused on injectable hydrogels and the methods for their preparation. For instance, Ruel-Gariepy and Leroux have studied the in situ formation of thermosensitive hydrogels from natural or synthetic polymers, while Jeong et al have focused on the fabrication of thermosensitive sol-gel reversible hydrogels [37], [38].

Injectable hydrogels present several inherent advantages over other preformed hydrogels. More specifically, these systems are aqueous solutions before administration and they rapidly turn into gel at the injection site under physiological conditions or in response to external stimuli such as temperature, pH, ion concentration or UV light. In addition, their injectable nature allows them to mould into the shape of the injection cavity minimising the adverse effects of invasive surgical approaches. Most importantly, injectable hydrogels based on natural polymers present a similar microstructure to the ECM rendering them one of the most promising biomaterials in the field of drug delivery and tissue engineering.

It is of paramount importance to exploit the advantages of using injectable hydrogels for a variety of applications including tissue engineering, wound healing and drug delivery systems for local cancer therapy that will be further discussed below [39], [40]. Intra-tumour drug delivery with injectable biodegradable hydrogels has attracted a lot of attention due to the fact that they can provide a sustained drug release within the tumour site and simultaneously minimising the adverse effects of

systemic exposure to the drug. Targeted therapy with injectable hydrogels can overcome the limitations of poor drug solubility observed with many chemotherapeutic agents, by decreasing the required amount of the drug and increasing the concentration that reaches the tumour site as discussed in Chapter 1 [41], [42]. Specifically, in case of brain tumours the presence of the BBB limits the effective delivery of drugs to the tumour site thus direct application of therapeutics to the brain has been tested [43], [44]. Recently, Kwon et al fabricated 5-fluorouracil (5-FU)-loaded Pluronic® F-127 thermosensitive hydrogels (5-FU-HP) with encapsulated formulations of DOX-loaded microcapsules (DOX-M) or FU-loaded di-block copolymer hydrogels (5-FU-HC) in order to optimise tumour toxicity from the synergistic action of the loaded drugs on the hydrogels as depicted in Figure 2.4 [45].

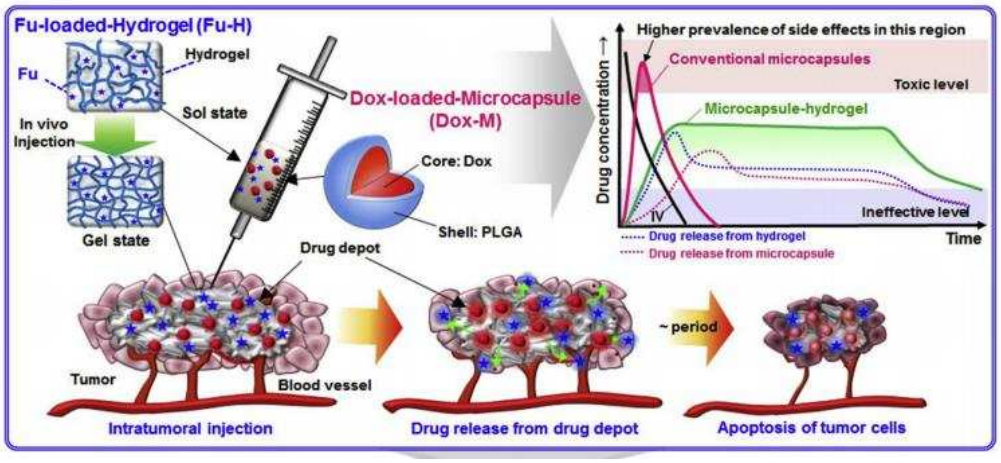

Figure 2.4: Schematic representation of synergistic tumour suppression via intratumoural injections of dual-drug depots and controlled release of DOX and 5-FU. Adapted from Kim et al [45].

These formulations were solutions at room temperature and formed gel at body temperature, indicating the injectability of the system. The results from the intratumoural injection of the above formulations containing DOX and 5-FU demonstrated significant antitumour activity, confirming the synergistic inhibitory effects of both drugs on tumour growth. To date, intratumoural injection of formulations loaded with combination of anticancer drugs on animals has received little attention, thus, further studies should be carried out for the development of an efficient in vivo drug delivery system.

Injectable pH-responsive hydrogels have been used for targeted drug delivery for the treatment of several cancers. For example, Wu et al synthesised pH-sensitive hydrogels through a Schiff-base reaction between aldehyde-functionalised four-arm PEG and 4-arm PEG-b-poly (l-lysine) for local delivery of metformin (ME) and 5-FU for colon carcinoma [42]. The pH-dependent release of the drugs exhibited a synergistic inhibitory effect on cell proliferation in C26 colon adenocarcinoma cells. In addition, animal studies revealed significant therapeutic outcome of the drug-loaded

hydrogel in terms of tumour growth inhibition and they demonstrated less toxicity than the free drugs in animal models.

Photopolymerisable hydrogels are of interest for several drug delivery and tissue-engineering applications due to their ability to be administered in aqueous solutions and form hydrogels in situ following photopolymerisation. Fourniols et al prepared TMZ-loaded photopolymerisable PEG dimethacrylate (PEG-DMA) injectable hydrogel by using Lucirin-TPO® as a photoinitiator for the treatment of GBM [46]. The hydrogel was photopolymerised rapidly (less than 2 minutes) in a brain tumour resection cavity using ultraviolet (UV) light allowing sustained release of TMZ. The antitumour activity of the TMZ-loaded hydrogel contributed to the regression of tumour in xenograft U87MG tumour-bearing mice and higher apoptosis at the centre of the tumour as summarised in Figure 2.5.

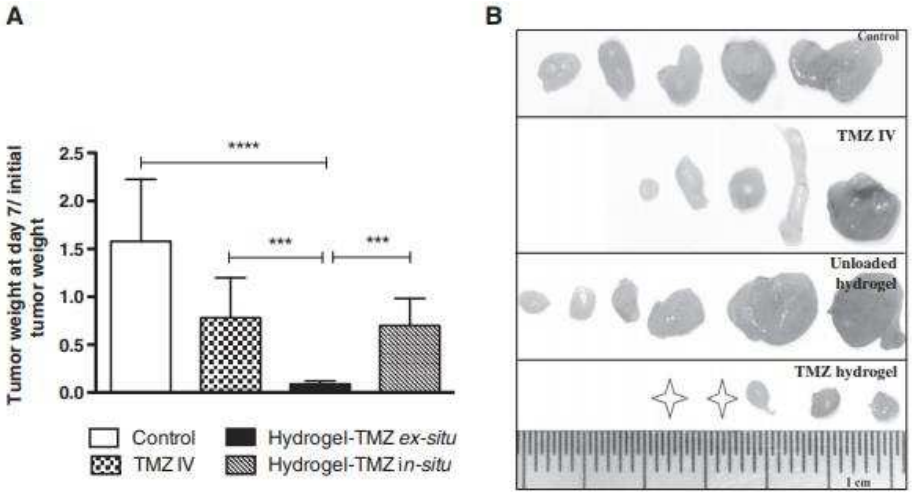

Figure 2.5: Antitumour efficacy of TMZ/PEG-DMA hydrogels. **A.** Ratios between tumour weights 7 days after treatment and initial tumour weights of xenografted human U87MG tumour-bearing nude mice untreated (control), treated with unloaded hydrogel, TMZ-loaded hydrogel, or intravenous injection of TMZ. TMZ dose was 4.75 mg/kg, **B.** Pictures of tumours after 7 days of post-implantation in nude mice (n = 5 to 7). Stars: Represent complete regression of tumours. Adapted from Fourniols et al [46].

In addition, except from polymeric hydrogels for localised drug delivery in cancer, low molecular gelators (LMWGs) have also been investigated. LMWGs are one of the most representative examples of self-assembly responsive systems including amino acids and sugars that can self-assemble into a 3D fibrous network by non-covalent interactions. Singh et al focused on the synthesis of LMWGs based on derivatives of L-alanine and they prepared injectable hydrogels loaded with DOX. These systems showed promising anticancer activity in mice models. Importantly though, subcutaneous injection of the DOX- loaded gel close to the proximity of the tumour achieved a greater decrease in tumour load than by intravenous injection of DOX alone and local injection of DOX alone at the tumour site [47]. However, the majority of LMWGs present poor mechanical properties and their applications as injectable scaffolds in drug delivery are limited.

In overall, the unique properties of the hydrogels render them very promising systems for localised drug delivery applications. Injectable hydrogels loaded with chemotherapeutic agents for drug delivery provide several advantages over the conventional intravenous delivery of the chemotherapeutics in terms of localised and sustained delivery of the drugs in the tumour vicinity. Several studies have been focused on the effectiveness of these drug delivery systems in vitro environment, however, further clinical trials in animal models or humans could address more precisely the efficiency of these drug delivery matrices for local chemotherapy and cancer treatment.

2.1.4 Polymeric hydrogels as engineered 3D microenvironments

As mentioned earlier, polymeric hydrogels are promising biomaterials due to their tunable mechanical properties and the structural similarity to the native ECM. These matrices have attracted significant attention as engineered 3D microenvironments because of the easy and not invasive manipulation and the fact that they can support cell growth due to the mechanical resemblance to the ECM.

Collagen type I is a protein of the ECM, responsible for the structural frame of cells and it promotes adhesion of cells through the cell-matrix interactions [48]. Collagen-based hydrogels can be prepared by physical crosslinking and the presence of environmental stimuli such as pH or temperature can trigger the gelation process. The formation of fibrillar collagen matrices can be induced by increasing the temperature and the pH of the acidic precursor solutions [49]. Despite its unique properties, collagen presents several disadvantages, mainly weak mechanical properties, susceptibility to enzymatic degradation and batch-to batch variation. To date, several chemical crosslinking methods have used genipin or PEG as crosslinkers or enzyme-mediated crosslinking reactions have been reported in order to produce stiffer and more stable hydrogels that are less prone to enzymatic degradation [50], [51]. Fibrin hydrogels have gained a lot of attention in a wide range of biomedical applications such as drug delivery or as therapeutic implants due to their innate biocompatibility, ease of fabrication and biodegradability. These hydrogels are mainly prepared by the ionic crosslinking of fibrinogen with thrombin where thrombin cleaves fibrinogen's N-terminal end that induces polymerisation of fibrin into fibrous hydrogel network [52]. However, fibrin-based hydrogels suffer from high degradation rates and ongoing studies intend to overcome this limitation.

Hydrogels prepared from synthetic polymers have also been used in neural engineering applications, demonstrating better mechanical properties and more tunable physicochemical characteristics. The most representative example is PEG which is a bioinert and hydrophilic polymer. Interestingly, the survival and proliferation of neural progenitor cells in vitro on photopolymerised hydrogels composed of polylysine and PEG has been reported [53]. Polylactic acid (PLA) is another biocompatible and biodegradable FDA approved synthetic polymer that has been used in several biomedical applications. To date, the majority of synthetic biomaterials that has been used for in

vivo delivery in brain is restricted to solid implants composed of polyglycolic acid (PGA) or poly (lactic-co-glycolic acid) (PLGA) scaffold particles and few have been applied to in vivo cell transplantation applications [54].

2.1.5 Polysaccharide-based hydrogels: the present and the future

Polysaccharides have been widely used in pharmaceutical and biomedical applications, particularly in regenerative medicine and drug delivery due to their high hydrophilicity, biocompatibility, structural diversity and biodegradability [55]. Commonly used polysaccharides include chitosan, cellulose, xanthan gum, alginate, chondroitin sulfate, dextran and hyaluronic acid [56], have received extensive interest due to their favourable properties and versatile chemical structures as presented in Figure 2.6.

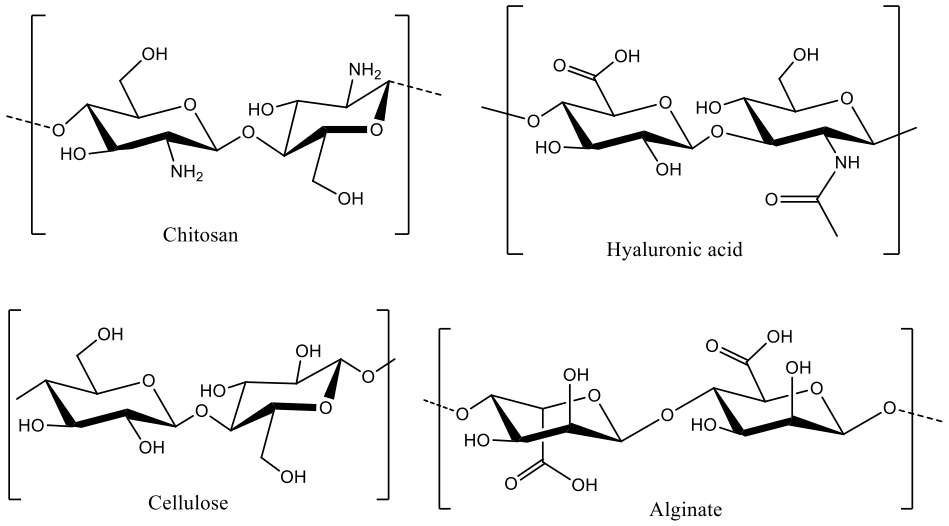

Figure 2.6: Chemical structures of commonly used polysaccharides: chitosan, hyaluronic acid, cellulose and alginate. These polysaccharides are the subject of much interest due to their physical characteristics and structural versatility.

Advantages of polysaccharides include natural abundance and the presence of functional groups which allow chemical modification of their backbone. Additionally, they are biodegradable since they can be degraded enzymatically or by hydrolysis and their tunable physicochemical properties contribute to their successful application as drug delivery systems.

Several polysaccharides have been used for the preparation of biocompatible hydrogels for biomedical applications. Natural polymers such as fibrin, collagen, alginate, hyaluronic acid and chitosan have already been used in clinical applications. The structural similarity with the ECM of the biological system is one of the most important unique features of polysaccharide-based hydrogels. Polysaccharides can form hydrogels through physical or chemical crosslinking. The high number of functional groups such as -OH, -COOH, -NH_2 that are present in the polysaccharides' backbone allow facile modification leading to a 3D polymeric network [57]. The chemical modification of the functional groups allows conjugation of polysaccharides with synthetic polymers

leading in the formation of stimuli responsive hydrogels [58]. Different types of crosslinking have been reported, including graft copolymerisation of a synthetic monomer on polysaccharide backbone in the presence of a crosslinker or direct crosslinking of the polysaccharide. For instance, Paulino et al fabricated thermoresponsive hydrogels from the graft copolymerisation of NIPAAM on the cellulose backbone [59].

Chitosan is a cationic polysaccharide and is obtained from alkaline deacetylation of chitin extracted from the external skeleton of marine crustaceans such as crabs and shrimps. It is widely used in a variety of applications including tissue engineering and drug delivery [60]. Chitosan-based hydrogels have received a lot of interest due to their unique properties such as easy manipulation, biocompatibility, biodegradability and bioadhesive nature. Commonly used methods of preparation of chitosan-based hydrogels include ionic gelation, chemical crosslinking or stimuli triggered gelation (pH or thermo-responsive gelation). The presence of the cationic amine groups in the chemical structure of chitosan allow ionic crosslinking with multivalent counter anions such as phosphate bearing molecules forming reversible hydrogels [61]. Several examples of ionically crosslinked chitosan hydrogels have been reported in the literature and the majority of them used in controlled drug delivery [62], [63]. Aldehydes such as glutaraldehyde and genipin have extensively been used as crosslinkers for the preparation of chemically crosslinked chitosan hydrogels demonstrating good biocompatibility [64], [65]. In terms of GBM treatment, chitosan has been used as an excipient for the preparation of nanoparticles due to its biodegradable and biocompatible nature. Van Woensel et al investigated the use of siRNA-loaded chitosan nanoparticles in order to inhibit the expression of Galectin-1 in human GBM cells. Galectin-1 is associated with tumour growth and it possesses a potential immune suppressing role in the tumour microenvironment [66]. Kim et al developed chitosan b-glycerophosphate (Ch/b-GP) thermo-sensitive hydrogel for the delivery of ellagic acid for the treatment of brain cancer. They investigated the release of ellagic acid from the chitosan hydrogels and the viability of human U87MG and rat C6 glioma cells was evaluated, demonstrating inhibition of cell growth [67].

Another widely used polysaccharide is alginate which is an anionic polysaccharide that is composed of β-D-mannuronic acid (M) and α-l-guluronic acid (G) units. Many clinical applications of alginate are connected with its ability to efficiently bind to divalent cations such as $Sr^{2+}$and Ca^{2+}, leading to formation of hydrogels [68], [69]. Hydrogels can be formed by physical or chemical crosslinking strategies or ionic crosslinking which is the most widely used. The gelation mechanism is based on the chelation of the divalent ions by the alginate chains which results in the fabrication of a swollen physical network under physiological conditions as illustrated in Figure 2.7.

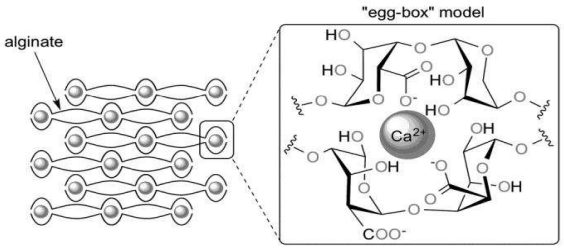

Figure 2.7: Schematic representation of alginate hydrogel formation. Ionic crosslinking with calcium-induces chain–chain association of guluronate blocks resulting in the formation of junction zones responsible for gelation (egg-box model). Adapted from Costa et al [70].

Alginate-based hydrogels due to their biocompatibility and easy fabrication process have numerous applications in wound healing, drug delivery, cell encapsulation and tissue regeneration. Degradation of ionically crosslinked hydrogels can be induced by the exchange between the divalent cations and monovalent cations that are present in the human body. Another benefit is that alginate, as chemically versatile molecule, allows the conjugation of peptide sequences such as RGD (arginine–glycine–aspartic acid) in order to promote cell adhesion [71]. Chitosan-alginate hydrogels have been used as mimic scaffolds of glioma tumour microenvironment. More specifically, Kievit et al studied the response of U87MG and C6 cells cultured on chitosan-alginate scaffolds and they observed that these scaffolds provided a 3D microenvironment for glioma cells that was representative of the in vivo tumour [72].

HA is an anionic glycosaminoglycan consisting of N-acetyl-D-glucosamine and D-glucuronic acid, is commonly used in a variety of clinical applications including tissue engineering and regenerative medicine [73]. Methylcellulose (MC) is a polysaccharide derived from cellulose by partial substitution of hydrophilic hydroxyl groups with hydrophobic methoxy groups. MC based hydrogels are promising materials for regenerative medicine and tissue engineering applications. Both polysaccharides will be discussed further in the following sections as they are main components of the fabricated hydrogels.

In overall, polysaccharide-based hydrogels demonstrate high biocompatibility and their structure closely resembles the ECM composition, maximising their potential for injection in human body. Additionally, the choice of the polysaccharide to form a hydrogel for a specific application it is of paramount importance and depends on the desirable features of the designed biomaterial. Moreover, it is also important to point out that the availability from renewable sources, the hydrophilic properties and the chemical modification of their backbone render them very promising candidates for the preparation of functional biomaterials. Further clinical studies with this group of biomaterials will broaden the comprehension of the unique interactions between the polysaccharide-based matrices and cells in animal models.

2.1.6 HA-based hydrogels

HA is a high molecular weight glycosaminoglycan and one of the main components of the brain ECM. It is ubiquitous in the native ECM throughout the human body at all ages, but is significantly abundant in the fetal brain, indicative of its critical role in the CNS development [74]. HA plays a substantial role in cellular processes such as cell proliferation, migration and cell adhesion since it interacts with cells through its surface receptors CD44 and RHAMM [75], [76]. HA has been used in a variety of medical and pharmaceutical applications due to its versatile structure, biodegradability, non-immunogenicity, biocompatibility and viscoelastic behaviour. Recently, the development of different strategies for chemical modification of its backbone has allowed the fabrication of new biomaterials that can be used in regenerative medicine and drug delivery applications.

HA in its innate structure, is characterised by poor mechanical properties and high degradation rates due to the presence of hyaluronidase which is an enzyme that catalyses the degradation of HA. Therefore, various chemical modifications of the HA backbone have been developed in order to prepare mechanically robust HA-based biomaterials that will demonstrate better mechanical properties and long-term stability in vivo environment [77]. There are three different target functional groups in the HA structure that are prone to chemical modification: the primary and secondary hydroxyl groups, the carboxylic group and the N-acetyl group after deacetylation as highlighted in Figure 2.8.

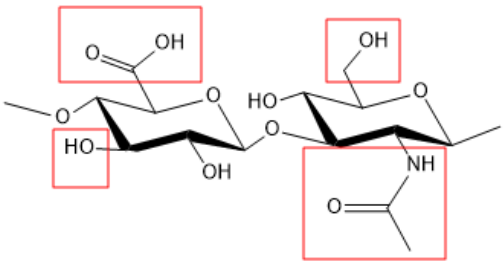

Figure 2.8: Chemical structure of HA with highlighted the three different target functional groups that are prone to chemical modification.

The hydroxyl groups can be modified through esterification, formation of ethers or crosslinking with divynilsulfone, while carboxyl groups are modified by esterification, amidation or carbodiimide-mediated reactions [78].

Although, HA solutions are highly viscous, chemical crosslinking is required for the formation of a stable hydrogel for in vitro and in vivo applications since it is less susceptible to enzymatic degradation. In the literature, there are several examples of HA-based hydrogels that have been used in a variety of clinical and biomedical applications. Seidlits et al studied the differentiation of neural progenitor cells on HA hydrogels with different mechanical properties [79]. HA was modified with photocrosslinkable methacrylate (MA) groups at different molar ratios for the fabrication of HA-MA

hydrogels. It was observed that the differentiation of neural cells was dependent on the mechanical properties of the hydrogels. Recently, Florczyk et al developed a 3D porous scaffold composed of HA and chitosan polyelectrolyte complex in order to mimic the ECM of GBM microenvironment [80]. The HA-chitosan matrix promoted tumour spheroid formation and increased the stem like properties of GBM cells as it was confirmed by the overexpression of the stem cell markers, indicating that this scaffold could be used for in vitro screening of cancer therapeutics or for other biomedical applications.

2.1.7 MC-based hydrogels

Cellulose is another well-known polysaccharide obtained from wood pulp or cotton and is commonly used in a variety of applications due to its biocompatibility and inexpensive resources. However, cellulose mainly suffers from low water solubility, due to the inter-molecular hydrogen bonds occurring between hydroxyl groups that are present in its backbone, leading to the formation of highly ordered crystalline structures. Therefore, cellulose is usually modified with methyl groups which disrupt its rigid crystalline structure and improve the polysaccharide's hydrophilicity [81]. The most commonly used derivative of cellulose is methylcellulose (MC) which is derived from the partial substitution of hydroxyl groups with methoxy groups. MC as FDA approved material is water soluble and is useful for numerous applications due to the mild gelation properties of its aqueous solutions [82].

MC dissolved in aqueous solutions forms thermoresponsive hydrogels that undergo sol-gel transition at specific temperatures depending on its concentration and the addition of salts. In addition, chemical crosslinking methods have been developed in order to develop MC-based hydrogels with long-term stability in vivo conditions. For example, Stalling et al fabricated photopolymerisable methacrylated methylcellulose (MA-MC) hydrogels through esterification with methacrylic anhydride [83]. They observed that MA-MC hydrogels maintained their shape and did not demonstrate any significant inflammatory response when they implanted in CD-1 mice as presented in Figure 2.9.

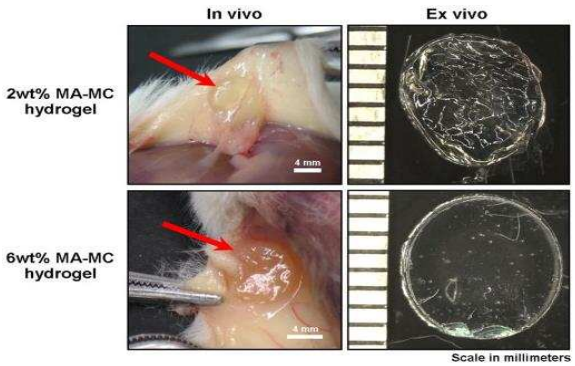

Figure 2.9: Representative images of MC-MA hydrogels at different concentrations implanted in CD-1 mice in vivo and ex vivo for 7 days. Adapted from Stalling et al [83].

Zhuo et al developed injectable HA-MC hydrogels using PEG as a crosslinker and they evaluated the cytotoxicity of this scaffold on L929 mouse fibroblasts [84]. Interestingly, they observed good relative cell viability proposing these scaffolds as a potential for tissue engineering applications. Kim et al fabricated thermosensitive hydrogels composed of soluble ECM (sECM) and MC for injectable stem cell delivery in skin wounds and as promising matrix for tissue regeneration [85].

2.2 Experimental

2.2.1 Materials

Hyaluronic acid (hyaluronic acid sodium salt, from Streptococcus equiv. MW = 1.5 -1.8 mDa) and Adipic Acid Dihydrazide (ADH, MW = 174.2 Da) were purchased from Sigma Aldrich. 1-Ethyl-3-(dimethylaminopropyl) carbodiimide hydrochloride (EDC, MW = 191.7 Da) and N-Hydroxysulfosuccinimide Sodium Salt (Sulfo-NHS, MW = 217.13) were purchased from TCI Europe. Bovine Serum Albumin (BSA) (lyophilised powder, ≥ 98 %, MW = 66 kDa), Methyl cellulose (MC, suitable for cell culture, MW = 14 kDa, viscosity: 15 cPs, D.S 1.5-1.9), Xanthan gum (XG) from Xanthomonas campestris (viscosity: 800-1200 cPs) all were purchased from Sigma Aldrich. Deionised water was prepared from 200 nm nylon membrane filters from Millipore. Phosphate buffer saline tablets (1 tablet dissolved in 200 mL of deionised water, yields 0.01 M phosphate buffer solution, pH 7.4) were purchased from Fischer Scientific.

2.2.2 Methods

2.2.2.1 Preparation of HA-ADH hydrogels

All hydrogels were prepared from HA of high molecular weight (1.5 - 1.8 mDa) and crosslinked with ADH as crosslinker and EDC as crosslinking agent similar as described by Prestwich et al [86]. The preparation protocol was slightly modified. Briefly, the ratios of ADH to HA and HA to EDC were adjusted to obtain hydrogels optimised for cell adhesion. Four different crosslinking densities of HA-ADH hydrogels were investigated and the detailed protocol for one of them is described below. HA sodium salt (10 mg, 6.25 nmoles) was dissolved in 800 µL of deionised water and EDC (0.26 mg, 1.35 µmoles) was dissolved in 100 µL of deionised water and added to the aqueous HA solution. EDC was allowed to dissolve before the addition of ADH. The crosslinker ADH (0.25 mg, 1.43 µmoles) was subsequently dissolved in 100 µL of deionised water and was added to the activated HA solution. The pH of the solution was adjusted at pH 5.5 with the addition of HCl 0.1 M. Gelation was allowed to occur with gentle vortexing. HA-ADH hydrogels were washed 3 times with PBS for the removal of any excess of unreacted crosslinker.

2.2.2.2 Preparation of HA-BSA hydrogels

All hydrogels were prepared from HA of high molecular weight. Four different crosslinking densities of HA-BSA hydrogels were prepared and the detailed protocol for one of them is described below. The ratios of BSA, sulfo-NHS and EDC were adjusted to obtain hydrogels optimised for cell

adhesion. Briefly, HA sodium salt (6 mg, 3.75 nmoles) was dissolved in 800 µL of deionised water and it was activated with EDC (2 mg, 10.4 µmoles) and sulfo-NHS (0.5 mg, 2.3 µmoles) mixture in a molar ratio 4:1 in 200 µL of deionised water and the pH was adjusted at pH 6.0 with the addition of HCl 0.1 M before the reaction with the protein. The reaction was allowed to proceed for 2 minutes by vortexing. Then BSA (3 mg, 45.4 nmoles) was added as a powder to the activated HA solution for further crosslinking and gelation was allowed to occur with gentle vortexing. HA-BSA hydrogels were washed 3 times with PBS for the removal of any excess of unreacted crosslinker.

2.2.2.3 Preparation of MC hydrogels

MC solutions were prepared by a dispersion technique similar as described by Tate et al [87]. MC powder with approximate viscosity of 15 cP according to the manufacturer's specifications, was used. Briefly, approximately half of the required volume of PBS was heated above 90 °C. The MC powder was mixed with heated PBS and agitated until all polymer particles were thoroughly wetted. The remainder of PBS was added cold and the mixture was gently stirred until MC was completely dissolved. As the temperature was lowered to 0 °C using an ice bath, the polymer became water-soluble, forming a clear solution and gentle agitation was continued for 30 minutes. The solutions were allowed to equilibrate at 4 °C overnight. Different compositions of MC solutions (2 % w/w, 4 % w/w, 6 % w/w and 8 % w/w in 1×PBS, 2 % w/w, 4 % w/w and 6 % w/w in 5×PBS, 2 % w/w and 4 % w/w in 10×PBS) were prepared and the solutions were heated until gelation was observed.

2.2.2.4 Preparation of blend XG/MC hydrogels

XG solutions were prepared by slow addition of XG powder into PBS solution with vigorous stirring until the polysaccharide was completely dissolved and the solution was kept at 4 °C overnight with gentle stirring as described by Liu et al [88]. MC solutions were prepared as described in Section 2.2.2.3. XG/MC composite solutions were prepared by adding XG powder into MC solution followed by overnight gentle stirring at 4 °C. XG/MC solutions were prepared at different compositions (XG 1% w/w and MC 3 % w/w, XG 1 % w/w and MC 6% w/w, XG 1% w/w, XG 1 % w/w and MC 8% w/w, XG 2 % w/w and MC 6 % w/w, XG 2 % w/w and MC 1% w/w, XG 3 % w/w and MC 1% w/w) and gelation was allowed to occur with heating.

2.2.2.5 Preparation of blend HA/MC hydrogels

HA and MC blend solutions were prepared as previously described by Gupta et al [89]. MC was dissolved in deionised water at 90 °C until all the particles were thoroughly wetted. Phosphate buffer saline (pH 7.4) was added to the solution in equal quantity to water and subsequently cooled to 0 °C using an ice bath for an additional 30 minutes, after which it was allowed to equilibrate at 4 °C overnight. HA was then added as a powder to the MC solutions at a range of concentrations and allowed to get completely dissolved at 4 °C overnight with gentle stirring. Gelation was allowed to occur with heating at 37 °C. HA/MC solutions were prepared at different compositions and they are

as follows: 0.25 % w/w HA and 0.5 % w/w MC, 0.5 % w/w HA and 0.5 % w/w MC, 0.5 % w/w HA and 1 % w/w MC, 0.5 % w/w HA and 3 % w/w MC, 0.75 % w/w HA and 0.75 % w/w MC, 1 % w/w HA and 2 % w/w MC.

2.3 Results and Discussion

2.3.1 Preparation of HA-ADH hydrogels at various crosslinking densities

Scaffolds prepared from polysaccharides are promising biomaterials for mimicking the in vivo tumour microenvironment. They structurally resemble glycosaminoglycans which are main components of the ECM. Particularly, HA is one of the major components of the brain ECM and is associated with the GBM growth and invasion [90]. HA presents several desirable properties such as biocompatibility, hydrophilicity, biodegradability, tunable viscoelastic properties and non-immunogenicity which are essential elements for its application in the biomedical field.

HA as a natural polymer in its native structure is characterised by its poor mechanical properties and rapid degradation in vivo conditions. It has been extensively used in the preparation of hydrogels for various biomedical applications such as wound healing and drug delivery [91]. For the preparation of HA-based hydrogels with good mechanical properties, various chemical crosslinking methods have been developed, although sometimes the cytotoxicity derived from the crosslinking agents is inevitable [92]. Many commercially available injectable HA hydrogels have been crosslinked with butanediol diglycidyl ether (BDDE) or divinylsulfone and glutaraldehyde as crosslinking agents [93]. In this study, HA was chosen as the main component of the hydrogels due to its numerous advantages over other polysaccharides. An inexpensive and straightforward approach for their preparation is proposed below.

HA of high molecular weight was chosen, since it has been found that high molecular weight HA presents anti-angiogenic and anti-inflammatory properties, whereas low molecular weight fragments (<100 kDa) show the opposite biological activity [94]. Herein, HA hydrogels were prepared by amidation reaction of the free carboxylic groups of HA in the presence of a carbodiimide as crosslinking agent. EDC is commonly used as crosslinking agent due to its high-water solubility and it is well known for its ability to crosslink carboxylic groups with amines. Different compounds with free amino groups were checked if they could react with the carboxylic groups of HA and form amide bonds. Particularly, 2,2′-(Ethylenedioxy) bis(ethylamine) (EBE), branched Polyethylenimine (PEI) and ADH as shown in Figure 2.10 were used and underwent screening under different experimental conditions but no reaction was observed in the case of the amines and they will not be further discussed. However, ADH successfully reacted with the carboxylic groups of HA at different molar ratios forming amide bond.

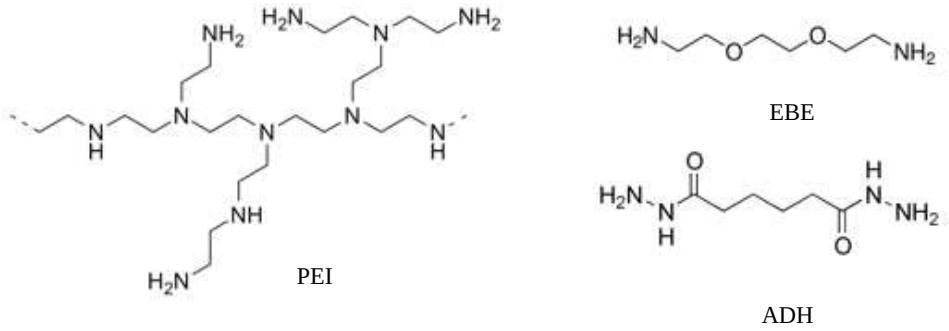

Figure 2.10: Chemical structures of 2,2′-(Ethylenedioxy) bis(ethylamine) (EBE), branched Polyethylenimine (PEI) and Adipic Acid Dihydrazide (ADH).

Therefore, ADH was used as a crosslinker and as a low molecular weight compound with a hydrazide group at each end, it was very reactive. Generally, dihydrazides have much lower pKa values of 2-3 than the diamines which allows the successful crosslinking with the HA in the presence of carbodiimide as crosslinking agent. On the other hand, amines have high pKa values (pKa > 9), which makes it more difficult to conjugate them to HA. ADH, due to its high-water solubility and low toxic properties, has commonly been used as a crosslinker in the preparation of hydrogels for biomedical applications [95]. For instance, Motokawa et al developed HA hydrogels crosslinked with ADH in the presence of bis(sulfosuccinimidyl) suberate (BS3) as crosslinking agent for the sustained release of erythropoietin [96], whereas Hu et al evaluated the in vitro and in vivo performance of oxidised HA-ADH hydrogels for the prevention of post-operative epidural fibrosis. These scaffolds presented reasonable biocompatibility for neural and Schwann cells [97].

Herein, HA was crosslinked with ADH at different crosslinking densities in the presence of EDC as a coupling agent. The reaction mechanism has been studied extensively by Nakajima and Ikada in 1995 [98]. Briefly, EDC activates the carboxylic group of HA forming an unstable reactive O-acyl isourea ester. The second step of the reaction is the nucleophilic attack of the chosen amine on the activated HA forming an amide bond. However, the O-acyl isourea intermediate can be further hydrolysed forming a stable water-soluble N-acyl urea by-product as it is demonstrated in Figure 2.11. In this reaction, the nucleophile was the ADH which supplied free amine groups and we hypothesised that the carboxylic groups of HA could react with EDC and form amide linkages with ADH. The reaction is strongly dependent on the pH and the activation of carboxylic acid by EDC takes place in acidic environment (pH 4.5-6.0). At higher pH values, EDC is hydrolysed into N-acyl urea which prevents further reaction with amines.

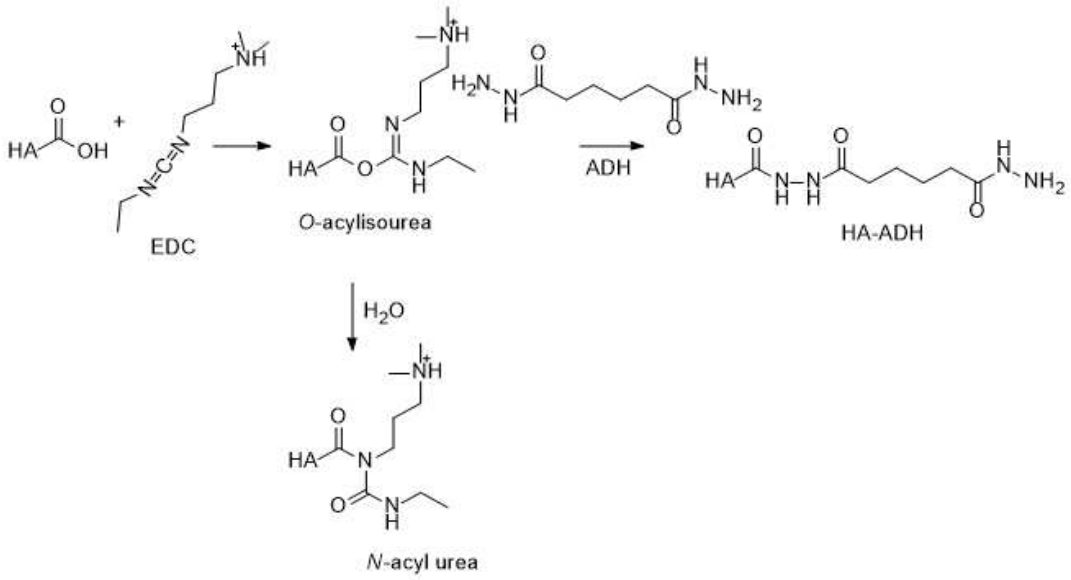

Figure 2.11: Plausible mechanism of crosslinking with EDC, which activates the carboxylic group of HA forming an unstable reactive O-acylisourea ester. Followed by the nucleophilic attack of the chosen amine on the activated HA leading to the formation of an amide bond. Hydrolysis of the O-acylisourea intermediate results in the formation of N-acyl urea as by-product.

Table 2.1 summarises the trials that have been made in order to obtain self-supporting hydrogels from the crosslinking of HA with ADH in the presence of EDC. Particularly, HA solutions of concentration 4.0 mg/mL and 8.0 mg/mL were prepared and crosslinked with different molar ratios of ADH and EDC at pH 5.5. In all cases, not self-supporting hydrogels were obtained, therefore it was considered necessary to increase the concentration of HA at 10 mg/mL.

Table 2.1: Summary of crosslinking reactions of HA with ADH at different molar ratios.

Sample abbreviation	HA (mg/nmole)	ADH (mg/μmole)	EDC (mg/μmole)	pH	Formation of hydrogel
HG1	4.0/2.5	0.25/1.43	0.26/1.36	5.5	Solution
HG2	4.0/2.5	0.5/2.87	0.6/3.12	5.5	Solution
HG3	4.0/2.5	1.5/8.6	1.6/8.35	5.5	Solution
HG4	4.0/2.5	3.5/20.1	3.6/18.8	5.5	Solution
HG5	4.0/2.5	8.0/45.9	8.1/42.2	5.5	Solution
HG6	8.0/5.0	0.25/1.43	0.26/1.36	5.5	Viscous solution
HG7	8.0/5.0	0.5/2.87	0.6/3.12	5.5	Viscous solution
HG8	8.0/5.0	2.5/14.3	2.6/13.6	5.5	Viscous solution
HG9	8.0/5.0	3.5/20.1	3.6/18.8	5.5	Viscous solution
L1	10.0/6.25	0.25/1.43	0.26/1.36	5.5	Self-supporting gel
L2	10.0/6.25	0.5/2.87	0.6/3.12	5.5	Self-supporting gel
H1	10.0/6.25	2.5/14.3	2.6/13.6	5.5	Self-supporting gel
H2	10.0/6.25	3.5/20.1	3.6/18.8	5.5	Self-supporting gel

Finally, four different crosslinking densities of HA-ADH hydrogels were prepared and the molar ratios of ADH to HA and HA to EDC were adjusted to obtain hydrogels optimised for cell adhesion

and culture. Table 2.2 summarises the critical conditions for the formation of HA-ADH hydrogels and their gelation time.

Table 2.2: Critical conditions for the preparation of HA-ADH hydrogels at different crosslinking densities.

Sample abbreviation	HA (mg/nmole)	ADH (mg/µmole)	EDC (mg/µmole)	pH	Gelation time (minutes)
L1	10.0/6.25	0.25/1.43	0.26/1.36	5.5	4
L2	10.0/6.25	0.5/2.87	0.6/3.12	5.5	3
H1	10.0/6.25	2.5/14.3	2.6/13.6	5.5	2
H2	10.0/6.25	3.5/20.1	3.6/18.8	5.5	2

Self-supporting hydrogels were prepared at four different crosslinking densities as shown in Figure 2.12. Briefly, HA sodium salt (10 mg, 6.25 nmoles) were dissolved in deionised water in a glass vial with inner diameter 12 mm and different molar ratios of ADH and EDC were added and gelation was allowed to occur with gentle vortexing. The transition from the solution (viscous) to the gel phase was monitored by the test tube inversion method as reported by Gupta et al [89]. The gelation time was determined as the time at which the gel did not flow and it was mainly dependent on the crosslinking density of the hydrogels. The higher crosslinking density of the hydrogels, the shorter gelation time observed.

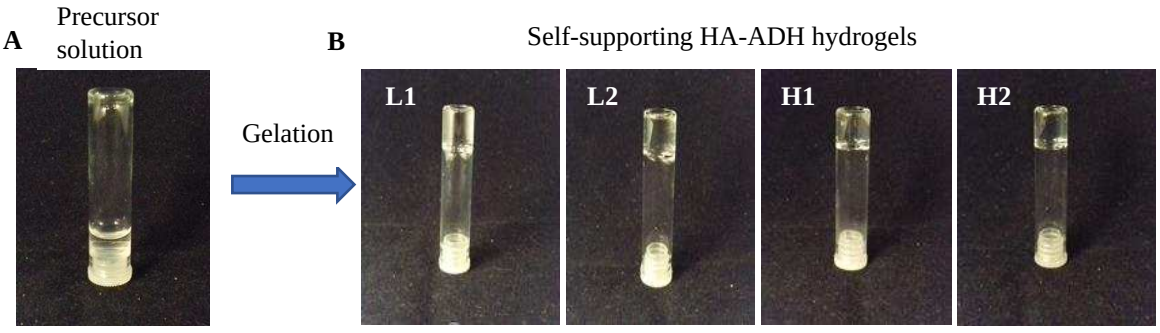

Figure 2.12: A. Photo of HA-ADH precursor solution before gelation. HA-ADH precursor solution is a viscous solution. **B.** Photos of HA-ADH hydrogels at four different crosslinking densities. The transition from the solution (viscous) to the gel phase was monitored by the test tube inversion method.

The successful crosslinking reaction of the HA with ADH was characterised by Fourier Transform Infrared Spectroscopy (FT-IR) as presented in Figure 2.13 and it will be further discussed in Chapter 3. Briefly, FT-IR spectroscopy was performed on HA, ADH and HA-ADH lyophilised hydrogel (xerogel) in order to confirm any changes in the structure of the HA backbone. In the spectrum of HA-ADH xerogel, the peak at 1686 cm^{-1} corresponds to the formation of a new amide bond (C=O stretch of secondary amide) and the peak at 1558 cm^{-1} is assigned to stretching vibration of N-H bond.

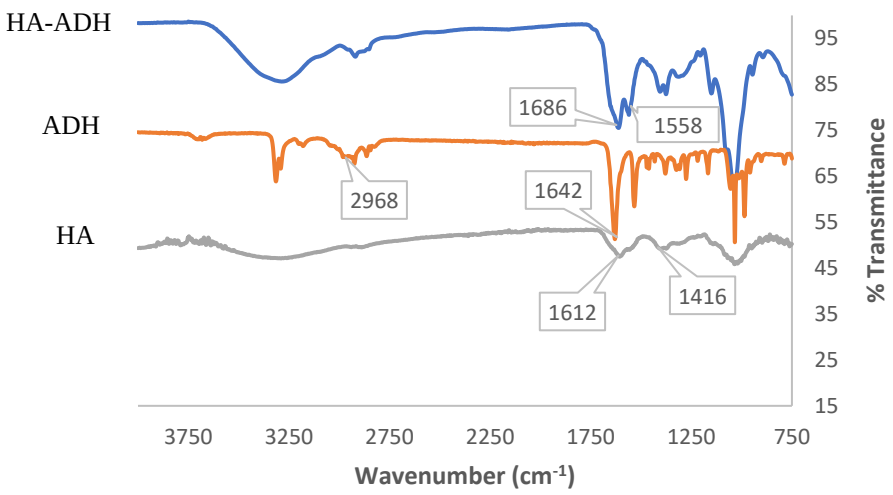

Figure 2.13: FT-IR spectra of native HA, ADH and HA-ADH xerogel. FT-IR spectroscopy confirmed the successful crosslinking reaction of HA-ADH.

2.3.2 Preparation of HA-BSA hydrogels at various crosslinking densities

In an effort to optimise the formulation of the aforementioned HA-based hydrogels and decrease the viscosity of the precursor gelator solution which will result in better injectability of the system, another method of crosslinking of HA is proposed in the presence of Bovine Serum Albumin. Albumin is the most abundant protein in human plasma and it has numerous biochemical applications including ELISA (Enzyme-Linked Immunosorbent Assay) and immunohistochemistry. Additionally, albumin is characterised by its unique physical properties such as stability, biodegradability and non-toxicity that contribute to its wide use in biomedical applications [99]. BSA is a single polypeptide of molecular weight of 66 kDa that consists of 59 lysine residues, of which 30-35 have primary amines that can react further with carboxylic groups and form amide bonds. In the literature, the chemical crosslinking of the lysine residues of BSA with different crosslinkers such as bis(sulfosuccinimidyl) suberate (BS3), disuccinimidyl suberate (DSS) or disuccinimidyl glutarate (DSG) for the characterisation of its 3D structure has been reported [100]. The 3D structure of BSA has been shown to be very similar to HSA (Human Serum Albumin), because the two proteins share 76 % sequence identity [101]. On that account, BSA was chosen as the model protein for crosslinking with HA.

In this work, HA was activated with EDC/sulfo-NHS and further crosslinked with the free amine groups that are present in the BSA molecule. Generally, sulfo-NHS is used to prepare amine-reactive esters of carboxylic groups for chemical crosslinking. The carboxylic groups of HA react with sulfo-NHS in the presence of EDC, resulting in a semi-stable sulfo-NHS ester, which may then be reacted with primary amines to form amide bond as shown in Figure 2.14. The presence of sulfo-NHS usually is not necessary in carbodiimide reactions, albeit their use significantly enhances the efficiency of the crosslinking reaction.

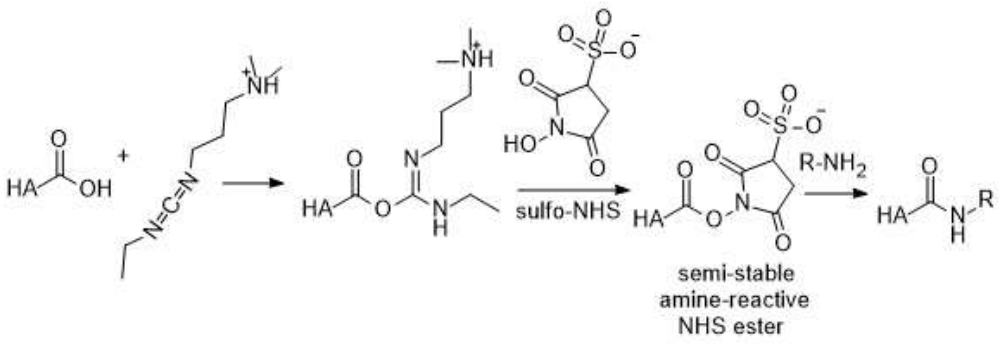

Figure 2.14: Plausible mechanism of crosslinking with EDC in the presence of sulfo-NHS. EDC activates the carboxylic group of HA forming an unstable reactive O-acylisourea ester which further reacts with sulfo-NHS forming a semi-stable reactive NHS ester. Then the reactive ester reacts with the chosen amine forming an amide bond.

The activation reaction with EDC and sulfo-NHS is most efficient at acidic pH, thus the pH of the HA solution was adjusted at pH 6.0 with the addition of HCl 0.1 M. Table 2.3 summarises the different molar ratios of EDC/sulfo-NHS that were investigated for the preparation of HA-BSA hydrogels at different crosslinking densities.

Table 2.3: Summary of crosslinking reactions of HA with BSA at different molar ratios in the presence of EDC/Sulfo-NHS.

Sample abbreviation	HA (mg/nmole)	Sulfo-NHS (mg/μmole)	EDC (mg/μmole)	BSA (mg/nmole)	pH	Formation of hydrogel
HB1	4.0/2.5	0.5/2.3	2.0/10.4	2.0/30.0	6.0	Solution
HB2	4.0/25	0.5/2.3	2.0/10.4	5.0/75.7	6.0	Solution
HB3	4.0/2.5	0.5/2.3	2.0/10.4	10.0/151.0	6.0	Solution
HB4	4.0/2.5	0.5/2.3	2.0/10.4	15.0/ 227.0	6.0	Solution
HB5	5.0/3.1	1.25/5.86	5.0/26.1	2.0/30.0	6.0	Viscous solution
HB6	5.0/3.1	1.25/5.86	5.0/26.1	5.0/75.7	6.0	Self-supporting gel
HB7	5.0/3.1	1.25/5.86	5.0/26.1	10.0/151.0	6.0	Formation of aggregate
HB8	5.0/3.1	1.25/5.86	5.0/26.1	15.0/227.0	6.0	Formation of aggregate
HB9	5.0/3.1	0.5/2.3	2.0/10.4	2.0/30.0	6.0	Viscous solution
HB10	5.0/3.1	2.5/11.5	10.0/52.2	2.0/30.0	6.0	Self-supporting gel
HB11	5.0/3.1	3.75/17.2	15.0/78.2	2.0/30.0	6.0	Self-supporting gel
HB12	5.0/3.1	0.5/2.3	2.0/10.4	3.0/45.4	6.0	Self-supporting gel
HB13	5.0/3.1	1.25/5.86	5.0/26.1	3.0/45.4	6.0	Self-supporting gel
HB14	5.0/3.1	2.5/11.5	10.0/52.2	3.0/45.4	6.0	Self-supporting gel
HB15	5.0/3.1	3.75/17.2	15.0/78.2	3.0/45.4	6.0	Self-supporting gel
HB16	6.0/3.7	0.5/2.3	2.0/10.4	3.0/45.4	6.0	Self-supporting gel
HB17	6.0/3.7	1.25/5.86	5.0/26.1	3.0/45.4	6.0	Self-supporting gel
HB18	6.0/3.7	2.5/11.5	10.0/52.2	3.0/45.4	6.0	Self-supporting gel
HB19	6.0/3.7	3.75/17.2	15.0/78.2	3.0/45.4	6.0	Self-supporting gel

As shown in Table 2.3, self-supporting hydrogels were formed at specific ratios of EDC/sulfo-NHS and BSA using an initial concentration of HA at 5 mg/mL. These hydrogels (HB10-HB15 samples) presented poor mechanical properties (data are not shown), therefore, higher concentration of HA (6

mg/mL) was used for the fabrication of mechanically robust hydrogels. Finally, four different crosslinking densities of HA-BSA hydrogels were further investigated and the characterisation of their physicochemical and mechanical properties will be discussed in Chapter 3. Table 2.4 presents the four chosen HA-BSA crosslinked hydrogels and their gelation time. The gelation time was determined as the time at which the gel did not flow and it was dependent on the crosslinking density of the hydrogels.

Table 2.4: Critical conditions for the preparation of HA-BSA hydrogels at different crosslinking densities.

Sample abbreviation	HA (mg/nmole)	Sulfo-NHS (mg/µmole)	EDC (mg/µmole)	BSA (mg/nmole)	pH	Gelation time (minutes)
HB16	6.0/3.7	0.5/2.3	2.0/10.4	3.0/45.4	6.0	2
HB17	6.0/3.7	1.25/5.86	5.0/26.1	3.0/45.4	6.0	3
HB18	6.0/3.7	2.5/11.5	10.0/52.2	3.0/45.4	6.0	6
HB19	6.0/3.7	3.75/17.2	15.0/78.2	3.0/45.4	6.0	8

Self-supporting hydrogels were prepared at four different crosslinking densities as presented in Figure 2.15. The transition from the solution to the gel phase was monitored by the test tube inversion method as described earlier. The precursor gelator solution underwent instant gelation once the pH of the reaction mixture was adjusted at pH 6.0 under gentle vortexing.

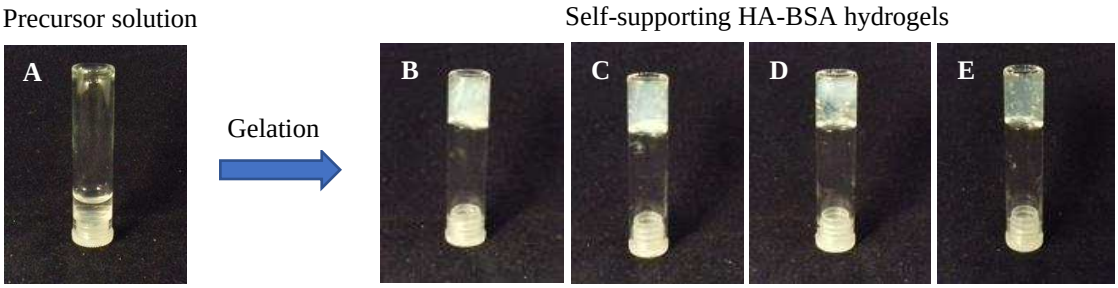

Figure 2.15: A. Photo of HA-BSA solution before gelation. Photos of HA -BSA hydrogels prepared at different crosslinking densities, **B.** HB16, **C.** HB17, **D.** HB18 and **E.** HB19 hydrogel. The transition from the solution to the gel phase was monitored by the test tube inversion method.

The successful crosslinking reaction of the HA with BSA was confirmed by FT-IR spectroscopy as shown in Figure 2.16. Briefly, FT-IR spectroscopy was performed on HA, BSA and HA-BSA xerogel in order to confirm the presence of characteristic peaks of HA and BSA in the HA-BSA conjugate. In the spectrum of HA-BSA xerogel, the main differences compared to that of the unmodified HA focused on the appearance of a peak at 1714 cm^{-1} which corresponds to the formation of an amide bond (C=O stretch of secondary amide), indicative of the successful crosslinking of HA with BSA. Additionally, the sharp peaks at 1676, 1556 and 1243 cm^{-1} assigned to C=O, N-H and C-N stretching vibrations of the amide bonds respectively, confirmed the presence of BSA in the structure of the xerogel.

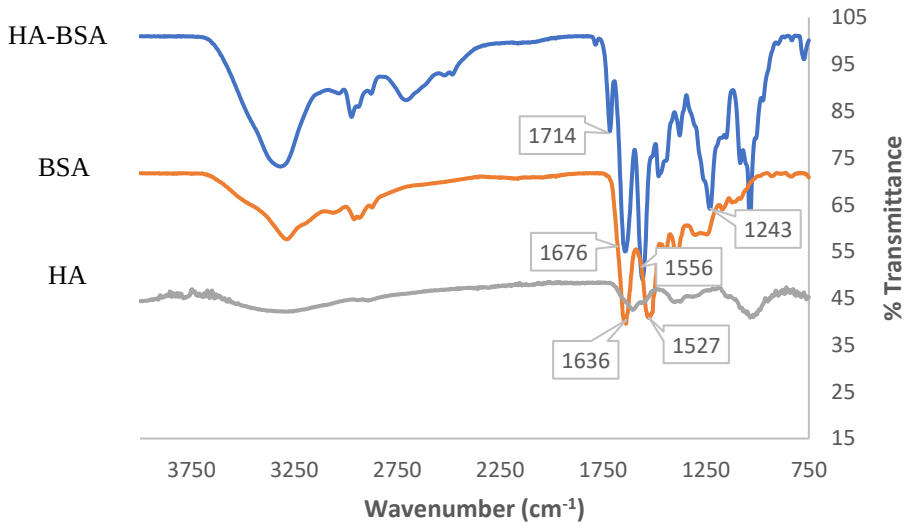

Figure 2.16: FT-IR spectra of native HA, BSA and HA-BSA xerogel. FT-IR spectroscopy confirmed the successful crosslinking reaction of HA-BSA.

2.3.3 Preparation of MC hydrogels in different compositions of PBS solution

MC is a biocompatible FDA approved material and is useful for numerous applications due to its mild gelation conditions. Its physicochemical properties allow gelation at physiological conditions and also injection as liquid precursor which turns into gel in any shape of cavity at body temperature. In 1997, Wells et al demonstrated that MC could promote nerve regeneration in peripheral nerve conduits, which indicated the potential of MC in brain tissue engineering [102]. Similarly, Tate et al investigated the use of injectable MC hydrogels for the repair of brain defects [103]. MC demonstrated low viscosity at room temperature, whereas at 37 °C a soft hydrogel was formed in the presence of salts. Subsequently, this minimally invasive polymer matrix was injected in the injury cavity in the brain of rats and its biocompatibility was assessed, highlighting the potential of this polymer in brain tissue engineering.

As described above, MC presents several advantages as injectable material in the brain tissue engineering, due to its mild gelation properties and the facile fabrication of hydrogels. Therefore, in this study MC hydrogels were prepared using various concentrations of the polysaccharide in PBS solution of different salt concentration in order to identify the optimal conditions for the formation of self-supporting hydrogels at 37 °C that will promote cell adhesion. Table 2.5 summarises the different concentrations of MC in different compositions of PBS solution that were investigated and their gelation temperature.

Table 2.5: Different concentrations of MC in various compositions of PBS solutions and their gelation temperature.

MC Concentration (% w/w)	PBS Composition	Gelation Temperature (°C)	Formation of hydrogel
2	1×PBS	-	Viscous solution
4	1×PBS	42	Self-supporting hydrogel
6	1×PBS	37	Self-supporting hydrogel
8	1×PBS	34	Self-supporting hydrogel
2	5×PBS	35	Self-supporting hydrogel
4	5×PBS	32	Self-supporting hydrogel
6	5×PBS	30	Self-supporting hydrogel
2	10×PBS	28	Self-supporting hydrogel
4	10×PBS	25	Self-supporting hydrogel

Table 2.6 summarises the different compositions of PBS solution that they were used for the preparation of MC hydrogels and the corresponding concentrations of the salts.

Table 2.6: Different compositions of PBS solutions and concentrations of the corresponding salts.

PBS composition	Na_2HPO_4 Concentration (M)	KH_2PO_4 Concentration (M)	NaCl Concentration (M)	KCl Concentration (M)	pH
1×PBS	0.0043	0.00147	0.137	0.0027	7.4
5×PBS	0.0215	0.00735	0.685	0.0135	7.4
10×PBS	0.043	0.0147	1.37	0.027	7.4

Briefly, different concentrations of MC solutions were prepared in PBS in glass vials with inner diameter 12 mm and they were placed in a Grant^{TM} digital block heater for the precise heating of the vials. The heating rate was 1 °C per min and the gelation behaviour was monitored by inversion of the vials. The transition from the solution to the gel phase was validated qualitatively by the test tube inversion method as described earlier and as shown in Figure 2.17. The gelation temperature was determined as the temperature at which the gel did not flow with inversion of the vial. Different phase transitions of the solutions at various temperatures were observed and can be classified into three distinct phases: clear solution, formation of soft gel and white, phase-separated gel. The transparency of MC hydrogels also decreased as the concentration of MC and salts increased as demonstrated in Figure 2.17.

It is widely known that MC is soluble in aqueous solutions at low temperatures due to the presence of ″cagelike″ water structures or hydrogen bonds surrounding MC chains. At higher temperatures, these structures are destroyed upon heating, leading to the formation of hydrophobic aggregates and the subsequent formation of a gel network. As shown in Table 2.5, all MC compositions presented gelation temperature below body temperature except for the second one, which turned into gel at higher temperature. The gelation temperature was highly dependent on the composition of PBS and the concentration of MC in the aqueous solutions. It has been reported that the gelation behaviour of MC is affected by salts concentration that are present in the solution. More specifically, Na_2HPO_4

and NaCl salts present strong polar interactions with water in the MC solution and consequently, the degree of polar interactions affects the gelation behaviour of MC. In this study, it was observed that the higher the concentration of the salts present in the MC solutions, the lower gelation temperature for MC solutions. Ions such as Cl^- tend to draw water molecules away from the MC polymer chains, as they can attract more water molecules to surround them due to their strong hydration abilities, leading to a poorer solubility of MC in water upon heating. As a result, there are more hydrophobic MC aggregates facilitating the formation of a gel network at lower temperatures.

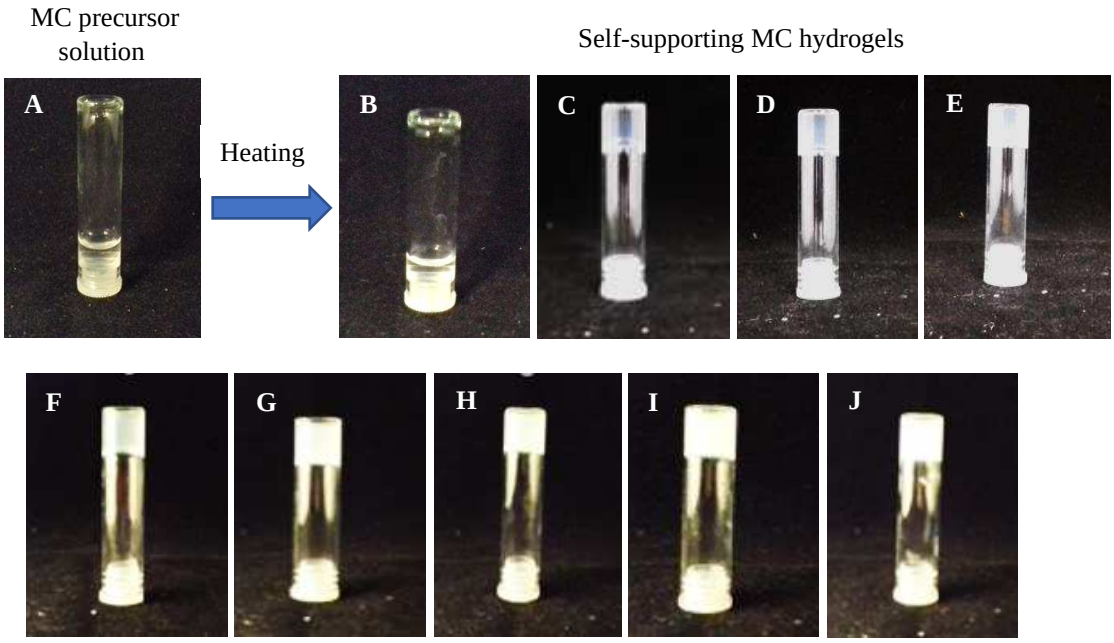

Figure 2.17: Photos of MC hydrogels. **A.** MC precursor solution , **B.** 2 % w/w MC in 1× PBS, **C.** 4 % w/w MC in 1× PBS, **D.** 6 % w/w MC in 1× PBS, **E.** 8 % w/w MC in 1×PBS, **F.** 2 % w/w MC in 5× PBS, **G.** 4 % w/w MC in 5× PBS, **H.** 6 % w/w MC in 5× PBS, **I.** 2 % w/w MC in 10× PBS, **J.** 4 % w/w MC in 10× PBS. The transparency of MC hydrogels decreased as the concentration of MC and salts increased. Due to the light artifacts, this is not clearly presented in the above photos.

The gelation mechanism of MC has been studied extensively including two main steps as described by Kobayashi et al [104]. Clustering of MC chains occurs which is driven by hydrophobic association, while at higher temperature the gelation is associated with liquid-liquid phase separation. Kato et al proposed that the association at low temperatures is addressed by aggregation of the most hydrophobic groups, whereas at high temperatures, the association is mainly caused by less hydrophobic groups [105]. At lower temperatures, water molecules in the presence of salts are attracted from ions and this results in hydrophobic association as stated above. The hydrogen bonds between water molecules and MC can be stronger than those at high temperatures and consequently water molecules will return to the hydrophobic groups progressively. In the presence of salts, the hydrophobic interactions are promoted from the salt-out effect and the strength of these interactions are highly dependent on the nature of the ions.

2.3.4 Preparation of different compositions of blend XG/MC hydrogels

Various blend hydrogels that combine two or more components with complementary shear thinning properties have been reported in the literature [106]. This group of hydrogels possesses the advantages of low cost, easy preparation and improved mechanical properties. Xanthan gum (XG) is a biocompatible and biodegradable high molecular weight anionic polysaccharide and is mainly produced from bacterial fermentation [107]. It consists of D-glucosyl, D-mannosyl, and D-glucuronyl acid residues in a 2:2:1 molar ratio and various ratios of O-acetyl and pyruvyl residues as shown in Figure 2.18.

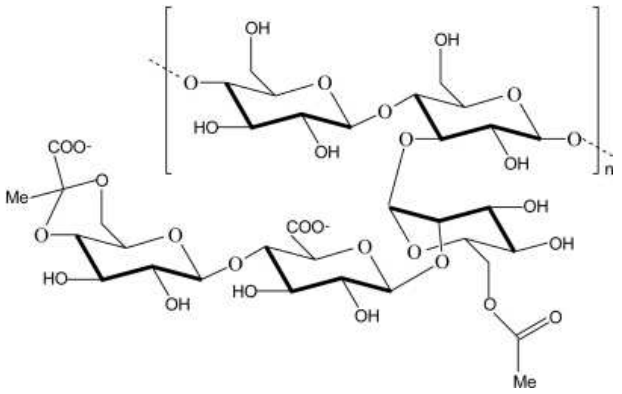

Figure 2.18: Chemical structure of xanthan gum which consists of D-glucosyl, D-mannosyl, and D-glucuronyl acid residues.

In aqueous solutions, XG adopts two different conformations. At low temperatures it obtains an ordered and rigid double helical conformation, whereas at high temperatures a disordered and flexible coil structure prevails [108]. XG forms a 3D network when the temperature is below its midpoint transition temperature (T_m) and it shows a weak gel-like behaviour. Dyondi et al prepared an injectable hydrogel from a blend of gellan gum and XG for growth factor delivery for bone regeneration, highlighting its potential as an injectable scaffold in tissue engineering [109].

Herein, commercially available XG and MC were used in order to prepare injectable, biocompatible blend XG/MC hydrogels. XG/MC blend solutions were prepared at different compositions in 1×PBS (pH 7.4) as summarised in Table 2.7 and the gelation properties were investigated. The transition from the solution to the gel phase was validated qualitatively by the test tube inversion method as described earlier and as shown in Figure 2.19. The gelation temperature was determined as the temperature at which the gel did not flow and it was highly dependent on the concentration of XG and MC in the blend solution. As described earlier, different compositions of XG/MC solutions were prepared in PBS as shown in Table 2.7 in glass vials with inner diameter 12 mm and they placed in a Grant^{TM} digital block heater for the precise heating of the vials. The heating rate was 1 °C per min and the gelation behaviour was monitored by inversion of the vials.

Table 2.7: XG and MC concentrations in various blend solutions of XG/MC in 1×PBS.

Sample abbreviation	MC Concentration (% w/w)	XG Concentration (% w/w)	Gelation temperature (°C)	Formation of hydrogel
XG1/MC0	0	1	-	Self-supporting hydrogel
XG1/MC3	3	1	35	Self-supporting hydrogel
XG1/MC6	6	1	34	Self-supporting hydrogel
XG1/MC8	8	1	29	Self-supporting hydrogel
XG2/MC1	1	2	37	Self-supporting hydrogel
XG2/MC6	6	2	28	Self-supporting hydrogel
XG3/MC1	1	3	32	Self-supporting hydrogel

All XG/MC compositions presented gelation temperature below body temperature as it was determined by the test tube inversion method. In addition, it can be concluded that the addition of XG decreased the gelation temperature of MC.

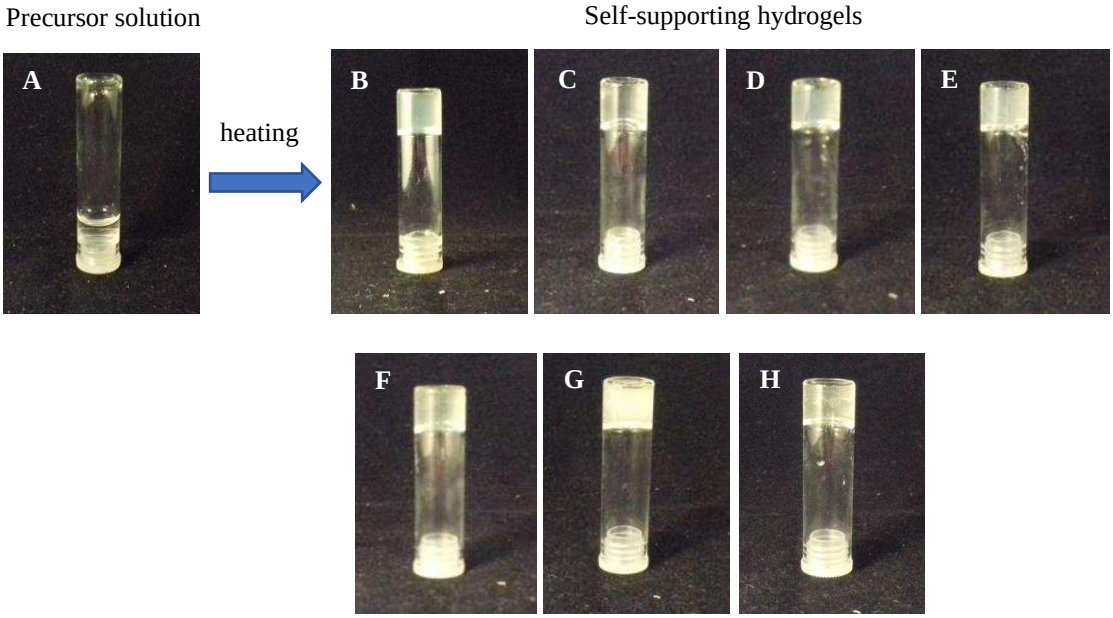

Figure 2.19: Photos of blend XG/MC hydrogels. **A.** Precursor solution of XG/MC, **B.** XG1/MC0, **C.** XG1/MC3, **D.** XG1/MC6, **E.** XG1/MC8, **F.** XG2/MC1, **G.** XG2/MC6, **H.** XG3/MC1 in 1×PBS.

XG contains carboxylic groups that could induce dehydration of the MC and thus decrease the gelation temperature of MC [89]. Additionally, the presence of salts in PBS cause dehydration of MC which results in lower gelation temperature for MC as explained in section 2.3.3. XG solutions present a weak gel behaviour and sheer thinning properties due to the 3D network formed by the helical conformation, while MC possesses thermal gelation properties. MC was used in higher concentration than XG in the blend solutions thus the 3D network of XG is partially interrupted from the MC molecules. In blend solutions, both components keep their own structures and their complementary sheer thinning properties contribute to the formation of self-supporting gels. To sum

up, the results demonstrated that the blend solutions of XG/MC are viscous at room temperature and after heating they form self-supporting hydrogels below body temperature, indicating their potential as injectable scaffolds.

2.3.5 Preparation of different compositions of blend HA/MC hydrogels

Blends of polysaccharides represent an emerging class of biomaterials due to the merge of the advantages of each component. The investigation of polysaccharide-based blend solutions that can form hydrogel network upon heating continued with the preparation of blend solutions composed of HA of high molecular weight and MC. HA/MC blend solutions can form hydrogels due to the dehydration of MC induced by the carboxylic groups of HA. HA as sodium salt when it is dissolved in water it is ionised and induces the salt-out effect which contributes to the development of hydrophobic interactions. Moreover, the addition of HA increases the viscosity of the MC solution by increasing the number of molecular entanglements. Recently, Shoichet et al developed an injectable blend hydrogel composed of HA and MC for drug delivery to the injured spinal cord [89]. They prepared different compositions of HA/MC blend solutions and they evaluated the injectability of the scaffold and its biocompatibility in vivo studies which showed that HA/MC is biocompatible in the intrathecal space. Blends of HA and MC have also been used for various applications, including wound healing and stroke repair [110], [111].

One specific aim of this work was to investigate the effect of HA of high molecular weight on the thermogelation and biocompatibility of its blends with MC. The rationale was to investigate a new possible scaffold for trapping glioma cells. MC is known for its thermoresponsive behaviour, while HA for its biocompatibility and biodegradability. HA/MC blend solutions were prepared at different compositions as summarised in Table 2.8 and they were evaluated for their gelation properties upon heating.

Table 2.8: XG and MC concentrations in various blend solutions of HA/MC. HA and MC were not used at higher concentrations as it was really difficult to manipulate them due to high viscosity of the precursor solutions.

Sample abbreviation	HA Concentration (% w/w)	MC Concentration (% w/w)	Formation of hydrogel
HA0.25/MC0.5	0.25	0.5	Solution
HA0.5/MC0.5	0.5	0.5	Solution
HA0.5/MC1	0.5	1.0	Solution
HA0.5/MC3	0.5	3.0	Solution
HA0.75/MC0.75	0.75	0.75	Solution
HA1/MC2	1.0	2.0	Viscous solution

In section 2.3.4, it was stated that XG/MC blend solutions are viscous solutions at 4 °C and they turn into gel upon heating. Herein, blends of HA/MC behave as solutions at room temperature and upon

heating they remain solutions and no formation of gel network was observed. The concentration of HA in the blends of HA/MC was chosen to be less than 1 % w/w as it was noticed that the manipulation of the precursor solution was really difficult due to high viscosity at higher concentrations. Finally, blend HA/MC solutions will not be studied further due to their poor gelation properties.

2.4 Conclusions

The first sections of this chapter aimed to provide a literature review on the hydrogels used for biomedical applications and their unique properties and versatility over other materials. Particular focus was given to polysaccharide-based hydrogels as potential scaffolds for attracting and trapping glioma cells. Scaffolds prepared from natural polysaccharides are promising biomaterials for mimicking the in vivo tumour microenvironment due to the fact that they structurally resemble glycosaminoglycans which are main components of the ECM. In the first experimental section of this work, HA was chosen as the main component for the preparation of hydrogels due to its unique advantages and structural versatility over other polysaccharides. HA is one of the main constituents of the brain ECM and is closely related to the proliferation and migration of GBM cells. Chemical modification of its backbone allows the formation of 3D polymeric hydrophilic networks that present viscoelastic properties similar to the elastic modulus of the brain tissue.

Herein, an inexpensive and relatively simple preparation of hydrogels based on HA was proposed. Hydrogels were prepared by amidation reaction of the free carboxylic groups of HA in the presence of EDC as crosslinking agent and ADH as crosslinker. HA of high molecular weight was chosen and it was crosslinked with different molar ratios of ADH and EDC. Transparent self-supporting HA-ADH hydrogels obtained at four different crosslinking densities and the characterisation of their physicochemical and mechanical properties will be discussed in Chapter 3 in order to identify the optimal crosslinking density that promotes cell adhesion. Moreover, in an effort to optimise the aforementioned formulation of hydrogels and improve the injectability of the formulation, another method of crosslinking of HA was developed in the presence of BSA. Taking into consideration the free primary amines that are present in lysine residues of the BSA molecule and the size of this protein, we proposed the potential crosslinking reaction of the carboxylic groups of HA with the primary amines of BSA which will result in the formation of amide bonds and the fabrication of a 3D network. HA-BSA self-supporting hydrogels were prepared at different crosslinking densities and they will be further characterised in the following chapter.

Furthermore, in the second experimental section of this chapter we investigated the use of MC for the fabrication of injectable hydrogels. MC presents several advantages as injectable material in the brain tissue engineering, due to its mild gelation properties. MC-based hydrogels were prepared using various concentrations of MC in PBS solutions of different salt concentration in order to identify the

optimal conditions for the formation of self-supporting hydrogels at 37 °C. It can be concluded that the concentration of MC and the composition of PBS affects the gelation behaviour of the polysaccharide. The preparation of blend hydrogels based on MC was investigated due to the fact that this group of hydrogels benefits from the physicochemical properties of each component. Blend solutions of XG/MC were successfully prepared at different compositions and their gelation properties were investigated upon heating, while HA/MC solutions presented poor gelation properties and they will not be discussed further in the following chapters.

References

[1] Hoffman A.S., Hydrogels for biomedical applications, Adv. Drug Deliv. Rev., 2002, 54, 3-12.

[2] El-Sherbiny I.M., Yacoub M.H., Hydrogel scaffolds for tissue engineering: Progress and challenges, Glob. Cardiol. Sci. Pract., 2013, 2013, 316-342.

[3] Fajardo A.R., Lopes L.C., Caleare A.O., Britta E.A., Nakamura C.V., Rubira A.F., Muniz E.C., Silver sulfadiazine loaded chitosan/chondroitin sulfate films for a potential wound dressing application, Mater. Sci. Eng., 2013, 33, 588-595.

[4] Buenger D., Topuz F., Groll J., Hydrogels in sensing applications, Prog. Polym. Sci., 2012, 37, 1678-1719.

[5] Nicolson P.C., Vogt J., Soft contact lens polymers: an evolution, Biomaterials, 2001, 22, 3273-3283.

[6] Qiu Y., Park K., Environment-sensitive hydrogels for drug delivery, Adv. Drug Deliv. Rev., 2001, 53, 321-339.

[7] Nishinari K., Some thoughts on the definition of a gel: structures, properties and functions, Springer, 2009, 97-94.

[8] Hunt J.A., Chen R., van Veen T., Bryan N., Hydrogels for tissue engineering and regenerative medicine, J. Mater. Chem. B, 2014, 2, 5319-5338.

[9] Mano J.F., Silva G.A., Azevedo H.S., Malafaya P.B., Sousa R.A., Silva S.S., Boesel L.F., Oliveira J.M., Santos T.C., Marques A.P., Neves N.M., Reis R.L., Natural origin biodegradable systems in tissue engineering and regenerative medicine: present status and some moving trends, J. R. Soc. Interface, 2007, 4, 999-1030.

[10] Tan H., Marra K.G., Injectable, Biodegradable Hydrogels for Tissue Engineering Applications, Materials, 2010, 3, 1746-1767.

[11] Yang J.Y., Xu C.Y., Kopeckova P., Kopecek P., Hybrid hydrogels self-assembled from HPMA copolymers containing peptide grafts, Macromol. Biosci., 2006, 6, 201-209.

[12] Li J.Y., Illeperuma W.B.K., Suo Z.G., Vlassak J.J., Hybrid hydrogels with extremely high stiffness and toughness, ACS Macro Lett., 2014, 3, 520-523.

[13] Akhtar M.F., Hanif M., Ranjha N.M., Methods of synthesis of hydrogels-A review, Saudi Pharm. J., 2016, 24, 554-559.

[14] Censi R., Fieten P.J., di Martino P., Hennink W.E., Vermonden T., In situ forming hydrogels by tandem thermal gelling and Michael addition reaction between thermosensitive triblock copolymers and thiolated hyaluronan, Macromolecules, 2010, 43, 5771-5778.

[15] Wilner I., Stimuli-Controlled Hydrogels and Their Applications, Acc. Chem. Res., 2017, 50, 657-658.

[16] Koetting M.C., Peters J.T., Steichen S.D., Peppas N.A., Stimulus-responsive hydrogels: Theory, modern advances and applications, Mat. Sci. Eng., 2015, 93, 1-49.

[17] Gupta P., Vermani K., Garg S., Hydrogels: from controlled release to pH-responsive drug delivery, Drug Discov. Today, 2002, 7, 569-579.

[18] Chan A.W., Whitney R.A., Neufeld R.J., Kinetic Controlled Synthesis of pH-Responsive Network Alginate, Biomacromolecules, 2008, 9, 2536-2545.

[19] Kim S.Y., Cho S.M., Lee Y.M., Kim S.J., Thermo- and pH-responsive behaviors of graft copolymer and blend based on chitosan and N-isopropylacrylamide, J. Appl. Polym. Sci., 2000, 78, 1381-1391.

[20] Park H.Y., Song I.H., Kim J.H., Kim W.S., Preparation of thermally denatured albumin gel and its pH-sensitive swelling, Int. J. Pharm.,1998, 175, 231-236.

[21] Welz M.M., Ofner C.M., Examination of self-crosslinked gelatin as a hydrogel for controlled release, J. Pharm. Sci., 1992, 81, 85-90.

[22] Na K., Lee E.S., Bae Y.H., Self-organised nanogels responding to tumour extracellular pH: pH-dependent drug release and in vitro cytotoxicity against MCF-7 cells, Bioconjugate Chem., 2007, 18, 1568-1574.

[23] Gil E.S., Hudson S.M., Stimuli-responsive polymers and their bioconjugates, Prog. Polym. Sci., 2004, 29, 1173-1222.

[24] Stabenfeldt S.E., Garcia A.J., LaPlaca M.C., Thermoreversible laminin-functionalised hydrogel for neural tissue engineering, J. Biomed. Mater. Res., 2006, 77A, 718-725.

[25] Bhattarai N., Matsen F.A., Zhang M., PEG-Grafted Chitosan as an Injectable Thermoreversible Hydrogel, Macromol. Biosci., 2005, 5, 107-111.

[26] Ohya S., Matsuda T., Poly (N-isopropylacrylamide) (PNIPAM)- grafted gelatin as thermoresponsive three-dimensional artificial extracellular matrix: molecular and formulation parameters vs. cell proliferation potential, J. Biomater. Sci. Polym., 2005, 16, 809-827.

[27] Shaker D.S., Shaker M.A., Klingner A., Hanafy M.S., In situ thermosensitive Tamoxifen citrate loaded hydrogels: An effective tool in breast cancer loco-regional therapy, J. Drug Deliv. Sci. Tec., 2016, 35, 155-164.

[28] Lee K.Y., Mooney D.J., Alginate: properties and biomedical applications, Prog. Polym. Sci., 2012, 37, 106-126.

[29] Patil J.S., Kamalapur M., Marapur S.C., Kadam, D.V., Ionotropic gelation and polyelectrolyte complexation: the novel techniques to design hydrogel particulate sustained, modulated drug delivery system: a review, Dig. J. Nanomater. Bios., 2010, 5, 241-248.

[30] Crompton K.E., Goud J.D., Bellamkonda R.V., Gengenbach T.R., Finkelstein D.I., Horne M.K., Forsythe J.S., Polylysine-functionalised thermoresponsive chitosan hydrogel for neural tissue engineering, Biomaterials, 2007, 28, 441-449.

[31] Berger J., Reist M., Mayer J.M., Felt O., Peppas N.A., Gurny R., Structure and interactions in covalently and ionically crosslinked chitosan hydrogels for biomedical applications, Eur. J. Pharm. Biopharm., 2004, 57, 19-34.

[32] Elisseeff J., McIntosh W., Anseth K., Riley S., Ragan P., Langer R., Photoencapsulation of chondrocytes in poly (ethylene oxide)-based semi-interpenetrating networks, J. Biomed. Mater. Res., 2000, 51, 164-171.

[33] Varghese S., Hwang N.S., Canver A.C., Theprungsirikul, P., Lin D.W., Elisseeff J., Chondroitin sulfate based niches for chondrogenic differentiation of mesenchymal stem cells, Matrix Biol., 2008, 27, 12-21.

[34] Leach J.B., Bivens K.A., Patrick C.W., Schmidt C.E., Photocrosslinked Hyaluronic Acid Hydrogels: Natural, Biodegradable Tissue Engineering Scaffolds, Biotechnol. Bioeng., 2003, 82, 578-589.

[35] Drury J.L., Mooney D.J., Hydrogels for tissue engineering: scaffold design variables and applications, Biomaterials, 2003, 24, 4337-4351.

[36] Brandl F., Sommer F., Goepferich A., Rational design of hydrogels for tissue engineering: Impact of physical factors on cell behaviour, Biomaterials, 2007, 28, 134-146.

[37] Ruel-Gariépy E., Leroux J.C., In situ-forming hydrogels-review of temperature-sensitive systems, Eur. J. Pharm. Biopharm., 2004, 58, 409-426.

[38] Jeong B., Kim S.W., Bae Y.H., Thermosensitive sol-gel reversible hydrogels, Adv. Drug Deliv. Rev., 2002, 54, 37-51.

[39] Dimatteo R., Darling N.J., Segura T., In situ forming injectable hydrogels for drug delivery and wound repair, Adv. Drug Deliv. Rev., 2018, 127, 167-184.

[40] Yang J.A., Yeom J., Hwang B.W., Hoffman A.S., Hahn S.K., In situ-forming injectable hydrogels for regenerative medicine, Prog. Polym. Sci., 2014, 39, 1973-1986.

[41] Norouzi M., Nazari B., Miller D.W., Injectable hydrogel-based drug delivery systems for local cancer therapy, Drug Discov. Today, 2016, 21, 1835-1849.

[42] Wu X., He C., Wu Y., Chen X., Synergistic therapeutic effects of Schiff's base cross-linked injectable hydrogels for local co-delivery of metformin and 5-fluorouracil in a mouse colon carcinoma model, Biomaterials, 2016, 75, 148-162.

[43] On N.H., Miller D.W., Transporter-based delivery of anticancer drugs to the brain: improving brain penetration by minimising drug efflux at the blood-brain barrier, Curr. Pharm. Des., 2014, 20, 1499-1509.

[44] Mishra V., Kesharwani P., Dendrimer technologies for brain tumour, Drug Discov. Today, 2016, 21, 766-778.

[45] Kim D.Y., Kwon D.Y., Kwon J.S., Park J.H., Park S.H., Oh H.J., Kim J.H., Min B.H., Park K., Kim M.S., Synergistic anti-tumour activity through combinational intratumoural injection of an in-situ injectable drug depot, Biomaterials, 2016, 85, 232-245.

[46] Fourniols T., Randolph L.D., Staub S., Vanvarenberg K., Leprince J.G., Préat V., des Rieux A., Danhier F., Temozolomide-loaded photopolymerisable PEG-DMA-based hydrogel for the treatment of glioblastoma, J. Control. Release, 2015, 210, 95-104.

[47] Singh M., Kundu S., Reddy M. A., Sreekanth V., Motiani R.K., Sengupta S., Srivastava A., Bajaj A., Injectable small molecule hydrogel as a potential nanocarrier for localised and sustained in vivo delivery of doxorubicin, Nanoscale, 2014, 6, 12849-12855.

[48] Leitinger B., Hohenester E., Mammalian collagen receptors, Matrix Biol., 2007, 26, 146-155.

[49] Kadler K.E., Baldock C., Bella J., Boot-Handford R.P, Collagens at a glance, J. Cell Sci., 2007, 120, 1955-1958.

[50] Lotz C., Schmid F.F., Oechsle E., Monaghan M.G., Walles H., Groeber-Becker F., Cross-linked Collagen Hydrogel Matrix Resisting Contraction to Facilitate Full-Thickness Skin Equivalents, ACS Appl. Mater. Interfaces, 2017, 9, 20417-20425.

[51] Orban J.M., Wilson L.B., Kofroth J.A., El-Kurdi M.S., Maul T.M., Vorp D.A., Crosslinking of collagen gels by transglutaminase, J. Biomed. Mater. Res. A., 2004, 68, 756-762.

[52] Ahmed T.A., Dare E.V., Hincke M., Fibrin: a versatile scaffold for tissue engineering applications, Tissue Eng. B., 2008, 14, 199-215.

[53] Hynes S., McGregor L., Rauch M., Lavik E., Photopolymerised poly(ethylene glycol)/poly(L-lysine) hydrogels for the delivery of neural progenitor cells J. Biomater. Sci. Polym., 2007, 18, 1017-1030.

[54] Pakulska M.M., Ballios B.G., Shoichet M.S., Injectable hydrogels for central nervous system therapy, Biomed. Mater., 2012, 7, 1-13.

[55] Matricardi P., Alhaique F., Coviello T., Polysaccharide hydrogels: Characterisation and biomedical applications, 2016, Pan Stanford Publishing, chapter 14, 499-507.

[56] Coviello T., Matricardi P., Marianecci C., Alhaique F., Polysaccharide hydrogels for modified release formulations, J. Control. Release, 2007, 119, 5-24.

[57] d'Ayala G.G., Malinconico M., Laurienzo P., Marine derived polysaccharides for biomedical applications: chemical modification approaches, Molecules, 2008, 13, 2069-2106.

[58] Qiu Y., Park K., Environment-sensitive hydrogels for drug delivery, Adv. Drug Deliv. Rev., 2012, 64, 49-60.

[59] Paulino A.T., Campese G.M., Favaro S. L., Guilherme M.R., Tambourgi E.B., Muniz E.C., Water absorption profile of PAAm-co-PNIPAAm/chitosan hydrogel with sandwich-like morphology, E-polymers, 2007, 122.

[60] Giri T.K., Thakur A., Alexander A., Ajazuddin, Badwaik H., Tripathi D.K., Modified chitosan hydrogels as drug delivery and tissue engineering systems: present status and applications, Acta Pharm. Sinic. B, 2012, 2, 439-449.

[61] Papadimitriou S.A., Achilias D.S., Bikiaris D.N., Chitosan-g-PEG nanoparticles ionically crosslinked with poly (glutamic acid) and tripolyphosphate as protein delivery systems, Int. J. Pharm., 2012, 430, 318-327.

[62] Ruel-Gariepy E., Chenite A., Chaput C., Guirguis S., Leroux J.C., Characterisation of thermosensitive chitosan gels for the sustained delivery of drugs, Int. J. Pharm., 2000, 203, 89-98.

[63] Chenite A., Chaput C., Wang D., Combes C., Buschmann M.D., Hoemann C.D., Leroux J.C., Atkinson B.L., Binette F., Selmani A., Novel injectable neutral solutions of chitosan form biodegradable gels in situ, Biomaterials, 2000, 21, 2155-2161.

[64] Mi F.L., Tan Y.C., Liang H.F., Sung H.W., In vivo biocompatibility and degradability of a novel injectable-chitosan-based implant, Biomaterials, 2002, 23, 181-191.

[65] Mi F.L., Tan Y.C., Liang H.C., Huang R.N., Sung H.W., In vitro evaluation of a chitosan membrane cross-linked with genipin, J. Biomater. Sci. Polym. Edn., 2001, 12, 835-850.

[66] Van Woensel M., Wauthoz N., Rosière R., Mathieu V., Kiss R., Lefranc F., Steelant B., Dilissen E., Van Gool S.W., Mathivet T., Gerhardt H., Amighi K., De Vleeschouwer S., Development of siRNA-loaded chitosan nanoparticles targeting Galectin-1 for the treatment of glioblastoma multiforme via intranasal administration, J. Control. Release, 2016, 227, 71-81.

[67] Kim S., Nishimoto S.K., Bumgardner J.D., Haggard W.O., Gaber M.W., Yang Y., A chitosan/beta-glycerophosphate thermo-sensitive gel for the delivery of ellagic acid for the treatment of brain cancer, Biomaterials, 2010, 31, 4157-4166.

[68] Augst A.D., Kong H.J., Mooney D.J, Alginate hydrogels as biomaterials, Macromol. Biosci., 2006, 6, 623-633.

[69] Lee K.Y., Mooney D.J., Alginate: properties and biomedical applications, Prog. Polym. Sci., 2012, 37,106-126.

[70] Costa M.J., Marques A.M., Pastrana L.M., Teixeira J.A., Sillankorva S.M., Cerqueira M.A., Physicochemical properties of alginate-based films: Effect of ionic crosslinking and mannuronic and guluronic acid ratio, Food Hydrocolloid, 2018, 81, 442-448.

[71] Rowley J.A., Madlambayan G., Mooney D.J., Alginate hydrogels as synthetic extracellular matrix materials, Biomaterials, 1999, 20, 45-53.

[72] Kievit F.M., Florczyk S.J., Leung M.C., Veiseh O., Park J.O., Disis M.L., Zhang M., Chitosan-alginate 3D scaffolds as a mimic of the glioma tumour microenvironment, Biomaterials, 2010, 31, 5903-5910.

[73] Highley C.B., Prestwich G.D., Burdick J.A., Recent advances in hyaluronic acid hydrogels for biomedical applications, Curr. Opin. Biotechnol., 2016, 40, 35-40.

[74] Margolis R.U., Margolis R.K., Chang L.B., Preti C., Glycosaminoglycans of brain during development, Biochemistry, 1975, 14, 85-88.

[75] Benarroch E.E., Extracellular matrix in the CNS, Neurology, 2015, 85, 1-11.

[76] Naor D., Interaction Between Hyaluronic Acid and Its Receptors (CD44, RHAMM) Regulates the Activity of Inflammation and Cancer, Front. Immunol., 2016, 7, 39-42.

[77] Xu X., Jha A., Harrington D., Farach-Carson M., Jia X., Hyaluronic acid-based hydrogels: from a natural polysaccharide to complex networks, Soft Matter, 2012, 8, 3280-3294.

[78] Bulpitt P., Aeschlimann D., New strategy for chemical modification of hyaluronic acid: Preparation of functionalized derivatives and their use in the formation of novel biocompatible hydrogels, J. Biomed. Mater. Res., 1999, 47, 152-169.

[79] Seidlits S., Khaing Z., Petersen R., Nickels J., Vanscoy J., Shear J., Schmidt C., The effects of hyaluronic acid hydrogels with tunable mechanical properties on neural progenitor cell differentiation, Biomaterials, 2010, 31, 3930-3940.

[80] Florczyk S., Wang K., Jana S., Wood D., Sytsma S., Sham J., Kievit F., Zhang M., Porous chitosan-hyaluronic acid scaffolds as a mimic of glioblastoma microenvironment ECM, Biomaterials, 2013, 34, 10143-10150.

[81] Sarkar N., Walker L.C., Hydration–dehydration properties of methylcellulose and hydroxypropyl methylcellulose, Carbohyd. Polym., 1995, 27, 177-185.

[82] Li L., Thangamathesvaran P.M., Yue C.Y., Tam K.C., Hu X., Lam Y.C., Gel Network Structure of Methylcellulose in Water, Langmuir, 2001, 17, 8062-8068.

[83] Stalling S.S., Akintoye S.O., Nicoll S.B., Development of photocrosslinked methylcellulose hydrogels for soft tissue reconstruction, Acta Biomater., 2009, 5, 1911-1918.

[84] Zhuo F., Liu X., Gao Q., Wang Y., Hu K., Cai Q., Injectable hyaluronan-methylcellulose composite hydrogel crosslinked by polyethylene glycol for central nervous system tissue engineering, Mater. Sci. Eng. C., 2017, 81, 1-7.

[85] Kim E.J., Choi J.S., Kim J.S., Choi Y.C, Cho Y.W., Injectable and Thermosensitive Soluble Extracellular Matrix and Methylcellulose Hydrogels for Stem Cell Delivery in Skin Wounds, Biomacromolecules, 2016, 17, 4-11.

[86] Prestwich G.D., Marecak D.M., Marecek J.F., Vercruysse K.P., Ziebell M.R., Controlled chemical modification of hyaluronic acid: synthesis, applications, and biodegradation of hydrazide derivatives, J. Control. Release, 1998, 53, 93-103.

[87] Tate M.C., Shear D.A., Hoffman S.W., Stein D.G., LaPlaca M.C., Biocompatibility of methylcellulose-based constructs designed for intracerebral gelation following experimental traumatic brain injury, Biomaterials, 2001, 22, 1113-1123.

[88] Liu Z., Yao P., Injectable thermo-responsive hydrogel composed of xanthan gum and methylcellulose double networks with shear thinning property, Carbohyd. Polym., 2015, 132, 490-498.

[89] Gupta D., Tator C.H., Shoichet M.S., Fast-gelling injectable blend of hyaluronan and methylcellulose for intrathecal, localised delivery to the injured spinal cord, Biomaterials, 2006, 27, 2370-2379.

[90] Sironen R.K., Tammi M., Tammi R., Auvinen P.K., Anttila M., Kosma V.M., Hyaluronan in human malignancies, Exp. Cell Res., 2011, 317, 383-391.

[91] Burdick J.A., Prestwich G.D., Hyaluronic Acid Hydrogels for Biomedical Applications, Adv. Mater., 2011, 23, 41-56.

[92] Schanté C., Zuber G., Herlin C., Vandamme T., Chemical modifications of hyaluronic acid for the synthesis of derivatives for a broad range of biomedical applications, Carbohyd. Polym., 2011, 85, 469-489.

[93] Collins M.N., Birkinshaw C., Physical properties of crosslinked hyaluronic acid hydrogels, J. Mater. Sci. Mater. Med., 2008, 19, 3335-3343.

[94] Stern R., Asari, A., Sugahara, K., Hyaluronan fragments: An information-rich system, Eur. J. Cell Biol., 2006, 85, 699-715.

[95] Shoham N., Sasson A.L., Lin F.H., Benayahu D., Haj-Ali R., Gefen A., The mechanics of hyaluronic acid/adipic acid dihydrazide hydrogel: towards developing a vessel for delivery of preadipocytes to native tissues, J. Mech. Behav. Biomed. Mater., 2013, 28, 320-331.

[96] Motokawa K., Hahn S.K., Nakamura T., Miyamoto H., Shimoboji T., Selectively crosslinked hyaluronic acid hydrogels for sustained release formulation of erythropoietin, J. Biomed. Mater. Res A, 2006, 78, 459-465.

[97] Hu M.H., Yang K.C., Sun Y.H., Chen Y.C., Yang S.H., Lin F.H., In situ forming oxidised hyaluronic acid/adipic acid dihydrazide hydrogel for prevention of epidural fibrosis after laminectomy, Eur. Cell. Mater., 2017, 34, 307-320.

[98] Nakajima N., Ikada Y., Mechanism of amide formation by carbodiimide for bioconjugation in aqueous media, Bioconjug. Chem., 1995, 6, 123-130.

[99] Zhao D., Zhao X., Zu Y., Preparation, characterisation, and in vitro targeted delivery of folate-decorated paclitaxel-loaded bovine serum albumin nanoparticles, Int. J. Nanomed., 2010, 5, 669-677.

[100] Huang B.X., Kim H.Y., Dass C., Probing three-dimensional structure of bovine serum albumin by chemical cross-linking and mass spectrometry, J. Am. Soc. Mass Spectrom., 2004, 15, 1237-1247.

[101] Curry S., Mandelkow H., Brick P., Franks N., Crystal Structure of Human Serum Albumin Complexed with Fatty Acid Reveals an Asymmetric Distribution of Binding Sites, Nature Struct. Biol., 1998, 5, 827-835.

[102] Wells M.R., Kraus K., Batter D.K., Blunt D.G., Weremowitz J., Lynch S. E., Antoniades H.N., Hansson H.A., Gel Matrix Vehicles for Growth Factor Application in Nerve Gap Injuries Repaired with Tubes: A Comparison of Biomatrix, Collagen, and Methylcellulose, Exp. Neurol., 1997, 146, 395-402.

[103] Tate M.C., Shear D.A., Hoffman S.W., Stein D.G., LaPlaca M.C., Biocompatibility of methylcellulose-based constructs designed for intracerebral gelation following experimental traumatic brain injury, Biomaterials, 2001, 22, 1113-1123.

[104] Kobayashi K., Huang C., Lodge T. P., Thermoreversible Gelation of Aqueous Methylcellulose Solutions, Macromolecules, 1999, 32, 7070-7077.

[105] Kato T., Yokoyama M., Takahashi A., Melting temperatures of thermally reversible gels IV. Methylcellulose-water gels, Colloid Polym. Sci., 1978, 256, 15-21.

[106] Guvendiren M., Lu H.D., Burdick J.A., Shear-thinning hydrogels for biomedical applications, Soft Matter, 2012, 8, 260-272.

[107] Bueno V.B., Bentini R., Catalani L.H., Siqueira Petri D.F., Synthesis and swelling behaviour of xanthan-based hydrogels, Carbohyd. Polym., 2013, 92, 1091-1099.

[108] Roy A., Comesse S., Grisel M., Hucher N., Souguir Z., Renou F., Hydrophobically modified xanthan: an amphiphilic but not associative polymer, Biomacromolecules, 2014, 15, 1160-1170.

[109] Dyondi D., Webster T.J., Banerjee R., A nanoparticulate injectable hydrogel as a tissue engineering scaffold for multiple growth factor delivery for bone regeneration, Int. J. Nanomed., 2013, 8, 47-59.

[110] Mayol L., De Stefano D., De Falco F., Carnuccio R., Maiuri M.C., De Rosa G., Effect of hyaluronic acid on the thermogelation and biocompatibility of its blends with methylcellulose, Carbohyd. Polym., 2014, 112, 480-485.

[111] Tuladhar A., Morshead C.M., Shoichet M.S., Circumventing the blood–brain barrier: Local delivery of cyclosporin A stimulates stem cells in stroke-injured rat brain, J. Control. Release, 2015, 215, 1-11.

Chapter 3: Physicochemical and mechanical characterisation of hydrogels

3.1 Introduction

The characterisation of the physicochemical and mechanical properties is of paramount importance in determining if a material is suitable for a specific application. As discussed in Chapter 2, hydrogels are crosslinked hydrophilic polymeric networks that can be prepared by physical or chemical crosslinking methods using natural or synthetic polymers. In the former case, hydrogels are prepared by the formation of physical bonds including hydrogen bonds, ionic or hydrophobic interactions. In the latter case, hydrogels are formed by covalent interactions between the polymer chains. The physicochemical and mechanical properties of the hydrogels are highly dependent on the method of crosslinking. Thus, the characterisation of the properties of hydrogels designed for biomedical applications is imperative.

The aim of this chapter is to present and discuss several experimental methods devoted to the characterisation of the fabricated hydrogels as described in Chapter 2. In particular, attention will be focused on the determination of swelling degree, characterisation of the surface morphology using Scanning Electron Microscopy, determination of the enzymatic degradation rate in vitro conditions, characterisation of the mechanical properties using oscillatory rheology and investigation of the drug release profile.

3.1.1 Characterisation of hydrogels by Fourier-Transform Infrared Spectroscopy

FT-IR (Fourier-Transform Infrared Spectroscopy) is a useful technique for the study of structural changes occurring during the formation of hydrogels. The principle of FT-IR spectroscopy relies on the fact that chemical bonds can be excited and absorb infrared light at specific frequencies which are typical of the chemical bonds. On the interaction with the infrared light, chemical bonds stretch, contract or bend in a specific wavelength as mentioned above. This technique is widely used to investigate structural changes and confirm the presence of specific chemical groups in the hydrogel network compared to the main components of the hydrogel [1], [2].

3.1.2 Scanning Electron Microscopy

To date, various imaging techniques have been applied to study the surface morphology of the hydrogels. Hydrogels morphology is usually investigated by Scanning Electron Microscopy (SEM) [3] as shown in Figure 3.1. This type of microscopy provides a large depth of field and a range of magnifications that allow to easily focus on the area of interest. SEM provides information about the surface morphology and the porosity of the hydrogels. In addition, estimation of the pore size and relevant information regarding the homogeneity or heterogeneity of the hydrogel network can be obtained from SEM analysis. SEM under standard operating conditions, requires lyophilisation of the hydrogel sample. Although, this method is not representative of the native state of the hydrogel structure, it is indicative of the morphology and porosity of the hydrogel. Lyophilised hydrogels are

usually coated before SEM analysis, in order to increase the conductivity of the sample. Typically, hydrogels are coated with a thin layer of a conductive metal such as chromium, palladium or gold.

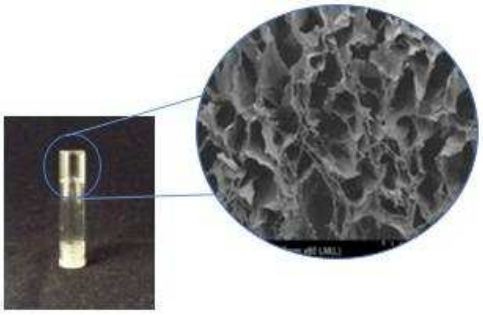

Figure 3.1: Schematic illustration of HA-based hydrogel and SEM image of its lyophilised form. SEM provides information on the morphology and porosity of the hydrogels.

3.1.3 Swelling studies

Due to their hydrophilic nature, hydrogels have the capacity to absorb large quantity of water, without the dissolution of the polymer as illustrated in Figure 3.2. During swelling, hydrogels as hydrophilic crosslinked structures continue to demonstrate properties of solid-like materials and present physical features similar to soft tissues [4]. The swelling capacity of hydrogels is highly dependent on the crosslinking density which defines the space within the polymer network [5]. In the case of highly crosslinked hydrogels, the swelling behaviour is mainly controlled by the diffusion mechanism.

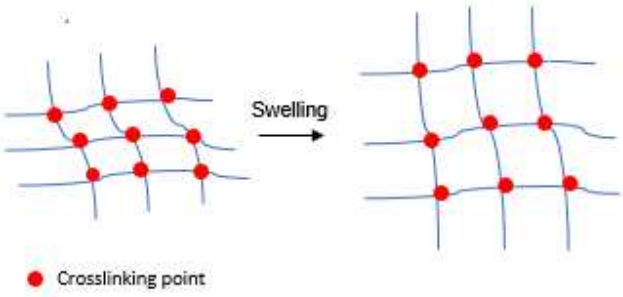

Figure 3.2: Schematic illustration of swelling process in a hydrogel network. Hydrogels due to their hydrophilic nature, absorb large amount of water and expand their volume.

The swelling process depends on the rate at which the water molecules can diffuse into the hydrogel network structure. For example, low crosslinked hydrogels demonstrate higher swelling capacity compared to high crosslinked hydrogels. In a polysaccharide-based hydrogel, the swelling is a consequence of the interactions between polymer and water molecules which increase with the hydrophilicity of the macromolecules. The swelling characteristics are of paramount importance in biomedical and pharmaceutical applications particularly in case of injectable hydrogels for tissue engineering. The determination of the swelling equilibrium of a hydrogel is necessary as uncontrollable swelling can cause adverse effects on the area of the injection.

When equilibrium in swelling of a hydrogel is reached, two opposing forces take place according to Flory and Rechner [6]. One is the thermodynamic force derived from the polymer-water mixing and contributes to swelling. While the other is the elastic force stored in the polymer chains preventing the swelling [7]. At equilibrium swelling, these two forces balance each other as described in the following equation (1) in terms of total Gibbs free energy:

$$\Delta G_{total} = \Delta G_{elastic} + \Delta G_{mixing} \qquad (1)$$

$\Delta G_{elastic}$ arises from the elastic forces stored in the polymer chains and ΔG_{mixing} comes from the mixing of the polymer chains with the water molecules. In terms of chemical potential, the above equation is modified as bellow (2):

$$\Delta \mu_{total} = \Delta \mu_{elastic} + \Delta \mu_{mixing} \qquad (2)$$

In the equilibrium state, the chemical potential outside the hydrogel should be equal with that inside the hydrogel. In the case of ionic hydrogels, an additional chemical potential factor is taken into consideration due to the contribution of the charged groups in the network as shown in the following equation (3):

$$\Delta \mu_{total} = \Delta \mu_{elastic} + \Delta \mu_{mixing} + \Delta \mu_{ionic} \qquad (3)$$

In ionic hydrogels, the swelling capacity is higher and increases with the content of the ionic groups. The number of counterions in the hydrogel network increase and this results in an additional osmotic pressure which induces swelling [8]. The extent of swelling of ionic hydrogels depends on the pH of the aqueous media. Cationic hydrogels demonstrate increased swelling in low pH, whereas anionic hydrogels swell more in aqueous media of high pH due to chain repulsion. The swelling behaviour of polymers with hydrophilic backbone and hydrophobic moieties is dependent on the temperature. This group of hydrogels present sensitivity to temperature due to the presence of hydrogen bonds and hydrophobic interactions which are highly dependent on the temperature [9].

3.1.4 Degradation of hydrogels

Besides swelling, the degradation of the hydrogels is another noteworthy characteristic which it should be taken into consideration for hydrogels designed for biomedical applications [10]. Controlled degradation of hydrogels is significantly desirable for biomedical purposes including soft tissue engineering and controlled drug release. Hydrogels are usually composed of degradable polymeric backbones, degradable side groups or degradable crosslinkers which allow degradation of the matrix. The degradation rate of the hydrogel network is highly dependent on the specific application of the degradable hydrogel. For example, for controlled release applications rapid degradation of the drug loaded hydrogel results in rapid release of the drug which can be desirable or cytotoxic depending on the specific application. Regarding tissue engineering applications, the degradation rate of the matrix should match the rate of formation of the new tissue [11]. The

degradation rate of the scaffold can be controlled by increasing the crosslinking density which results in smaller pores size, increased mechanical resistance and consequently slower degradation. Smaller pores size limits the penetration of the degradable molecules such as enzymes within the hydrogel due to lower diffusion rate [12]. The rate of degradation can be influenced by the chemical nature of the degradable crosslinker which is conjugated to the hydrogel. For example, side chains conjugated to the polymer backbone including esters, amides or ethers can be degraded by hydrolysis [13].

Hydrogels can be degraded by several mechanisms including enzymatic degradation, hydrolysis, reversible click reactions or light-mediated degradation as summarised in Figure 3.3. As mentioned previously, synthetic hydrogels containing esters linkages can be degraded by hydrolysis resulting in the formation of a carboxylic acid and an alcohol. The degradation rate can be controlled by the crosslinking density of the network and the local pH. Thomas et al synthesised biodegradable crosslinkers with lactate and glycolate esters. The fabricated hydrogels consisted of specific ratio of crosslinker incorporated into 2-hydroxypropyl methacrylate (HPMA). The authors investigated the hydrolytic degradation rate of the hydrogels at 37 °C and at pH 7.4 by varying the number of lactate and glycolate residues [14]. Enzymatic degradation mainly takes place in hydrogels composed of natural polymers or proteins. The mechanism of the enzymatic hydrolysis is based on the catalytic role of the enzyme during the hydrolysis process. For instance, HA-based hydrogels can be degraded in the presence of hyaluronidase which is an enzyme that catalyses the hydrolysis of C–O, C–N and C–C bonds. Lee et al studied the degradation of HA-tyramine hydrogel for protein delivery in the presence of hyaluronidase [15]. Sustained release of the protein was observed due to the subsequent degradation of the hydrogel network by hyaluronidase.

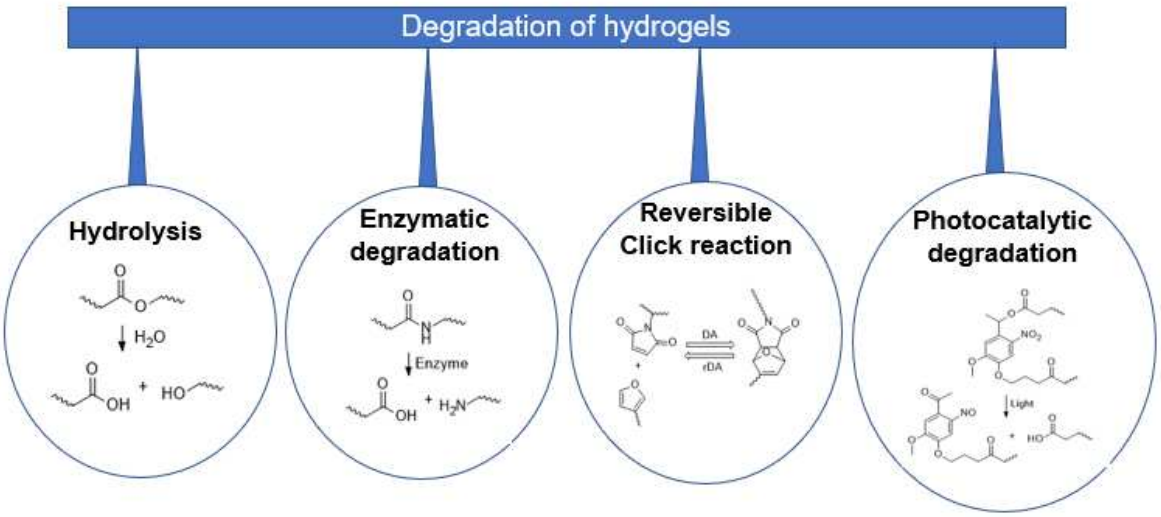

Figure 3.3: Different degradation mechanisms of hydrogels mainly including hydrolysis, enzymatic degradation, reversible click reactions and light-mediated degradation.

The hydrogel degradation rate can be influenced by the enzyme concentration, pH, temperature and the crosslinking density. Enzymatically degradable hydrogels are mainly used for targeted drug delivery applications due to the fact that the enzyme concentration is highly dependent on the cell or tissue type, which acts as trigger for the drug release. Hydrogels susceptible to enzymatic hydrolysis have also been used in bone regeneration and wound healing [16], [17].

Degradation of synthetic hydrogels induced by reversible click reactions is not commonly used despite their advantages on the formation of the hydrogel network. Reversible click reactions mainly include Michael-type addition and retro Diels-Alder cycloreversion which are necessary tools to mediate hydrogel degradation. Baldwin et al studied the degradation of heparin-based hydrogels prepared by Michael-type addition reaction between the multifunctional PEG-thiols and maleimide -functionalised heparin [18]. Interestingly, they found that the pKa and the hydrophobicity of the scaffolds affected the degradation rate of the fabricated hydrogels. In another study, Koehler et al investigated the degradation of PEG-maleimide-based hydrogels loaded with furan functionalised peptides derived from the thermally reversible Diels-Alder reaction of the furan and maleimide moieties. Specifically, dexamethasone was conjugated to the furan containing peptide and sustained release was achieved by the mediated degradation of the hydrogel [19].

Furthermore, hydrogels can be degraded by light-mediated hydrolysis. This degradation mechanism requires hydrogels composed of photoresponsive moieties. Anseth et al prepared photodegradable PEG-based hydrogels consisted of an acrylated nitrobenzyl ether-derived moiety attached to PEG-bis-amine or amine-terminated peptides [20]. The hydrogel photodegradation was induced by UV irradiation. In another complementary study, Anseth et al studied the light-mediated degradation of disulfide-bonded PEG hydrogels using photoinitiators [21]. By irradiation, free radicals were formed from the photoinitiator which resulted in the fragmentation of the disulfide bonds and the subsequent hydrogel degradation.

Degradation on hydrogels can occur by surface or bulk erosion which depends on the crosslinking density and the water diffusion rate or diffusion of the enzymes to the interior of the hydrogel [22]. Surface degradation occurs when water molecules or enzymes can not penetrate the hydrogel network due to the high crosslinking density, whereas bulk erosion takes place when the hydrogel network is degraded homogeneously. Degradation by bulk erosion is more common on hydrogels prepared at lower crosslinking densities.

In summary, degradation of hydrogels can be induced by different mechanisms in accordance to their specific application. Ideally, the degradation rate of the hydrogels should be controlled and tunable in order to avoid the formation of by-products that are not biocompatible and eliminate any potential side effects. Importantly though, balance between the biodegradability and the mechanical properties

including the elastic modulus and the integrity of the scaffold is critical and fundamental to ensure the functionality of the hydrogel within a desirable period of time.

3.1.5 Oscillatory rheology

The mechanical characterisation of the hydrogels is of significant importance for several biomedical applications such as tissue engineering. The viscoelastic properties of the hydrogels should be similar to the mechanical characteristics of the tissue since cellular activities such as adhesion, migration and differentiation are highly dependent on the stiffness of the matrix as it will be discussed further in Chapter 4. Undoubtedly, hydrogels are complex systems and their rheological characterisation is an important tool to investigate further their properties and evaluate their potential use in various biomedical applications. Their hydrophilic nature contributes to their soft and viscoelastic consistency which closely resembles the mechanical properties of the living tissues [23], [24]. The structural, chemical and mechanical properties of the hydrogels can be addressed to mimic those of the native ECM, rendering these scaffolds as attractive biomaterials in tissue engineering as stated above.

A wide range of methods have been used to characterise the mechanical properties of the hydrogels including tensile testing for the characterisation of the elastic behaviour, dynamic mechanical analysis for the characterisation of viscoelastic materials and compression tests [25], [26]. For tensile tests, hydrogel samples are cut and prepared into dumb-bell shape and placed between two clamps. The applied force and elongation of the hydrogel are used to obtain stress-strain curve and determine several mechanical properties including Young's modulus. In compression testing which can be confined or unconfined, hydrogels are usually prepared as round samples and compressed between two non-porous plates as shown in Figure 3.4. Similar to the tensile test, the force and the displacement for the compression of hydrogels are recorded and the Young's modulus can be determined. During dynamic mechanical analysis a sinusoidal stress is applied and the strain in the material is measured, allowing to determine the complex modulus of the hydrogels.

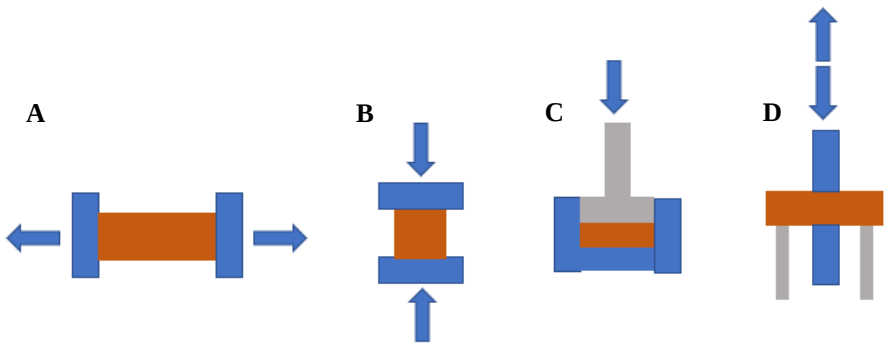

Figure 3.4: Schematic illustration of different types of set up for the mechanical characterisation of hydrogels. **A.** Tensile testing, **B.** Compression, **C.** Confined compression and **D.** Dynamic mechanical analysis.

Oscillatory rheology is another mechanical characterisation technique that enables the investigation of the viscoelastic properties of the hydrogels. The principle of oscillatory rheology relies on measuring the stress response induced by a sinusoidal shear deformation on hydrogel at a constant frequency [27]. The shear strain and the oscillatory stress in the hydrogel sample are described by the following equations (4) and (5) respectively:

$$\gamma = \gamma^{o}\sin(\omega t) \qquad (4)$$

$$\tau = \tau^{o}\sin(\omega t+\delta) \qquad (5)$$

where ω is the applied angular frequency, γ is the shear strain, t is the time, τ is the oscillatory stress and δ is the phase angle. In particular, the mechanical response in terms of shear stress is obeyed to the following equation (6):

$$\tau = G'(\omega)\gamma\sin(\omega t) + G''(\omega)\gamma\cos(\omega t) \qquad (6)$$

and it is intermediate between an ideal pure elastic solid (obeying to the Hooke's law) and an ideal pure viscous liquid (obeying to the Newton's law). G′ is the storage or elastic modulus and provides information on the elasticity or the energy stored in the material during the deformation. In contrast, G′′ is the loss or viscous modulus which describes the viscous behaviour of the material or the energy lost as heat. The ratio between the viscous and elastic modulus defines the loss tangent or the loss factor as described in the following equation (7):

$$\tan\delta = G''/G' \qquad (7)$$

The phase angle δ is equal to 90° for a viscous material, 0° for an elastic material and $0° < \delta < 90°$ for viscoelastic materials. For the determination of the viscoelastic behaviour of a material, amplitude strain sweep experiments are performed at a constant oscillation frequency. Regarding viscoelastic materials such as hydrogels, both moduli are constant and strain dependent across a range of strain values. However, above a critical strain value γ, viscoelastic materials lose their nondestructive behaviour. Amplitude sweep tests establish the region of the linear viscoelastic behaviour and the determination of the strain value at which a crossover of both moduli G′ and G′′ takes place and the viscous behaviour prevails as shown in Figure 3.5.

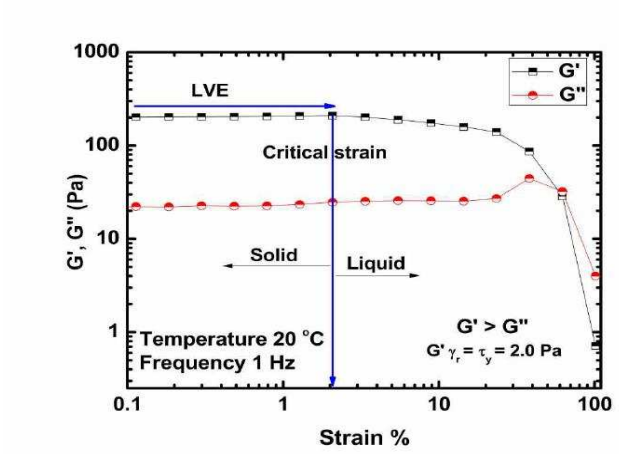

Figure 3.5: Amplitude strain sweep experiment of a hydrogel. Typical strain dependence of the viscoelastic moduli within the linear viscoelastic regime. Above a critical strain value, crossover of both moduli takes place and the viscous behaviour is predominant. Adapted from Matricardi et al [28].

The viscoelastic behaviour of the hydrogels is also characterised by the frequency dependence of the viscoelastic moduli G′ and G′′. On this account, frequency sweep experiments are performed by keeping constant the oscillation amplitude strain within the linear viscoelastic regime (LVR) determined by performing the amplitude sweep experiment. In case of hydrogels, both G′ and G′′ are almost independent of the frequency and the elastic modulus G′ is much higher than the viscous modulus G′′ as demonstrated in Figure 3.6. Frequency sweep experiments have proved to be indicative for the determination of the viscoelastic behaviour and measurement of the stiffness of the hydrogels.

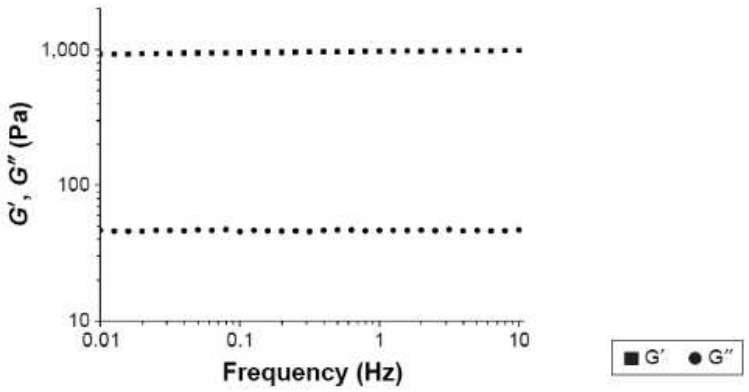

Figure 3.6: Frequency sweep experiment of a hydrogel conducted in a range of frequency from 0.01 to 10 Hz keeping constant the LVR strain amplitude determined by performing the amplitude sweep experiment before. Both moduli are almost independent of the frequency and G′ is greater than G′′ confirming the viscoelastic behaviour of the hydrogel. Adapted from Liu et al [29].

3.1.6 Differential Scanning Calorimetry

The thermal behaviour of hydrogels is mostly assessed by Differential Scanning Calorimetry (DSC). As illustrated in Figure 3.7, DSC is a thermoanalytical technique which allows the measurement of the difference in the amount of heat required to increase the temperature of a sample and a reference as function of temperature [30]. Both the sample and the reference are maintained at the same temperature during the experiment. Depending on the physical transformations such as phase transitions that a sample can undergo, more or less heat is required to it than to the reference to keep both at the same temperature. Specifically, when more heat flow to the sample is required then an endothermic phase transition takes place, while when less heat flow is required to increase the temperature of the sample, an exothermic transition exists.

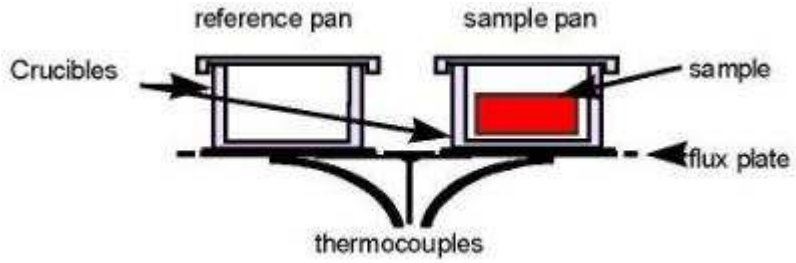

Figure 3.7: Illustration of set-up of a differential scanning calorimeter. It consists of a sample pan where the sample is inserted and a reference pan (typically empty). Both pans are maintained at the same temperature during the experiment. Adapted from reference [31].

The thermal transitions that are usually observed in hydrogels, take place due to the presence of different states of water in the hydrogel network. In particular, two types of water can be found in the hydrogel, including the bound and the free state. The bound state exists when the water molecules are attached to the polymer chain via the development of hydrogen bonds, while in the free water state the molecules of the water do not interact with the polymer [32]. In case of hydrogels, DSC thermographs usually demonstrate changes in the glass transition temperature (T_g) for crosslinked hydrogels and their initial components. For example, Zarzyka et al studied the influence of crosslinker on the glass transition temperature of poly (N-isopropylacrylamide) and poly (sodium acrylate) hydrogels using conventional DSC [33]. They observed that the addition of crosslinker resulted in an increase in the T_g of the polymer and the transition range became broader. These observations can be explained by the fact that the higher crosslinking density reduces the mobility of the polymer chains, so that the glass transition temperature increases. Overall, conventional DSC is employed for the characterisation of the thermal behaviour of hydrogels.

3.1.7 Drug release from hydrogels

In the last decades, due to their unique tunable physical properties, hydrogels have attracted significant attention in drug delivery applications for the treatment of various types of cancer [34]. Their hydrophilic nature and the structural resemblance to tissues contribute to their potential as drug delivery carriers. Their highly porous structure also allows the loading of drugs into the hydrogel matrix which protects labile drugs from degradation. In addition, their controllable degradability induces the release of the encapsulated drugs in a controlled manner which is highly dependent on the diffusion coefficient of the drug molecules through the hydrogel network. The release of the therapeutic agents from hydrogels mainly occurs through three main mechanisms including diffusion-controlled mechanism, swelling-controlled and degradation-controlled mechanism [35], as illustrated in Figure 3.8.

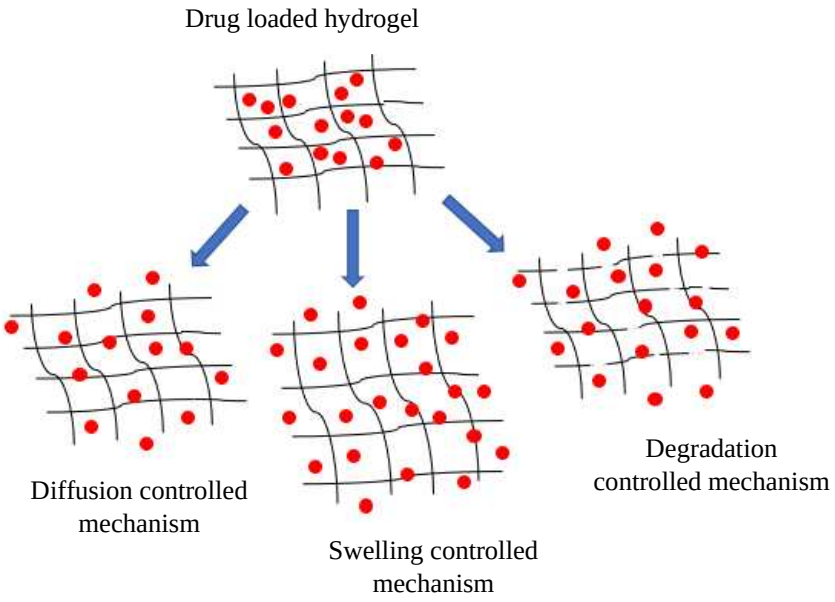

Figure 3.8: Illustration of mechanisms of drug release from hydrogels. Drugs can be released from hydrogels through three main mechanisms including diffusion-controlled, swelling-controlled and degradation-controlled mechanism with subsequent diffusion.

The diffusion is the most common mechanism for the controlled release of drugs from hydrogels. The rate of drug release depends on the crosslinking density and external stimuli such as pH and temperature. In addition, the mesh size of the hydrogels determines how quickly a drug can be released from the 3D matrix. The mesh size is the distance between the crosslinking points. For example, when the mesh size is larger than the drug molecule then the small drug molecules can be easily diffused through the network. In swelling-controlled mechanism, the diffusion of the drug is faster than the swelling. As discussed previously, the extent of the swelling is dependent on the crosslinking density of the hydrogels and the presence of external stimuli including ionic strength, pH and temperature. For example, in oral drug delivery systems the pH responsive swelling of the hydrogel is of paramount importance. In the acidic environment of the stomach, the swelling of the

drug loaded hydrogels is negligible which protects the physically entrapped drug. In contrast, in neutral pH in intestinal tract a dramatic increase in swelling occurs which allows the burst release of the drug. The pH triggered release is also used in the targeted drug delivery to tumours where the environment is more acidic than the normal tissues which allows the diffusion of the drug to the tumour site. The controlled network degradation is another mechanism that induces the release of drugs entrapped in hydrogels. Hydrogels can be degraded by hydrolysis or enzymatic activity that results in the increase of mesh size allowing the drugs to diffuse out from the hydrogel network.

3.2 Experimental

3.2.1 Materials

Hyaluronic acid (hyaluronic acid sodium salt, from Streptococcus equiv. MW = 1.5 -1.8 mDa) and ADH (MW = 174.2 Da) were purchased from Sigma Aldrich. EDC (MW = 191.7 Da) and Sulfo-NHS (MW = 217.13 Da) were purchased from TCI Europe. BSA (lyophilised powder, ≥ 98 %, MW = 66 kDa), Methyl cellulose (MC, suitable for cell culture, MW = 14 kDa, viscosity: 15 cPs, D.S 1.5-1.9), Xanthan gum (XG) from Xanthomonas campestris (viscosity = 800-1200 cPs) all were purchased from Sigma Aldrich. Phosphate buffer saline tablets were purchased from Fischer Scientific. Hyaluronidase from bovine testes was purchased from Sigma Aldrich. Human Urotensin UII (MW = 1388. 55 Da) and FITC-UII (MW = 1777 Da) were purchased from PolyPeptide Laboratories. TMZ (MW = 194.15 Da) and DOX HCl (MW = 543.52 Da) were purchased from Sigma Aldrich. Aluminum crucibles with lids for DSC analysis were purchased from Mettler Toledo.

3.2.2 Methods

3.2.2.1 Lyophilisation- Preparation of xerogels

Lyophilisation or freeze-drying has been extensively used for the fabrication of porous hydrogels in order to characterise further their morphology, structure and thermal properties [36], [37]. This method involves rapid cooling of the hydrogel which results in thermodynamic instability within the network. Subsequently, the solvent which is mostly water is removed by sublimation under vacuum. In particular, hydrogels were prepared according to the protocol described in section 2.2.2.1 in small centrifuge tubes and then frozen by immersion in a block of dry ice at a temperature of -78.5 °C. The frozen hydrogels were lyophilised using a ScanVac Coolsafe freeze drier and xerogels were obtained. Xerogels are defined as solids formed by dehydration of hydrogels and they usually retain high porosity [38].

3.2.2.2 FT-IR spectroscopy

The structure of the fabricated hydrogels was investigated by using a Perkin Elmer Spectrum One FT-IR spectrometer equipped with a diamond crystal. FT-IR spectra of the xerogels were obtained in the range of wavenumber from 4000 to 750 cm^{-1} by accumulating 16 scans.

3.2.2.3 SEM characterisation

The microstructure of the hydrogels was evaluated using a FEG-SEM Hitachi SU8030 Scanning Electron Microscope. Prior to the SEM analysis, hydrogels were previously swollen in PBS for at least 24 h at 37 °C and subsequently were frozen by immersion in a block of dry ice in order to preserve the microstructure of the hydrogels. Frozen gels were then fractured with a scalpel and immediately placed on a lyophiliser for freeze drying as described in section 3.2.2.1. Subsequently, the hydrogels were affixed to a metal stub with carbon film and they were sputter-coated with a layer of gold for 2 minutes at 25 mA prior to observation using an Edwards Au coater. Several magnifications using accelerating voltage of 1.0 kV were obtained to study further the surface morphology and pore sizes of the hydrogels.

3.2.2.4 Swelling studies on hydrogels

The swelling behaviour of the hydrogels was calculated using a conventional gravimetric method [39]. Preweighed hydrogels prepared in glass vials with inner diameter 12 mm were immersed in phosphate buffered saline solution (pH 7.4 or pH 6.0) and incubated at 37 °C for predetermined periods of time. At regular time intervals, the solution was taken out carefully from the swollen hydrogels and wiped with a filter paper for the removal of any excess of PBS and then weighed in order to measure the weight of the swollen hydrogels. The % Swelling Degree (% SD) was calculated using the following equation (8):

$$\% \text{ SD} = W_s\text{-}W_i/W_i \times 100 \qquad (8)$$

where W_s is the weight of the swollen hydrogel at a specific time and W_i is the initial dry weight of the hydrogel. The measurements were carried out in triplicate and the results represent the mean with the corresponding standard deviation.

3.2.2.5 *In vitro* enzymatic degradation of hydrogels

In vitro degradation of hydrogels was performed by incubation with hyaluronidase enzyme solution at various concentrations at 37 °C. Briefly, hydrogels were incubated in PBS at 37 °C for 2 h. After this period, hydrogels were weighed (W_i) and subsequently incubated in 1 mL of PBS with hyaluronidase at 37 °C under constant agitation in a horizontal orbital shaker at 180 rpm. Weight loss of the initially weighed hydrogels was monitored as a function of incubation time in PBS at 37 °C. At specified time intervals, the hydrogels were weighed (W_f) and the degradation medium was replaced with freshly prepared enzyme solution every 24 h. In order to verify the absence of degradation phenomena due to temperature, a degradation test was carried out on control samples mixed with PBS and incubated at 37 °C. Measurements were performed until complete degradation of the hydrogels was observed. All measurements were performed in triplicate. The degradation was expressed as percentage of hydrogel mass and calculated using the following equation (9):

$$\% \text{ hydrogel mass} = W_f / W_i \times 100 \qquad (9)$$

where W_i is the initial weight of the hydrogel before degradation and W_f is the weight of the hydrogel after degradation at regular time intervals.

3.2.2.6 Differential Scanning Calorimetry

DSC analysis was performed on hydrogels using a conventional differential scanning calorimeter Mettler Toledo DSC 822. Samples were precisely weighed into an aluminum pan on which aluminum lid with a centrally pierced hole was crimped. The thermal analysis of the xerogels was obtained as the temperature was increased from room temperature to 280 °C at a rate of 10 °C/min under N_2.

3.2.2.7 Oscillatory rheology

The rheological characterisation of the hydrogels was performed on an Anton Paar MCR 302 Rheometer using a cylinder (relative, ST10-4V-8.8/97.5) geometry configuration. Hydrogels were prepared into glass vials with inner diameter 14 mm as lower geometry and then the upper geometry (relative cylinder) was inserted into the hydrogel. Before each measurement, a delay time of 30 minutes was set as for the hydrogel to settle. Oscillatory rheological measurements were performed to measure the viscoelastic moduli of the hydrogels as a function of shear strain (Amplitude sweep experiment) and as a function of frequency (Frequency sweep experiment). All the experiments were performed at 37 °C and this temperature was controlled throughout the measurement. The measurements were repeated at least three times to ensure reproducibility.

Amplitude sweep test: Amplitude sweep experiments were performed to determine the LVR of deformation for each hydrogel at increasing shear strains. Strain scans were performed from 0.01 to 100 % with a constant frequency of 1 Hz. The critical strain was determined as the point at which the elastic modulus G′ starts to deviate from linearity and crosses over the viscous modulus G′′. The average elastic modulus G′ and viscous modulus G′′ were plotted vs amplitude strain. Subsequently, frequency sweep experiments were carried out at a strain amplitude that was within the LVR.

Frequency sweep test: Frequency sweep experiments were performed at a strain amplitude determined by the amplitude sweep test. Typically, angular frequencies in the range of 0.1 to 100 rad/sec were tested at a strain amplitude of 5 % for all hydrogels. The average elastic modulus G′ and viscous modulus G′′ were plotted vs angular frequency.

3.2.2.8 DOX loading into HA-ADH hydrogels

DOX was loaded in hydrogels prepared at different crosslinking densities. Briefly, different crosslinking densities of hydrogels were investigated and the detailed protocol for one of them is described below. HA sodium salt (10 mg, 6.25 nmoles) was dissolved in 800 µL of sterile deionised water and EDC (0.26 mg, 1.35 µmoles) was dissolved in 100 µL of deionised water and added at different molar ratios to the aqueous HA solution. EDC was allowed to dissolve before the addition

of ADH. The crosslinker ADH (0.25 mg, 1.43 μmoles) was then dissolved in 100 μL of deionised water and was added to the activated HA solution. Subsequently, 75 μL of DOX solution of concentration 0.66 mg/mL was added on the gelator solution. The final concentration of the drug in the hydrogels was 0.05 mg/mL. Gelation was allowed to occur with gentle vortexing. In order to ensure the drug encapsulation efficiency, DOX-loaded hydrogels were washed with PBS three times and the UV absorbance of the washing solutions was measured at 484 nm for the detection of DOX.

3.2.2.9 TMZ loading into HA-ADH hydrogels

Hydrogels of different crosslinking densities were loaded with various concentrations of TMZ. Hydrogels were prepared as described earlier in section 3.2.2.8 and 75 μL of TMZ solution of concentration 0.64 mg/mL were loaded on the gelator solution. The final concentration of TMZ in the hydrogels was 0.05 mg/mL. Gelation was allowed to occur with gentle vortexing. As mentioned previously, in order to confirm the TMZ encapsulation efficiency, the UV absorbance of the washing solutions was measured at 330 nm.

3.2.2.10 DOX loading into HA-BSA hydrogels

DOX was loaded into HA-BSA hydrogels at different crosslinking densities. Briefly, the protocol for the preparation for one of them is described below. HA sodium salt (6.0 mg, 3.75 nmoles) was dissolved in 800 μL of deionised water. Then HA was activated with EDC (2.0 mg, 10.4 μmoles) and sulfo-NHS (0.5 mg, 2.3 μmoles) mixture in a molar ratio 4:1 in 200 μL of deionised water and the pH was adjusted at pH 6.0 with the addition of HCl 0.1 M before the reaction with the protein. The reaction was allowed to proceed for 2 minutes by vortexing. BSA (3 mg, 45.4 nmoles) was added as a powder to the activated HA solution for further crosslinking. Subsequently, 75 μL of DOX solution of concentration 0.66 mg/mL was mixed with the precursor solution and gelation was allowed to occur with gentle vortexing. The final concentration of DOX in the hydrogels was 0.05 mg/mL.

3.2.2.11 TMZ loading into HA-BSA hydrogels

Hydrogels were prepared as described in section 3.2.2.10 and then 75 μL of TMZ solution of concentration 0.64 mg/mL was loaded on the gelator solution. The final concentration of TMZ in the hydrogels was 0.05 mg/mL. Gelation was allowed to occur with gentle vortexing. As mentioned previously, in order to confirm the TMZ encapsulation efficiency, the UV absorbance of the washing solutions was measured at 330 nm.

3.2.2.12 Drug release from hydrogels

Drug loaded hydrogels were prepared in glass vials as described in the previous sections and they were allowed to settle for 24 h so the drug could be diffused throughout the hydrogel network. Subsequently, 1 mL of PBS as release medium was slowly added on hydrogels and they were incubated at 37 °C under constant agitation in a horizontal orbital shaker at 180 rpm. The

concentration of the drug in the release medium was measured at regular time intervals. To satisfy the perfect sink conditions, the release medium was replaced with fresh PBS pre-equilibrated at 37 °C at each time point. The concentration of the released drug was determined by measuring the absorbance of the release medium using quartz cuvettes at 484 nm for DOX and 330 nm for TMZ. The UV absorbance was measured using a WPA Biowave II spectrophotometer. The concentration of the drug released from the hydrogel was determined using a calibration curve plotted for DOX and TMZ respectively (refer to the Appendix). All measurements were performed in triplicate and the % drug release was calculated using the following equation (10):

$$\% \text{ Drug release} = \frac{\text{Concentration of released drug}}{\text{Initial concentration of drug in the hydrogel}} \times 100 \qquad (10)$$

3.2.2.13 Release of FITC-Urotensin (FITC-UII) from HA-ADH hydrogels

Four different crosslinking densities of HA-ADH hydrogels were prepared in the wells of a 96-well plate and the detailed protocol for the preparation for one of them is described below. HA sodium salt (10.0 mg, 6.25 nmoles) was dissolved in 800 µL of deionised water and EDC (0.26 mg, 1.35 µmoles) was dissolved in 100 µL of deionised water and added at different molar ratios to the aqueous HA solution. EDC was allowed to dissolve before the addition of ADH. The crosslinker ADH (0.25 mg, 1.43 µmoles) was subsequently dissolved in 100 µL of deionised water and was added to the activated HA solution. A stock solution of the FITC labelled UII of concentration 10^{-4} M was prepared in DMEM and added in the gelator solution. The final concentration of the labelled chemoattractant in the hydrogel was 10^{-6} M. The pH of the solution was adjusted at pH 5.5 with the addition of HCl 0.1 M. Gelation was allowed to occur with gentle vortexing. Subsequently, FITC-UII loaded hydrogels were incubated in DMEM at 37 °C. The release of the FITC-UII from the hydrogels was determined by measuring the fluorescence of the release medium at 520 nm at predetermined time intervals. The concentration of the FITC-UII released from the hydrogel was determined using a calibration curve and the % release was calculated as described in the previous section.

3.3 Results and Discussion

3.3.1 Physicochemical and mechanical characterisation of HA-ADH hydrogels

HA-based hydrogels demonstrate advantageous properties such as high biocompatibility, easy manipulation, biodegradability and tunable viscoelastic properties which lead to their various applications in biomedical and pharmaceutical field. In the present work, inexpensive and relatively simple methods of preparation of biocompatible hydrogels based on HA were proposed and they were extensively discussed in Chapter 2. Hydrogels were prepared by chemical crosslinking of the

carboxylic groups of HA with ADH or BSA as crosslinkers. HA of high molecular weight was chosen and it was crosslinked with different molar ratios of ADH and EDC resulting in the fabrication of self-supporting hydrogels. HA was activated by EDC/sulfo-NHS chemistry and then crosslinked with BSA resulting in the formation of self-supporting hydrogels. Subsequently, the physicochemical and mechanical properties of the fabricated hydrogels were characterised and they will be discussed further in the following sections.

3.3.1.1 FT-IR spectroscopy of HA-ADH hydrogels

The fabrication of HA-based hydrogels requires chemical modification of the HA backbone in order to obtain chemically and mechanically robust materials. Herein, HA-based hydrogels were obtained by crosslinking HA with EDC as a carboxyl-activating agent and ADH as a crosslinker. As mentioned previously, HA-ADH hydrogels were obtained at different crosslinking densities and they are summarised in Table 3.1. Crosslinked hydrogels were analysed by FT-IR using Transmittance mode. FT-IR spectroscopy of the fabricated xerogels was conducted using a Perkin Elmer Spectrum One FT-IR spectrometer equipped with a diamond crystal. FT-IR spectroscopy was performed in order to investigate the structural changes of the prepared hydrogels compared to the structure of their precursor components and the nature of formation of the new bonds.

Table 3.6: HA-ADH hydrogels prepared at different crosslinking densities.

Sample abbreviation	HA (mg/nmole)	ADH (mg/μmole)	EDC (mg/μmole)
L1	10.0/6.25	0.25/1.43	0.26/1.36
L2	10.0/6.25	0.5/2.87	0.6/3.12
H1	10.0/6.25	2.5/14.3	2.6/13.6
H2	10.0/6.25	3.5/20.1	3.6/18.8

As discussed in Chapter 2, during the crosslinking reaction, ADH with its free amine groups acts a nucleophile which attacks the activated by EDC carboxyl groups of HA resulting in the formation of amide bonds. The successful crosslinking of the activated HA with the amine moieties of the ADH was confirmed by FT-IR spectroscopy. The corresponding IR spectra of the hydrogel precursor components and HA-ADH xerogel demonstrated similar patterns as shown in Figure 3.9.

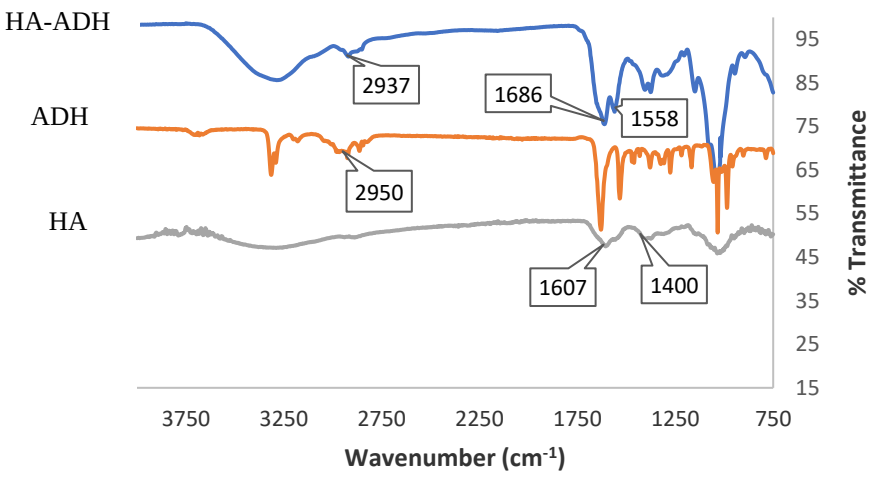

Figure 3.9: FT-IR spectra of HA, ADH and HA-ADH xerogel. FT-IR spectroscopy was performed in order to investigate the structural changes of the prepared hydrogels compared to the structure of their precursor components and the nature of formation of new bonds. Graph adapted from Chapter 2.

As depicted above, HA presents spectral characteristics typical for carboxylates anions, which are mainly absorption bands at 1607 and 1400 cm^{-1} assigned to the asymmetric and symmetric stretching vibrations of the carboxylate anions respectively. In the IR spectrum of the HA-ADH xerogel, the main differences compared to that of the unmodified HA are the appearance of the characteristic peaks of the ADH modification at 1686 cm^{-1} which corresponds to the formation of the amide bond (C=O stretch of secondary amide) and 1558 cm^{-1} (N-H bend of amide) [40]. Moreover, in the HA-ADH spectrum, the absorption band at 2937 cm^{-1} represents the -CH_2 stretching vibrations from the ADH moiety.

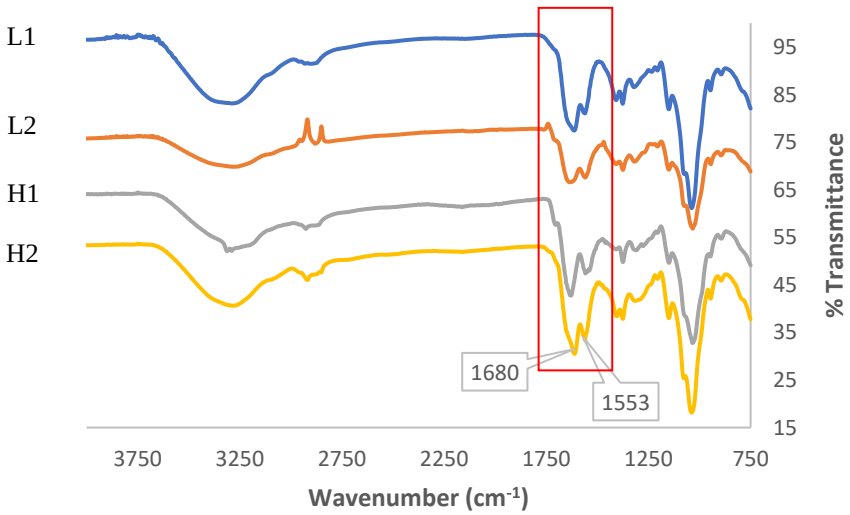

Figure 3.10: FT-IR spectra of HA-ADH xerogels prepared at different crosslinking densities.

As shown in Figure 3.10, the FT-IR spectra of the HA-ADH xerogels are identical and they presented the main characteristic peaks arising from the HA backbone and the crosslinker, confirming the

successful crosslinking reaction in all cases. In addition, it is noteworthy that the increasing concentration of the crosslinker did induce a slight increase in the intensity of the peaks as highlighted in the above graph corresponding to the formation of the amide bond at approximately 1680 and 1550 cm^{-1}.

3.3.1.2 Characterisation of surface morphology and porosity of HA-ADH hydrogels

The scanning electron microscopy has been commonly used to provide important information regarding the morphology of the hydrogels and their characteristic network structure [41]. In addition, estimation of the average pore size and relevant information regarding the homogeneity or heterogeneity of the hydrogel network can be obtained from SEM. The average pore size, the pore size distribution and the pore interconnections are important factors of a hydrogel matrix that are usually difficult to determine. Hydrogels prior to SEM analysis, are usually freeze-dried and xerogels are obtained for the characterisation of their surface morphology. Despite the fact that freeze-drying method is not representative of the native state of the hydrogel network, it is indicative of the morphology and porosity of the hydrogel.

Herein, HA-ADH hydrogels prepared at different crosslinking densities and they were flash frozen by immersion in dry ice. Frozen hydrogels were fractured into thin slices and lyophilised. Lyophilised hydrogels were coated before SEM analysis, in order to increase the conductivity of the samples and achieve better resolution. Thin slices of lyophilised hydrogels were coated with a thin layer of gold under Argon atmosphere as shown in Figure 3.11.

Figure 3.11: Representative photo of lyophilised hydrogels coated by a thin layer of Au prior to SEM analysis. Hydrogels were coated using an Edwards Au coater under Ar atmosphere.

Figure 3.12 shows the representative scanning electron micrographs of the obtained xerogels prepared at four different crosslinking densities. The SEM images were taken at three different magnifications as shown below. The xerogels derived from the crosslinking of HA with different concentrations of the crosslinker, presented a disorganised interconnected porous structure. Porous structure of hydrogels plays a critical role in swelling kinetics as these scaffolds allow penetration of water or surrounding media through the interconnected pores [42]. The porosity of scaffolds plays important role in cell adhesion and proliferation due to the fact that effective distribution of cell nutrients and metabolic waste is ensured through the 3D network. In the literature, it has been reported that the optimal pore size of scaffolds for potential application in tissue engineering should

be in a range of 20-200 μm. Scaffolds with these pore sizes allow cells sufficient space to grow and adhere to the matrix [43]. Moreover, besides the pore size, cell diffusion or migration within a scaffold is controlled by the total porosity, interconnectivity of the pores and the surface area of the scaffold.

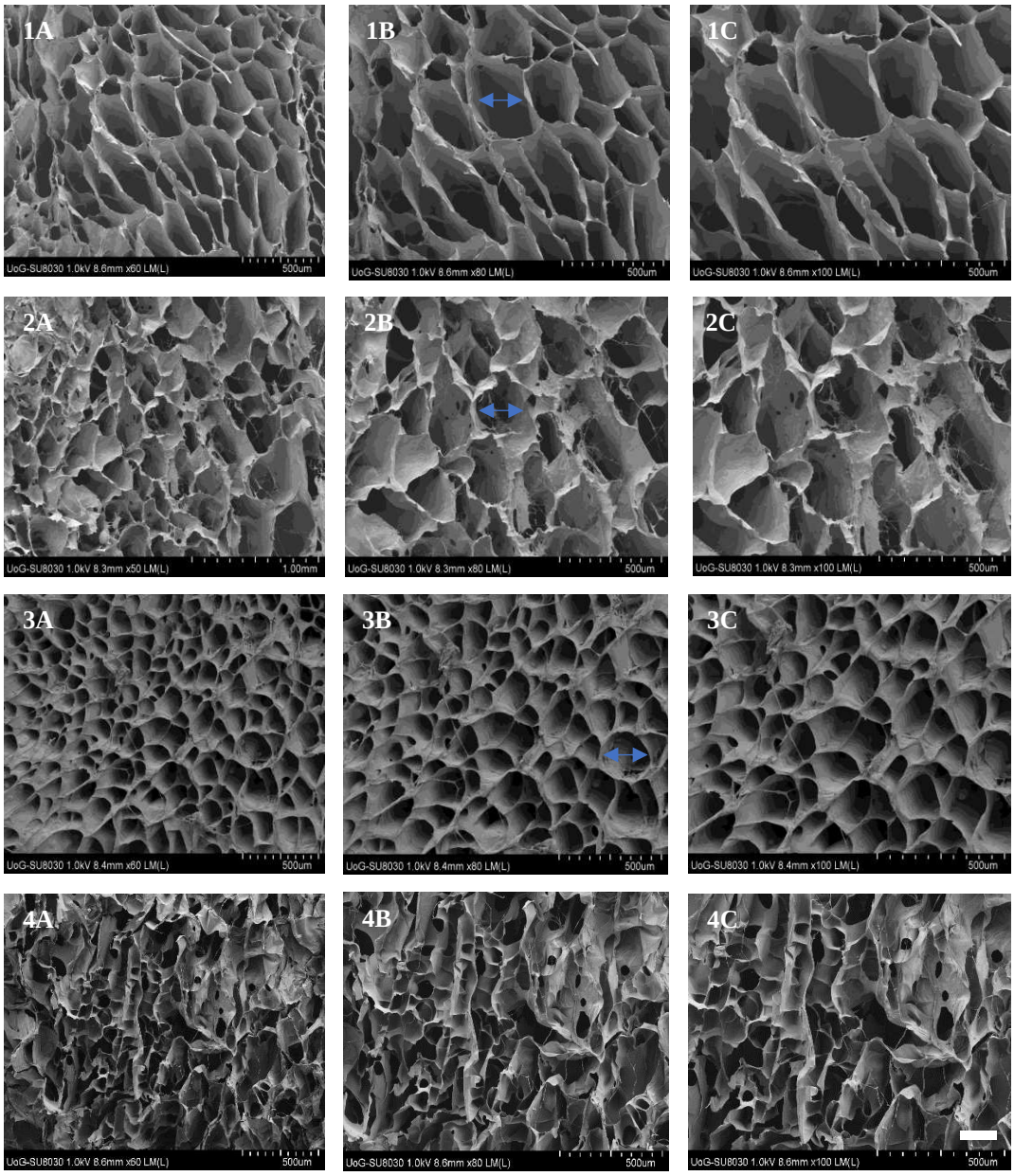

Figure 3.12: SEM images of HA-ADH xerogels prepared at different crosslinking densities. **1A-1B-1C**: L1 hydrogel at magnifications 60x, 80x and 100x respectively, **2A-2B-2C**: L2 hydrogel at magnifications 60x, 80x and 100x respectively, **3A-3B-3C**: H1 hydrogel at magnifications 60x, 80x and 100x respectively and **4A-4B-4C**: H2 hydrogel at magnifications 60x, 80x and 100x respectively. Scale bar: 500 μm.

An interconnected network of pores improves the diffusion of oxygen and nutrients across the scaffold and multiple studies have proposed that highly porous scaffolds facilitate cell seeding and migration throughout the matrix [44]. As presented in Figure 3.12, all xerogels were characterised

by interconnected porous structure with various pore sizes. As expected, the hydrogel network was significantly denser with increasing concentration of the crosslinker. As mentioned in section 3.2.2.3, hydrogels were previously swollen in PBS for at least 24 h at 37 °C and the determination of the pore sizes of the lyophilised scaffolds was performed. The pore size was measured by choosing at least 15 random pores from each image and measuring their diameter (as highlighted with arrows in the above images) using ImageJ software. The histogram in Figure 3.13 summarises the pore size of xerogels prepared at different crosslinking densities.

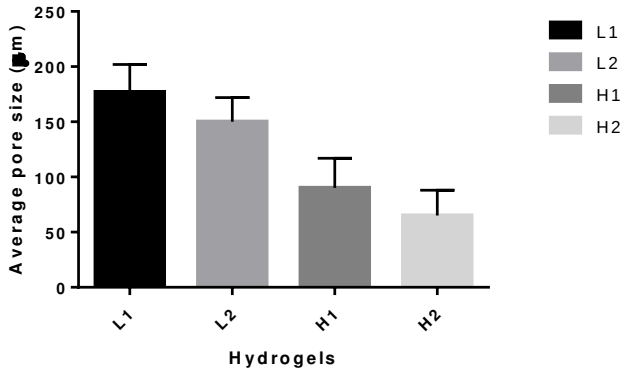

Figure 3.13: Histogram summarises the average pore size of HA-ADH xerogels prepared at different crosslinking densities. Error bars were calculated by the corresponding standard deviation.

Hydrogels prepared at low crosslinking densities L1 and L2, presented an average pore size of 177 and 150 μm respectively after swelling. In contrast, increasing concentration of ADH resulted in significantly smaller pores ranging from 90 to 65 μm for H1 and H2 crosslinking densities respectively. It can be concluded that the pore size of the hydrogels was highly dependent on the crosslinking density. Increasing degree of crosslinking resulted in increased pore density in the hydrogel network. Zhang et al reported a similar effect of the crosslinking density on the porous network of the fabricated PNIPAAm hydrogels [45]. The authors observed that the least crosslinked hydrogels presented larger average pore sizes compared to those with the highest level of crosslinking.

3.3.1.3 Swelling studies of HA-ADH hydrogels

Hydrogels are 3D dimensional crosslinked hydrophilic polymeric networks that are able to swell in an aqueous environment without dissolution [46]. The swelling profile of hydrogels is of paramount importance in biomedical and pharmaceutical applications particularly in case of injectable hydrogels for tissue engineering. The determination of the swelling degree of hydrogels designed for brain tissue engineering applications is a critical factor that should be taken into consideration. As stated in Chapter 2, hydrogels can obtain different shapes and fill amorphous cavities in the brain due to their tunable mechanical characteristics. The volume of the injectable hydrogel and the extent of the swelling capacity should be precisely determined before the injection due to the limited open space within the brain tissue. For example, a large volume of hydrogel can present adverse effects on the

brain by increasing the pressure in the brain tissue surrounding the hydrogel. However, swelling in the brain is less of a concern due to the fact that the increase in overall size because of swelling is restricted by the counter forces of the surrounding tissue [47].

Generally, the swelling capacity of hydrogels under biological conditions renders them an interesting class of materials for biomedical applications including tissue engineering and drug delivery. The determination of the swelling characteristics of hydrogels is significant because the equilibrium degree of swelling affects their surface and mechanical properties. The degree to which a polymer network is able to swell is determined by the equilibrium between the elastic retractive forces arised from the polymer chains and the thermodynamic interaction of the polymer with the solvent molecules.

In the present work, the swelling behaviour of the crosslinked hydrogels was calculated using a conventional gravimetric method [39]. Hydrogels prepared at different crosslinking densities in glass vials with inner diameter 12 mm were initially weighed (W_i) and afterwards, they were immersed in PBS at pH 7.4 and incubated at 37 °C for predetermined periods of time. At regular time intervals, the PBS solution was removed carefully from the swollen hydrogels, wiped with a filter paper and then the weight of the swollen hydrogels was measured (W_s). Subsequently, the % SD of the hydrogels was calculated using the following equation (8):

$$\% \text{ SD} = W_s\text{-}W_i/W_i \times 100 \qquad (8)$$

After 3 days of incubation in PBS, the low crosslinking densities of hydrogels L1 and L2 presented an equilibrium % swelling degree of 42 and 24 respectively, while H1 and H2 hydrogels reached equilibrium after 24 h, presenting a mass increase of 6 and 5 % respectively as shown in Figure 3.14. After 6 days of incubation, low crosslinked hydrogels started undergoing hydrolytic degradation, whereas hydrogels prepared at high crosslinking densities remained relatively stable until the completion of the experiment. Also, hydrogels were prepared in the presence of the chemoattractant at a concentration of 10^{-8} M and as shown in Figure 3.14, it did not induce significant change in the % SD. It can be concluded that the swelling profile of the hydrogels highly depends on the crosslinking density of the hydrogels. The lower the crosslinking density of the hydrogels, the higher % SD, whereas high crosslinking densities resulted in lower % SD due to the increased density of the crosslinks which was also confirmed by the SEM analysis of the lyophilised networks. The increase of the concentration of ADH resulted in an increase of the crosslinking density which decreased the swelling capacity of the hydrogels.

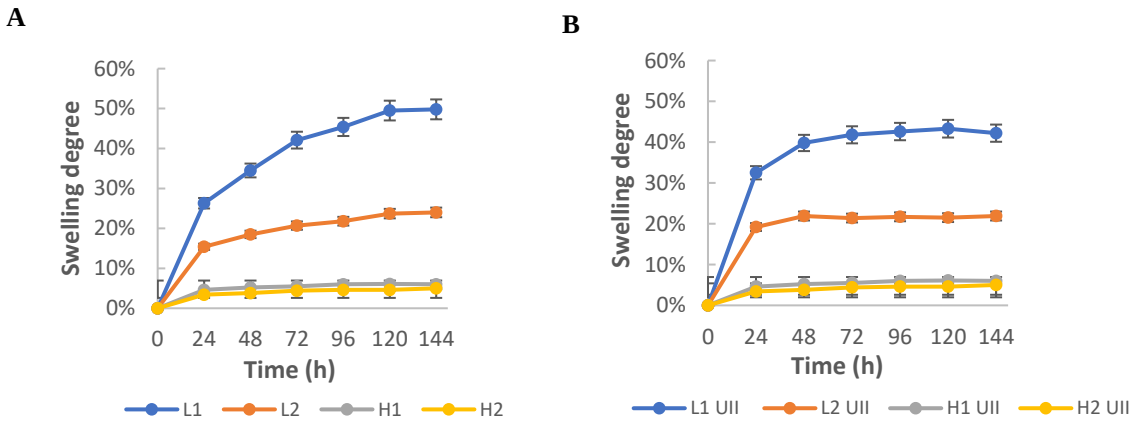

Figure 3.14: A. Swelling profile of hydrogels prepared at different crosslinking densities in PBS at 37 °C. **B.** Swelling profile of hydrogels prepared at different crosslinking densities loaded with the chemoattractant UII in PBS at 37 °C. The presence of UII did not affect the % SD of the hydrogels. The data represent the average of triplicate with the corresponding error bar calculated by standard deviation.

Similarly, Zhou et al observed that the pore size and the swelling ratio of the fabricated composite gelatin-hyaluronic acid hydrogels decreased with increasing concentration of EDC as crosslinker [48]. The higher crosslinking density renders the network more dense resulting in smaller pores which limits the diffusion of the solvent into the scaffolds. Highly crosslinked hydrogels started to undergo syneresis on the fourth day of the swelling experiment. Syneresis is defined as the shrinkage of the hydrogels with simultaneous release of water that results in a lower volume of hydrogel. Typically, syneresis increases with increasing crosslinking density and can be problematic for applications that the gel integrity is important [49].

Moreover, the effect of the pH and ionic strength on the swelling behaviour of the HA-ADH hydrogels prepared at low crosslinking densities L1 and L2 was investigated, as demonstrated in Figure 3.15. Hydrogels were prepared as described earlier in glass vials and immersed in DMEM (pH 7.8), PBS (pH 7.4) and deionised water (pH 6.5). They were incubated at 37 °C and the % SD was determined after specific time intervals as described previously. The degree of crosslinking in the polymer network is critical as it determines the extent of swelling as discussed earlier. As summarised in the graphs below, HA-ADH hydrogels swelled extensively in water reaching equilibrium % SD of 96 and 48 for the L1 and L2 crosslinking densities respectively after 48 h of incubation. This extensive swelling is facilitated by the presence of the free carboxylic acid groups on the HA backbone, which strongly interact with water molecules. The swelling behaviour of the HA-based hydrogels depends on the pH and it is closely related to the ionisation of the carboxylic acid groups. These groups are easily ionisable and sensitive to changes of pH and ionic strength [50].

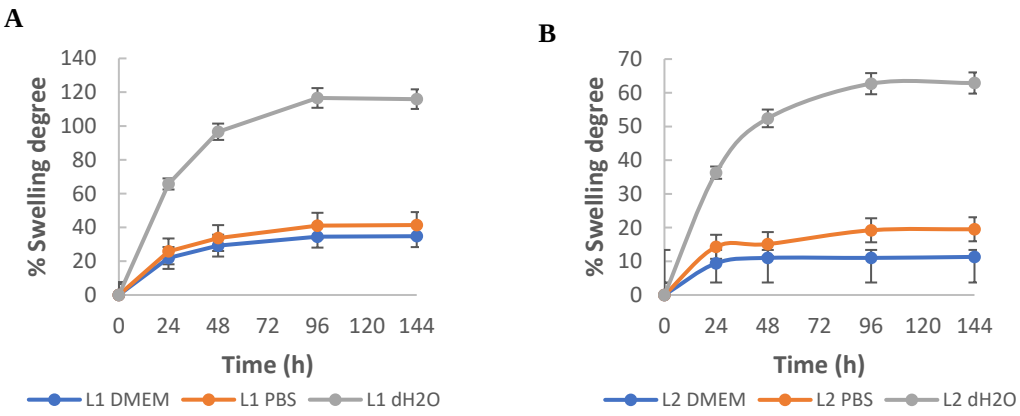

Figure 3.15: Swelling profile of hydrogels prepared at low crosslinking densities in solutions of various pH and ionic strength. Changes in the pH and ionic strength presented significant effect on the swelling behaviour of the hydrogels. The data represent the average of triplicate with the corresponding error bar calculated by standard deviation.

The ionisation of the carboxyl group induces the formation of anionic carboxylate moieties and consequently the electrostatic repulsion between the negatively charged groups results in dramatic swelling behaviour. In case of DMEM and PBS, lower swelling was observed for both hydrogels as it can be confirmed by the following photos of the swollen hydrogels in Figure 3.16. The concentration of the cations in the buffer increased which resulted in lower osmotic pressure due to decreased anion-anion electrostatic repulsion.

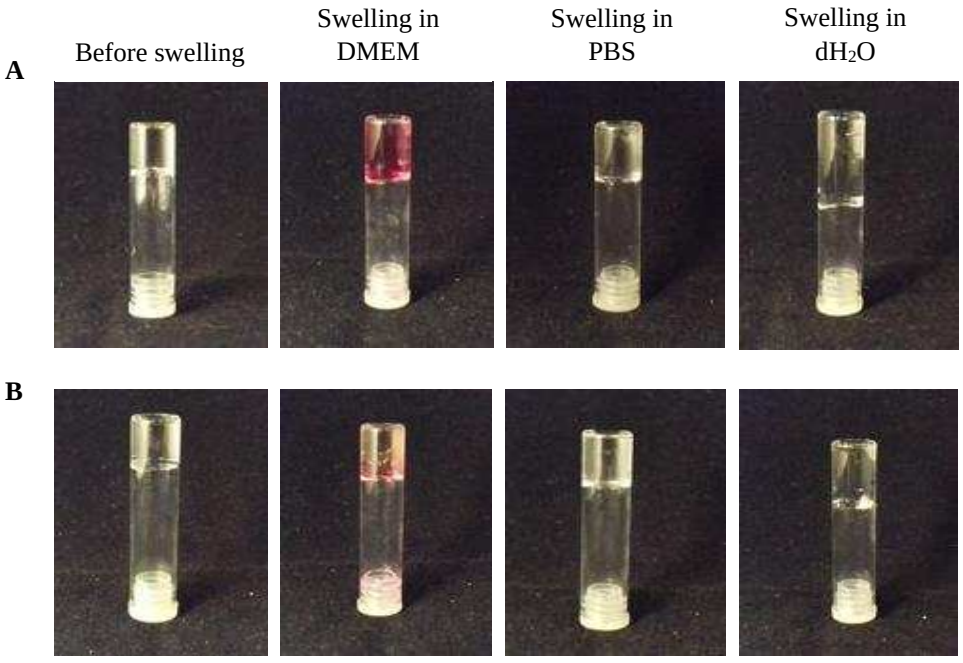

Figure 3.16: Representative photos of HA-ADH hydrogels prepared at low crosslinking densities before and after swelling at 37 °C. **A.** Photos of L1 hydrogel before swelling (top left), after swelling in DMEM and PBS (in the middle), after swelling in dH_2O (top right). **B.** Photos of L2 hydrogel before swelling (bottom left), after swelling in DMEM and PBS (in the middle), after swelling in dH_2O (bottom right).

3.3.1.4 *In vitro* enzymatic degradation studies of HA-ADH hydrogels

The majority of the hydrogels designed for tissue engineering or release of therapeutic molecules, are formulated to be biodegradable. In the brain tissue engineering, the ability of a hydrogel to degrade is critical due to the occurrence of inevitable glial scarring in close proximity to the implant site [51]. Therefore, the temporary presence of a biodegradable hydrogel is more preferable compared to a permanent implant which can induce a lasting immune response and glial scarring. The process of degradation involves the cleavage of degradable chemical sites within the polymer chain leading to the formation of smaller biocompatible molecules that can be eliminated from the implant area.

Typically, as mentioned in section 3.1.4, degradation takes place mainly through hydrolysis or enzymatic cleavage of chemical bonds that are present in the polymer chain. Hydrolytic degradation usually occurs in polymers containing chemical bonds such as ester, ether or amide bonds. For example, in the case of hydrogels consist of poly (α-hydroxy acids), the ester bonds between poly-lactic or poly-glycolic acid moieties undergo hydrolysis resulting in the formation of lactic or glycolic acid units as shown in Figure 3.17. Hydrogels can undergo degradation by enzymatic cleavage of chemical sequences present in the polymer chain that are recognised by specific enzymes. For instance, HA-based hydrogels can be degraded in the presence of hyaluronidase which is an enzyme that catalyses the hydrolysis of C–O, C–N and C–C bonds.

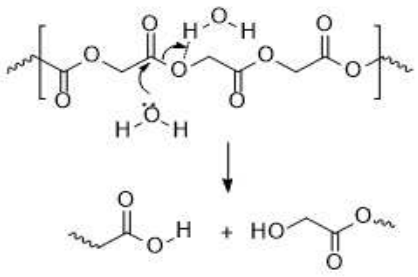

Figure 3.17: Hydrolytic degradation of poly (α-hydroxy acids) results in the formation of molecules containing carboxyl or hydroxyl groups.

HA in its native form as biopolymer, presents short in vivo resistance due to its poor mechanical properties and the enzymatic degradation induced by hyaluronidase. Hyaluronidase specifically degrades HA by cleavage of glycosidic bonds between HA monosaccharides [52]. To overcome these limitations, crosslinking of HA takes place in order to form 3D scaffolds that demonstrate better mechanical properties and longer resistance to this enzyme.

Herein, the integrity of the crosslinked HA hydrogels upon exposure to hyaluronidase was investigated. The in vitro degradation of hydrogels was initially performed by incubation with hyaluronidase enzyme solution at a concentration of 10 U/mL at 37 °C which is within the range of

concentrations that can be found in physiological conditions (0.0059 ± 0.0012 U/ml in human plasma to 38.5 U/ml in human ovaries) [53]. Briefly, hydrogels were prepared at different crosslinking densities in glass vials and incubated in PBS at 37 °C for 2 h. After this incubation period, hydrogels were weighed (W_i) and subsequently 1 mL of PBS with hyaluronidase at 37 °C was added on the top of the hydrogels. At specified time intervals, the enzyme solution was removed and the hydrogels were weighed (W_f). The degradation medium was replaced with freshly prepared enzyme solution of the same composition every 24 h. The degradation was determined as the % hydrogel mass left as function of incubation time with the enzyme solution and it was calculated using the following equation (9):

$$\% \text{ hydrogel mass} = W_f / W_i \times 100 \qquad (9)$$

In order to verify the absence of degradation phenomena due to temperature or PBS, degradation test was carried out on control samples mixed with PBS and incubated at 37 °C. Measurements were performed until complete degradation of the hydrogels was observed. As shown in Figure 3.18, after 2 days of incubation with hyaluronidase, low crosslinking densities of hydrogels L1 and L2, demonstrated significant % mass loss compared to the control hydrogels that started to undergo swelling reaching equilibrium on the third day of incubation. After incubation with hyaluronidase, L1 and L2 hydrogels were completely degraded after 4 and 5 days respectively. In contrast, as shown in Figure 3.18, hydrogels prepared at high crosslinking densities H1 and H2, presented longer degradation times of 10 and 14 days respectively. In addition, in case of control hydrogels a slight decrease in the % hydrogel mass was observed due to syneresis similarly to that during the swelling experiment. The longer degradation rate of H1 and H2 hydrogels compared to the lower crosslinked hydrogels, is correlated with the increased crosslinking density of their network. High crosslinking density results in the formation of a dense network that restricts the diffusion of the enzyme through the scaffold and prolongs the degradation rate. The degradation profile reported here is consistent with the results obtained from swelling studies. The higher % SD of the low crosslinked hydrogels resulted in higher degradation rate due to the increased interactions of the swollen scaffolds with the enzyme solution. It can be concluded that the degradation behaviour of the hydrogels is highly dependent on the crosslinking density. Similarly, Bulpitt et al reported that HA-based hydrogels with 25% of ADH modification degree presented an eight-fold faster degradation rate than those with 65% modification degree, highlighting the significant effect of crosslinking density on the degradation rate [54].

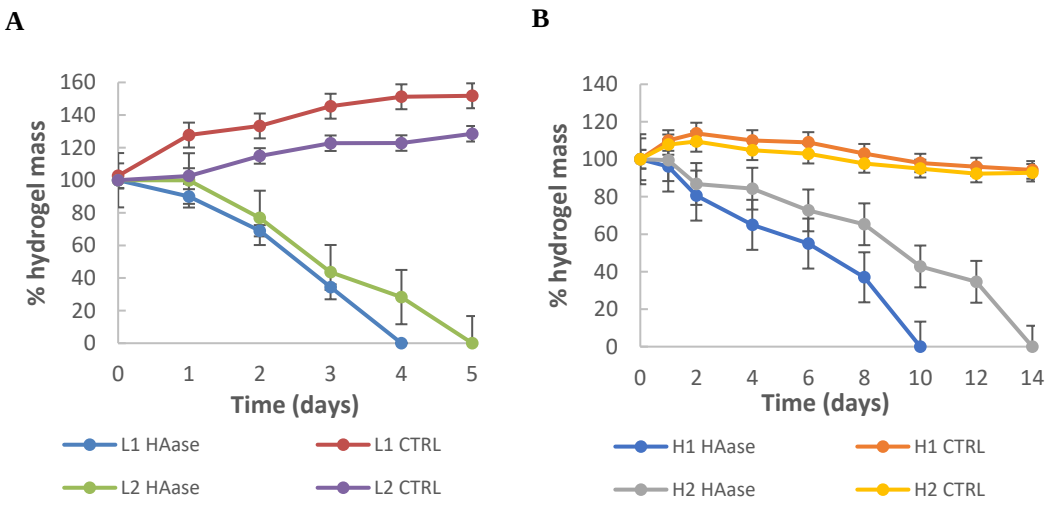

Figure 3.18: Degradation profile of HA-ADH hydrogels prepared at different crosslinking densities in hyaluronidase solution of concentration 10 U/mL at 37 °C. **A.** Degradation profile of low crosslinked hydrogels L1 and L2, **B.** Degradation profile of high crosslinking densities of hydrogels H1 and H2. Hydrogels were prepared as control and incubated in PBS at 37 °C in order to ensure the absence of degradation phenomena due to PBS or temperature. The data represent the average of triplicate with the corresponding error bar calculated by standard deviation.

Hydrogels were also incubated with different concentrations of hyaluronidase 10-200 U/mL and the effect on their degradation rate was investigated. Briefly, hydrogels were prepared at low and high crosslinking densities and digested with different concentrations of hyaluronidase as summarised in Figure 3.19. A linear relationship was observed between the degradation rate and the increasing concentrations of the enzyme applied for both crosslinking densities. The degradation rate of the crosslinked hydrogels was proportionally increased with increasing concentrations of hyaluronidase.

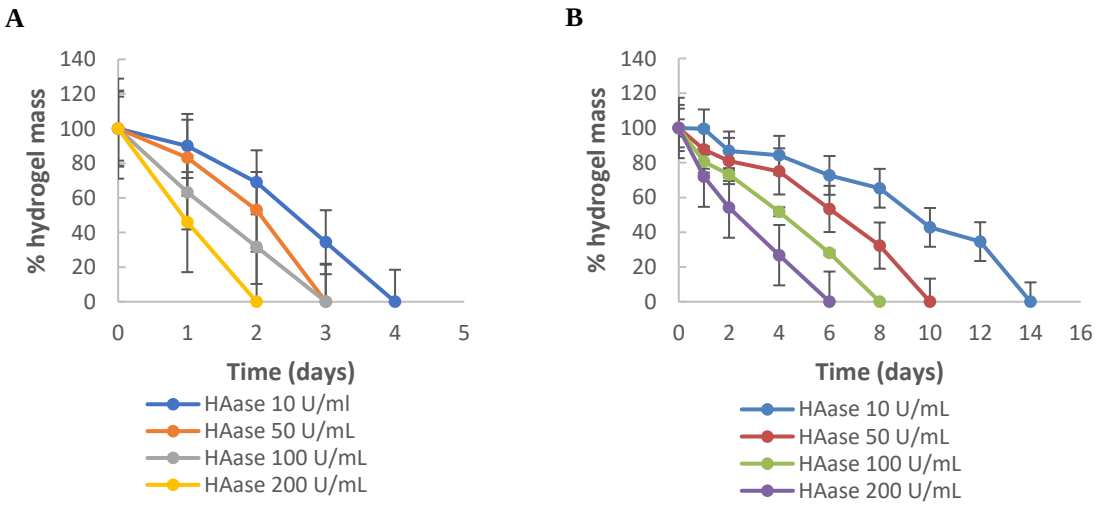

Figure 3.19: Degradation rate of hydrogels prepared at L2 and H2 crosslinking densities. Hydrogels were incubated with different concentrations of hyaluronidase (10-200 U/mL) in PBS at 37 °C. The degradation was determined as the % hydrogel mass left as function of incubation time with the enzyme. **A.** Degradation profile of L2 hydrogels and **B.** Degradation profile of hydrogels prepared at H2 crosslinking density. The data represent the average of triplicate with the corresponding error bar calculated by standard deviation.

The obtained results are indicative of the degradation behaviour of the hydrogels and they do not represent the real-life scenario. Hydrogels were incubated directly with solution of hyaluronidase in vitro conditions that do not mimic the in vivo environment, where the response of the hydrogels would be different. The degradation of the scaffolds is expected to be slower in vivo conditions since the water content in the human body is relatively lower which decreases the hydrolysis rate of the hydrogels [55]. Recently, Kong et al reported the difference in the degradation rate of crosslinked alginate hydrogels in vitro and in vivo conditions. Hydrogels presented faster degradation rate in vitro conditions, whereas in the in vivo environment they maintained their integrity over the entire period of the experiment [56].

3.3.1.5 Rheological measurements on HA-ADH hydrogels

The mechanical features of the hydrogels are important to be considered for the design of scaffolds for pharmaceutical and tissue engineering applications. The mechanical profile of these 3D scaffolds play crucial role in the regulation of cell phenotype, cellular functions including cell proliferation and migration and it will be discussed further in Chapter 4. The chemical properties determine the crosslinking density of the hydrogels which consequently defines their physical and mechanical properties including the stiffness of these materials [57]. Crosslinking density can be modified by varying the amount of the crosslinker or changing the molecular weight of the polymer. Generally, higher crosslinking density results in stiff hydrogels suitable for bone tissue engineering, while lower crosslinking density produces softer hydrogels ideal for brain and neural tissue engineering. For example, Lampe et al observed that neuron cells demonstrated higher viability on soft hydrogels compared to cells seeded on stiffer environment. In contrast, Chatterjee et al using osteoblasts, demonstrated that osteogenesis was improved when the cells were cultured on hydrogels with higher stiffness close to that of bone tissue [58], [59]. Generally, the mechanical properties of the culture environments should be modified and mimic the stiffness of the specific cell types or tissues as summarised in Figure 3.20. Neural cell types prefer to grow on relatively soft substrates with elastic modulus being within the range of 100-1000 Pa.

Therefore, in the present work taking into consideration all the critical mechanical features that the fabricated hydrogels should have in order to be applied as injectable scaffolds in the brain, the mechanical characterisation of the prepared hydrogels was performed. Oscillatory rheological measurements of the elastic modulus G′ and the viscous modulus G′′ as function of shear strain (Amplitude sweep experiment) and as function of frequency (Frequency sweep experiment) were performed using an Anton Paar MCR 302 Rheometer equipped with a cylinder (relative, ST10-4V-8.8/97.5) geometry configuration.

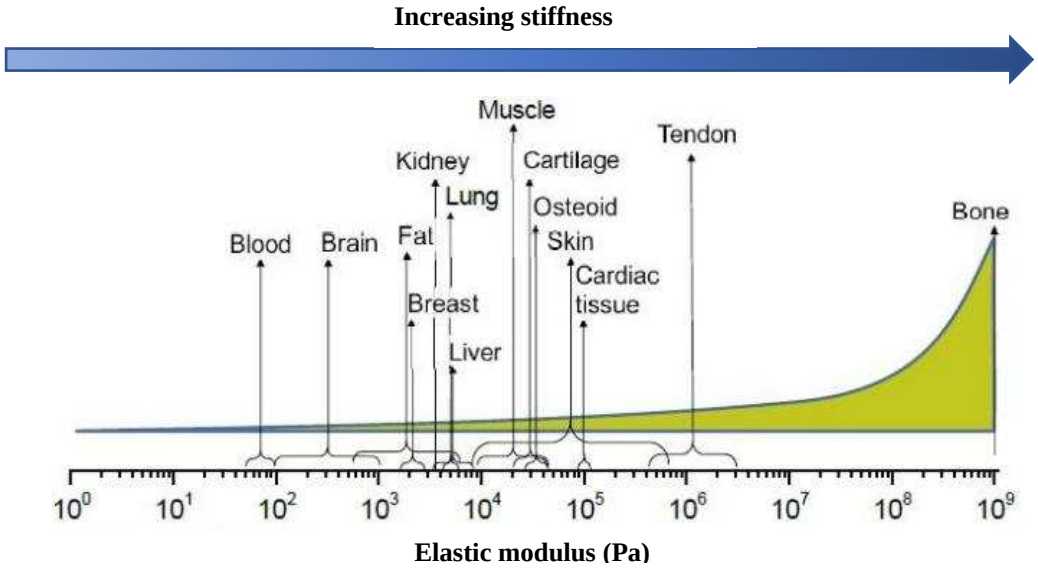

Figure 3.20: Stiffness of different healthy tissues found in the human body. The elastic modulus is expressed in logarithmic scale and measured in Pa. Adapted from Sachot et al [60].

Briefly, hydrogels with a volume of 1 mL were prepared into glass vials with inner diameter of 14 mm as lower geometry and then the upper geometry (relative cylinder) was inserted into the hydrogel as shown in Figure 3.21. Before each measurement, a delay time of 30 minutes was set as for the hydrogel to settle. All the experiments were performed at 37 °C and this temperature was controlled throughout the measurement. The measurements were repeated at least three times to ensure reproducibility.

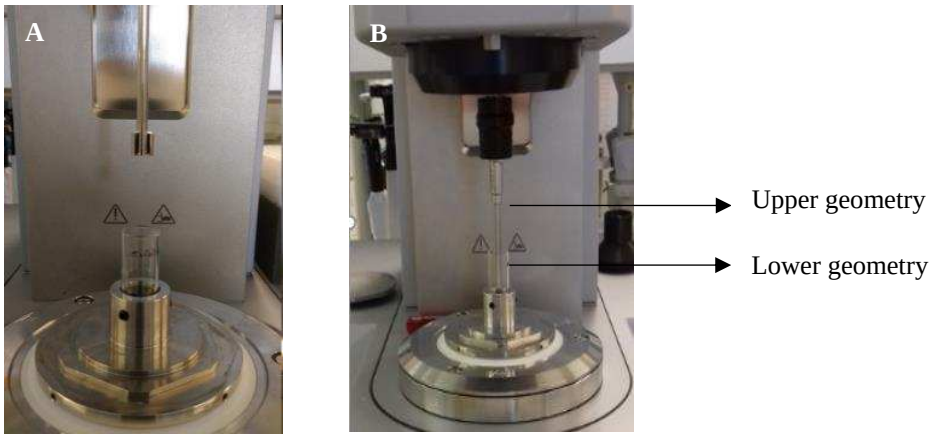

Figure 3.21: A. Photo of relative cylinder used as upper geometry. **B.** Photo of the set up of rheometer used, equipped with a relative cylinder geometry configuration which was inserted into a glass vial containing 1 mL of hydrogel. The illustrative photo A was provided by Dr. E. Sitsanidis.

Initially, amplitude sweep experiment was performed to determine the LVR of deformation for each crosslinking density of hydrogels at increasing shear strains. Strain scans were performed from 0.01 to 100 % with a constant frequency of 1 Hz. The critical strain was determined as the point at which the elastic modulus G´ starts to deviate from linearity and crosses over the viscous modulus G´´. The elastic modulus G´ and viscous modulus G´´ were plotted vs amplitude strain as presented in Figure 3.22.

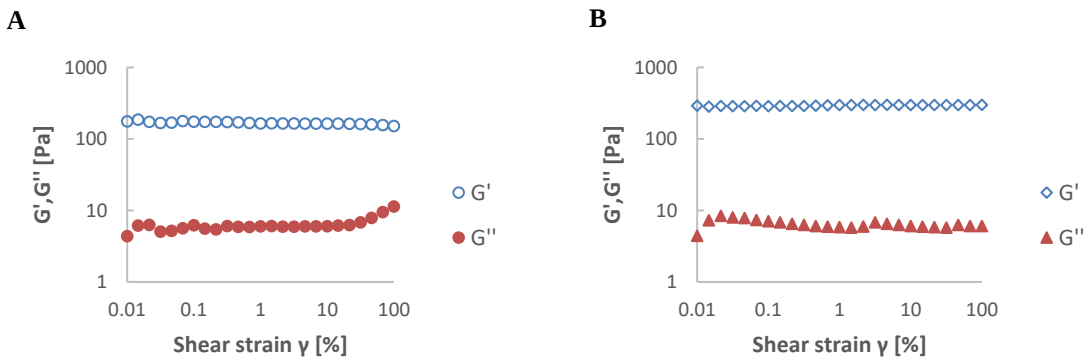

Figure 3.22: Amplitude sweep experiments performed on **A.** L2 and **B.** H1 crosslinking densities of HA-ADH hydrogels. Strain scans were performed from 0.01 to 100 % keeping constant frequency at 1 Hz.

Both moduli demonstrated constant and strain dependent relationship across the range of strain values measured which is typical behaviour of viscoelastic materials. As shown in Figure 3.22, L2 and H1 crosslinking densities indicated linear viscoelastic behaviour up to a critical strain value of 10 %. Therefore, a strain value of 5 % within the LVR was chosen for all hydrogels and applied subsequently to the frequency sweep experiment (for amplitude sweep experiment on L1 and H2 crosslinking densities refer to the Appendix). Amplitude sweep experiment was run on the same sample (L1 crosslinking density) for 3 times in order to ensure the reversibility of the linear viscoelastic behaviour, when the same sample is subjected to increasing amplitude oscillation strain. As presented in Figure 3.23, the three measurements were identical which indicated that the hydrogel can reverse to its initial state, highlighting the elasticity of the material.

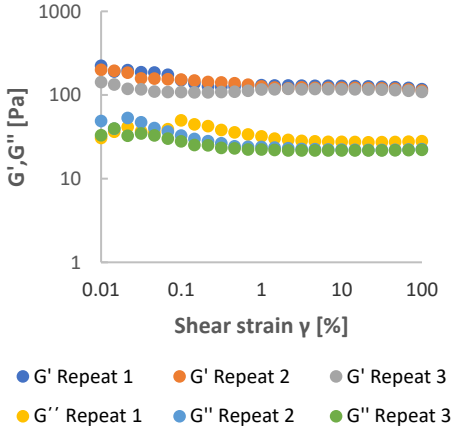

Figure 3.23: Amplitude sweep experiment on L1 hydrogel was repeated three times on the same sample. The graph demonstrates the reproducibility of the measurements and the high elasticity of the hydrogel.

The effect of the increasing concentration of the crosslinker on the viscoelastic properties of the hydrogels was investigated by the frequency sweep test. The frequency sweep experiment was performed within the LVR at a constant strain of 5 % and angular frequencies in the range of 0.1 to 100 rad/sec. The average elastic modulus G´ and viscous modulus G´´ were plotted vs angular frequency as shown in Figure 3.24. All crosslinking densities demonstrated viscoelastic behaviour

as the elastic modulus G´ was higher than viscous modulus G´´ throughout the entire frequency range [61]. The frequency dependence of the moduli is a feature critical of hydrogels and indicative of the homogeneous crosslinked hydrogel network. As summarised in Figure 3.24, hydrogels prepared at high crosslinking densities H1 and H2 presented average elastic moduli of 254 and 289 Pa respectively higher than those of low crosslinked hydrogels. L1 and L2 hydrogels presented elastic moduli of 88 and 138 Pa respectively. The rheological measurements demonstrated that both G´ and G´´ moduli were significantly dependent on the crosslinking density of hydrogels. Similarly, Jeon et al investigated the effect of crosslinking density of HA hydrogels on the mechanical properties and they observed that increasing crosslinking density of HA hydrogels resulted in increased elastic moduli [62].

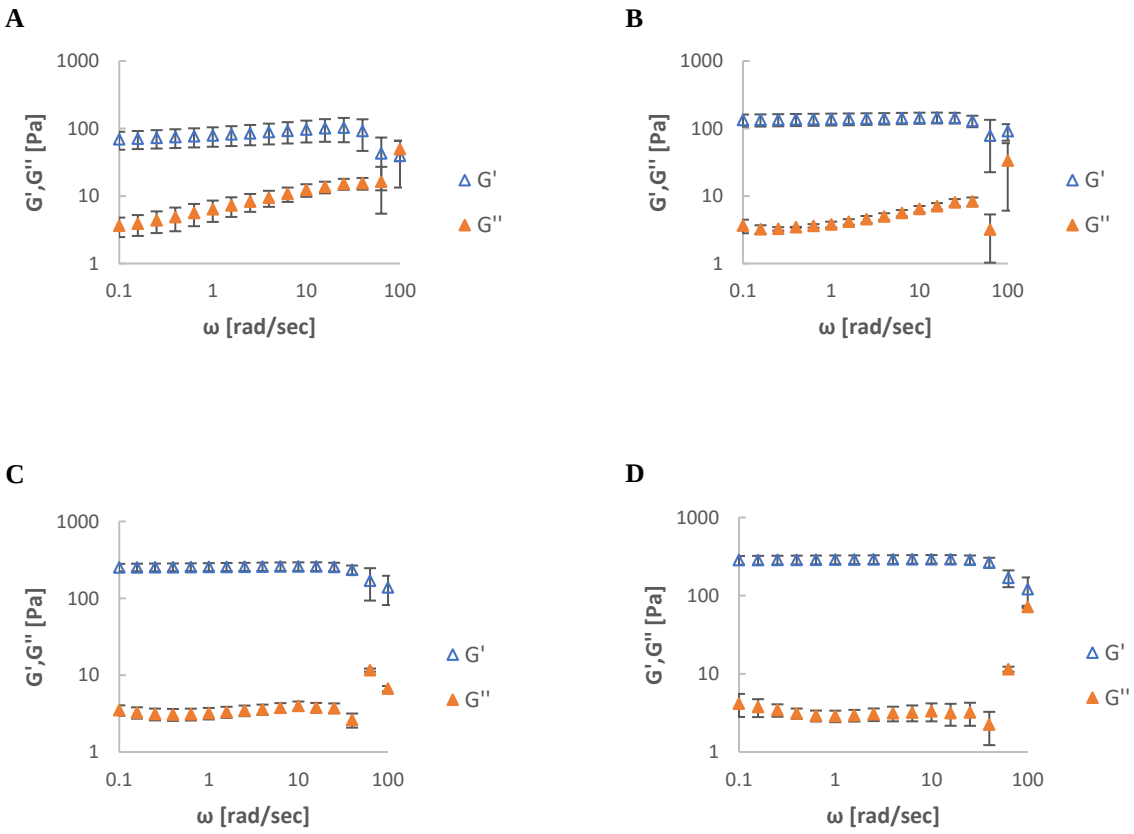

Figure 3.24: Frequency sweep experiments performed on **A.** L1, **B.** L2, **C.** H1 and **D.** H2 crosslinking densities of HA-ADH hydrogels using a constant strain of 5 % in angular frequencies in the range of 0.1 to 100 rad/sec. The data represent the average of three independent measurements with the corresponding error bar calculated by standard deviation.

In summary, the rheological measurements revealed that the elastic moduli of the fabricated hydrogels were within the range of those of neural tissues and brain (100-1000 Pa), highlighting the potential of these hydrogels as injectable scaffolds in the brain.

3.3.1.6 DSC analysis of HA-ADH hydrogels

The thermal behaviour of the crosslinked HA hydrogels was investigated by DSC analysis. In case of hydrogels, DSC thermographs usually demonstrate changes in the glass transition temperature (T_g) for crosslinked hydrogels and their initial components. Herein, the DSC thermographs of HA, ADH and HA-ADH xerogels were recorded using a conventional differential scanning calorimeter Mettler Toledo DSC 822 as shown in Figure 3.25. HA presented a broad endothermic peak approximately at 99 °C and a sharp exothermic peak at 237 °C. The endothermic peak is associated with the loss of water from the HA molecule, while the exothermic peak can be attributed to the thermal degradation of the polysaccharide [63]. ADH demonstrated a sharp endothermic peak at 181 °C that is related to its melting point.

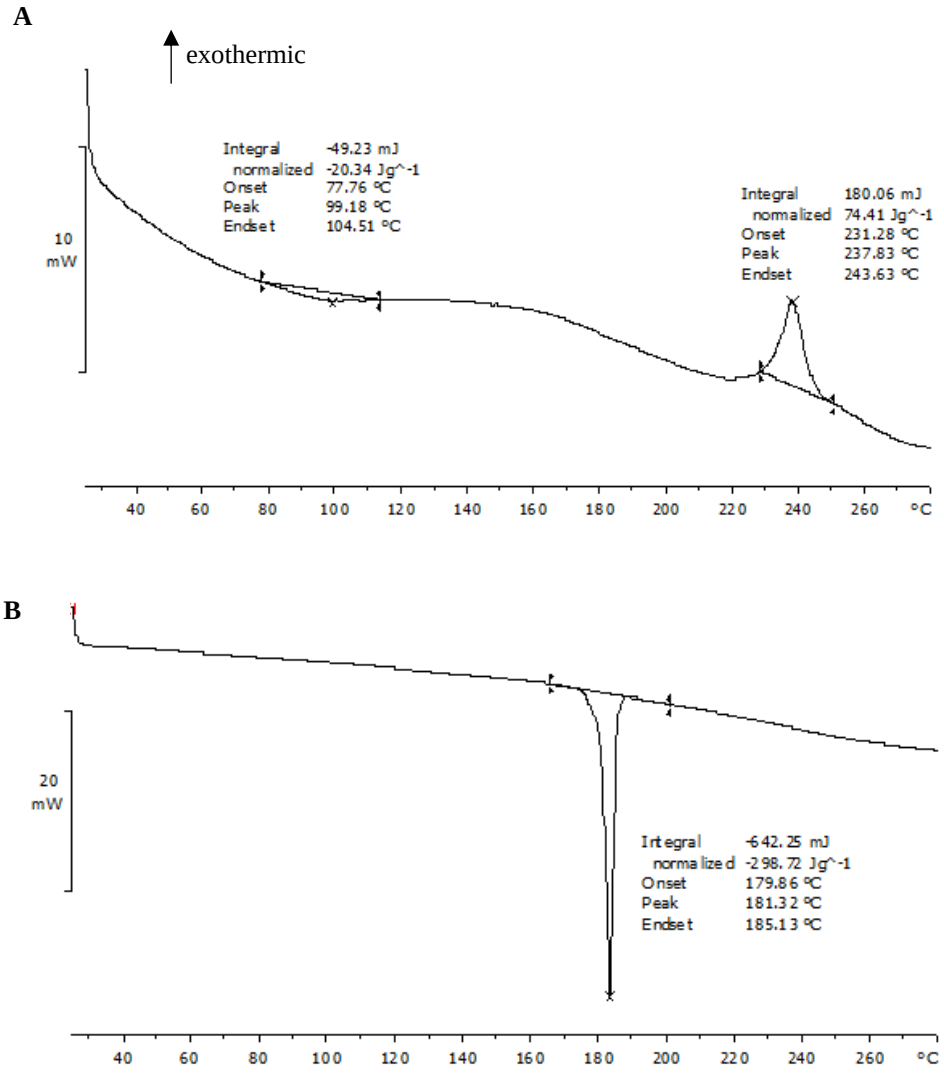

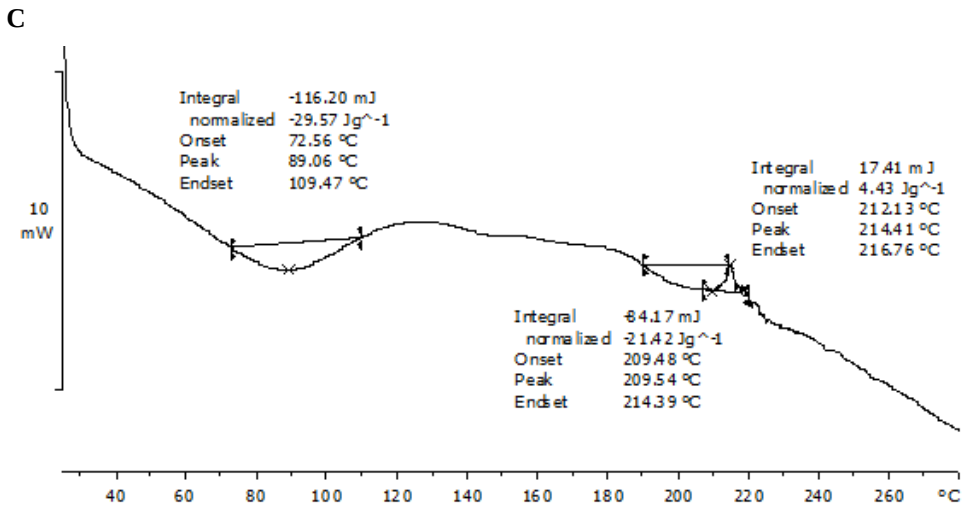

Figure 3.25: DSC thermographs of crosslinked HA xerogel and its components. **A.** DSC thermograph of HA, **B.** ADH and **C.** HA-ADH xerogel.

HA-ADH xerogel showed the presence of a broad endothermic peak at 89 °C which is associated with the loss of water and a small exothermic peak at 214 °C that is connected with the thermal decomposition of the polymer. In overall, the DSC thermographs demonstrated that the endothermic and exothermic peaks of HA shifted after the successful crosslinking with ADH, indicating the altered polymer structure.

3.3.1.7 Drug release from HA-ADH hydrogels

As briefly discussed in section 3.1.7, the efficacy of cancer chemotherapy is restricted by the systemic mechanisms of administration including oral or intravenous routes. Therefore, there is an urgent need to develop localised drug delivery systems that will allow the targeted sustained release of the drug with negligible side effects. Among the drug delivery systems that have been investigated so far, hydrogels can provide all the necessary features for effective targeted controlled drug release close to the tumour site. The delivery of various drugs to the brain has always been challenging due to the unique morphology of the brain microenvironment and the presence of delicate barriers such as the blood-brain barrier as discussed in Chapter 1.

In this study, crosslinked HA hydrogels were loaded with DOX or TMZ and their release profile was investigated. Hydrogels can be loaded with drugs in two different ways. In the first approach, the drug is mixed with the precursor polymer solution and gelation occurs with the drug within the matrix, while in the second approach the hydrogel is allowed to swell in a drug solution until equilibrium swelling is reached [64]. Herein, the drug was mixed with the gelator solution and the polymerisation took place with the drug being physically encapsulated in the hydrogel. Briefly, hydrogels loaded with DOX or TMZ were prepared in glass vials as described in detail in sections 3.2.2.8 and 3.2.2.9. In order to ensure the drug encapsulation efficiency, DOX or TMZ-loaded hydrogels were washed with PBS three times and the UV absorbance of the washing solutions was

measured at 484 nm or 330 nm for the detection of DOX or TMZ respectively. All hydrogels demonstrated facile encapsulation of DOX or TMZ and self supporting hydrogels were formed as shown in Figure 3.26.

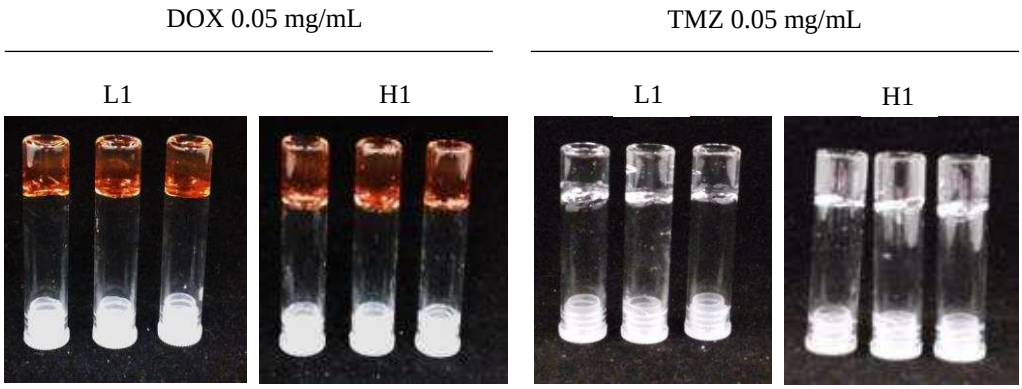

Figure 3.26: Photos of DOX-loaded and TMZ-loaded hydrogels prepared at L1 and H1 crosslinking densities. Self-supporting hydrogels were prepared in triplicate.

DOX or TMZ were physically entrapped within the hydrogel network and any chemical interactions with the main components of the hydrogel were observed. The drug release profile of the DOX or TMZ-loaded hydrogels in PBS at pH 7.4 and 6.0 was studied as function of incubation time at 37 °C. In the literature, it has been reported that the pH of solid tumours varies in the range of approximately 5.7 to 7.6 due to accumulation of acidic metabolites due to low blood pressure and hypoxia caused by abnormal tumour vessels [65]. At predetermined time intervals, the release medium was removed and the concentration of the drug was determined by measuring the absorbance at 484 nm or 330 nm respectively using a WPA Biowave II spectrophotometer. The concentration of the drug released from the hydrogel was determined using a calibration curve plotted for DOX or TMZ respectively (refer to the Appendix). Figure 3.27 summarises the results from the in vitro DOX and TMZ release from the hydrogels in PBS at pH 7.4. The drug release results performed in PBS at pH 6.0 are not shown due to insignificant changes in the release profile of the hydrogels.

It can be observed that hydrogels presented a sustained release of DOX and TMZ which was dependent on the crosslinking density. L1 and L2 hydrogels loaded with DOX presented a cumulative release of 55 and 47.5 % respectively after 96 h, while hydrogels prepared at higher crosslinking densities showed cumulative release of approximately 38 %. Similarly, L1 and L2 hydrogels loaded with TMZ presented a cumulative release of 62.8 and 51.9 % respectively, whereas in case of H1 and H2 hydrogels the cumulative release was 36.1 and 24.4 % respectively, significantly lower at the same period of time. Overall, hydrogels promoted sustained release of DOX or TMZ under physiological conditions over a specific period of time. This sustained drug release is desirable as one of the critical features of the fabricated hydrogels is the release of the loaded drug in a controlled

manner in order to induce gradually apoptosis of the cells that remain in the margins of the resection cavity.

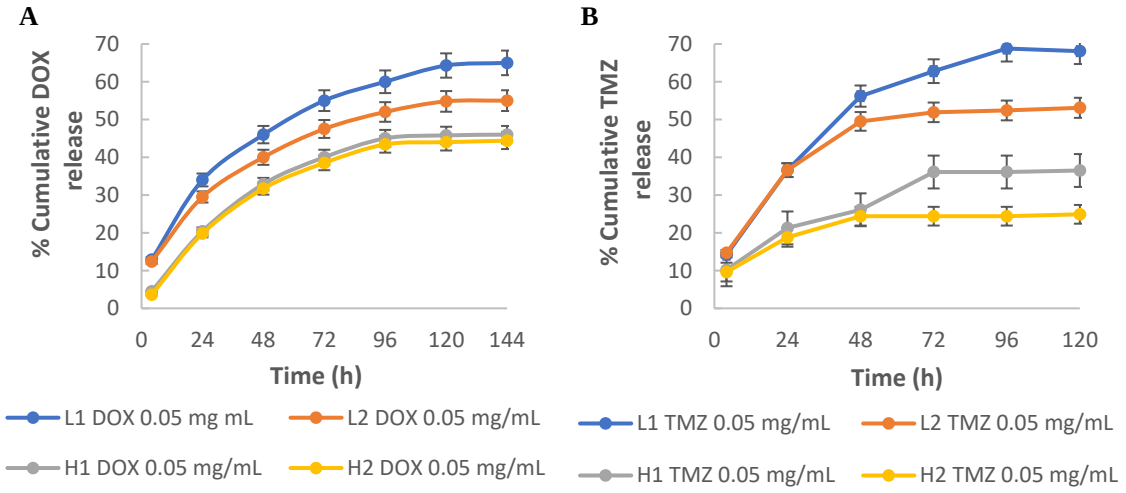

Figure 3.27: Drug release profiles of HA-ADH hydrogels prepared at different crosslinking densities. **A.** Drug release profile of DOX-loaded hydrogels and **B.** Drug release profile of TMZ-loaded hydrogels in PBS at 37 °C. The data represent the average of triplicate with the corresponding error bar calculated by standard deviation.

3.3.1.8 FITC-UII release studies from HA-ADH hydrogels

One of the main objectives of this thesis, was the formulation of a chemoattractant loaded crosslinked network that would allow the formation of chemoattractant gradient. It has been reported that gradient concentration of UII promotes the migration of glioma cells and this will be discussed further in Chapter 4. Hence, the sustained release of the chemokine from the hydrogel to the margins of the tumour site will induce the migration of the invasive glioma cells that have not been removed by the surgery into the scaffold. Herein, the release profile of the chemoattractant loaded HA-ADH hydrogels was investigated. Hydrogels were prepared as described in section 3.2.2.13 and the FITC-UII was efficiently entrapped in the matrix. The successful encapsulation of the chemoattractant in the hydrogel was confirmed by fluorescence spectroscopy of the washing supernatant solutions.

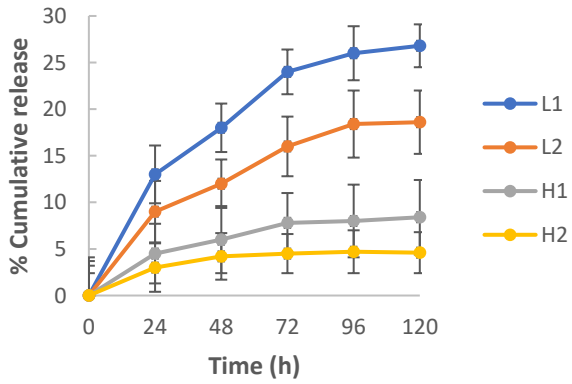

Figure 3.28: % Cumulative release of FITC-UII from HA-ADH hydrogels prepared at different crosslinking densities. The data represent the average of n=5 with the corresponding error bar calculated by standard deviation.

The kinetics of the chemokine release from the hydrogels was determined by incubation of the hydrogels with 100 μL of DMEM as releasing buffer at 37 °C. At specific time points, the supernatant solution was removed and the concentration of the released chemokine was determined by measuring the fluorescence at 520 nm.

As presented in Figure 3.28, the release of the chemoattractant was highly dependent on the crosslinking density of the hydrogels. The highest % release was observed in low crosslinking densities. Specifically, L1 and L2 hydrogels presented cumulative release of 24 and 16 % respectively, while the release from the high crosslinked hydrogels H1 and H2 was 7.8 and 4.5 % respectively. These results indicated that hydrogels can promote the sustained release of the chemoattractant while high concentration of the chemokine remains entrapped in the scaffold which is desirable for our application. As stated previously, one of the main aims of this work, was the formation of a gradient concentration of UII in the drug loaded matrix that will allow release of the chemoattractant while most of it will remain within the matrix as illustrated in Figure 3.29. The above results showed that some of the loaded chemoattractant can be released reaching highest cumulative release of 24 %, while most of it remains inside the hydrogel facilitating the migration of glioma cells towards the scaffold.

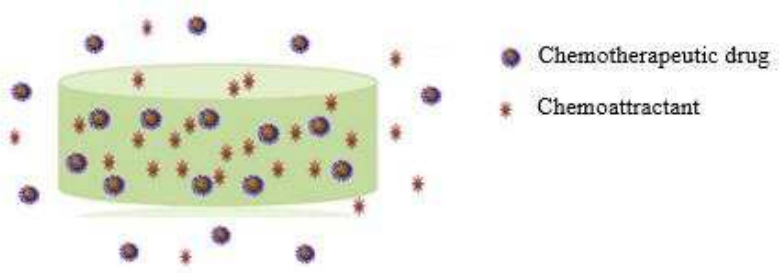

Figure 3.29: Illustration of a hydrogel loaded with a chemotherapeutic drug and chemoattractant that allows sustained release of the drug and chemoattractant while most of it remains within the matrix.

3.3.2 Physicochemical and mechanical characterisation of HA-BSA hydrogels

3.3.2.1 FT-IR spectroscopy of HA-BSA hydrogels

In an effort to optimise the aforementioned formulation of hydrogels, another method of crosslinking of HA was developed in the presence of BSA. Taking into consideration the free primary amines that are present in lysine residues of the BSA molecule and the size of this protein, we proposed the potential crosslinking reaction of the carboxylic groups of HA with the primary amines of BSA which will result in the formation of amide bonds and the fabrication of a 3D network. As discussed in Chapter 2, the carboxyl groups of the HA were activated by EDC/sulfo-NHS chemistry and the activated polysaccharide was further crosslinked with the free amine groups that were present in the BSA molecule. HA-BSA hydrogels were prepared at different crosslinking densities as summarised in Table 3.2 and they were characterised by FT-IR spectroscopy.

Table 3.7: HA-BSA hydrogels prepared at different crosslinking densities.

Sample abbreviation	HA (mg/nmole)	Sulfo-NHS (mg/µmole)	EDC (mg/µmole)	BSA (mg/nmole)
HB16	6.0/3.7	0.5/2.3	2.0/10.4	3.0/45.4
HB17	6.0/3.7	1.25/5.86	5.0/26.1	3.0/45.4
HB18	6.0/3.7	2.5/11.5	10.0/52.2	3.0/45.4
HB19	6.0/3.7	3.75/17.2	15.0/78.2	3.0/45.4

The FT-IR spectra of the HA-BSA xerogel and its main components were recorded and compared as shown in Figure 3.30. In the spectrum of HA, the main absorption bands at 1611 and 1417 cm^{-1} can be assigned to the asymmetric and symmetric stretching vibrations of the carboxylate anions respectively. In the FT-IR spectrum of BSA, there are three main characteristic peaks that are unique to the secondary structure of the protein. The sharp peak at 1640 cm^{-1} is due to the stretching vibration of C=O bond of the amide I band, while the sharp peak at 1527 cm^{-1} is assigned to the bending vibration of N-H of the amide II band.

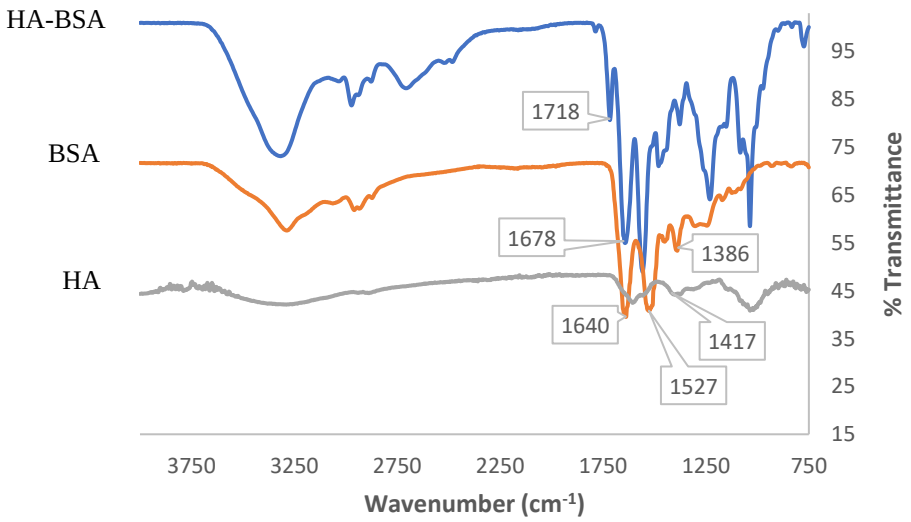

Figure 3.30: FT-IR spectra of HA, BSA and HA-BSA xerogel were recorded and compared. Graph adapted from Chapter 2.

The smaller peak at 1386 cm^{-1} is due to the C-N stretching vibration [66]. Regarding the spectrum of the HA-BSA xerogel, the main differences compared to that of the unmodified HA focused on the the appearance of a peak at 1718 cm^{-1} which corresponds to the formation of an amide bond (C=O stretch of secondary amide), indicative of the successful crosslinking reaction of HA with BSA. The sharp peaks at 1678, 1556 and 1286 cm^{-1} assigned to C=O, N-H and C-N stretching vibrations of the amide bonds respectively, confirmed the presence of BSA in the structure of the xerogel. FT-IR spectra of HA-BSA xerogels prepared at different crosslinking densities were also recorded and

compared as demonstrated in Figure 3.31. All xerogels presented a sharp characteristic peak around 1715 cm^{-1} indicative of the formation of a new amide bond in the structure of HA. As highlighted in Figure 3.31, it is also notable the increase in the intensity of this peak as the crosslinking density increases.

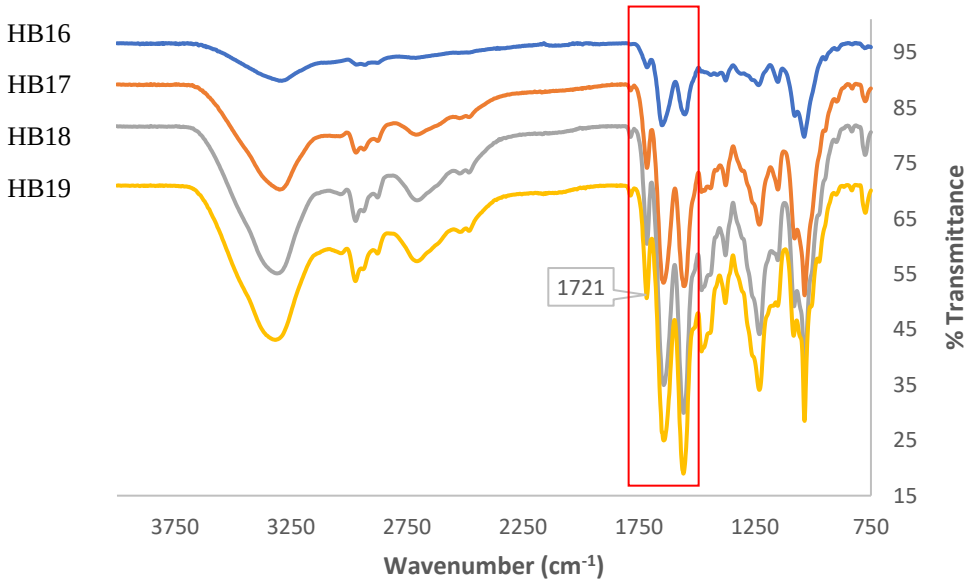

Figure 3.31: FT-IR spectra of HA-BSA xerogels prepared at different crosslinking densities.

3.3.2.2 SEM characterisation of HA-BSA hydrogels

The effect of the increasing crosslinking density on the morphology and porosity of HA-BSA hydrogels was investigated by SEM analysis. Briefly, HA-BSA hydrogels were prepared at different crosslinking densities as described above and they were allowed to swell for 24 h in PBS. After this period, hydrogels were flash frozen by immersion in dry ice and subsequently, frozen hydrogels were fractured into thin slices and prepared for freeze-drying. Xerogels were obtained after 24 h of freeze-drying and coated before SEM characterisation. The thin slices of xerogels were coated with a thin layer of gold as described previously and SEM images were taken at different magnifications as demonstrated in Figure 3.32. Xerogels presented an interconnected porous network similar to that of HA-ADH xerogels with variable porosity.

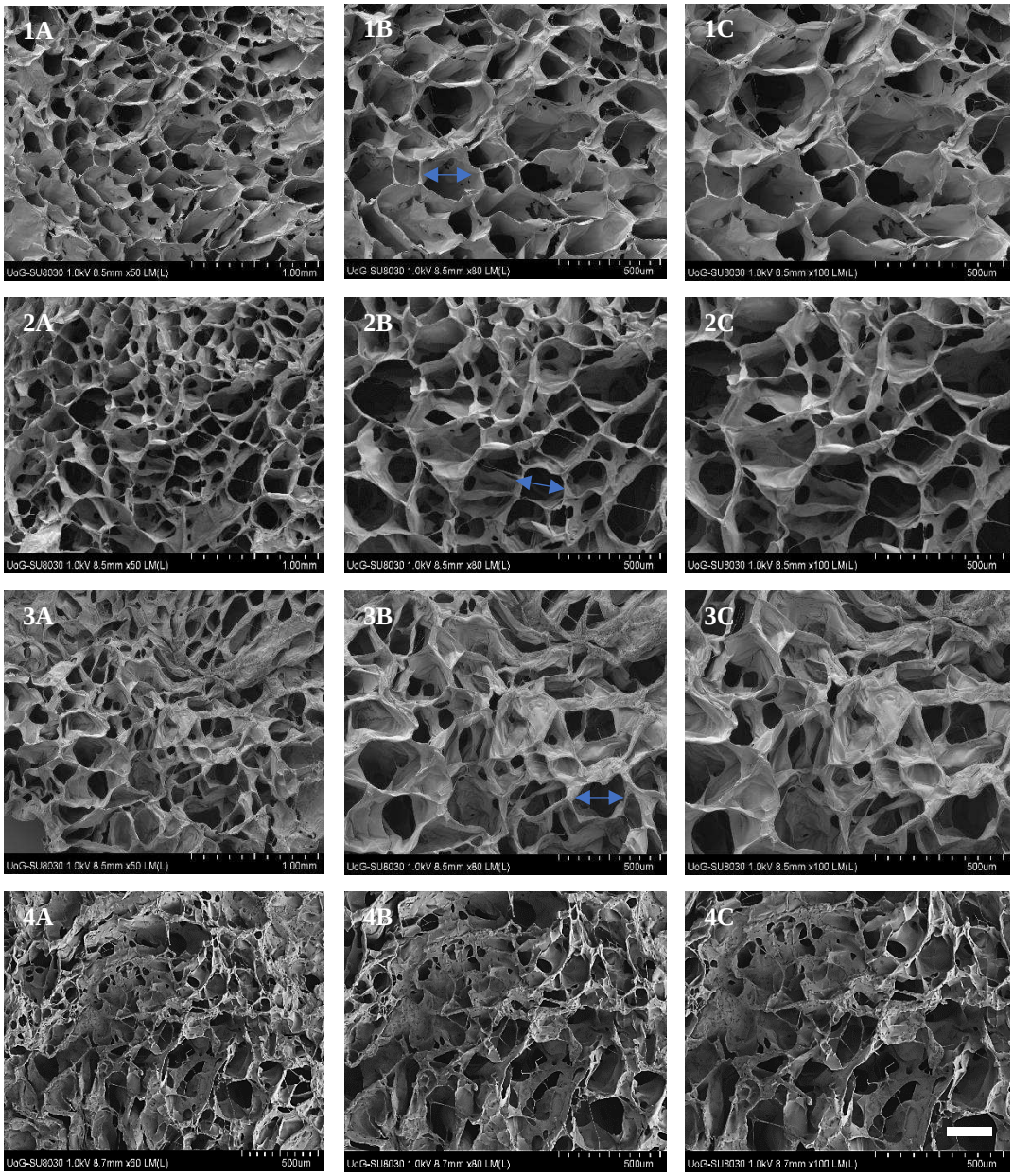

Figure 3.32: SEM images of HA-BSA xerogels prepared at different crosslinking densities. **1A-1B-1C**: HB16 xerogel at magnifications 50x, 80x and 100x respectively, **2A-2B-2C**: HB17 xerogel at magnifications 50x, 80x and 100x respectively, **3A-3B-3C**: HB18 xerogel at magnifications 50x, 80x and 100x respectively and **4A-4B-4C**: HB19 xerogel at magnifications 60x, 80x and 100x respectively. Scale bar: 500 μm-1mm.

The pore size was highly dependent on the crosslinking density. The histogram in Figure 3.33 presents the average pore size of each crosslinking density as it was calculated by ImageJ. Xerogels prepared at low crosslinking densities HB16 and HB17 presented pore size of 250 and 195 μm respectively. In contrast, high crosslinked xerogels HB18 and HB19 were characterised with a pore size of 138 and 105 μm respectively. Overall, xerogels with these pore sizes can facilitate cells sufficient space to grow and adhere to the matrix. Moreover, it is notable that these xerogels presented higher pore sizes than those of HA-ADH xerogels due to the lower concentration of the polysaccharide used as summarised in the graphs in Figure 3.33.

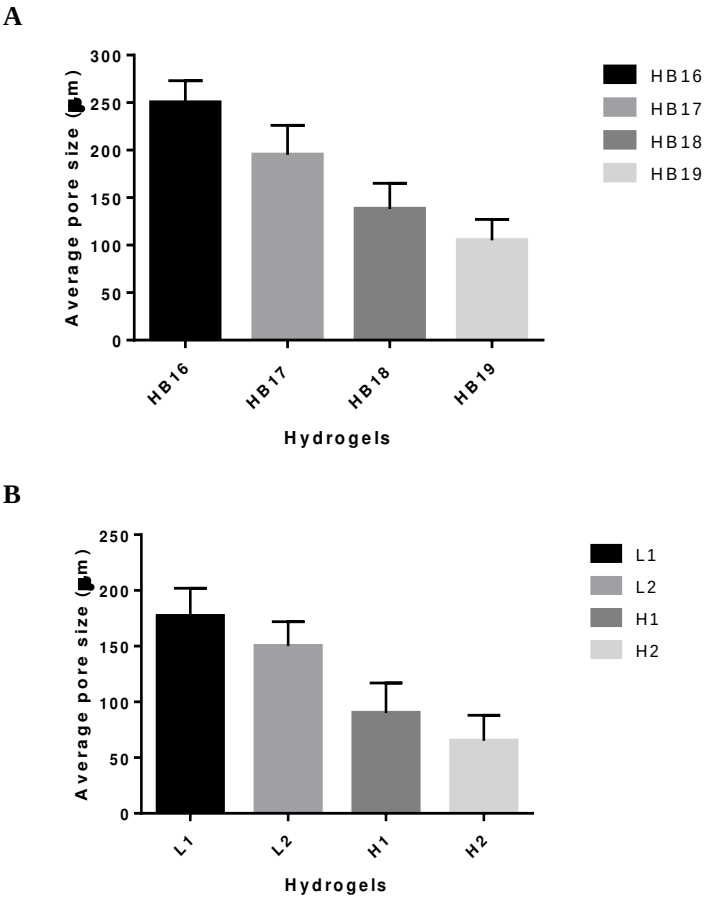

Figure 3.33: Histograms demonstrate the average pore size of **A.** HA-BSA xerogels and **B.** HA-ADH xerogels prepared at different crosslinking densities measured by ImageJ. Error bars were calculated by the corresponding standard deviation.

3.3.2.3 Swelling studies of HA-BSA hydrogels

The porous structure of the crosslinked hydrogels presented above enables them to swell in aqueous environment. The crosslinking density determines the extent of the swelling capacity. Herein, the effect of the crosslinking density on the swelling behaviour of the crosslinked HA hydrogels was investigated. Hydrogels prepared at different crosslinking densities in glass vials with inner diameter 12 mm were allowed to swell in PBS (pH 7.4) at 37 °C. At predetermined time intervals, the PBS solution was removed carefully from the swollen hydrogels, wiped with a filter paper and then the weight of the hydrogels was measured. The % SD was calculated as a function of incubation time as described previously and the obtained results from the swelling experiment are summarised in Figure 3.34. After 2 days of incubation in PBS at 37 °C, the low crosslinking densities of hydrogels HB16 and HB17 showed an equilibrium % SD of 49 and 38 respectively. On the other hand, HB18 and HB19 hydrogels presented an equilibrium % SD of 25.2 and 15.8 respectively. Compared to HA-ADH hydrogels, those fabricated by the crosslinking of HA with BSA, demonstrated higher % swelling degree which is also consistent with the data obtained from the SEM analysis. The expected higher swelling capacity of these hydrogels can be assigned to the higher porosity of the scaffolds.

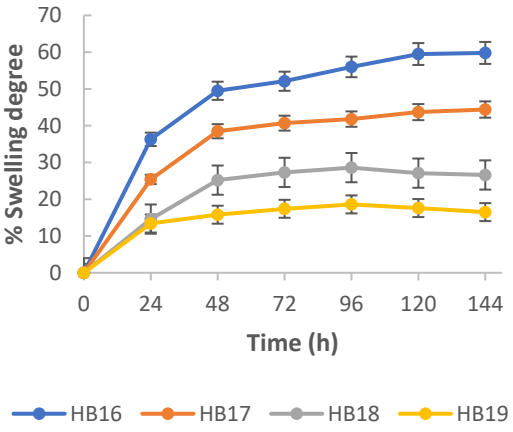

Figure 3.34: Swelling profile of HA-BSA hydrogels prepared at different crosslinking densities in PBS at 37 °C. The data represent the average of triplicate with the corresponding error bar calculated by standard deviation.

3.3.2.4 *In vitro* enzymatic degradation of HA-BSA hydrogels

The degradation rate of the HA-BSA hydrogels upon exposure to hyaluronidase was investigated. The in vitro degradation of hydrogels was performed by incubation with hyaluronidase solution at a concentration of 10 U/mL at 37 °C which is within the range of enzyme concentrations that can be found in physiological conditions. Briefly, hydrogels were prepared at different crosslinking densities in glass vials and incubated in PBS at 37 °C for 2 h. After this incubation time, hydrogels were weighed and subsequently 1 mL of PBS with hyaluronidase at 37 °C was added on the top of the hydrogels. At predetermined time intervals, the enzyme solution was removed and the hydrogels were weighed. The degradation medium was replaced with freshly prepared enzyme solution of the same composition every 24 h. The degradation was determined as the % hydrogel mass left as a function of incubation time as presented in Figure 3.35.

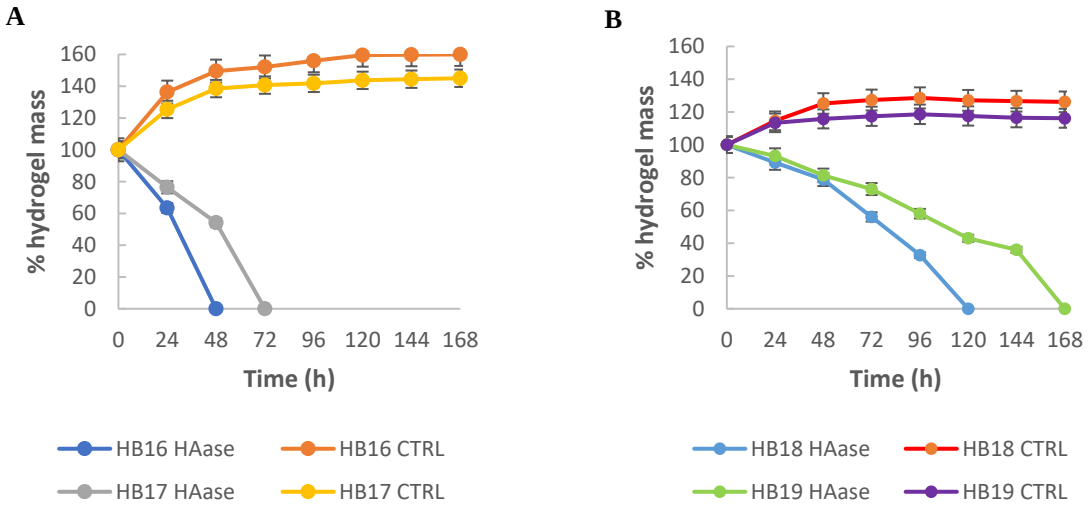

Figure 3.35: Degradation profile of HA-BSA hydrogels prepared at different crosslinking densities in hyaluronidase solution of concentration 10 U/mL at 37 °C. **A.** Degradation profile of low crosslinked hydrogels HB16 and HB17, **B.** Degradation profile of high crosslinking densities of hydrogels HB18 and HB19. Hydrogels were also prepared as control and incubated in PBS at 37 °C in order to ensure the absence of degradation phenomena due to PBS or temperature. The data represent the average of triplicate with the corresponding error bar calculated by standard deviation.

Hydrogels were also incubated in PBS at 37 °C in the absence of hyaluronidase in order to verify that the degradation process is not induced by temperature or the presence of PBS. Measurements were performed until complete degradation of the hydrogels was observed. As shown in Figure 3.35, low crosslinking densities of hydrogels HB16 and HB17 demonstrated significant % mass loss and complete degradation was observed after 2 and 3 days of incubation respectively. On the other hand, control hydrogels in the absence of the enzyme, started to undergo swelling. The degradation rate for the high crosslinked hydrogels was slower than that of lower crosslinking densities. HB18 and HB19 hydrogels were completely degraded within 5 and 7 days respectively. In addition, in case of control hydrogels a slight increase in the hydrogel mass was observed due to swelling. These results are consistent with the corresponding swelling profile of the hydrogels. The high porosity of these scaffolds resulted in higher swelling capacity and increased interactions with the enzyme solution leading to shorter degradation time compared to HA-ADH hydrogels.

3.3.2.5 Rheological characterisation of HA-BSA hydrogels

The characterisation of the mechanical properties of the fabricated scaffolds prepared at different crosslinking densities was investigated by oscillatory rheology. HA-BSA hydrogels with a volume of 1 mL were prepared into glass vials with inner diameter of 14 mm as lower geometry and subsequently the upper geometry (relative cylinder) was inserted into the hydrogel as described previously. Before each measurement, a delay time of 30 minutes was set as for the hydrogel to settle. All the experiments were performed at 37 °C. Amplitude sweep experiment on the crosslinked hydrogels, was performed to determine the LVR of deformation for each crosslinking density at increasing shear strains. Strain scans were performed within a range from 0.01 to 100 % with a

constant frequency of 1 Hz. The elastic modulus G′ and viscous modulus G′′ were plotted vs amplitude strain as shown in Figure 3.36.

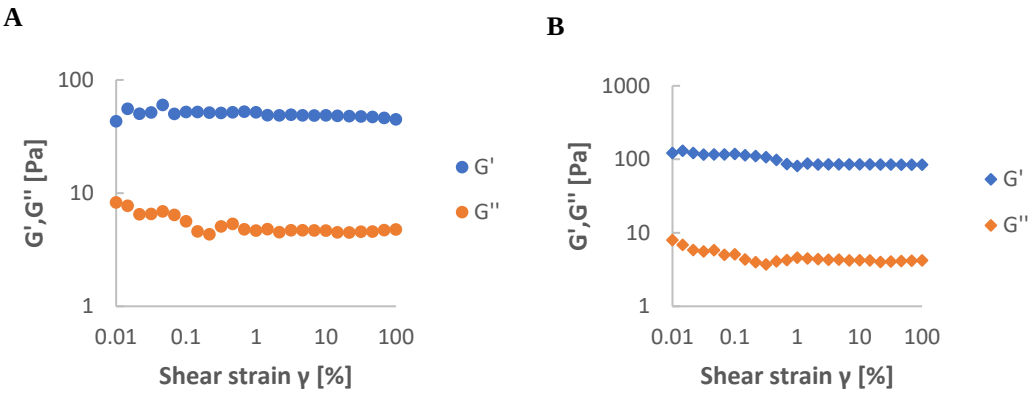

Figure 3.36: Amplitude sweep experiments performed on **A.** HB17 and **B.** HB18 crosslinking densities of HA-BSA hydrogels. Strain scans were performed within a range from 0.01 to 100 % keeping constant frequency at 1 Hz.

Both viscoelastic moduli demonstrated strain dependent relationship across the range of strain values measured which indicated the viscoelastic behaviour of these materials. As presented in Figure 3.36, hydrogels showed linear viscoelastic behaviour up to a critical strain value of 10 %. Therefore, a strain value of 5 % within the LVR was chosen for all hydrogels and applied subsequently to the frequency sweep test. In addition, the reversibility of the viscoelastic behaviour of the hydrogels was investigated by amplitude sweep experiment which was run on the same sample (HB17 crosslinking density) for 3 times. The sample was subjected to increasing shear strain and the viscoelastic behaviour was identified. As presented in Figure 3.37, the three measurements showed the same trend which indicated that the hydrogel can reverse to its initial viscoelastic profile, highlighting the elasticity of the 3D matrix.

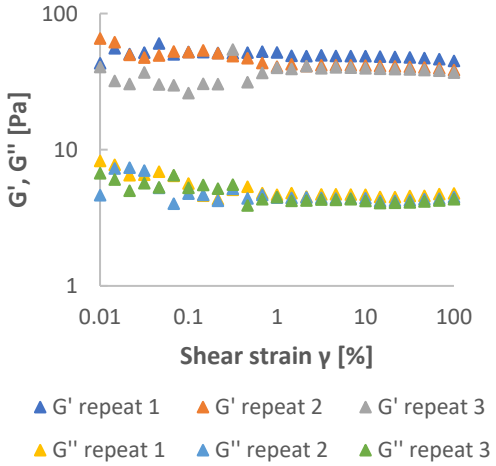

Figure 3.37: Amplitude sweep experiment on HB17 hydrogel was run three times on the same sample. The graph demonstrates the reversibility of the viscoelastic properties of the material.

Frequency sweep test was performed within the LVR at a constant strain of 5 % and angular frequencies in the range of 0.1 to 100 rad/sec. The average elastic modulus G´ and viscous modulus G´´ were plotted vs angular frequency as demonstrated in Figure 3.38. The frequency sweep experiment indicated that the fabricated scaffolds prepared at different crosslinking densities, presented viscoelastic behaviour as the elastic modulus G´ was higher than the viscous modulus G´´ throughout the entire frequency range. The frequency dependence of both viscoelastic moduli was indicative of the homogeneous formation of a crosslinked hydrogel network. As shown in Figure 3.38, the increasing crosslinking density presented significant effect on the stiffness of the hydrogels. Hydrogels prepared at high crosslinking densities HB18 and HB19 presented average elastic moduli of 100 and 180 Pa respectively.

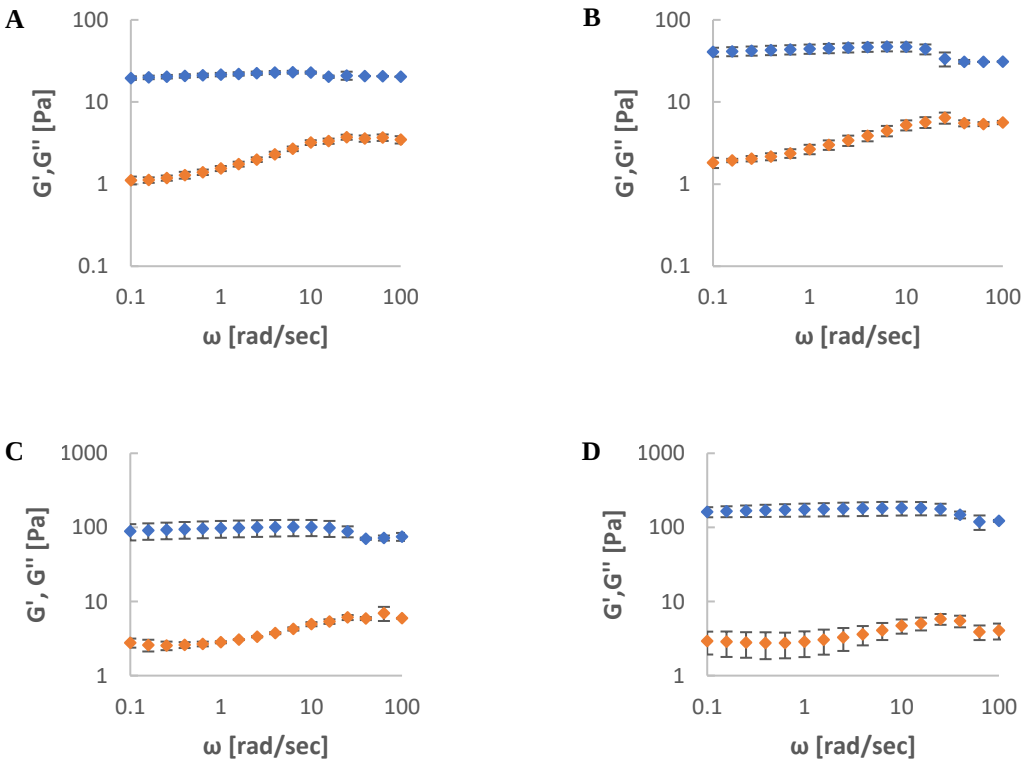

Figure 3.38: Frequency sweep experiments performed on **A.** HB16, **B.** HB17, **C.** HB18 and **D.** HB19 crosslinking densities of HA-BSA hydrogels using a constant strain of 5 % in angular frequencies in the range of 0.1 to 100 rad/sec. The data represent the average of three independent measurements with the corresponding error bar calculated by standard deviation.

In contrast, low crosslinking degree resulted in softer hydrogels HB16 and HB17 with elastic moduli of 22 and 45 Pa respectively. In comparison with the HA-ADH hydrogels, the crosslinking method using BSA as crosslinker produced softer hydrogels within the range of elastic modulus of the brain tissue.

3.3.2.6 DSC analysis of HA-BSA hydrogels

DSC measurements were performed to confirm the results obtained from FT-IR regarding the structural change of HA backbone. The FT-IR analysis showed that the crosslinking reaction between HA and BSA could have happened as there was slight change in the carbonyl region of the spectra. Figure 3.39 depicts the DSC thermographs of HA, BSA and HA-BSA xerogel. HA presented a broad endothermic peak approximately at 99 °C and a sharp exothermic peak at 237 °C. The endothermic peak is associated with the loss of water from the HA molecule, while the exothermic peak can be attributed to the thermal degradation of the polymer. BSA showed a broad endothermic peak at 204 °C that can be assigned to the thermal degradation of the protein [67]. The DSC thermograph of the HA-BSA xerogel presented a broad endothermic at 74.1 °C due to the loss of water and a broad exothermic peak at 215 °C that corresponds to the thermal degradation of the system. Overall, the DSC curve of HA-BSA xerogel presented differences compared to the curves of the pure compounds. The DSC thermographs demonstrated that the endothermic and exothermic peaks of the HA slightly shifted after the crosslinking reaction with BSA which confirms the altered polysaccharide's structure.

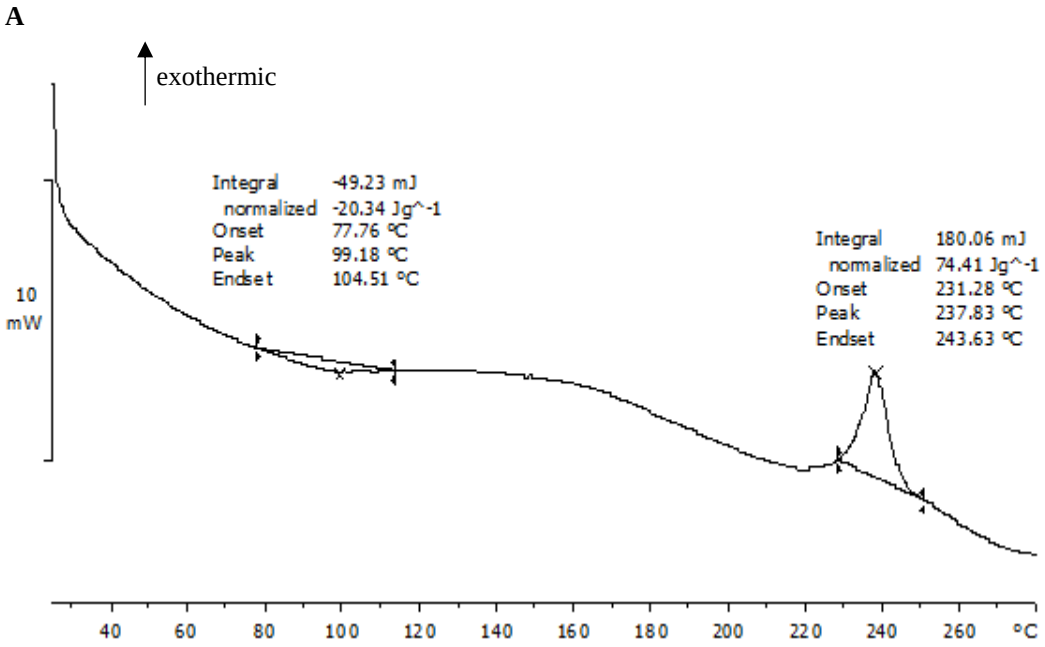

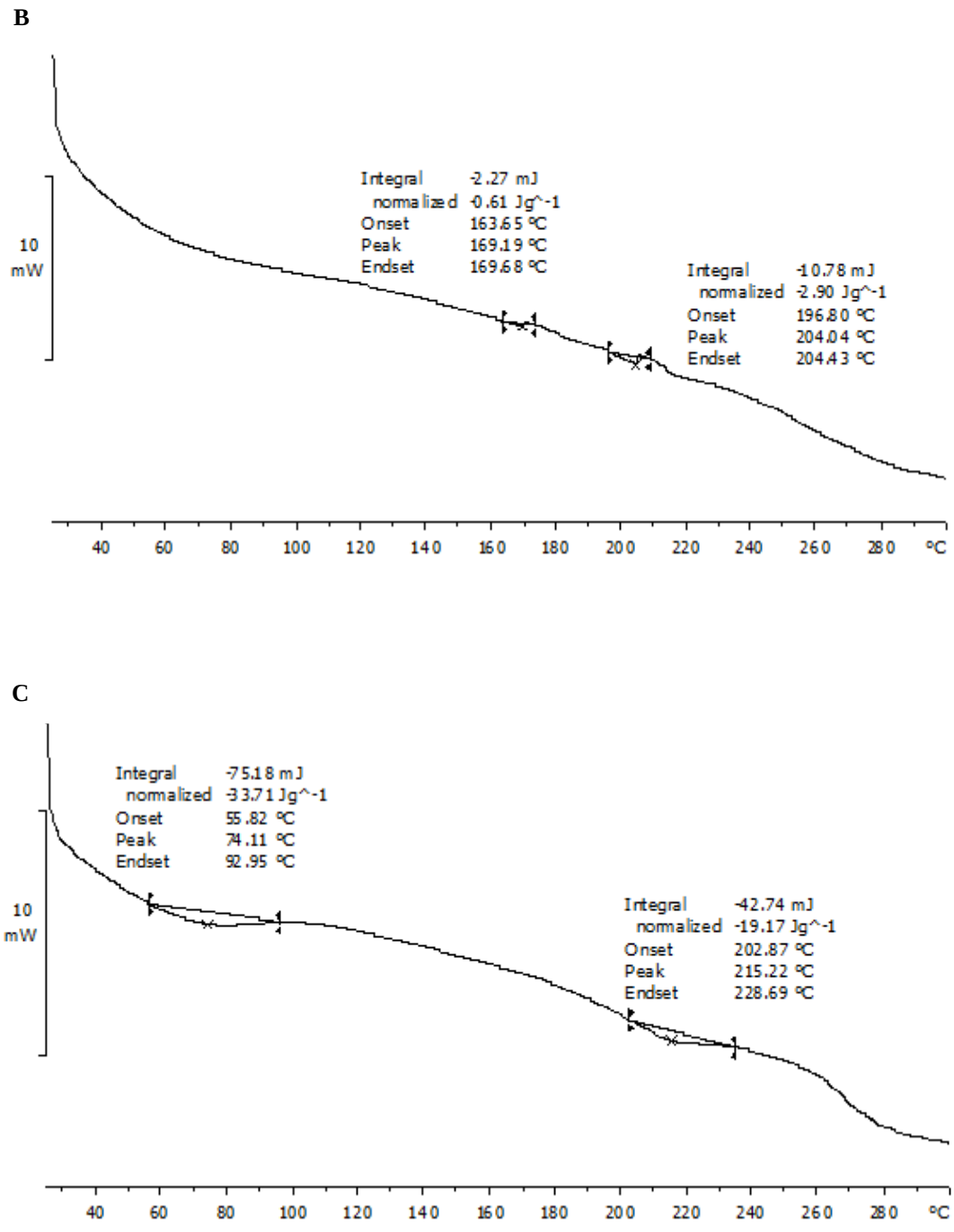

Figure 3.39: DSC thermographs of **A.** HA, **B.** BSA and **C.** HA-BSA xerogel.

3.3.2.7 Drug release from HA-BSA hydrogels

The drug release profile of the HA-BSA hydrogels loaded with DOX or TMZ was studied. Similar to the protocol followed for the drug loading on the HA-ADH hydrogels, the drug was mixed with the precursor polymer solution and gelation was allowed to occur with the drug encapsulated within the hydrogel network. Briefly, the crosslinked hydrogels loaded with DOX or TMZ were prepared in glass vials according to the protocols described in sections 3.2.2.10 and 3.2.2.11. All hydrogels demonstrated facile encapsulation of DOX or TMZ and self supporting hydrogels were formed as shown in Figure 3.40.

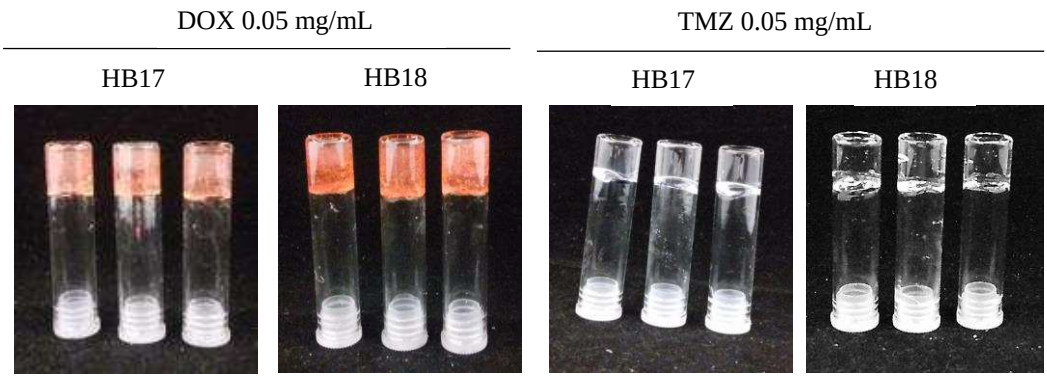

Figure 3.40: Photos of DOX-loaded and TMZ-loaded hydrogels prepared at HB17 and HB18 crosslinking densities. Self-supporting hydrogels were prepared in triplicate.

Subsequently, hydrogels were incubated in PBS (pH 7.4) at 37 °C and at specific time intervals the release medium was removed. The concentration of the released drug was determined and the % cumulative release was calculated as described in previous sections. Figure 3.41 summarises the % cumulative release profiles of HA-BSA hydrogels loaded with DOX or TMZ. The % drug release from hydrogels was affected by the crosslinking density as decreased % drug release was observed with an increase in the crosslinking density. A cumulative DOX release of 64 and 53 % for low crosslinked hydrogels HB16 and HB17 respectively was observed, while the % DOX release for HB18 and HB19 hydrogels was 42 and 26.3 respectively. Similarly, the % TMZ release was higher in low crosslinking densities reaching % cumulative release of 49 and 31 for HB16 and HB17 hydrogels respectively and lower in high crosslinking densities HB18 and HB19 reaching cumulative release of 23 and 15 % respectively. These results indicated that the fabricated hydrogels promoted the sustained release of the loaded drugs over a period of time and they can be suitable candidates for the localised treatment of GBM.

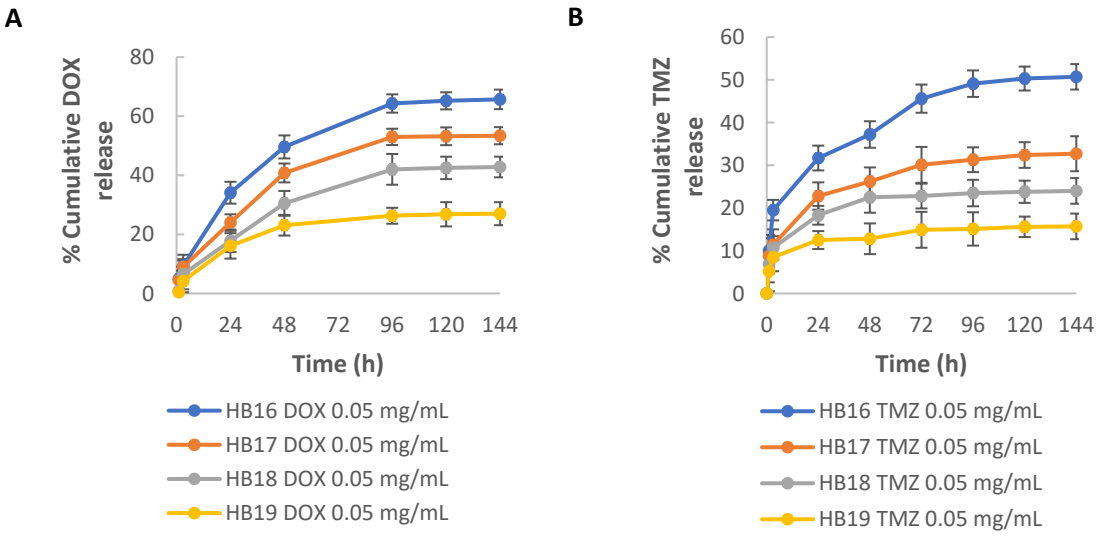

Figure 3.41: Drug release profiles of HA-BSA hydrogels prepared at different crosslinking densities. **A.** Drug release profile of DOX-loaded hydrogels and **B.** Drug release profile of TMZ-loaded hydrogels in PBS at 37 °C. The data represent the average of triplicate with the corresponding error bar calculated by standard deviation.

3.3.3 Characterisation of blend XG/MC hydrogels

3.3.3.1 FT-IR characterisation of blend XG/MC hydrogels

As discussed in Chapter 2, XG and MC were used in order to prepare injectable, biocompatible blend XG/MC hydrogels, alternative to HA gels. Different compositions of blend hydrogels were prepared as described in Table 3.3 and they will be briefly characterised by FT-IR spectroscopy and Scanning Electron Microscopy due to their poor biocompatibility as it will be discussed in the following chapter. Self-supporting hydrogels were formed and xerogels were obtained according to the protocol described earlier. The changes in the structure of the XG/MC xerogels compared to the structure of the native polysaccharides were investigated by FT-IR spectroscopy.

Table 3.8: XG and MC concentrations in various blend solutions of XG/MC in 1×PBS.

Sample abbreviation	XG Concentration (% w/w)	MC Concentration (% w/w)
XG1/MC0	1	0
XG1/MC3	1	3
XG1/MC6	1	6
XG1/MC8	1	8
XG2/MC1	2	1
XG2/MC6	2	6
XG3/MC1	3	1

Figure 3.42 presents the FT-IR spectra of the XG/MC xerogel and its main components XG and MC. In the spectrum of the native XG, the broad peak at 3296 cm^{-1} is associated to the O-H stretch band, while the small peak at 2885 cm^{-1} is attributed to the -CH_2 stretching vibrations. Moreover, the C=O band at 1738 cm^{-1} corresponds to the acetate groups of the mannose moiety, while the peak at 1605 cm^{-1} is assigned to the carboxylate groups of the pyruvate unit and glucuronic acid [68].

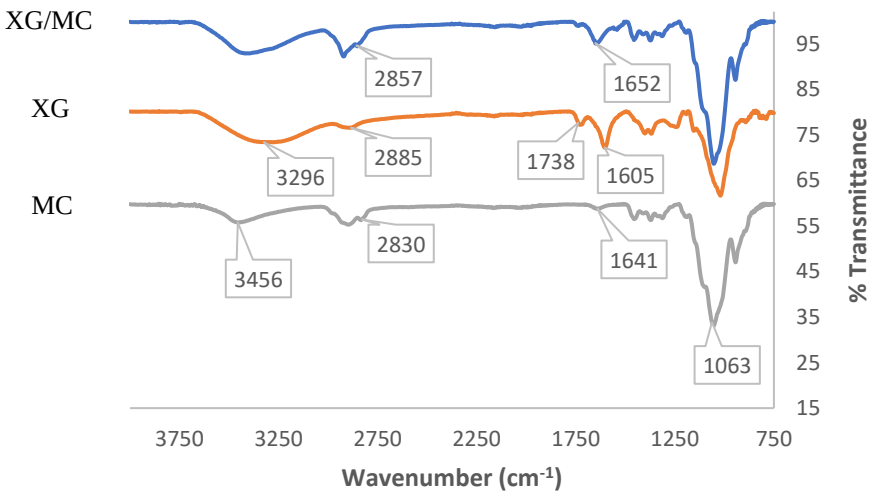

Figure 3.42: FT-IR spectra of native XG, MC and blend XG/MC xerogel.

The small characteristic peak at 2830 cm^{-1} presented in the spectrum of the native MC is associated to the stretching vibration of C-H in the methyl ester group. The broad peak at 3456 cm^{-1} corresponds to the O-H stretching vibration [69]. The C=O stretching vibration observed at 1641 cm^{-1} and the sharp peak at 1063 cm^{-1} is related to the stretching vibration of C-O bond. In the spectrum of XG/MC xerogel the characteristic peak at 2857 cm^{-1} that is attributed to the C-H band of the methyl ester group confirmed the presence of MC. The peak at 1652 cm^{-1} that represents the C=O stretching of the acetate groups was slightly shifted. In overall, the results from FT-IR analysis indicated that there was not formation of a new chemical bond and both polysaccharides kept their own chemical structures.

3.3.3.2 SEM characterisation of blend XG/MC hydrogels

Blend XG/MC hydrogels prepared at different compositions were freeze-dried and coated with gold as described previously. SEM micrographs were obtained at different magnifications as shown in Figure 3.43. XG1/MC0 xerogel presented a disorganised porous structure with various pore sizes, while in case of higher concentration of MC in XG1/MC6 xerogel the density of the network was significantly higher with low porosity. XG2/MC1 xerogel demonstrated a disorganised interconnected porous structure, whereas XG2/MC6 similar to XG1/MC6 sample presented a network consisted of dense polymer sheets. On the other hand, the porosity was higher in XG3/MC1 xerogel.

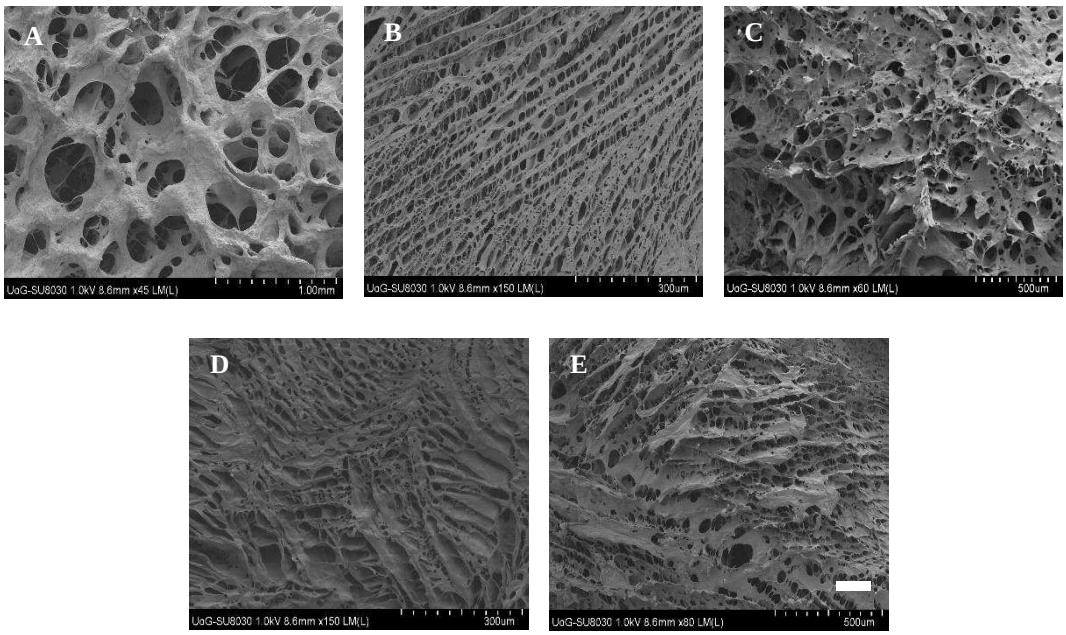

Figure 3.43: SEM micrographs of XG/MC xerogels prepared at various compositions. **A.** XG1/MC0, **B.** XG1/MC6, **C.** XG2/MC1, **D.** XG2/MC6 and **E.** XG3/MC1 hydrogel. SEM photos were obtained at different magnifications. Scale bar: 300-500 μm.

As stated in the previous sections, the porous structure is beneficial for rapid diffusion of nutrients throughout the network, improving the efficacy in cell adhesion, proliferation and migration. In

summary, these observations indicated that the presence of XG promoted porosity of the fabricated scaffolds, in contrast to MC which induced the formation of a denser network. The high incorporation of MC significantly changed the morphology of XG xerogels which resulted in lower porosity and low cell viability as it will be discussed further in Chapter 4.

3.4 Conclusions

The characterisation of the physicochemical and mechanical properties of hydrogels designed for biomedical applications is of paramount importance. The aim of this thesis was to prepare injectable biocompatible hydrogels that will mimic the mechanical properties of the brain tissue and facilitate cell invasion and migration in response to the loaded gradient chemoattractant UII. The first half of Chapter 2 focused on the preparation of HA-based hydrogels formed at differerent crosslinking densities, while in the second half, the preparation of blend hydrogels based on MC was discussed.

The current chapter focused on the main experimental methods devoted to the characterisation of the fabricated hydrogels. In particular, attention focused on the determination of swelling degree, characterisation of the surface morphology using SEM, characterisation of their structure using FT-IR, determination of the enzymatic degradation rate in vitro conditions, characterisation of the mechanical properties using oscillatory rheology and investigation of the release profile of hydrogels. FT-IR spectroscopy allowed to investigate the changes in the structure of the polysaccharides after the crosslinking reaction, while the surface morphology and porosity of the fabricated crosslinked scaffolds were investigated by SEM. HA based hydrogels presented an interconnected porous structure and porosity that was highly dependent on the crosslinking density. In addition, the high porosity of the hydrogels enabled them to swell and the equilibrium swelling degree was determined. The degradation rate of the fabricated hydrogels incubated with hyaluronidase solution was found to be significantly dependent on the swelling degree and the enzyme concentration. The mechanical characterisation of the hydrogels revealed that their viscoelastic properties were close to those of the brain tissue, highlighting their potential as injectable scaffolds in the brain. The drug release studies performed on hydrogels showed that these crosslinked networks can promote sustained release of the drug over a specific period of time, while the release experiments of the FITC-loaded hydrogels demonstrated low amount of the chemoattractant is released as most of it remains inside the gel, which is desirable for the specific application.

Overall, the physicochemical and mechanical features of the fabricated hydrogels showed that could facilitate cell growth and migration. The in vitro biocompatibility of the crosslinked hydrogels and the potential to promote migration of glioma cells when loaded with a gradient concentration of the chemoattractant will be investigated in the following chapter.

References

[1] Garcia H., Barros A.S., Gonçalves C., Gama F.M., Gil A.M., Characterisation of dextrin hydrogels by FTIR spectroscopy and solid-state NMR spectroscopy, Eur. Polym. J., 2008, 44, 2318-2329.

[2] Mansur H.S., Sadahira C.M., Souza A.N., Mansur A.A.P., FTIR spectroscopy characterisation of poly (vinyl alcohol) hydrogel with different hydrolysis degree and chemically crosslinked with glutaraldehyde, Mater. Sci. Eng. C, 2008, 28, 539-548.

[3] Stadtländer C. T. K.H., Scanning Electron Microscopy and Transmission Electron Microscopy of Mollicutes: Challenges and Opportunities, Modern Research and Educational Topics in Microscopy, 2007, 122-131.

[4] Nguyen K.T., West J.L., Photopolymerisable hydrogels for tissue engineering applications, Biomaterials, 2002, 23, 4307-4314.

[5] Pacios I.E., Molina M.J., Gomez-Anton M.R., Pierola I.F., Correlation of Swelling and Crosslinking Density with the Composition of the Reacting Mixture Employed in Radical Crosslinking Copolymerisation, J. Appl. Polym. Sci., 2007, 103, 263-269.

[6] Flory P.J., Rehner J., Statistical mechanics of cross-linked polymer networks II. Swelling, J. Chem. Phys., 1943, 11, 521-526.

[7] De S.K., Aluru N., Johnson B., Crone W., Beebe D.J., Moore J., Equilibrium swelling and kinetics of pH-responsive hydrogels: Models, experiments, and simulations, J. Microelectromech. Syst., 2002, 11, 544-555.

[8] Brannon-Peppas L., Peppas N.A., Equilibrium swelling behaviour of dilute ionic hydrogels in electrolytic solutions, J. Control. Release, 1991, 16, 319-329.

[9] Xue W., Hamley I.W., Thermoreversible swelling behaviour of hydrogels based on N-isopropylacrylamide with a hydrophobic comonomer, Polymer, 2002, 43, 3069-3077.

[10] Kharkar P.M., Kiick K.L., Kloxin A.M., Designing degradable hydrogels for orthogonal control of cell microenvironments, Chem. Soc. Rev., 2013, 42, 7335-7372.

[11] Zhang H., Zhou L., Zhang W., Control of scaffold degradation in tissue engineering: a review, Tissue Eng. Part B Rev., 2014, 20, 492-502.

[12] Aimetti A.A., Machen A.J., Anseth K.S., Poly(ethylene glycol) hydrogels formed by thiol-ene photopolymerisation for enzyme-responsive protein delivery, Biomaterials, 2009, 30, 6048-6054.

[13] Zhang Z., Ni J., Chen L., Yu L., Xu J., Ding J., Biodegradable and thermoreversible PCLA-PEG-PCLA hydrogel as a barrier for prevention of post-operative adhesion, Biomaterials, 2011, 32, 4725-4736.

[14] Thomas A.A., Kim I.T., Kiser P.F., Symmetrical biodegradable crosslinkers for use in polymeric devices, Tetrahedron Lett., 2005, 46, 8921-8925.

[15] Lee F., Chung J.E., Kurisawa M., An injectable hyaluronic acid–tyramine hydrogel system for protein delivery, J. Control. Release, 2009, 134, 186-193.

[16] Patterson J., Siew R., Herring S.W., Lin A.S., Guldberg R., Stayton P.S., Hyaluronic acid hydrogels with controlled degradation properties for oriented bone regeneration, Biomaterials, 2010, 31, 6772-6781.

[17] Yang C., Xu L., Zhou Y., Zhang X.M., Huang X., Wang M., Han Y., Zhai M.L., Wei S.C., Li J.Q., A green fabrication approach of gelatin/CM-chitosan hybrid hydrogel for wound healing, Carbohyd. Polym., 2010, 82, 1297-1305.

[18] Baldwin A.D., Kiick K.L., Reversible maleimide–thiol adducts yield glutathione-sensitive poly (ethylene glycol)–heparin hydrogels, Polym. Chem., 2013, 4, 133-143.

[19] Koehler K.C., Alge D.L., Anseth K.S., Bowman C.N., A Diels-Alder modulated approach to control and sustain the release of dexamethasone and induce osteogenic differentiation of human mesenchymal stem cells, Biomaterials, 2013, 34, 4150-4158.

[20] Kloxin A.M., Kasko A.M., Salinas C.N., Anseth K.S., Photodegradable hydrogels for dynamic tuning of physical and chemical properties, Science, 2009, 324, 59-63.

[21] Fairbanks B.D., Singh S.P., Bowman C.N., Anseth K.S., Photodegradable, Photoadaptable Hydrogels via Radical-Mediated Disulfide Fragmentation Reaction, Macromolecules, 2011, 44, 2444-2450.

[22] Burkersroda, F., Schedl L., Göpferich A., Why degradable polymers undergo surface erosion or bulk erosion, Biomaterials, 2002, 23, 4221-4231.

[23] Lee J.H., Kim H.W., Emerging properties of hydrogels in tissue engineering, J. Tissue Eng., 2018, 9, 1-4.

[24] Vedadghavami A., Minooei F., Mohammadi M.H., Khetani S., Rezaei Kolahchi A., Mashayekhan S., Sanati-Nezhad A., Manufacturing of hydrogel biomaterials with controlled mechanical properties for tissue engineering applications, Acta Biomater., 2017, 62, 42-63.

[25] Xiao Y., Friis E.A., Gehrke S.H., Detamore M.S., Mechanical testing of hydrogels in cartilage tissue engineering: beyond the compressive modulus, Tissue Eng. B Rev., 2013, 19, 403-412.

[26] Oyen M.L., Mechanical characterisation of hydrogel materials, Int. Mater. Rev., 2014, 59, 44-59.

[27] Yan C., Pochan D.J., Rheological properties of peptide-based hydrogels for biomedical and other applications, Chem. Soc. Rev., 2010, 39, 3528-3540.

[28] Matricardi P., Alhaique F., Coviello T., Polysaccharide hydrogels: Characterisation and biomedical applications, Pan Stanford Publishing, 2016, 84-126.

[29] Liu Y., Zhang L., Wei W., Effect of noncovalent interaction on the self-assembly of a designed peptide and its potential use as a carrier for controlled bFGF release, Int. J. Nanomed., 2017, 12, 659-670.

[30] Kodre K.V., Attarde S.R., Yendhe P.R., Patil R.Y., Barge V.U., Differential Scanning Calorimetry: A Review, Res. Rev. J. Pharm. Anal., 2014, 3, 11-22.

[31] http://www.materialssolutions.info/thermal.html (accessed on 08/2018).

[32] Sánchez M.S., Pradas M.M., Ribelles J.L.G., Thermal transitions in PHEA hydrogels by thermomechanical analysis. A comparison with DSC data, Eur. Polym. J., 2004, 40, 329-334.

[33] Zarzyka I., Pyda M., Di Lorenzo M.L., Influence of crosslinker and ionic comonomer concentration on glass transition and demixing/mixing transition of copolymers poly(N-isopropylacrylamide) and poly (sodium acrylate) hydrogels, Colloid Polym. Sci., 2014, 292, 485-492.

[34] Hoare T.R., Kohane D.S., Hydrogels in drug delivery: Progress and challenges, Polymer, 2008, 49, 1993-2007.

[35] Li J., Mooney D. J., Designing hydrogels for controlled drug delivery, Nat. Rev. Mater., 2016, 1, 1-17.

[36] Rich M.H., Lee M.K., Marshall N., Clay N., Chen J., Mahmassani Z., Boppart M., Kong H., Water-Hydrogel Binding Affinity Modulates Freeze-Drying-Induced Micropore Architecture and Skeletal Myotube Formation, Biomacromol., 2015, 16, 2255-2264.

[37] Sornkamnerd S., Okajima M.K., Kaneko T., Tough and Porous Hydrogels Prepared by Simple Lyophilisation of LC Gels, ACS Omega, 2017, 2, 5304-5314.

[38] Ganesan K., Dennstedt A., Barowski A., Ratke L., Design of aerogels, cryogels and xerogels of cellulose with hierarchical porous structures, Mater. Design, 2016, 92, 345-355.

[39] Gupta N.V., Shivakumar H.G., Investigation of Swelling Behaviour and Mechanical Properties of a pH-Sensitive Superporous Hydrogel Composite, Iran J. Pharm. Res., 2012, 11, 481-493.

[40] Wang M.D., Zhai P., Schreyer D.J., Zheng R.S., Sun X.D., Cui F.Z., Chen X.B., Novel crosslinked alginate/hyaluronic acid hydrogels for nerve tissue engineering, Front. Mater. Sci., 2013, 7, 269-284.

[41] Hui Wong R.S., Ashton M., Dodou K., Effect of Crosslinking Agent Concentration on the Properties of Unmedicated Hydrogels, Pharmaceutics, 2015, 7, 305-319.

[42] Malik N.S., Ahmad M., Minhas M.U., Murtaza G., Khalid Q., Polysaccharide hydrogels for controlled release of acyclovir: development, characterisation and in vitro evaluation studies, Polym. Bull., 2017, 74, 4311-4328.

[43] Hutmacher D.W., Scaffolds in tissue engineering bone and cartilage, Biomaterials, 2000, 21, 2529-2543.

[44] Van Tienen T.G., Heijkants R.G., Buma P., de Groot J.H., Pennings A.J., Veth R.P., Tissue ingrowth and degradation of two biodegradable porous polymers with different porosities and pore sizes, Biomaterials, 2002, 23, 1731-1738.

[45] Zhang X.Z., Wu D.Q., Chu C.C., Effect of the Crosslinking Level on the Properties of Temperature-Sensitive Poly(N-isopropylacrylamide) Hydrogels, J. Polym. Sci.: Part B: Polymer Physics, 2003, 41, 582-593.

[46] Hoffman A.S., Hydrogels for biomedical applications. Adv. Drug Deliver. Rev., 2002, 43, 3-12.

[47] Lampe K.J., Kern D.S., Mahoney M.J., Bjugstad K.B., The administration of BDNF and GDNF to the brain via PLGA microparticles patterned within a degradable PEG-based hydrogel: Protein distribution and the glial response, J. Biomed. Mater. Res. A., 2011, 96A, 595-607.

[48] Zhou Z., Yang Z., Huang T., Liu L., Liu Q., Zhao Y., Zeng W., Yi Q., Cao D., Effect of Chemical Cross-linking on Properties of Gelatin/Hyaluronic Acid Composite Hydrogels, Polymer-Plastics Tech. Eng., 2013, 52, 45-50.

[49] Castilla A.M., Wallace M., Mears L.E., Draper E.R., Doutch J., Rogers S., Adams D.J., On the syneresis of an OPV functionalised dipeptide hydrogel, Soft Matter, 2016, 12, 7848-7854.

[50] Kim J.T., Lee D.Y., Kim Y.H., Lee I.K., Song Y.S., Effect of pH on Swelling Property of Hyaluronic Acid Hydrogels for Smart Drug Delivery Systems, J. Sensor Sci. Tech., 2012, 21, 256-262.

[51] Spencer K.C., Sy J.C., Ramadi K.B., Graybiel A.M., Langer R., Cima M.J., Characterisation of Mechanically Matched Hydrogel Coatings to Improve the Biocompatibility of Neural Implants, Sci. Rep., 2017, 7, 1952-1967.

[52] Shi L., Zhang Y., Ossipov D., Enzymatic degradation of hyaluronan hydrogels with different capacity for in situ bio-mineralisation, Biopolymers, 2017, e23090.

[53] Yeo Y., Highley C.B., Bellas E., Ito T., Marini R., Langer R., Kohane D.S., In situ cross-linkable hyaluronic acid hydrogels prevent post-operative abdominal adhesions in a rabbit model, Biomaterials, 2006, 27, 4698-4705.

[54] Bulpitt P., Aeschlimann D., New strategy for chemical modification of hyaluronic acid: preparation of functionalised derivatives and their use in the formation of novel biocompatible hydrogels, J. Biomed. Mater. Res., 1999, 47, 152-169.

[55] Park M.R., Cho C.S., Song S.C., In vitro and in vivo degradation behaviours of thermosensitive poly(organophosphazene) hydrogels, Polym. Degrad. Stabil., 2010, 95, 935-944.

[56] Kong H.J., Alsberg E., Kaigler D., Lee K.Y., Mooney D.J., Controlling Degradation of Hydrogels via the Size of Cross-Linked Junctions, Adv. Mater., 2004, 16, 1917-1921.

[57] Vanderhooft J.L., Alcoutlabi M., Magda J.J., Prestwich G.D., Rheological properties of cross-linked hyaluronan-gelatin hydrogels for tissue engineering, Macromol. Biosci., 2009, 9, 20-28.

[58] Lampe K.J., Namba R.M., Bjugstad K.B., Mahoney M.J., Effect of macromer weight percent on neural cell growth in 2D and 3D nondegradable PEG hydrogel culture, J. Biomed. Mater. Res A., 2010b, 94A, 1162-1171.

[59] Chatterjee K., Lin-Gibson S., Wallace W.E., Parekh S.H., Lee Y.J., Cicerone M.T., Young M.F., Simon C.G., The effect of 3D hydrogel scaffold modulus on osteoblast differentiation and mineralisation revealed by combinatorial screening, Biomaterials, 2010, 31, 5051-5062.

[60] Sachot N., Engel E., Castaño O., Hybrid Organic-Inorganic Scaffolding Biomaterials for Regenerative Therapies, Curr. Org. Chem., 2014, 18, 2299-2314.

[61] Zuidema J.M., Rivet C.J., Gilbert R.J., Morrison F.A., A protocol for rheological characterisation of hydrogels for tissue engineering strategies, J. Biomed Mater. Res. B, 2014, 102, 1063-1073.

[62] Jeon O., Song S.J., Lee K.J., Park M.H., Lee S.H., Hahn S.K., Kim S., Kim B.S., Mechanical properties and degradation behaviours of hyaluronic acid hydrogels cross-linked at various cross-linking densities, Carbohyd. Polym., 2007, 70, 251-257.

[63] Collins M.N., Birkinshaw C., Comparison of the effectiveness of four different crosslinking agents with hyaluronic acid hydrogel films for tissue-culture applications, J. App. Polym. Sci., 2007, 104, 3183-3191.

[64] Mishra B., Upadhyay M., Reddy Adena S.K., Vasant B.G., Muthu M.S., Hydrogels: An Introduction to a Controlled Drug Delivery Device, Synthesis and Application in Drug Delivery and Tissue Engineering, Austin J. Biomed. Eng., 2017, 4, 1-13.

[65] Bashir S., Teo Y.Y., Naeem S., Ramesh S., Ramesh K., pH responsive N-succinyl chitosan/Poly (acrylamide-co-acrylic acid) hydrogels and in vitro release of 5-fluorouracil, PLoS ONE, 2017, 12, e0179250.

[66] Tang I.M., Krishnamra N., Charoenphandhu N., Hoonsawat R., Pon-On W., Biomagnetic of Apatite-Coated Cobalt Ferrite: A Core-Shell Particle for Protein Adsorption and pH-Controlled Release, Nanoscale Res. Lett., 2011, 6, 19-28.

[67] Park M.H., Baek J.S., Lee C.A., Kim D.C., Cho C.W., The effect of Eudragit type on BSA-loaded PLGA nanoparticles, J. Pharm. Investig., 2014, 44, 339-349.

[68] Mendes A.C., Baran E.T., Nunes C., Coimbra M.A., Azevedo H.S., Reis R.L., Palmitoylation of xanthan polysaccharide for self-assembly microcapsule formation and encapsulation of cells in physiological conditions, Soft Matter, 2011, 7, 9647-9658.

[69] Viera R.G.P., Filho G.R., de Assunção R.M.N., da S. Meireles C., Vieira J.G., Synthesis and characterisation of methylcellulose from sugar cane bagasse cellulose, Carbohyd. Polym., 2007, 67, 182-189.

Chapter 4: *In vitro* evaluation of glioma cells response on polysaccharide-based hydrogels

4.1 Introduction

Glioma cells are known for their aggressive and invasive nature which results in inevitable tumour recurrences. Current targeted strategies for GBM treatment including hydrogels as drug delivery systems lack of several limitations. As discussed in Chapter 1, the majority of the studies have employed these matrices as injectable anticancer drug delivery depots to the tumour site after resection of the tumour. The introduction of artificial scaffolds that can not mimic the structure and properties of the ECM is one of the key reasons why most of these systems are not functional. Moreover, these systems lack of effective chemoattractants, allowing residual glioma cells that have not been removed from the surgery to infiltrate healthy brain tissue and increase the risk for tumour reformation. Therefore, there is a number of reasons for the development of viable GBM treatment based on hydrogels derived from molecules that naturally exist in the brain ECM that can promote migration of glioma cells in response to loading of chemoattractants.

Herein, in order to address the limitations of the anticancer drug-loaded hydrogels that have been used in the treatment of GBM, we proposed an easy and cost-effective fabrication of chemoattractant-loaded hydrogels mainly consisted of molecules that naturally exist in the brain ECM such as HA. Specifically, fabricated hydrogels were loaded with human UII as chemoattractant at a ″potentially gradient concentration″ and subsequently with an anticancer drug in order to achieve cell migration in the hydrogel and apoptosis of migrated glioma cells into the hydrogel matrix.

The first section of this chapter provides a brief review on the structure of the brain ECM and the scaffolds that have been fabricated so far in order to mimic this matrix. Chapters 2 and 3 have already presented the preparation methods and the physicochemical and mechanical characterisation of the hydrogels. In this chapter, the biocompatibility of the fabricated hydrogels and the in vitro response of glioma cells on them will be investigated.

4.1.1 Brain ECM

The ECM in the brain occupies up to 20 % of the adult brain volume and plays a vital role in neural development and function, whereas the majority of the CNS volume is composed of neural cells, e.g. neurons, astrocytes, oligodendroglial cells, microglia and blood vessels [1]. Although, the brain ECM has many components that can be found in the ECM of other tissues, there are some distinct differences in its composition. As illustrated in Figure 4.1, it is mainly composed of water, sulfated proteoglycans (PGs) such as chondroitin sulfate and glycosaminoglycans (GAGs) such as hyaluronan or hyaluronic acid (HA) which are long linear polysaccharides and they are localised at the intercellular spaces. In contrast, fibrillar components such as laminin present in the basal membrane for elasticity, fibronectin (mainly produced by fibroblasts) and collagen (mainly produced

by vascular components) that are typical constituents expressed in other tissues, are rarely found in the brain parenchyma, while their levels are rather low compared with the connective tissue [2].

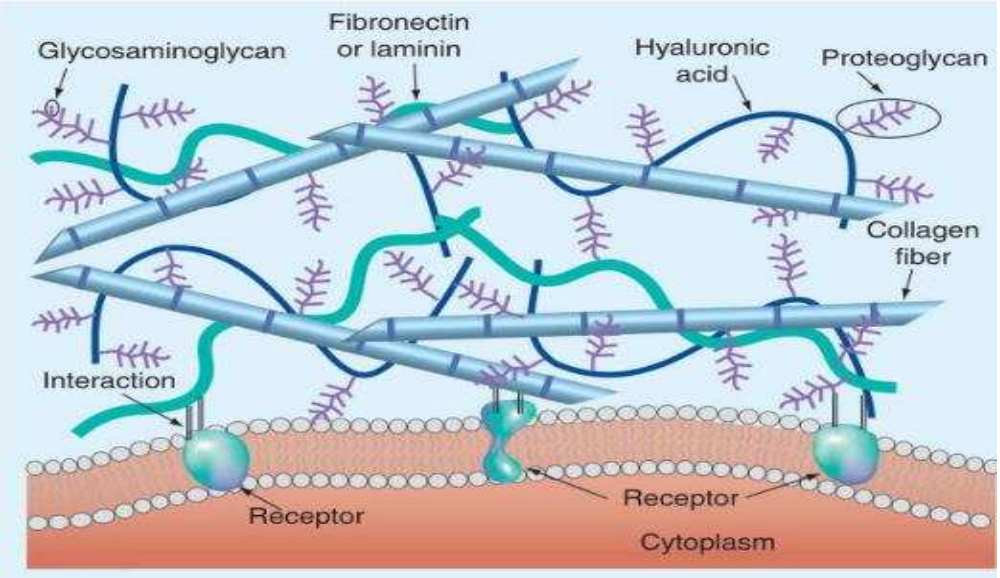

Figure 4.1: The main components of the CNS ECM including specific proteoglycans, low amounts of fibrillar adhesive proteins such as laminin, fibronectin, collagen and integrins as the major ECM adhesion receptors. Adapted from Zhu et al [3].

ECM proteins play a key role in cell-matrix interactions due to the fact they are recognised by cell surface receptors and are involved in physiological cellular processes e.g. proliferation, differentiation and migration. Cells express specific receptors on their surface for components of ECM, which mediate these responses. For example, HA binds to specific cell receptors such as the cluster determinant adhesion molecule (CD44) and to receptor for hyaluronan-mediated motility (RHAMM) that can regulate cell proliferation, adhesion and motility.

4.1.2 ECM in brain tumours

Many alterations occur in the composition of the ECM in case of brain tumours, as summarised in Table 4.1. The changes involve increased secretion of non-typical ECM components in the vicinity of the invading cells in front of the tumour bulk. Some of the secreted molecules such as vitronectin, tenascin C or some specific αvβ integrins are associated with cell motility and angiogenesis which are both critical for tumour growth. This increased production of tumorous ECM molecules results in a significant increase in its volume through adhesion which contributes to intracranial pressure and oedema in the restricted extracellular space [4]. Extensive degradation of the ECM in close proximity to the tumour bed occurs, specifically in high-grade glioma. Then tumour cells overexpress αvβ integrin receptors on their surface and are allowed to detach from the core tumour and migrate along tract structures within the brain.

Furthermore, glycosaminoglycans such as HA is expressed in case of high-grade gliomas at high levels, which can be 20 times higher than in normal adult brain. Moreover, chondroitin sulfate

proteoglycans in the normal brain, are known for their inhibitory effect on stem cell migration, whereas in glioma they are upregulated and promote glioma cell migration [5]. In the context of GBM growing, fibrous proteins rarely found in normal brain, appear to be highly expressed by GBM cells [6], [7]. Tenascins (C and R) consist a family of glycoproteins present in the ECM and they are involved in proliferation, migration, and morphogenesis, playing an important role in the development of CNS. Galectins are also upregulated in glioma and they are involved in glioma cell migration and angiogenesis. Particularly, levels of Gal-1 are indicative of the aggressiveness of many tumours [8].

Table 4.1: Representative ECM molecules present in the brain and brain tumours (+ indicates the presence of the molecule, +++ indicates the presence at high levels, - indicates the absence of the molecule).

Molecules	Location	
	Brain	Glioma
Glycosaminoglycans (GAGs): Hyaluronan (HA)	+	+++
Proteoglycans (PGs): Chondroitin sulfate	+	+++
Glycoproteins: Tenascin: C and R	+	+++
Galectins	+	+++
Fibrous proteins (collagen, laminin, fibronectin)	-	+

4.1.3 Scaffolds to mimic the brain ECM properties

The complexity and the diversity in the composition of brain ECM plays a significant role in GBM invasion, highlighting the significance of studying further glioma cells-ECM interactions. To date, several studies have focused on the development of biocompatible matrices in order to mimic the properties of the ECM and study extensively glioma cells behaviour. Yang et al fabricated composite hydrogels consisted of blends of collagen-chondroitin sulfate and collagen-HA in order to mimic the ECM surrounding high-grade gliomas [9]. The effect of chondroitin sulfate and HA on glioma invasion was investigated. Chondroitin sulfate demonstrated an inhibitory role on glioma invasion, whereas HA did not present any important effect. Kievit et al developed a 3D scaffold that was composed of chitosan and alginate as model microenvironment to study the behaviour of glioma cells cultured on these scaffolds [10]. They found that these scaffolds were able to provide a growth environment for glioma cells in vitro. On the other hand, Pedron et al reported the use of gelatin modified with methacrylic anhydride for the preparation of scaffolds to investigate the impact of biophysical properties such as crosslinking density and stiffness on the glioma phenotype [11].

4.1.4 HA as main component of brain ECM and its role in glioma

HA as a non-sulfated glycosaminoglycan is one of the main components of the native brain ECM and occupies a large part of the extracellular volume of the brain, mainly located in the white matter tracts [12], [13]. There is a lot of evidence that HA plays a critical role in glioma progression but most importantly higher levels of HA are present in malignant gliomas than in the normal brain tissue. HA through interaction with CD44 or RHAMM expressed by glioma cells promotes migration and invasion of glioma cells [14] as illustrated in Figure 4.2. CD44 is a membrane glycoprotein frequently overexpressed in gliomas and is correlated with increased malignancy and reduced mean survival time [15]. RHAMM is also well-known as a HA-binding protein and is expressed on the cell surface and in the cytoplasm, as well as in the cytoskeleton and nucleus [16]. As it was mentioned earlier, this protein regulates cell proliferation, adhesion and motility. The cellular signalling pathways involving RHAMM and CD44 receptors will not be discussed further as it is beyond of the scope of this thesis.

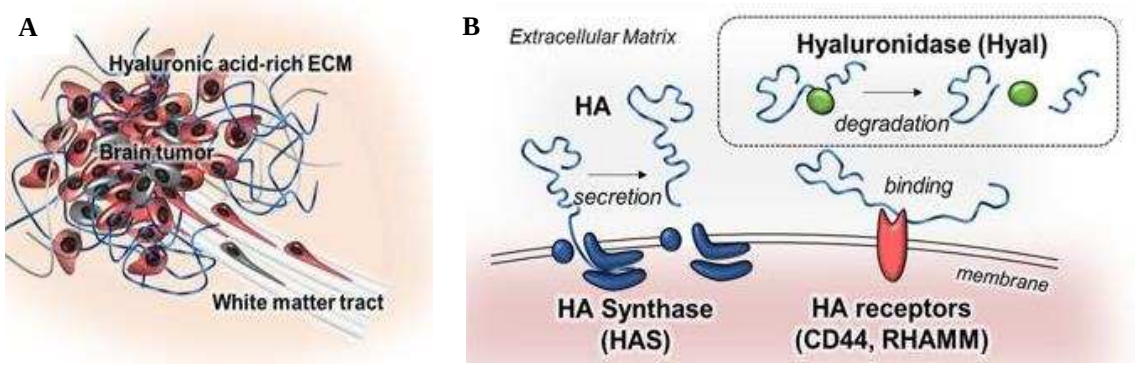

Figure 4.2: A. Schematic illustration of brain tumour-favourable microenvironment highlighting the HA enriched ECM, **B.** Illustration of the three major components in HA production and degradation that are present in the ECM. Adapted from Cha et al [17].

Recently, there has been a growing interest in the development of hydrogels to understand tumour biology. Glioma cells-ECM interactions have been investigated on 3D matrices and they are mainly restricted to collagen or Matrigel based scaffolds [18], [19]. Limitations of these scaffolds due to the different consistency and structural organisation of brain parenchyma, render the understanding of invasion mechanism complicated. In chapter 2, some of the biomedical applications of HA-based hydrogels were noted, but only few studies have investigated the use of these matrices to study the cell-matrix interactions in GBM invasion. Rao et al developed multicomponent composite hydrogels composed of collagen and HA. Consequently, they studied glioma cell morphology and migration on these scaffolds. Glioma cells obtained rounded morphology and their migration was mainly dependent on the concentration of HA [20]. Ananthanarayanan et al fabricated HA-based hydrogels of various stiffness, functionalised with Arg-Gly-Asp (RGD) peptides to facilitate cell adhesion and

study the mechanobiology of glioma cell morphology and invasion which was dependent on RGD concentration as shown in Figure 4.3 [21].

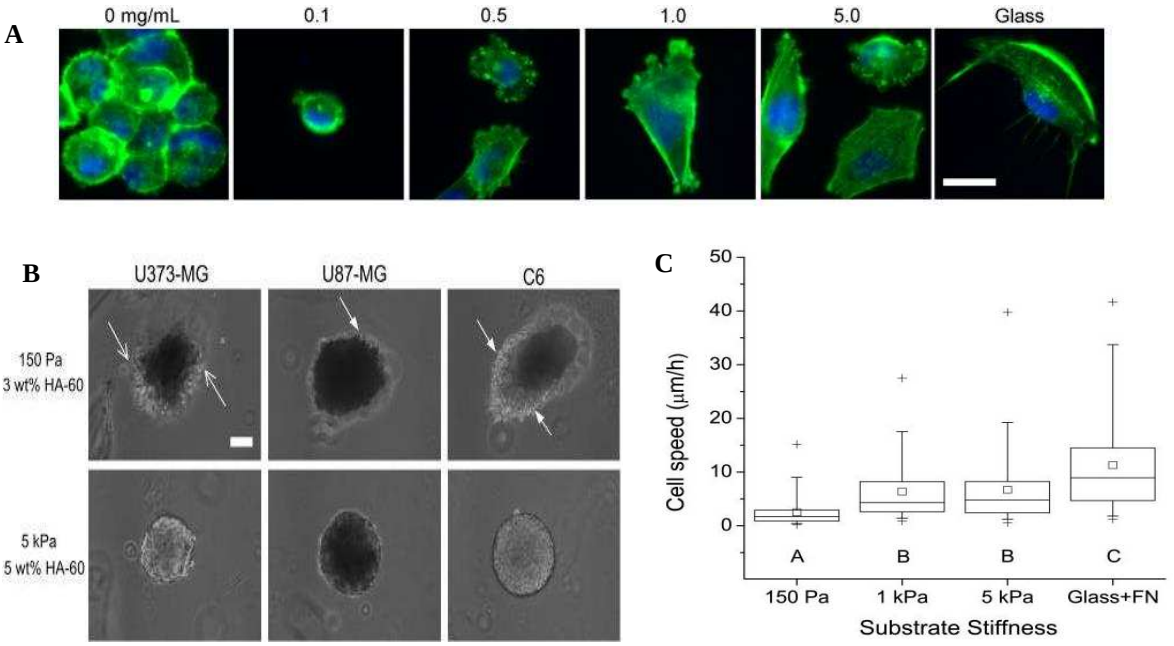

Figure 4.3: A. Morphology of glioma cells adhered to RGD-functionalised HA gels with various concentrations of RGD peptide, **B.** 3D invasion of glioma spheroids through HA-RGD hydrogels. U373 MG cells dispersed and invaded as single cells (open arrows) whereas U87MG and C6 cells retained spheroid borders with cells invading at the edges (filled arrows). No cells invaded the dense 5 kPa hydrogel, **C.** Regulation of glioma cell motility by matrix stiffness. The graph depicts the average speed of random motility of U373 MG cells cultured on RGD functionalised HA gels of constant RGD peptide density and varying stiffness. Cell motility was higher on glass surface compared with hydrogel matrix. Adapted from Ananthanarayanan et al [21].

Pedron et al reported the development of gelatin and PEG based hydrogels with the incorporation of HA into the hydrogel network [22]. They investigated the glioma cell phenotype on these scaffolds, highlighting the formation of clusters and the increased expression of malignancy associated genes in the HA containing hydrogels.

4.1.5 Human Urotensin II as chemoattractant

In the late 1970s, Conlon et al demonstrated the presence of urotensin in the brain of a tetrapod, the green frog Rana ridibunda [23]. Urotensin II (UII) is a cyclic peptide consisting of 11 amino acids in humans, including the presence of a cyclic hexapeptide C-terminal Cys-Phe-Trp-Lys-Tyr-Cys, connected by a disulfide bond as shown in Figure 4.4.

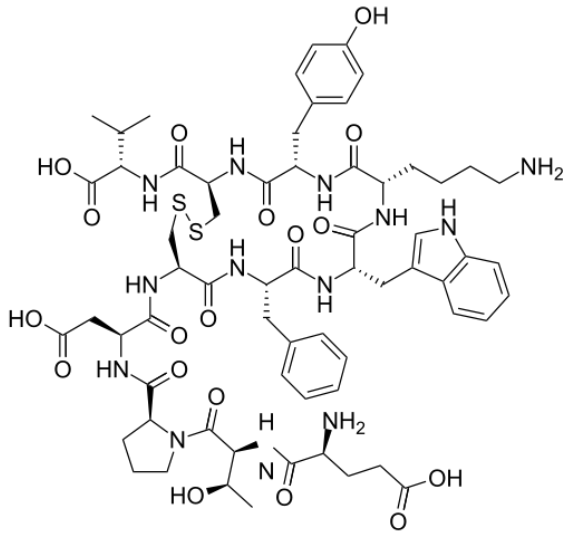

Figure 4.4: Chemical structure of human Urotensin II, including the presence of a cyclic hexapeptide.

UII is mainly located in the cardiovascular, renal and endocrine systems as well as within the CNS [24]. In humans, high expression levels of UII are found in the myocardium, the atria, and the ventricles [25]. Additionally, low amount of this peptide was detected in extracts of cerebrospinal fluid (CSF) in humans [26]-[28].

Recently, it has been reported that UII promoted proliferation of A549 lung adenocarcinoma cells and tumour growth in a nude mouse xenograft model [29]. This vasoactive peptide has been involved in the release of proinflammatory cytokines and matrix metalloproteinase-9 in the tumour microenvironment of lung adenocarcinoma [30]. In this context, UII overexpressed in malignant gliomas could play a key role in the tumour growth and the invasion of these tumour cells. As discussed in Chapter 1, one of the unique features of GBM is the highly invasive nature of glioma cells. The invasive behaviour can be attributed not only to chemoattractant factors such as growth factors but also chemokines or vasoactive peptides which activate G protein coupled receptors (GPCRs). Among these receptors, the chemokine receptor CXCR4 is widely recognised by glioma cells [31]. It is noteworthy that vasoactive peptide receptors have been involved in migration of various cancer cell lines such as neuropeptide Y on a breast cancer cell line and bradykinin on glioma cells [32], [33]. Most importantly, it has been demonstrated that UII can induce chemoattraction of human monocytes through its GPCR receptor (UT), highlighting its potential as a new chemokine [34]. Recently, Castel et al reported that GBMs highly express UII and demonstrated that gradient concentrations of UII (10^{-8} M) exhibited chemoattracting behaviour on glioma cells and HEK 293 cells expressing human UT as presented in Figure 4.5 [35]. In contrast, it was observed that homogenous concentrations of UII (10^{-8} -10^{-10} M) drastically blocked cell motility of glioma cells.

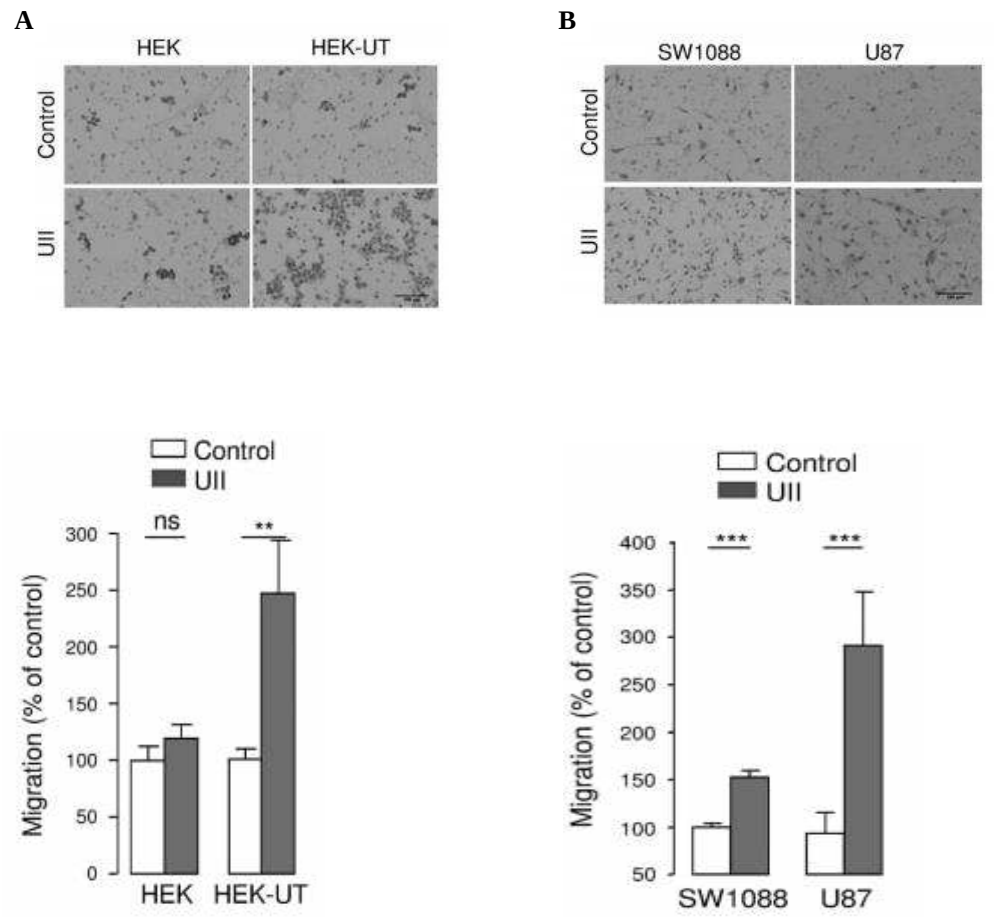

Figure 4.5: Migration profile of HEK and SW1088 cells in response to gradient concentration of UII. **A.** Migration of human UT expressing HEK293 cells in the presence or absence of UII (10^{-9} M). **B.** Migration of astrocytoma SW1088 cells in the presence or absence of UII (10^{-9}). Cell migration was evaluated by counting hemotoxylin stained cells on the transwell membranes. The histograms represent the percentage of migrated cells in comparison with the control (untreated cells). Each bar corresponds to mean ± SEM obtained from 3 to 12 independent experiments in triplicates. Data adapted from Lecointre et al [35].

4.2 Experimental

4.2.1 Materials

Human UII (MW=1388.56 Da, purity: 86.2 %) was purchased from PolyPeptide Laboratories. Human fibronectin 0.1 % v/v was purchased from Sigma Aldrich. Dulbecco's Modified Eagle Medium (DMEM), Antibiotic/Antimicotic (AA, Penicillin 10.000 U/mL, Streptomycin 10.000 µg/mL and 25 µg/mL Fungizone™) and Fetal Bovine Serum (FBS) were purchased from Gibco by Life Technologies. Sodium pyruvate solution and Dulbecco's phosphate buffered saline (1×DPBS) were purchased from Sigma Aldrich. Trypsin-EDTA solution (0.05 %) was purchased from Gibco by Life Technologies. The human glioblastoma cell lines U87MG (ATCC, HTB-14, grade IV WHO classification) were purchased from American Type Culture Collection (ATCC Manassas, VA, USA). The other glioma cell lines 42 MG were provided by Professor J. Honnorat (CRNL, Lyon, France). The cell culture flasks, 24, 48 and 96-well plates were purchased from Thermo Fischer Scientific. Cell viability was assessed by MTS (Cell Titer 96 Aqueous One Solution Cell

Proliferation Assay) and it was purchased from Promega. Live/Dead Cell Viability/Cytotoxicity kit was purchased from Molecular Probes. Ki-67 antibody was purchased from Santa Cruz Biotechnology, 4',6-Diamidino-2-Phenylindole (DAPI) was purchased from Invitrogen. Normal Donkey Serum was purchased from Abcam. Alexa Fluor anti-goat 488 antibody was purchased from Molecular Probes. Corning Transwell polycarbonate membrane cell culture inserts and hematoxylin solution (Harris Modified) were purchased from Sigma Aldrich. CitiFluor™ mounting solution was purchased from Science Services and Mowiol mounting solution was purchased from Sigma Aldrich. DOX HCl, TMZ and Paraformaldehyde were purchased from Sigma Aldrich.

4.2.2 Methods

4.2.2.1 Cell culture

Glioma cell lines (U87MG, 42 MG) were cultured in DMEM supplemented with 10 % FBS, 1% AA and 1 % sodium pyruvate at 37 °C and 5 % CO_2 in a fully humidified incubator. Cells were routinely passaged upon reaching confluency using Trypsin EDTA 0.05 % for their detachment from the culture flask.

4.2.2.2 Preparation of chemoattractant (UII)-loaded HA-ADH hydrogels

Four different crosslinking densities of HA-ADH hydrogels were investigated and the detailed protocol for one of them is described below. HA sodium salt (10.0 mg, 6.25 nmoles) was dissolved in 800 μL of sterile deionised water and EDC (0.26 mg, 1.35 μmoles) was dissolved in 100 μL of deionised water and added at different molar ratios to the aqueous HA solution. EDC was allowed to dissolve before the addition of ADH. The crosslinker ADH (0.25 mg, 1.43 μmoles) was subsequently dissolved in 100 μL of sterile deionised water and was added to the activated HA solution. A stock solution of the chemoattractant UII of 10^{-4} M concentration was prepared and added in the gelator solution. The final concentration of the chemoattractant in the hydrogel was 10^{-8} M. The pH of the solution was adjusted at pH 5.5 with the addition of HCl 0.1 M. Gelation was allowed to occur with gentle vortexing. HA-ADH hydrogels were washed 3 times with PBS for the removal of any excess of unreacted crosslinker.

4.2.2.3 Preparation of chemoattractant (UII)-loaded HA-BSA hydrogels

Four different crosslinking densities of HA-BSA hydrogels were prepared and the detailed protocol for one of them is described below. The ratios of BSA, sulfo-NHS and EDC were adjusted to obtain hydrogels optimised for cell adhesion. Briefly, HA sodium salt (6.0 mg, 3.75 nmoles) was dissolved in 800 μL of sterile deionised water. HA was activated with EDC, (2.0 mg, 10.4 μmoles) and N-hydroxysulfosuccinimide (sulfo-NHS) (0.5 mg, 2.3 μmoles) mixture in a molar ratio 4:1 in 200 μL of sterile deionised water and the pH was adjusted at pH 6.0 with the addition of HCl 0.1 M before the reaction with the BSA molecule. The reaction was allowed to proceed for 2 minutes by vortexing. A stock solution of the chemoattractant UII of concentration 10^{-4} M was prepared and added in the

gelator solution. The final concentration of the chemoattractant in the hydrogel was 10^{-8} M. Then BSA (3.0 mg, 45.4 nmoles) was added as a powder to the activated HA solution for further crosslinking and gelation was allowed to occur with gentle vortexing. HA-BSA hydrogels were washed 3 times with PBS for the removal of any excess of unreacted crosslinker.

4.2.2.4 Preparation of DOX-loaded HA-ADH hydrogels

Different crosslinking densities of HA-ADH hydrogels were investigated and the detailed protocol for one of them is described below. HA sodium salt (10 mg, 6.25 nmoles) was dissolved in 800 μL of sterile deionised water and EDC (0.26 mg, 1.35 μmoles) was dissolved in 100 μL of deionised water and added at different molar ratios to the aqueous HA solution. EDC was allowed to dissolve before the addition of ADH. The crosslinker ADH (0.25 mg, 1.43 μmoles) was subsequently dissolved in 100 μL of deionised water and was added to the activated HA solution. A stock solution of DOX of concentration 100 μM was prepared and 100 μL were added to the reaction mixture. The final concentration of the drug in the hydrogels was 10 μM. Gelation was allowed to occur with gentle vortexing. Hydrogels were washed with PBS for the removal of any excess of unreacted crosslinker.

4.2.2.5 Preparation of DOX-loaded HA-BSA hydrogels

Different crosslinking densities of HA-BSA hydrogels were prepared and the detailed protocol for one of them is described below. Briefly, HA sodium salt (6.0 mg, 3.75 nmoles) was dissolved in 800 μL of sterile deionised water. HA was activated with EDC (2.0 mg, 10.4 μmoles) and sulfo-NHS (0.5 mg, 2.3 μmoles) mixture in a molar ratio 4:1 in 200 μL of deionised water and the pH was adjusted at pH 6.0 with the addition of HCl 0.1 M before the reaction with the protein. The reaction was allowed to proceed for 2 minutes by vortexing. Then BSA (3.0 mg, 45.4 nmoles) was added as a powder to the activated HA solution for further crosslinking. A stock solution of DOX of concentration 100 μM was prepared and 100 μL were added to the reaction mixture. The final concentration of the drug in the hydrogels was 10 μM. Gelation was allowed to occur with gentle vortexing.

4.2.2.6 Preparation of MC hydrogels for U87MG cell culture

For detailed protocol refer to chapter 2 (Section 2.2.2.3).

4.2.2.7 Preparation of blend XG/MC hydrogels for U87MG cell culture

For detailed protocol refer to chapter 2 (Section 2.2.2.4).

4.2.2.8 Glioma cell culture on HA-ADH hydrogels

HA-ADH hydrogels at different crosslinking densities were prepared into the wells of a 48-well plate with a final volume of 250 μL in the presence or absence of the chemoattractant UII (10^{-8} M). The hydrogels were rinsed three times with PBS and they were incubated with 200 μL of DMEM (1 %

AA, 1 % sodium pyruvate, in the absence of FBS) for 2 h for buffer exchange. Then glioma cells (U87MG, 42 MG) were passaged and seeded on the surface of the hydrogels at a density of 5×10^3 cells per well. Subsequently, the cells were seeded for 4 days in DMEM supplemented with 1 % of AA and 1 % of sodium pyruvate in the absence of serum at 37 °C in a fully humidified incubator (IGO150 CELL life CO_2 Incubator, Thermo Fischer Scientific). The culture medium was replaced every second day. The morphology of glioma cells seeded on the hydrogels was monitored as a function of incubation time and cultures were imaged using a camera connected to a NIKON inverted microscope.

4.2.2.9 U87MG cell culture on HA-BSA hydrogels

HA-BSA hydrogels at different crosslinking densities were prepared into the wells of a 96-well plate with a final volume of hydrogel 50 µL in the presence or absence of the chemoattractant (10^{-8} M). The hydrogels were rinsed three times with PBS and they were incubated with 100 µL of DMEM (1% AA, 1 % sodium pyruvate, in the absence of FBS) for 2 h for buffer exchange. Then U87MG cells were passaged and seeded on the surface of the hydrogels at a density of 5×10^3 cells per well. The cells were seeded for 2 days in DMEM supplemented with 1 of % AA and 1% of sodium pyruvate in the absence of serum at 37 °C. The morphology of glioma cells seeded on the hydrogels was monitored as a function of incubation time and cultures were imaged using an EVOS FLoid Cell Imaging station.

4.2.2.10 Cell viability-MTS assay on HA-ADH hydrogels

The viability of U87MG and 42 MG cells seeded on HA-ADH hydrogels, measured as a function of mitochondrial activity, was determined by MTS assay. Briefly, U87MG and 42 MG cells were seeded on 50 µL of different crosslinking densities of HA-ADH hydrogels at a density of 5×10^3 cells per well in a 96-well plate in 100 µL of DMEM supplemented with 10 % of FBS, 1 % of AA and 1 % of sodium pyruvate in a fully humidified incubator. The cells were seeded on the hydrogels for 24 and 48 h. After 24 and 48 h of incubation, MTS solution (20 µL) was added to the wells as per manufacturer's protocol and the plate was placed in the incubator for 1 h. The absorbance was measured at 490 nm using a microplate reader (Tecan Infinite M200 Pro).

% Cell viability was calculated assuming the well containing only U87MG or 42 MG cells as positive control (100 % viability). The resulting viability of the hydrogels was calculated using the following equation:

% Cell viability = subtracted absorbance average hydrogel/subtracted absorbance average control × 100.

As background for the positive control, wells contained only DMEM and MTS solution. As background for the conditions with the hydrogels, wells contained only hydrogels in DMEM and MTS. The background absorbance was subtracted from the absorbance of the wells containing cells.

4.2.2.11 Cell viability-MTS assay on HA-BSA, MC and on blend XG/MC hydrogels

The viability of U87MG cells on HA-BSA, MC and XG/MC hydrogels was evaluated by MTS assay as described above. For the detailed protocol refer to section 4.2.2.10.

4.2.2.12 Live/Dead assay on HA-ADH hydrogels

Live/Dead Cell Viability Assay Kit was performed in order to evaluate qualitatively the viability of cells seeded on HA-ADH hydrogels after 24 and 48 h of incubation. The Live/Dead assay kit containing Calcein AM (2 μg/mL in PBS) and ethidium homodimer (4 μg/mL in PBS) reagents was prepared as per manufacturer's protocol. Briefly, U87MG and 42 MG cells seeded on the hydrogels as described above were washed with DPBS and incubated with 100 μL of Live/Dead staining solution for 25-30 minutes at room temperature. Images of the cultured cells were taken with an EVOS FLoid Cell Imaging station or a camera connected to a NIKON inverted microscope respectively. Viable cells were stained green because of their reaction with the Calcein AM and damaged cell membranes were stained red due to their reaction with ethidium homodimer. The green and red fluorescence images from viable and dead cells respectively were merged to one using ImageJ.

4.2.2.13 Live/Dead assay on HA-BSA hydrogels

Live/Dead Cell Viability Assay was performed in order to evaluate qualitatively the viability of cells seeded on HA-BSA hydrogels after 24 and 48 h of incubation. For the detailed protocol, refer to section 4.2.2.12.

4.2.2.14 Immunofluorescence

Immunofluorescence analysis was performed on U87MG and 42 MG cells cultured on HA-ADH hydrogels for 2 days. To isolate the cells seeded on the hydrogels, trypsin-EDTA solution was added on each hydrogel and with thorough mixing with DMEM, the cell solutions were transferred into centrifuge tubes. Cell pellets were obtained after centrifugation at 125g for 5 minutes. Glass coverslips were coated with fibronectin (1:50 dilution) and placed in a 24-well plate. Cell pellet was resuspended and cells were allowed to adhere on the coverslips for 24 h. Next day, cells were fixed with 4 % paraformaldehyde (PFA), permeabilised using 0.05 % Triton-1× PBS and blocked using 2 % NDS (Normal Donkey Serum), 10 % FBS in 1×PBS for 1 h at room temperature. After blocking, cells were incubated with the primary antibody Ki-67 (1:300 dilution) overnight at 4 °C. After 24 h, cells were washed with PBS and incubated with Alexa-conjugated secondary antibody Alexa Fluor anti-goat 488 (1:250 dilution) for 2 h at room temperature. Finally, cell nuclei were counterstained

with 4′,6-diamidino-2-phenylindole (DAPI) in 1:1000 dilution (stock concentration 1 μg/μL) and they were imaged by confocal microscopy (Leica TCS SP5 confocal laser scanning microscope).

4.2.2.15 Boyden Chamber invasion and migration assay on HA-ADH hydrogels

HA-ADH hydrogels were prepared at two different crosslinking densities (L1 and L2 conditions) according to the preparation protocol. A thin layer of hydrogel (100 μL) was applied to the upper part of the polycarbonate membranes with pore size 8 μm. U87MG and 42 MG cells were harvested by trypsinisation and 5×10^4 cells resuspended in 100 μL of DMEM in the absence of serum. Subsequently, cells were seeded on the hydrogel layer, whereas the lower chamber was filled with 600 μL of DMEM in the absence of serum (control buffer) or in the presence of UII (10^{-8} M). U87MG and 42 MG cells were allowed to invade and migrate through the thin layer of hydrogel for 48 h at 37 °C. At the end of the assay, the upper chambers were removed from the transwell unit and cells that had not migrated from the upper surface of the membrane were removed gently with a cottonwool swab. Then U87MG and 42 MG cells were fixed and stained with hematoxylin solution. Polycarbonate membranes with fixed cells were mounted on microscope slides. Photos of the membranes were taken with EVOS FLoid Cell Imaging station and quantification of the migrated cells was performed with ImageJ.

4.2.2.16 Boyden Chamber invasion and migration assay on HA-BSA hydrogels

HA-BSA hydrogels were prepared at three different crosslinking densities (HB16, HB17 and HB18 conditions) according to the protocol. A thin layer of hydrogel (100 μL) was applied to the upper part of the membrane. U87MG cells were passaged and 5×10^4 cells resuspended in 100 μL of DMEM in the absence of FBS and they were seeded on the thin layer of the hydrogel. As described above, U87MG were allowed to invade the thin layer of hydrogel and migrate through the porous membranes for 48 h at 37 °C. Then cells were fixed and stained with hematoxylin and photos of the membranes were taken with an EVOS FLoid Cell Imaging station.

4.2.2.17 *In vitro* cytotoxicity of DOX on U87MG cells

The in vitro cytotoxicity of DOX on U87MG cells was evaluated by MTS assay. Briefly, U87MG cells were passaged, seeded into the wells of a 96-well plate at a density of 5×10^3 cells per well and allowed to adhere in DMEM supplemented with 10 % FBS, 1 % AA and 1 % sodium pyruvate for 24 h. Subsequently, glioma cells were treated with various concentrations of DOX (0.01-100 μM) for 24, 48 and 72 h. After these incubation times, MTS solution (20 μL) was added to the wells as per manufacturer's protocol and cells were incubated at 37 °C for 1 h. The absorbance was measured at 490 nm and the % cell viability was calculated. The IC_{50} value of DOX was determined as the concentration of the drug that demonstrated 50 % inhibition of cell growth in vitro after 72 h of incubation.

4.2.2.18 *In vitro* cytotoxicity of DOX-loaded HA-ADH hydrogels

The in vitro cytotoxicity of DOX-loaded hydrogels was determined using MTS assay. Briefly, DOX-loaded hydrogels were prepared into the wells of a 96-well plate as described above in section 4.2.2.4. U87MG cells were passaged and seeded on the drug-loaded hydrogels at a density of 5×10^3 cells per well for 24 and 48 h. After these incubation times, MTS solution (30 μL) was added on the hydrogels and cells were incubated for 1 h at 37 °C. The absorbance was measured at 490 nm and the % cell viability was calculated as described above. Blank HA-ADH hydrogels were also prepared as negative control.

4.2.2.19 *In vitro* cytotoxicity of TMZ on U87MG cells

The cytotoxicity of TMZ on U87MG cells was evaluated by MTS assay. U87MG cells were passaged and seeded into the wells of a 96-well plate at a density of 5×10^3 cells per well and allowed to adhere overnight in DMEM as described previously. Fresh solutions of TMZ of various concentrations were obtained by diluting the stock solution with DMEM. The stock solution of TMZ in DMSO was diluted more than 1000 times in order to prevent adverse effects on cells. Subsequently, the cells were incubated with increasing concentrations of TMZ (50-515 μM) for 24, 48 and 72 h. After these incubation periods, MTS solution (20 μL) was added and the % cell viability was calculated.

4.2.2.20 Statistical analysis

Statistical analysis was performed using GraphPad Prism and the level of significance was determined by using Mann and Whitney's test. Statistical difference was set at a probability of $^{***}P < 0.001$, $^{**}P < 0.01$ and $^{*}P < 0.05$.

4.3 Results and discussion

4.3.1 Glioma cell culture on HA-ADH hydrogels

4.3.1.1 Morphology and proliferation of glioma cells on HA-ADH hydrogels

As discussed in Chapter 2, four different crosslinking densities of HA-ADH hydrogels were prepared and the molar ratios of ADH to HA and HA to EDC were adjusted to obtain hydrogels optimised for cell adhesion. Glioma cells were seeded on the fabricated hydrogels and the morphology and proliferation was investigated. The experimental conditions for the preparation of HA-ADH hydrogels at different crosslinking densities are provided in Table 4.2. Briefly, hydrogels were prepared into the wells of a 48-well plate with a final volume of 250 μL in the presence or absence of the chemoattractant. Stock solution of the chemoattractant UII of concentration 10^{-4} M in DMEM in the absence of serum, was prepared. Subsequently, HA-ADH hydrogels were loaded with UII with final concentration of the chemoattractant in the hydrogels to be 10^{-8} M. In addition, hydrogels were prepared in the absence of chemoattractant as control condition in order to control whether the chemokine peptide UII affects the morphology and proliferation of glioma cells.

Table 4.2: Experimental conditions for the preparation of HA-ADH hydrogels at different crosslinking densities.

Sample abbreviation	HA (mg/nmole)	ADH (mg/µmole)	EDC (mg/µmole)	pH
L1	10.0/6.25	0.25/1.43	0.26/1.36	5.5
L2	10.0/6.25	0.5/2.87	0.6/3.12	5.5
H1	10.0/6.25	2.5/14.3	2.6/13.6	5.5
H2	10.0/6.25	3.5/20.1	3.6/18.8	5.5

Different glioma cell lines (U87MG and 42 MG) were passaged and seeded on the surface of the hydrogels at a density of 5×10^3 cells per well. U87MG and 42 MG cell cultures are shown in Figures 4.6 and 4.7. The cells were seeded for 4 days in DMEM supplemented with 1 % of AA and 1 % of sodium pyruvate in the absence of FBS at 37 °C.

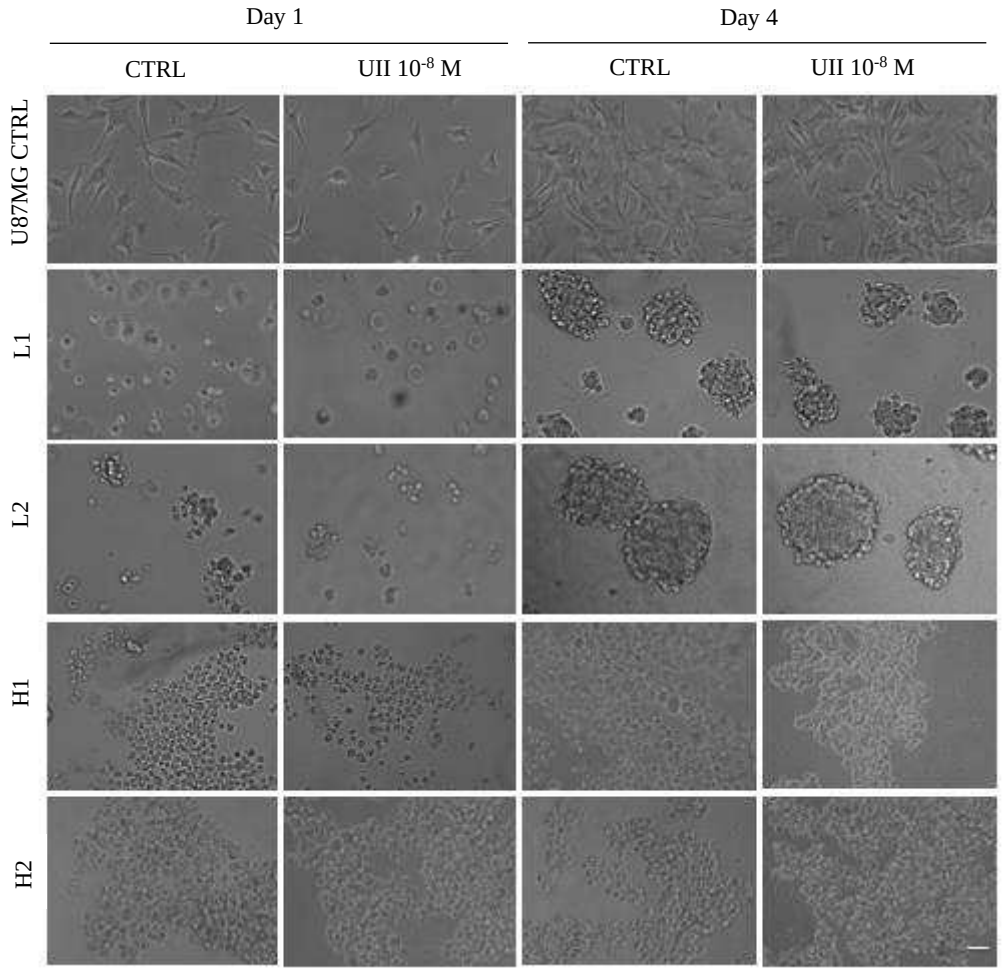

Figure 4.6: Morphology of U87MG cells cultured on different crosslinking conditions of HA-ADH hydrogels in the absence or the presence of UII (10^{-8} M). Cells were seeded onto the hydrogels for 4 days in DMEM in the absence of FBS. Representative photos of cell cultures were taken using a NIKON inverted microscope. Magnification: 20x, Scale bar: 50 µm.

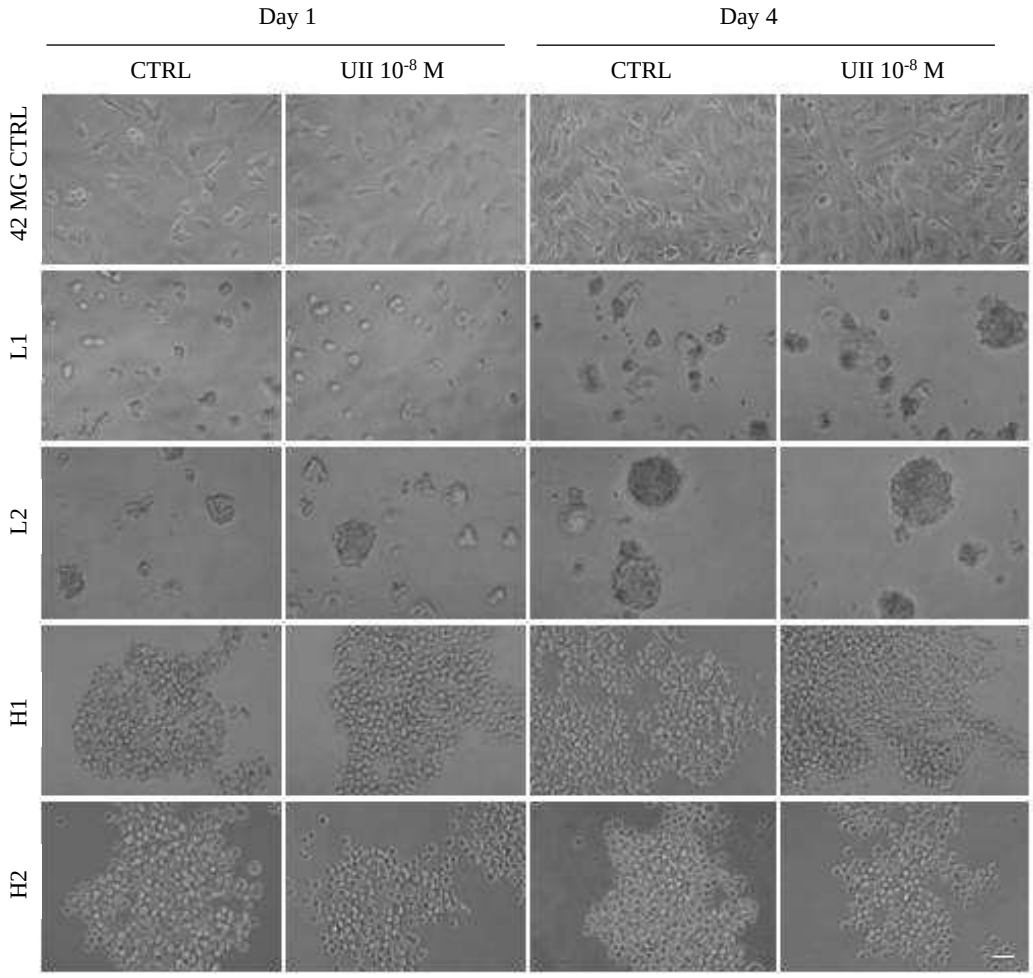

Figure 4.7: Morphology of 42 MG cells cultured on different crosslinking conditions of HA-ADH hydrogels in the absence or the presence of UII (10^{-8} M). Cells were seeded onto the hydrogels for 4 days in DMEM in the absence of FBS. Representative photos of cell cultures were taken using a NIKON inverted microscope. Magnification: 20x, Scale bar: 50 µm.

As discussed earlier, U87MG and 42 MG cells were seeded on HA-ADH scaffolds and 2D culture surfaces for 4 days. To ensure that HA-ADH hydrogels at different crosslinking densities in the absence or presence of UII demonstrate different cell adhesive properties, the morphology of glioma cells seeded on the hydrogels was monitored as function of incubation time. As shown in Figures 4.6 and 4.7, U87MG and 42 MG cells presented morphology, which was highly dependent on the stiffness of the matrix. After one day of incubation, U87MG and 42 MG cells seeded on the standard culture surface obtained their typical elongated morphology with long cell protrusions associated with migration [36], whereas both cell lines cultured on the surface of the hydrogels started to adopt rounded morphology with loss of cell adhesion. More specifically, cells seeded on the hydrogels of low crosslinking density (L1 and L2 conditions) showed rounded morphology and progressive clustering of glioma cells forming well-defined spherical shape of neurospheres. In contrast, in the case of hydrogels of high crosslinking density (H1 and H2 conditions), cell spreading was relatively

higher on the surface and cells appeared included in irregular clusters with uneven external rims and isolated, possibly due to low porosity and poor diffusion of the cell nutrients across the hydrogel network. In addition, it is noteworthy that the presence of UII had negligible effect on the morphology, shape and proliferation of glioma cells. These results suggest that glioma cells are sensitive to the mechanical properties of the designed hydrogels and their morphology alters accordingly to hydrogel's stiffness and crosslinking density. Recently, Pedron et al found that the hydrogel porosity and the matrix mechanical properties significantly impact glioma cell morphology [11]. Particularly, they observed that stiffer microenvironments induced cell spreading, while softer hydrogels induced low cell spreading, favouring the formation of cell aggregates or neurospheres. Similarly, Jiglaire et al observed that U87MG cells cultured on 2D environment after 8 days had elongated morphology with small filopodia, while cells seeded on hydrogels obtained rounded morphology with less developed lamellipodia or filopodia as shown in Figure 4.8 [37].

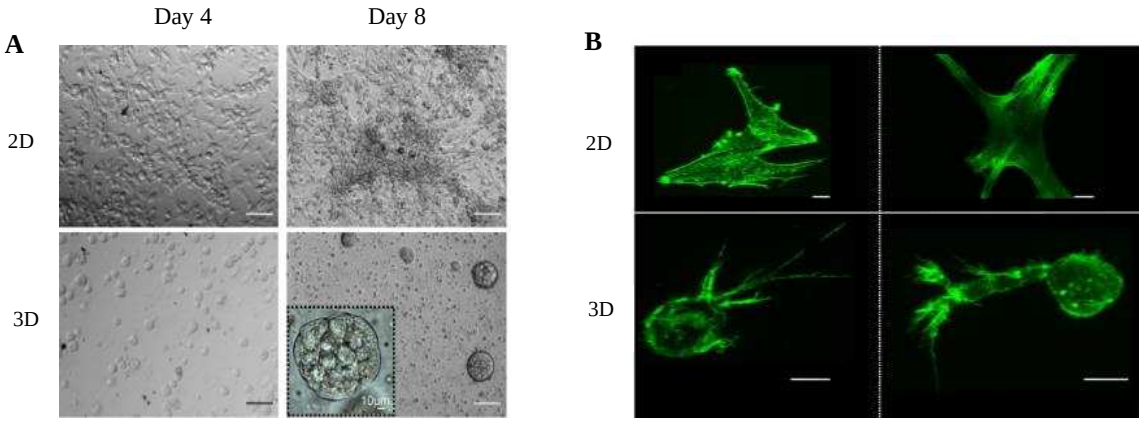

Figure 4.8: A. Morphology of U87MG cells seeded on 2D and 3D environment. After 8 days of culture, the cells seeded under 3D conditions adopted rounded morphology, while cells on 2D environment adopted elongated morphology, **B.** Confocal microscopy photos indicating U87MG cells with small filopodia on 2D condition and rounded cells with lamellipodia or filopodia under 3D conditions. Scale bars represent 10 μm. Photos adapted from Jiguet et al [37].

Moreover, as presented in Figures 4.6 and 4.7, U87MG and 42 MG cells seeded on the standard culture surface adopted a flattened and elongated morphology from the first day of culture, leading to a typical 2D culture after 4 days of incubation. In contrast, as mentioned earlier, after 1 day of culture, cells started to form rounded clusters over time with significantly increased size after 4 days of seeding on hydrogels of low crosslinking density, suggestive of proliferation. Interestingly, Pedron et al reported that neurospheres of glioma cells were observed on hydrogels containing HA [23]. U87MG cells encapsulated within PEG-based hydrogels remained as individuals or as small groups, whereas with increasing concentration of methacrylated HA (HAMA) into the hydrogel network, formation of large cell aggregates was observed as depicted in Figure 4.9.

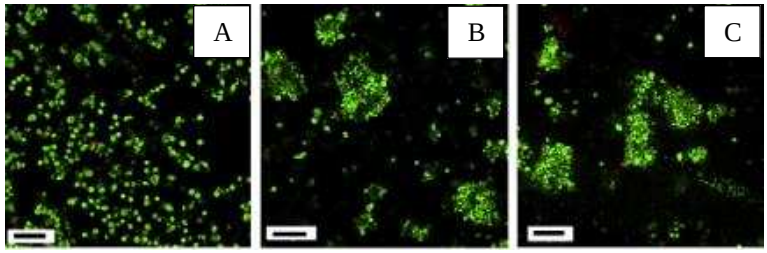

Figure 4.9: Morphology of U87MG cells seeded on PEG-based hydrogels with increasing concentration of HAMA 2 weeks after seeding. **A.** In the absence of HAMA, **B.** In the presence of 0.5 % w/w HAMA and **C.** In the presence of 1% w/w HAMA. Progressive clustering of U87MG cells was observed with increasing concentration of HAMA. Photos adapted from Conlon et al [23].

Furthermore, it can be concluded that U87MG and 42 MG cell motility is higher on softer hydrogels such as L1 and L2 due to the looser hydrogel network, leading to the formation of large clusters through aggregation but also proliferation. On the other hand, cells seeded on stiffer surfaces, due to the denser network, are tightly encapsulated and remain as single cells. Moreover, it is noteworthy that slow proliferation rate was observed within cells seeded on L1 and L2 hydrogels compared with the cells seeded on the standard culture plate as demonstrated in the graph in Figure 4.10. The cell number was calculated based on the standard curve created for U87MG cells (refer to the Appendix).

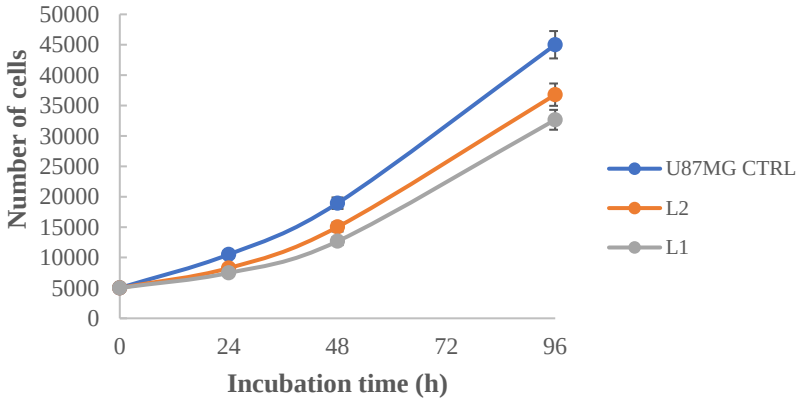

Figure 4.10: Graph summarises the proliferation of U87MG cells seeded on the standard culture surface and on the surface of HA-ADH hydrogels over 4 days. Slower proliferation rate was observed within cells cultured on L1 and L2 hydrogels. The data represent the average of triplicate with the corresponding standard deviation.

This slow rate of proliferation is common as the cells adjust to the porous hydrogel network and due to 3D environmental factors such as limited diffusion of nutrients and bigger surface to colonise [38]. Additionally, in the literature it has been reported that human GBM cells proliferate in a stiffness-dependent manner with higher proliferation observed on stiffer surfaces, which partially explains the difference on the number of glioma cells seeded on HA-ADH hydrogels. Overall, it can be concluded that variations in crosslinking density and the viscoelastic properties of the hydrogels affect cell morphology and viability, when no clear effect of UII can be observed.

4.3.1.2 Viability of glioma cells on HA-ADH hydrogels

The viability of U87MG and 42 MG cells seeded on the surface of HA-ADH hydrogels at different crosslinking densities was determined using MTS assay. MTS assay allows the evaluation of cell viability by measuring cells metabolic activity. The method is based on the reduction of the MTS tetrazolium compound (3-(4,5-dimethylthiazol-2-yl)-5-(3-carboxymethoxyphenyl)-2-(4-sulfophenyl)-2H-tetrazolium) by viable cells to form formazan which is directly soluble in the cell culture medium as shown in Figure 4.11. This reaction is catalysed by NADPH or NADH produced by dehydrogenase enzymes in metabolically active cells. The formazan produced by viable cells is quantified by measuring the absorbance at 490 nm.

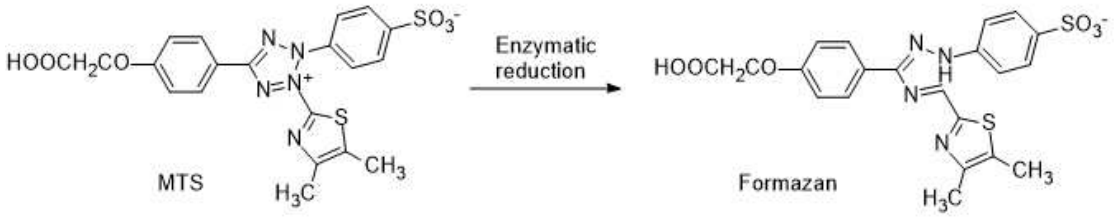

Figure 4.11: Enzymatic reduction of MTS tetrazolium compound to formazan. The formazan produced by viable cells is quantified by measuring the absorbance at 490 nm.

Briefly, U87MG and 42 MG cells were seeded on HA-ADH hydrogels in the presence or absence of UII (10^{-8} M) at a density of 5×10^{3} cells per well. The viability of glioma cells was evaluated after 24 and 48 h of incubation as summarised below in graphs A and B in Figure 4.12. It can be concluded that the presence of the chemoattractant UII displayed insignificant effect on glioma cells viability.

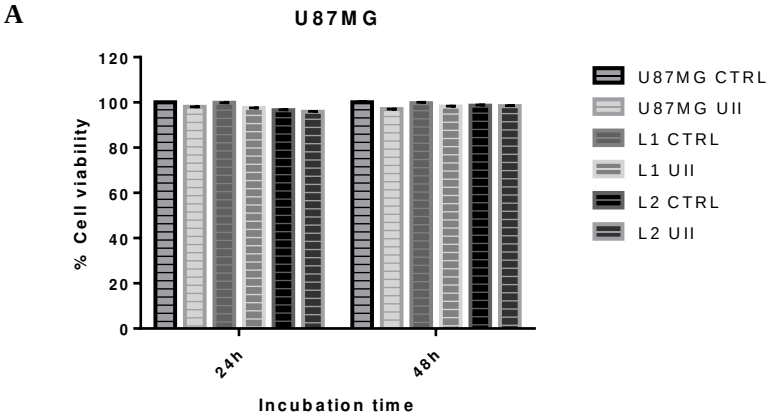

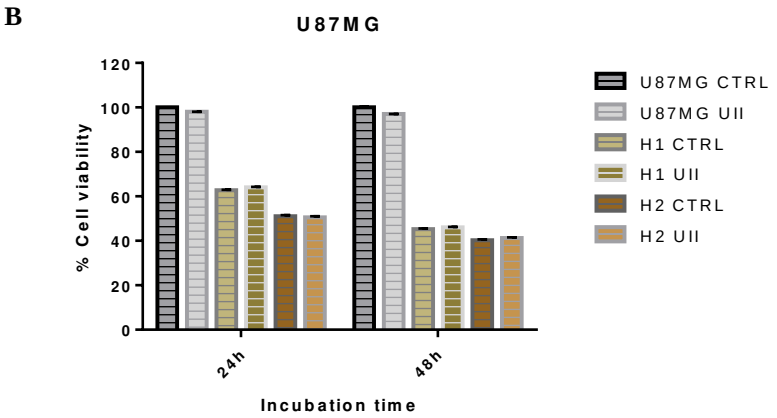

Figure 4.12: Viability of U87MG cells seeded on different crosslinking densities of HA-ADH hydrogels in the absence or presence of UII (10^{-8} M). **A.** Viability of cells seeded on low crosslinked hydrogels. **B.** Viability of cells on high crosslinking density of hydrogels. The viability of glioma cells was evaluated after 24 and 48 h of incubation. The data represent the average of n=6 with the corresponding standard deviation.

Glioma cells seeded on HA-ADH hydrogels of low crosslinking density (L1 and L2 conditions) in the absence or presence of UII showed viability > 95 % after 24 and 48 h of incubation. On the other hand, at higher crosslinking densities of HA-ADH hydrogels (H1 and H2 conditions), cell viability was much lower, 62 % and 51 % respectively with cell number reduced even after 24 h seeded culture, suggesting cell death. A possible reason for this, is the high crosslinking density of the hydrogels which results in low porosity and poor diffusion of the cell nutrients, with adverse effects on cell viability. In addition, culture of 42 MG cells on hydrogels in the absence or presence of UII resulted in a similar viability profile with U87MG cells as shown in graphs A and B in Figure 4.13. These observations support that glioma cells seeded on highly crosslinked hydrogels were either less metabolically active, less proliferative or both than those seeded on low crosslinked hydrogels. The results are consistent with the work of Kaufman et al reported that the increased collagen I concentration resulted in decreased U87MG glioma viability and metabolic activity due to increased hydrogel crosslinking density [39].

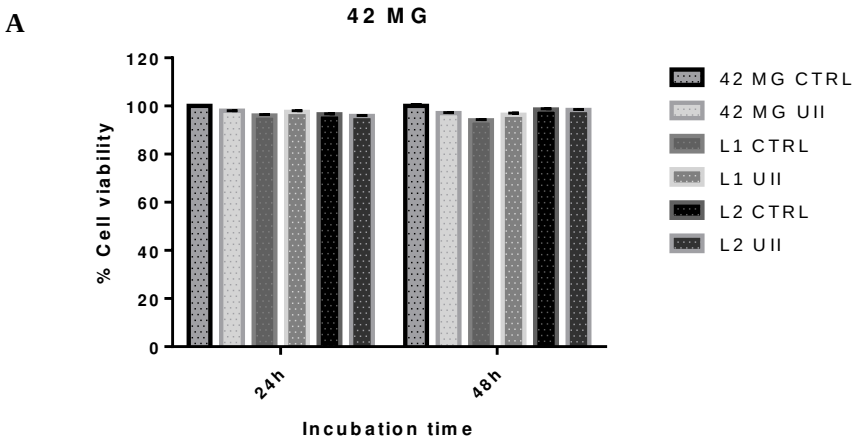

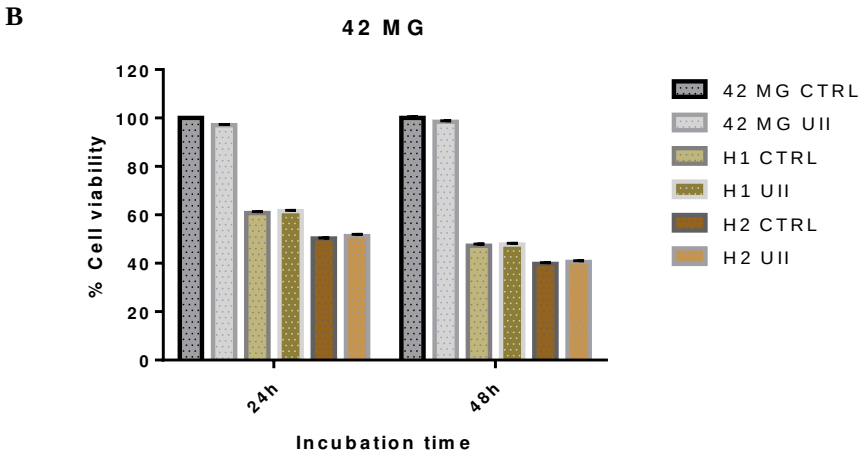

Figure 4.13: Viability of 42 MG cells seeded on different crosslinking densities of HA-ADH hydrogels in the presence or absence of UII (10^{-8} M). **A.** Cell viability on low crosslinking density of hydrogels. **B.** Cell viability on highly crosslinked hydrogels. The viability of glioma cells was evaluated after 24 and 48 h of incubation. The data represent the average of n=6 with the corresponding standard deviation.

In order to better clarify whether crosslinking density affects GBM cells viability through metabolic activity or cell death, qualitative Live/Dead Cell Viability Assay was conducted. Briefly, U87MG and 42 MG cells were seeded on the hydrogels at different crosslinking densities as described previously and the Live/Dead staining solution was added after 24 h of culture. Viable cells were stained green due to their reaction with the Calcein AM and damaged cell cytoplasmic and nuclear membranes were stained red because of the reaction with ethidium homodimer. The green and red fluorescence images taken from viable and dead cells respectively were merged to one using ImageJ as shown in Figure 4.14. The fluorescence microscopy was challenging due to the presence of hydrogels leading to loss of constant focal planes, resulting sometimes in blurry images as depicted in Figure 4.14. After 24 h of seeding, glioma cells on the standard culture surface were elongated with a spreading shape. U87MG cells seeded on low crosslinking densities of hydrogels (L1 and L2 conditions) were mostly viable (green) with rounded morphology and progressive formation of clusters over time. Cells cultured on highly crosslinked hydrogels (H1 and H2 conditions), started to undergo cell death as evidenced by the occurrence of red nuclei. These results are consistent with the data obtained from the MTS assay, confirming high cell viability on L1 and L2 hydrogels indicating their biocompatibility. In contrast, high crosslinking density demonstrated adverse effect on the viability of glioma cells.

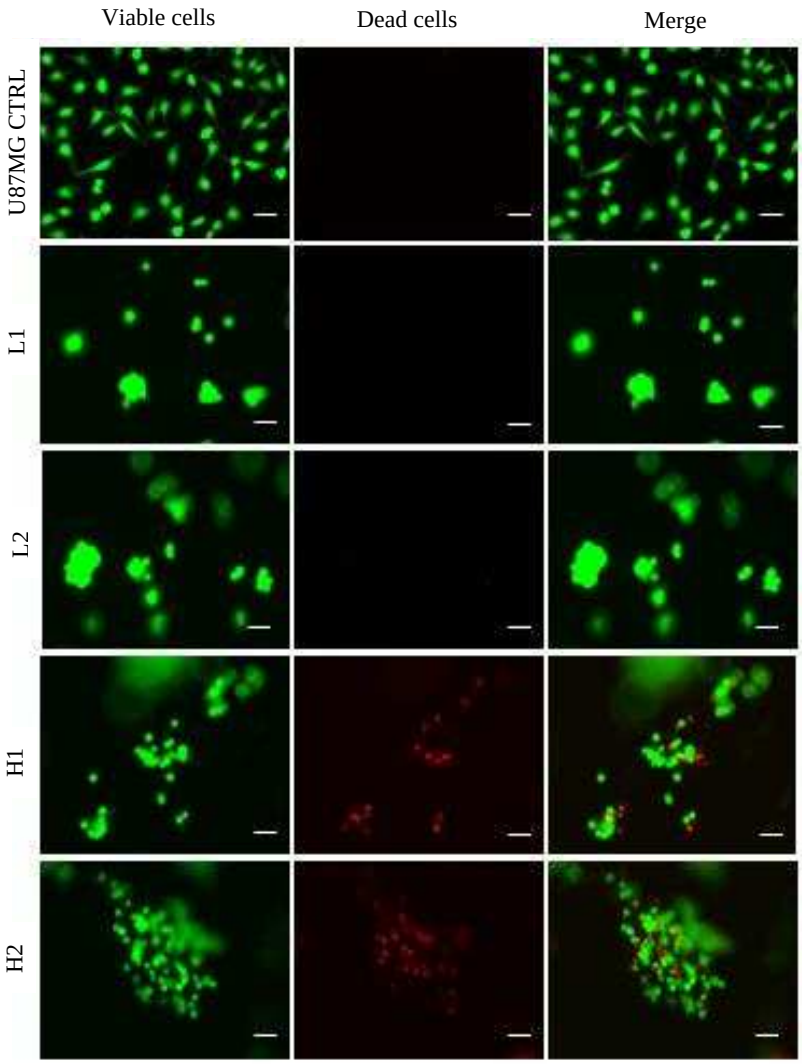

Figure 4.14: Representative Live/Dead photos of U87MG cells seeded on different crosslinking densities of HA-ADH hydrogels. Viable cells were stained green and dead cell nuclei were stained red. L1 and L2 hydrogels presented good biocompatibility. Magnification: 20×, Scale bar: 50 μm.

As shown in Figure 4.15, after 24 h of culture 42 MG cells demonstrated consistent results compared with U87MG cell culture. In overall, it can be concluded that L1 and L2 hydrogels promoted the formation of cell clusters allowing to grow as neurospheres, whereas the highly crosslinked hydrogels H1 and H2 inhibited cell growth with considerable decrease in cell viability after 24 h of culture.

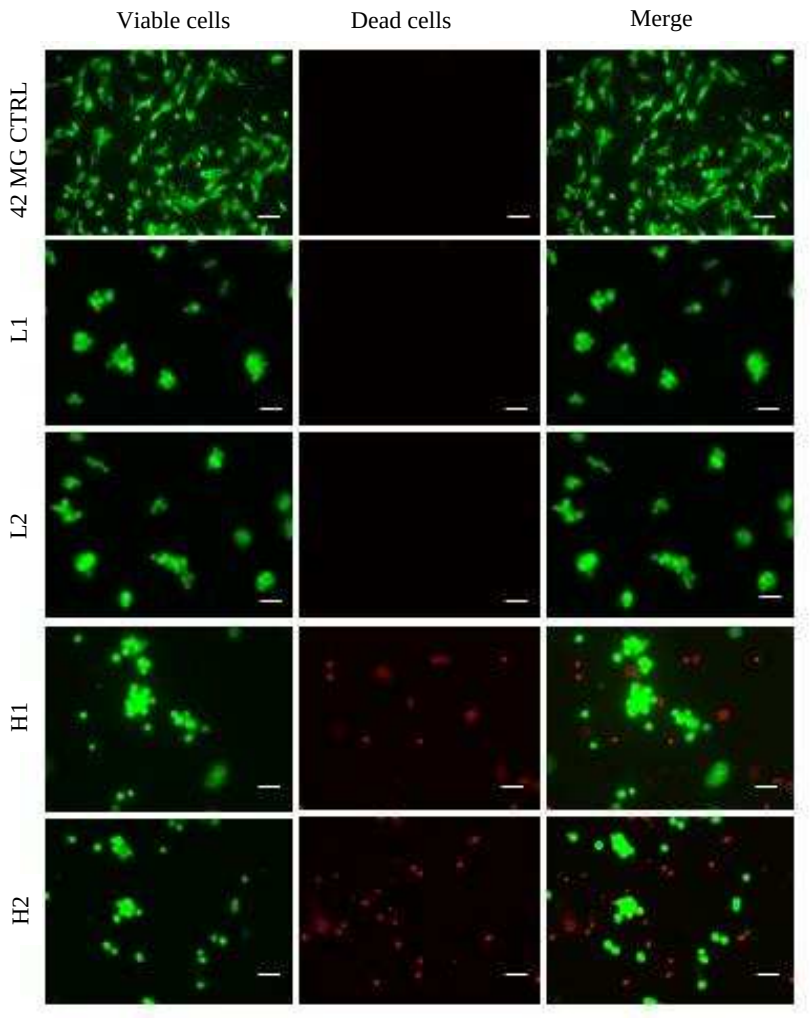

Figure 4.15: Representative Live/Dead photos of 42 MG cells seeded on different crosslinking densities of HA-ADH hydrogels. Viable cells were stained green while dead cell nuclei were stained red. Magnification: 20×, Scale bar: 50 μm.

4.3.1.3 Modified Boyden Chamber invasion and migration assay on HA-ADH hydrogels

It is generally known that directional cell migration is crucially important in biological processes such as wound healing and malignancy and further studies on chemotactic factors should contribute to this essential process. Cell migration can be triggered by a variety of molecules that act as chemoattractants including peptides and large proteins. Traditionally, cell migration is studied in vitro 2D environment, where cells are organised in monolayers such as in wound assays [40], [41]. Albeit, this type of setting provides crucial information regarding directional cell migration, it suffers from several limitations since cells are not included in a 3D matrix microenvironment. For instance, in wound healing assays cells in monolayers contact only the standard coated plastic surface, whereas in a 3D environment, cells interact with the matrix which modifies their shape and migration kinetics [42]. Additionally, microfluidics devices have been employed to direct cell migration in the presence of chemokine gradients but this system is quite expensive and difficult to set up [43]. Chemotactic cell migration is often measured using the modified Boyden chamber assay [44]. This assay

exploiting the chemokine gradient between upper and lower chambers to address cell invasion and migration, is well adapted to study migration in 2D (migration) and 3D (invasion) environment. The principle of this assay is based on two chambers containing medium separated by a porous membrane. Cells are loaded on the upper chamber and they are allowed to migrate through membrane pores (usually 8 μm pore size for adherent cells) toward chemoattractants added in the lower chamber. Then, cells that managed to migrate and stayed adhered on the lower side of the porous membrane, are fixed, stained and quantified.

Several in vitro studies have provided relevant insights into the migratory or invasive ability of cancer cells within 3D extracellular matrices. Campbell et al investigated the invasion and migration of breast cancer cell lines using modified Boyden Chamber assay [45]. Specifically, the upper chamber of the Boyden was coated with lyophilised porous 3D collagen-based scaffolds and subsequently breast cancer cell lines were seeded on them. The lower chamber was filled with media containing gradient FBS in order to stimulate cell migration within the scaffold depth. Cells were attracted to invade the scaffold and displayed increased migration in response to the presence of the FBS gradient. Similarly, Topman et al studied the directional migration of 3T3L1 (preadipocyte) cells seeded on HA-ADH hydrogel-based 3D matrix using cell culture inserts [46]. The bottom of the inserts was coated with a thin layer of transparent HA-ADH hydrogel while the lower compartment was filled with growth medium to generate a chemotaxis stimulus for directional migration as shown in Figure 4.16.

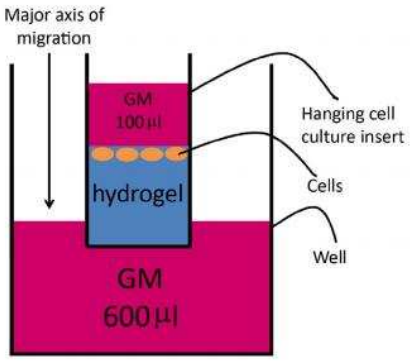

Figure 4.16: Schematic illustration of the experimental set up used by Topman et al for the investigation of the directional cell migration in a 3D matrix. The upper chamber was coated with HA-ADH hydrogel and the lower chamber was filled with media containing FBS. Adapted from Topman et al [46].

Herein, a modified version of the traditional Boyden chamber assay was applied in order to evaluate glioma cells ability to invade and migrate through the hydrogel network. Migration is defined as the directed movement of cells on a substrate such as ECM fibers or coated culture plates in response to specific stimuli such as gradient of chemoattractants, whereas invasion occurs when cells move through a 3D matrix. Briefly, glioma cell invasion and migration were investigated using transwell cell culture chambers coated with a thin layer of hydrogels as shown in the illustration of Figure 4.17.

Low crosslinking densities of hydrogels (L1 and L2 conditions) were chosen for the invasion assay, as highly crosslinked hydrogels H1 and H2 did not present good biocompatibility. Different thicknesses of hydrogels have been tested and a volume of hydrogel of 100 µL (thickness of 3 mm) was applied finally to the upper part of the polycarbonate membranes. U87MG cells were passaged, resuspended in DMEM in the absence of FBS and seeded on the hydrogels at a density of 5×10^4 cells. The lower compartment was filled with 600 µL of DMEM in the absence of FBS as control condition or with 600 µL of DMEM in the presence of the chemoattractant UII (10^{-8} M) in order to evaluate the invasive and migratory ability of glioma cells.

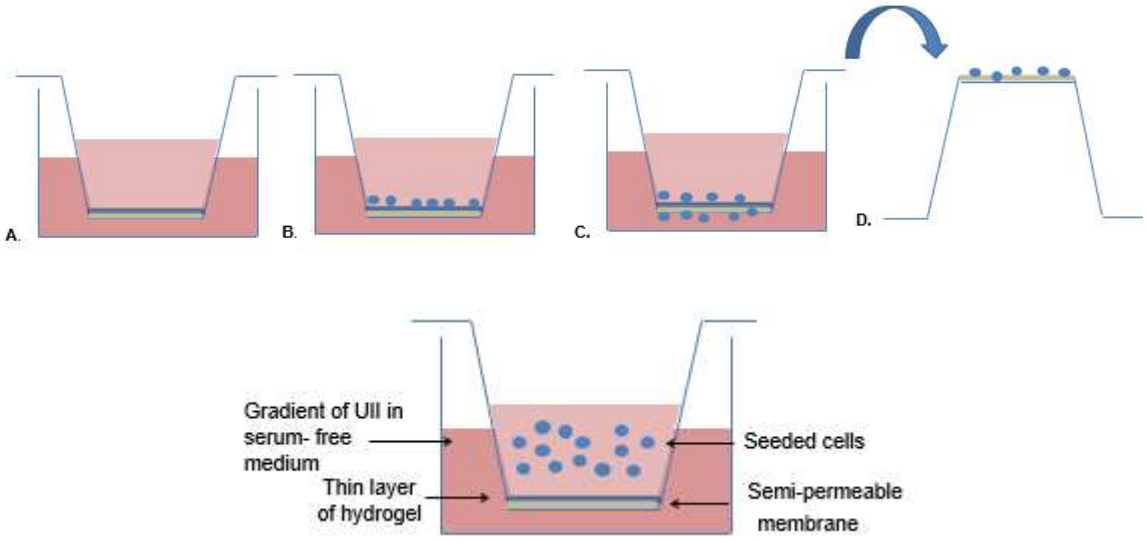

Figure 4.17: Schematic illustration of transwell cell culture chambers. Glioma cells invasion and migration were investigated using transwell cell culture chambers coated with a thin layer of hydrogel. Cells migrated within 48 h, were fixed, stained and quantified.

U87MG cells were allowed to invade and migrate through the thin layer of the hydrogel for 48 hours at 37 °C. This incubation time was chosen because after 24 h of incubation only few cells invaded the hydrogel. After 48 h, cells having migrated were fixed, stained with hematoxylin, photos of the membranes were taken and migrated cells were quantified using ImageJ. As summarised in the histogram below in Figure 4.18, the addition of UII to the lower migration chamber resulted in a significant increase in the number of migrating glioma cells in the absence of the thin layer of hydrogel (control condition) and in the presence of the matrix. These results are consistent with the previous work of Lecointre et al and Coly et al, in which the presence of UII promoted increase in the number of migrating HEK293 cells expressing UT and glioma cells [35], [36]. Moreover, it is observed that less U87MG cells migrated towards the hydrogel compared with the control condition (without hydrogel) due to the fact that glioma cells had to invade the hydrogel matrix.

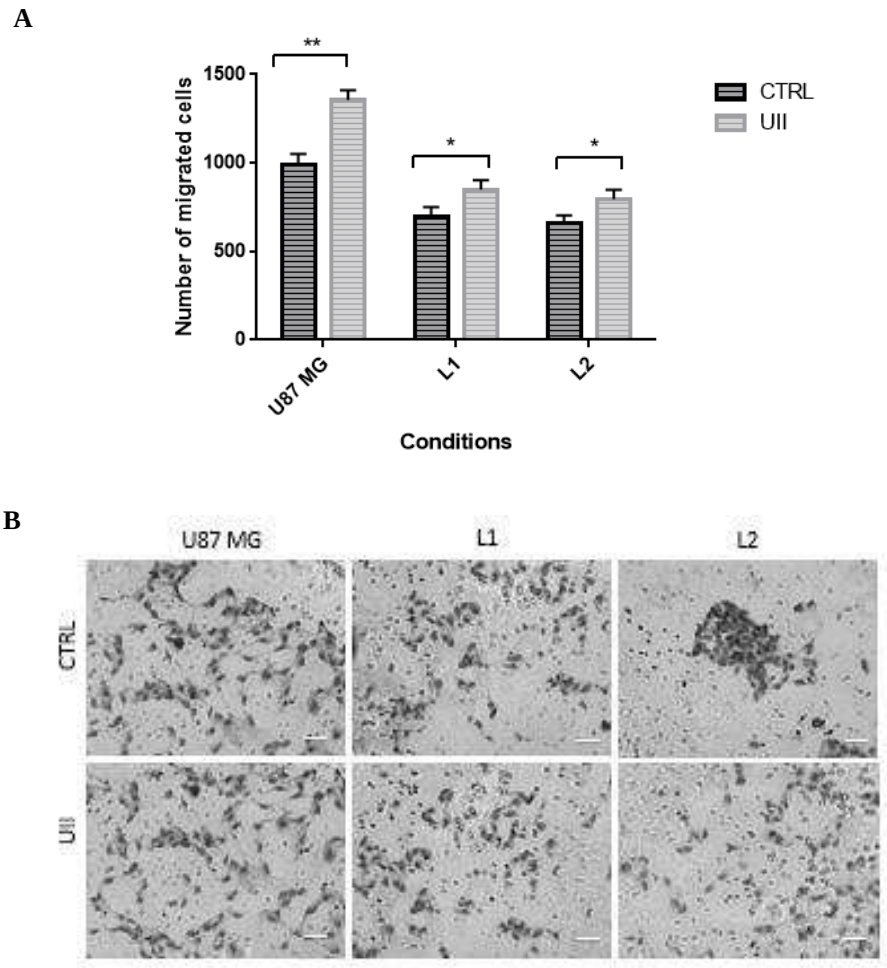

Figure 4.18: Cell migration was evaluated by counting U87MG cells on the membranes after staining with hematoxylin in the absence or presence of UII (10^{-8} M). **A.** Histogram shows the quantification of the migrating cells exposed to gradient UII after invasion of the thin layer of the hydrogel compared with the control (CTRL). The data obtained from one representative experiment in triplicate with the corresponding standard deviation. Mann and Whitney test; $^{**}P < 0.01$, $^{*}P < 0.05$. **B.** Representative photos of the membranes after staining with hematoxylin. Magnification: 20×, Scale bar: 50 μm.

Furthermore, 42 MG cells ability to invade and migrate through the thin layer of the hydrogel was evaluated. Similarly, as described above, 42 MG cells were resuspended in DMEM in the absence of FBS and seeded on the thin layer of hydrogels at a density of 5×10^4 cells. The lower compartment was filled with 600 μL of DMEM in the absence of FBS and in the presence of UII (10^{-8} M). 42 MG cells were allowed to invade and migrate through the hydrogel matrix for 48 h. Again, cells were fixed, stained and quantified on the porous membranes as described earlier. As shown in the histogram in Figure 4.19, 42 MG cells demonstrated migratory behaviour resembling that of U87MG cells, highlighting that glioma cells were able to invade the hydrogel network and migrate in response to the chemoattractant UII.

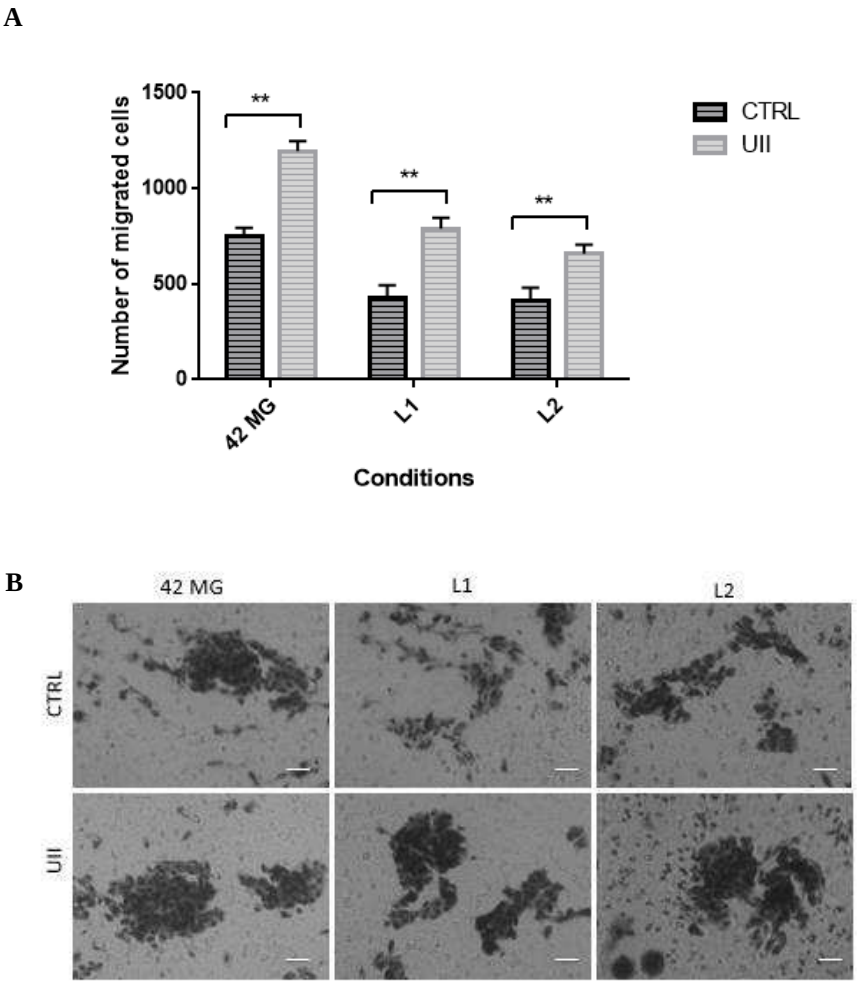

Figure 4.19: Cell migration was evaluated by counting 42 MG cells on the membranes after staining with hematoxylin in the absence or presence of UII (10^{-8} M). **A.** Histogram shows the quantification of the migrating cells through the thin layer of the hydrogel compared with the control. Data obtained from one representative experiment in triplicate with the corresponding standard deviation. Mann and Whitney test; $^{**}P < 0.01$. **B.** Representative photos of the membranes after staining with hematoxylin. Magnification: 20×, Scale bar: 50 µm.

4.3.1.4 Immunofluorescence

Immunofluorescence analysis was performed on U87MG and 42 MG cells cultured on standard culture surface and on HA-ADH hydrogels for the expression of the proliferative marker Ki-67 expressed in nuclei of divided cells. Hydrogels were prepared at the lowest crosslinking density (L1 condition) in the absence or presence of the chemoattractant UII (10^{-8} M) to evaluate glioma cell cycle in the context of 3D matrix and the chemokine peptide. Briefly, after 2 days of culture, glioma cells isolated from 2D standard culture surface or 3D hydrogels were seeded on glass coverslips coated with fibronectin for 24 h. Next day, cells were fixed, permeabilised using 0.05 % Triton-1× PBS and non-specific sites were blocked using 2 % NDS. After rinsing, cells were immunostained with primary antibody directed against Ki-67. Cell nuclei were counterstained with DAPI. Images of U87MG and 42 MG cells were taken by confocal fluorescence microscope (Normandie Rouen University, PRIMACEN platform) as shown in Figure 4.20.

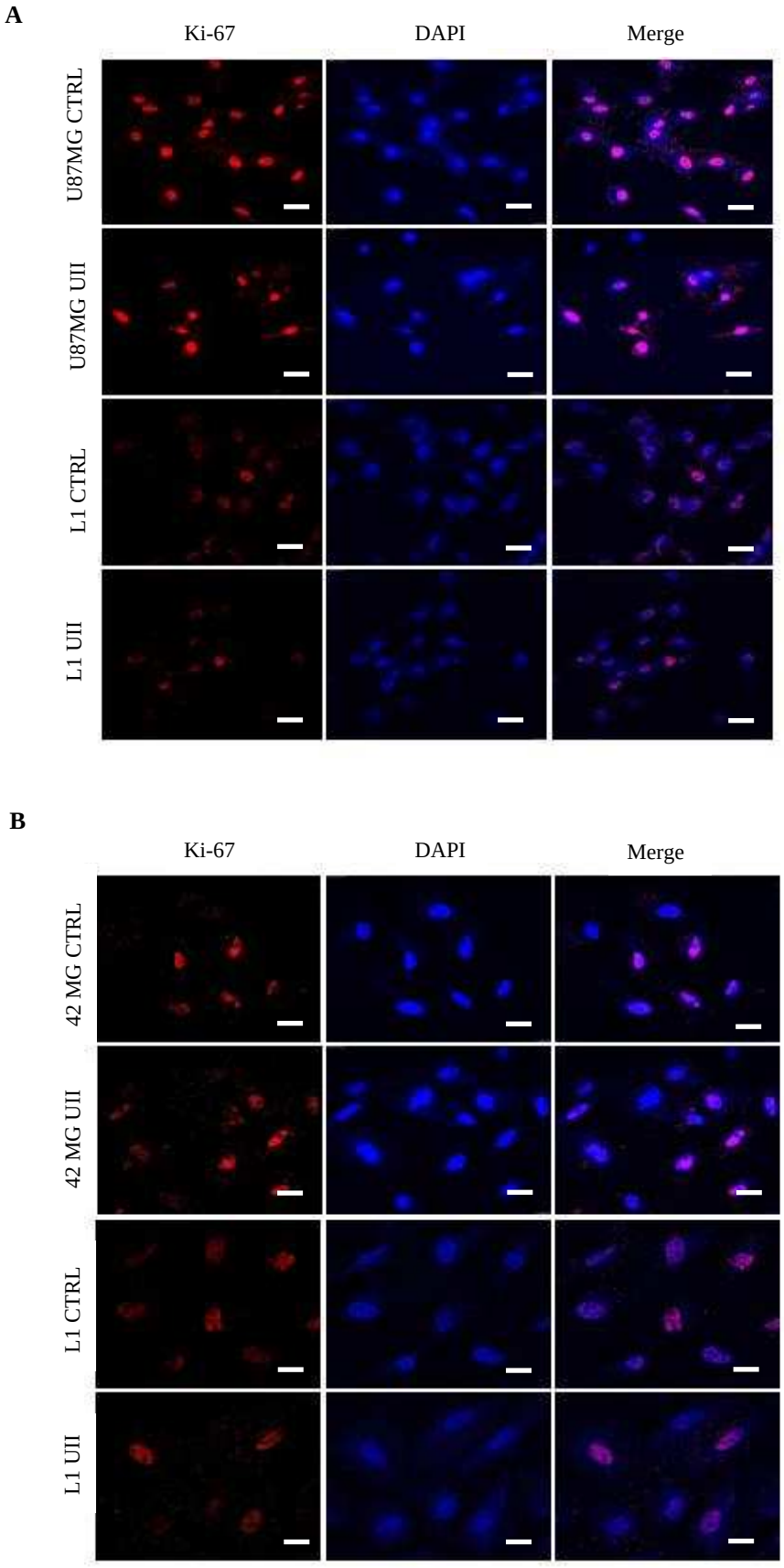

Figure 4.20: Representative immunofluorescence images of glioma cells. **A.** U87MG cells seeded on 2D culture surface or on hydrogels were immunostained with antibody against Ki-67. Cell nuclei were counterstained with DAPI. **B.** 42 MG cells seeded on 2D culture surface or on hydrogels were immunostained with antibody against Ki-67. Scale bar: 10 μm.

Ki-67 is a marker associated with cell proliferation and it is commonly used in immunofluorescence studies as well as for diagnostics [47]. Ten representative images of DAPI and Ki-67 labelled cells were taken covering different surface areas. Subsequently, relative quantification of the Ki-67 stained cells by measuring the fluorescence intensity of Ki-67 stained cells under the different culture conditions was conducted with ImageJ. As summarised in graphs A and B in Figure 4.21, it was found approximately fourfold increase in the fluorescence intensity of cells seeded on the standard culture surface compared with the cells seeded on the hydrogels, indicating higher cell proliferation activity on the 2D culture surface than in 3D. Moreover, it is noteworthy that the presence of the chemoattractant UII (10^{-8} M) did not affect the proliferation rate of glioma cells in both culture conditions. 42 MG cells demonstrated similar proliferative activity with U87MG cells with higher expression of Ki-67 on cells cultured on the standard 2D culture surface.

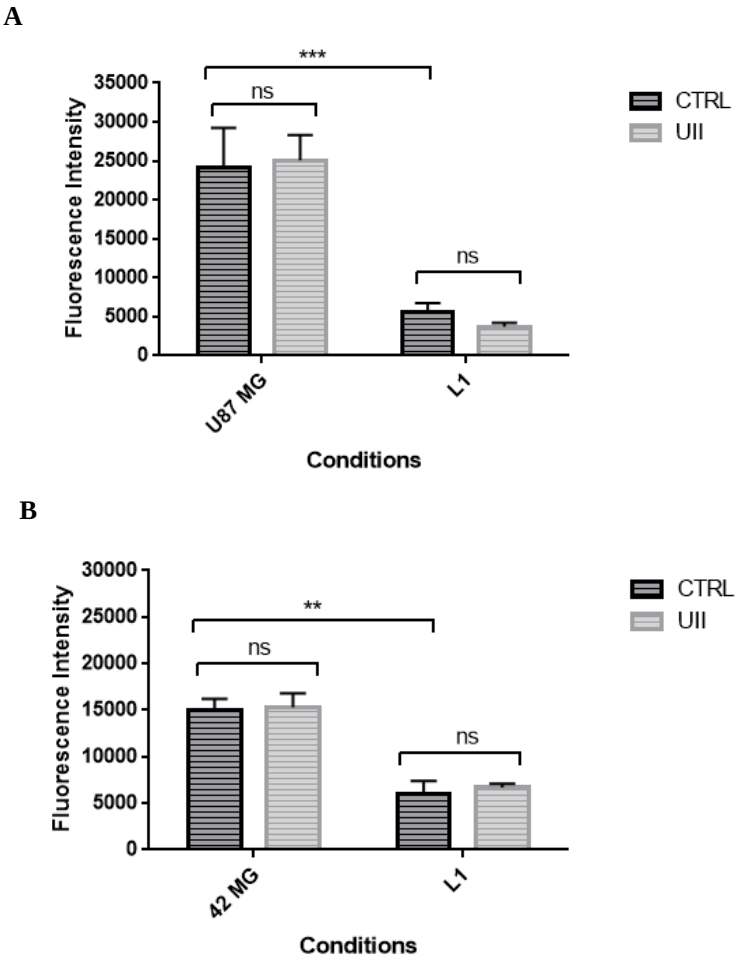

Figure 4.21: Ki-67 staining revealed increase in proliferation rate of glioma cells seeded on the standard 2D culture surface. **A.** Quantification of fluorescence intensity of Ki-67 stained U87MG cells. **B.** Quantification of fluorescence intensity of Ki-67 stained 42 MG cells seeded on the standard culture surface compared with cells cultured on HA-ADH hydrogels. Background was subtracted from the total fluorescence per cell using ImageJ. Bar graph represent the average of n=6 with the corresponding standard deviation. Mann and Whitney test; ns, not significant; $^{***}P< 0.001$, $^{**}P< 0.01$.

4.3.1.5 *In vitro* cytotoxicity of DOX on U87MG cells

DOX, also known as Adriamycin, is a cytotoxic anthracycline compound isolated from cultures of Streptomyces peucetius in 1960s whose structure is shown in Figure 4.22 [48]. This drug is commonly used as chemotherapeutic agent for the treatment of various types of human cancer including breast, bladder, lung, ovarian, liver cancer, acute lymphocytic leukemia, neuroblastoma and Hodgkin's lymphoma [49].

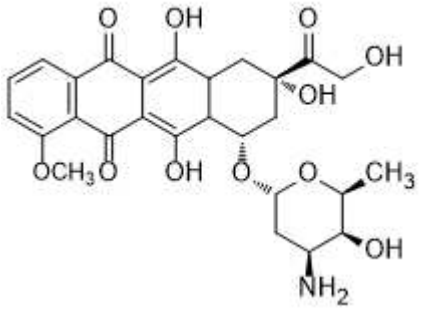

Figure 4.22: Chemical structure of DOX consists of a sugar moiety attached to a tetracyclic ring. It is the lead compound of the broad anthracycline family.

The action mechanism of DOX is based on acting as DNA interchelator which inhibits topoisomerase II activity by interchelating between the bases of the DNA double helix, leading to disruption of DNA replication and transcription and thus cell death. Another possible mechanism proposes that DOX generates free radicals responsible for DNA and cell membrane damage. DOX is mainly administered intravenously with inevitable adverse effects. Common side effects involve vomiting, hair loss, bone marrow suppression, inflammation of the mouth and heart failure [50], [51]. DOX is most commonly used to treat various types of cancer but it is little known for its possible use as chemotherapeutic agent in the treatment of brain tumours due to a poor blood-brain barrier penetration capacity, despite in vitro efficacy on glioma cell lines [52], [53]. Annovazzi et al reported the in vitro cytotoxicity of DOX on different glioma cell lines, by reducing significantly the number of viable cells [54]. In addition, in vivo studies on animal models of malignant glioma have suggested DOX as an effective anti-glioma agent [55], [56]. Albeit, as mentioned previously the limitations of penetrating the BBB effectively, prevents its broad use in the treatment of GBM. Intratumoural injections of DOX have prolonged the survival of patients diagnosed with malignant gliomas, highlighting its potential as an anticancer drug [57]. To allow penetration of the BBB, several studies have investigated the delivery of anticancer drugs using colloidal carriers such as liposomes, nanoparticles or hydrogels in order to achieve targeted and effective drug delivery. As extensively discussed in Chapter 1, DOX has been loaded on nanoparticles or encapsulated in the liposomes core for higher accumulation of the drug close to the tumour site.

In the present work, we hypothesised that the local delivery of DOX via the hydrogel matrix might be beneficial and more effective method of delivery in the treatment of GBM. More specifically, we

investigated the cytotoxicity of DOX on U87MG cells in vitro and the cytotoxicity induced by HA-ADH hydrogels loaded with DOX. The in vitro cytotoxicity on U87MG cells was evaluated by MTS assay and qualitatively with Live/Dead assay. Briefly, human U87MG cells were incubated with increasing concentrations of DOX (0.01-100 μM) for 72 h and the IC_{50} concentration was determined as shown in the graph in Figure 4.23. It was observed that increasing concentration of DOX reduced significantly U87MG cell viability. With the range of DOX concentration employed, the IC_{50} was calculated to be ~1 μM after 72 h of incubation. The IC_{50} value was defined as the concentration of DOX that caused 50 % inhibition of cell growth after 72 h of treatment. In the literature, IC_{50} values for U87MG cells treated with various concentrations of DOX vary between 3.85 to 1.06 μM [58], [59].

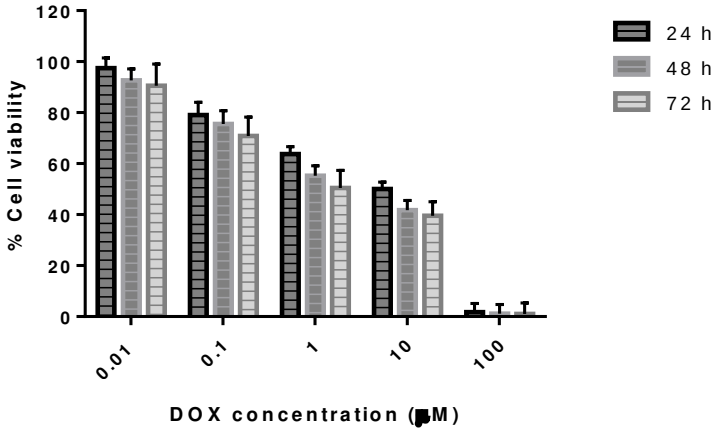

Figure 4.23: In vitro cytotoxicity of DOX on U87MG cells. % Cell viability of glioma cells after 24, 48 and 72 h of treatment with increasing concentrations of DOX. The IC_{50} concentration was determined to be ~1 μM. Data represent the average of n=4 with the corresponding standard deviation.

Moreover, the cytotoxicity of DOX on U87MG cells was assessed using Live/Dead assay. Briefly, U87MG cells were treated for 48 h with various concentrations of DOX and the Live/Dead staining solution was added. As shown in Figure 4.24, inhibition of cell proliferation and higher cytotoxicity were observed on cells treated with high concentrations of DOX compared with the control condition, confirming its significant cytotoxicity on glioma cells.

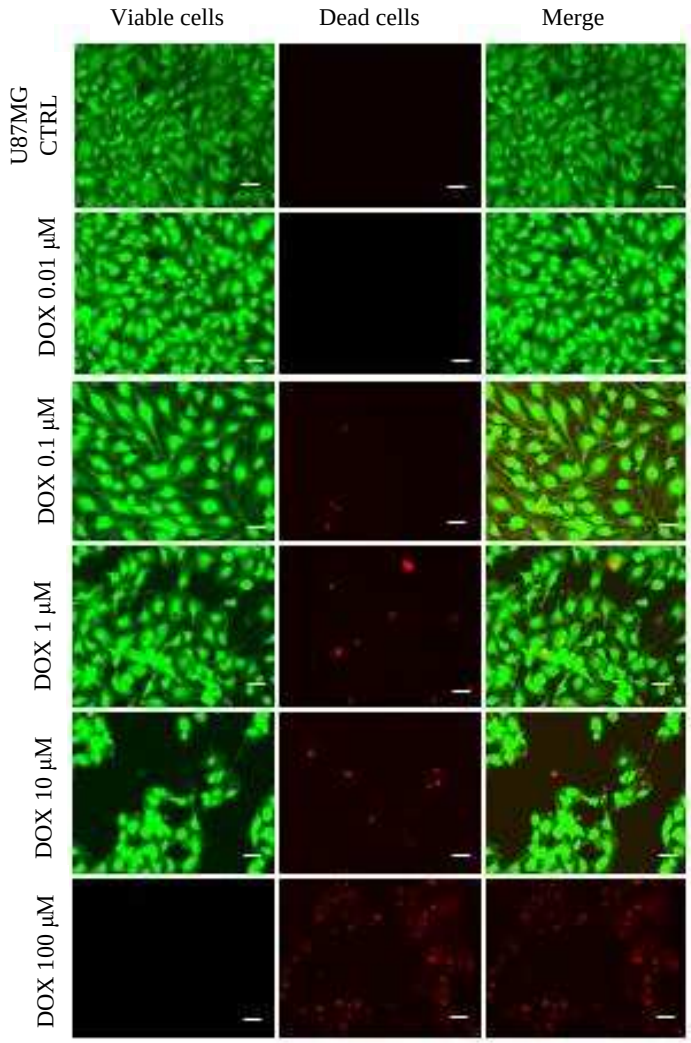

Figure 4.24: Representative Live/Dead photos of U87MG cells treated with increasing concentrations of DOX after 48 h of treatment. Inhibition of cell proliferation and significant cytotoxicity were observed on higher concentrations of DOX. Magnification: 20×, Scale bar: 50 µm.

4.3.1.6 *In vitro* cytotoxicity of DOX loaded HA-ADH hydrogels

To date, there are more than 100 types of chemotherapeutic drugs including cisplatin, paclitaxel, carmustine, 5-fluorouracil (5-FU) and doxorubicin. The majority of these drugs are administered via intravenous injection to the human body. However, it is challenging to reach therapeutic concentrations of the drug in the tumour tissue due to the limitations of the drug delivery methods and the presence of the BBB [60]. Recently, hydrogels have gained a lot of attention in drug delivery applications due to their unique physical properties. Their porous interconnected structure allows loading of various drugs into the gel matrix and subsequent release of the drug through the hydrogel network [61]. Loaded drugs can be precisely released from hydrogels in close proximity to the tumour sites. Herein, HA-ADH hydrogels loaded with DOX were prepared at different crosslinking densities (L1 and L2 conditions) as described in section 4.2.2.4 and their in vitro cytotoxicity on U87MG cells was further investigated. The cytotoxicity of the drug-loaded hydrogels was evaluated

by MTS assay and Live/Dead assay. Low crosslinking densities of HA-ADH hydrogels were prepared as described earlier into the wells of a 96-well plate and loaded with DOX at concentration 100 μM. The final concentration of the drug into the hydrogels was 10 μM. Hydrogels were washed with PBS and with measurement of UV absorbance of the washing solutions, the encapsulation of DOX in the hydrogels was confirmed. In addition, hydrogels were prepared in the absence of DOX as negative control. U87MG cells were seeded on the blank and DOX-loaded hydrogels and treated with solution of free DOX for 24 and 48 h at 37 °C. Subsequently, glioma cell viability was determined by measuring the metabolic activity of cells using MTS assay as summarised in Figure 4.25.

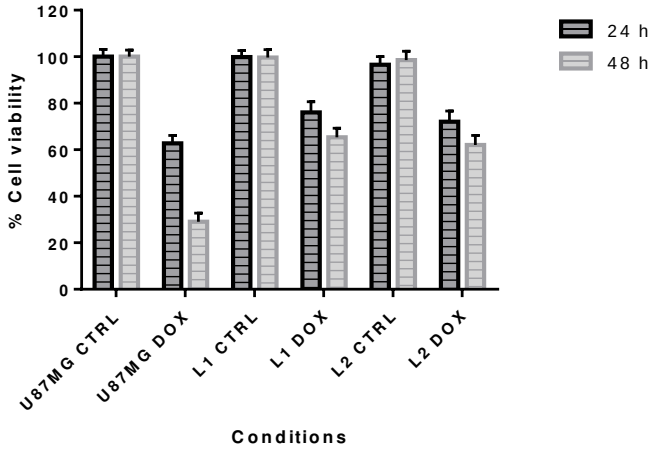

Figure 4.25: % Cell viability of U87MG cells seeded on blank hydrogels and DOX-loaded hydrogels after 24 and 48 h of incubation. Data represent the average of n=4 with the corresponding standard deviation.

As shown in Figure 4.25, glioma cells seeded on the L1 and L2 hydrogels in the absence of DOX presented good viability > 95 %, indicative of their biocompatibility. In contrast, L1 and L2 hydrogels loaded with DOX after 24 and 48 h of incubation, demonstrated significant cytotoxicity with cell viability lower than 80 % suggesting inhibition of cell growth. In addition, DOX-loaded hydrogels presented lower cytotoxic effect than that from the free DOX in the culture medium. This observation suggests that hydrogels either induced higher glioma cell resistance to DOX treatment, and/or less DOX delivery and cell access reducing toxicity.

Furthermore, Live/Dead assay was performed on U87MG cells treated with solution of free DOX and seeded on DOX-loaded hydrogels as shown in Figure 4.26. After 48 h of treatment, Live/Dead staining qualitatively revealed that free DOX caused significant cytotoxicity confirmed by substantial changes in the morphology of U87MG cells. On the other hand, glioma cells seeded on DOX-loaded hydrogels demonstrated higher viability with few cells engaging death. This indicates as mentioned earlier more resistance and/or the sustained release of DOX from the hydrogels as discussed in detail in Chapter 3. Overall, these results demonstrate that HA-ADH hydrogels could be used for localised

therapeutic delivery of DOX for the treatment of GBM, mimicking a better way the brain physiopathological conditions.

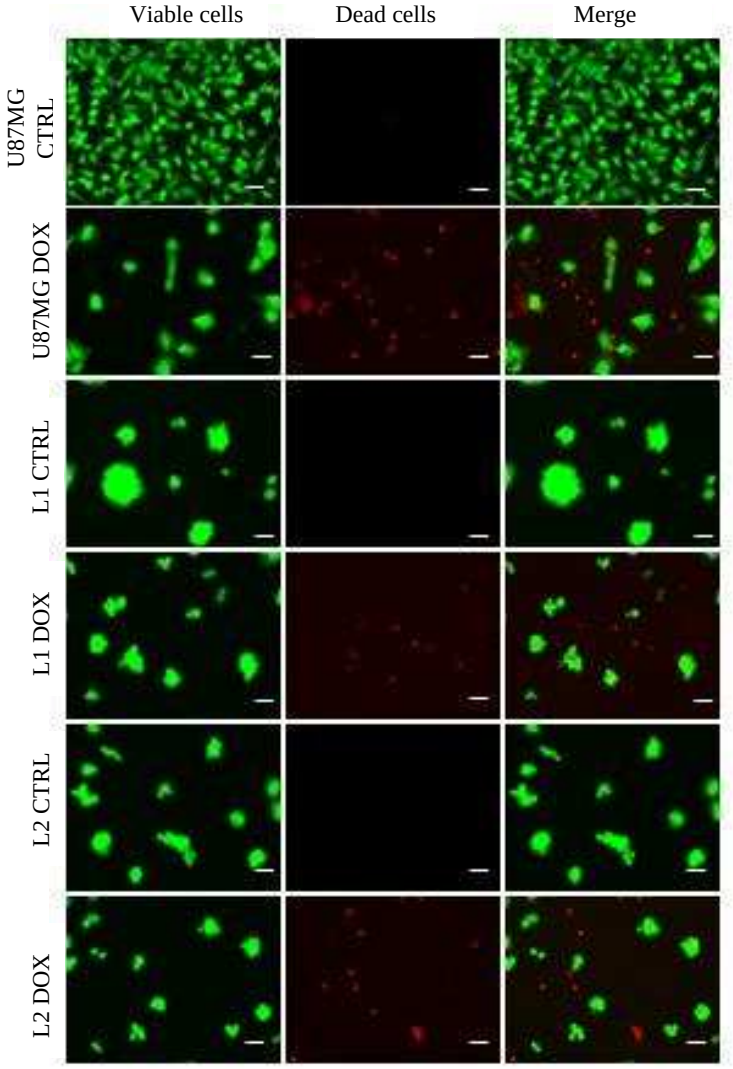

Figure 4.26: Representative Live/Dead photos of U87MG cells seeded on DOX-loaded HA-ADH hydrogels after 48 h of incubation. Free DOX caused higher cytotoxicity on glioma cells compared with the sustained release of DOX from the hydrogels. Magnification: 20×, Scale bar: 50 μm.

4.3.1.7 *In vitro* cytotoxicity of TMZ on U87MG cells

TMZ, also known as 3-methyl-4-oxoimidazo[5,1-d][1,2,3,5]tetrazine-8-carboxamide, is an imidazotetrazine derivative of the alkylating agent dacarbazine and prodrug of the commercially available anticancer chemotherapeutic drug Temodar [62]. TMZ belongs to a new class of second generation imidazotetrazine prodrugs that undergo conversion to the active alkylating agent (5E)-5-(methylaminohydrazinylidene)imidazole-4-carboxamide (MTIC) under physiological conditions [63] as shown in Figure 4.27.

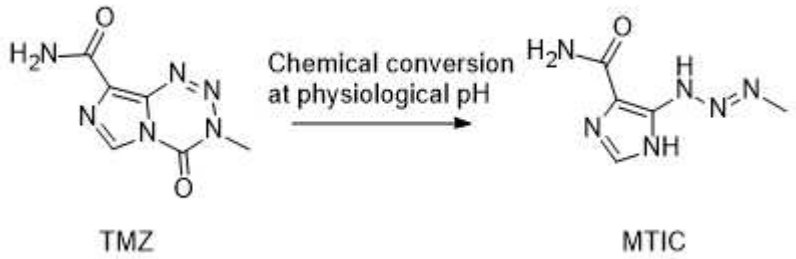

Figure 4.27: Chemical conversion of the prodrug TMZ to the active alkylating agent MTIC under physiological conditions.

TMZ is commonly used as chemotherapeutic drug in the treatment of brain tumours including astrocytoma and GBM. In 1999, it was approved by FDA for its use in the treatment of anaplastic astrocytoma in adults and in 2005, in the treatment of patients with newly diagnosed GBM [64]. In preclinical studies, TMZ due to its lipophilic nature has demonstrated the ability to penetrate CNS and cross successfully the BBB [65]. Although, as discussed in Chapter 1, the BBB restricts the penetration of nearly all commonly used chemotherapeutic agents, leading to ineffective chemotherapy.

Therefore, TMZ is mainly used in conjunction with radiotherapy for the treatment of GBM. Clinical studies from the National Cancer Institute of Canada demonstrated that the median survival rate was increased on patients received radiotherapy in combination with TMZ compared with those received only radiotherapy [66]. The standard scheme of treatment consists of TMZ at a dose of 75 mg/m^2 and 60 Gy of radiotherapy (2 Gy daily) for 4-6 weeks, followed by a TMZ subsequent dose of 150-200 mg/m^2 for 5 days every 28 days for 6 cycles. It has been observed that adjuvant radiation enhances the efficacy of TMZ and improves its antitumour activity in the treatment of brain cancer.

Its mechanism of action is based on its ability of methylating DNA at the N^7 and O^6 positions of guanine residues or at the O^3 position on adenine. The methylation of the O^6 on guanine moiety results in the insertion of a thymine molecule instead of cytosine during the DNA replication which mediates the cytotoxicity of TMZ. However, the cytotoxicity of TMZ against glioma cell lines is still controversial. In the literature, several glioma cell lines have been identified as TMZ sensitive or TMZ resistant [67]. In the current work, in order to identify if human U87MG cells are sensitive to TMZ, in vitro cytotoxicity assay was conducted. Briefly, glioma cells were seeded into the wells of a 96-well plate at a density of 5×10^3 cells per well and allowed to adhere overnight in DMEM as described previously. Subsequently, the cells were incubated with increasing concentrations of TMZ (50-515 μM) for 24, 48 and 72 h. After treatment, the TMZ cytotoxicity was quantified using the MTS assay and the relative cell viability was evaluated as summarised in Figure 4.28. After 72 h of treatment, TMZ within the range of concentrations used, did not induce substantial cytotoxicity on

glioma cells as U87MG cells presented viability > 80 %. Moreover, the cytotoxic effect of TMZ on glioma cells was also evaluated qualitatively using Live/Dead assay.

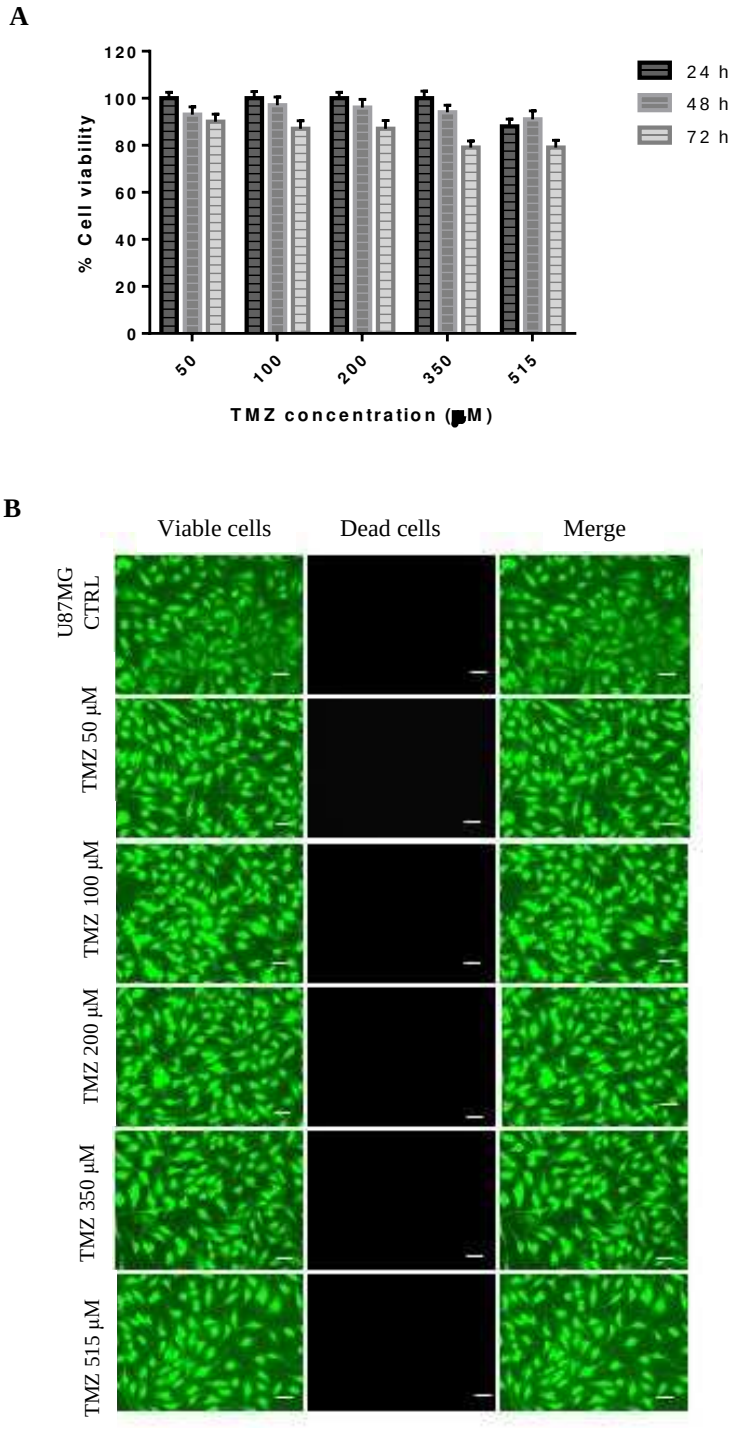

Figure 4.28: A. Cell viability was measured after 24, 48 and 72 h of incubation with increasing concentrations of TMZ (50-515 µM). TMZ did not induce any significant cytotoxicity on U87MG cells. All the results presented are the mean of n=6 with the corresponding standard deviation. **B.** Representative Live/Dead photos of U87MG cells treated with increasing concentrations of TMZ after 48 h of incubation. Magnification: 20×, Scale bar: 50 µm.

As described earlier, U87MG cells were treated with increasing concentrations of TMZ for 48 h and the Live/Dead staining solution was added. The Live/Dead assay results were consistent with those obtained from MTS assay, confirming the resistance of U87MG cells to TMZ even treated with high concentrations of this drug as shown in Figure 4.28.

In the literature, the IC_{50} value of TMZ on glioma cells vary. For example, Montaldi et al and Hermisson et al found that the IC_{50} of TMZ on U87MG cells was 7 μM and 10 μM respectively, while Baer et al and Ryu et al reported it as 172 μM and < 500 μM [68]-[71]. In addition, to date several studies have investigated the possible factors that contribute to the TMZ resistance. The O^6-methylguanine methyltransferase (MGMT) which acts to reverse methylation of the O^6 position of guanine has been associated with the drug-resistance mechanism as shown in Figure 4.29. Particularly, it has been reported that cells expressed high levels of MGMT protein, showed TMZ resistance [72]. Expression of the Mismatch Repair Protein (MMR) induces TMZ cytotoxicity, while in theory defective MMR leads to cell resistance to TMZ. Moreover, Agnihotri et al reported that TMZ resistance can be induced not only by the expression of the MGMT protein but also the expression of alkylpurine-DNA-N-glycosylase (APNG) protein [73]. This protein mainly regulates the repair of O^3- methyladenine and N^7- methylguanine. Higher expression of APNG protein has been correlated with poor survival time on patients diagnosed with GBM. Furthermore, the expression of the Base Excision Repair (BER) which is mainly responsible for the repair of N^7-methylguanine and O^3-methyladenine, is associated with the resistance to TMZ. Blough et al found that the expression of the gene mutation p53 has also been associated with the TMZ resistance but its contribution, is not clear yet [74]. These observations are at least in part explaining the complexity of GBM treatment in vivo and the high level of tumour recurrence.

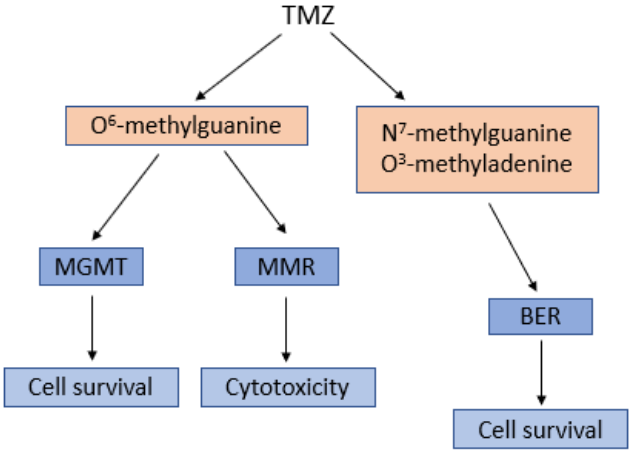

Figure 4.29: Mechanism of TMZ resistance on glioma cells. TMZ modifies DNA at N^7 or O^6 positions on guanine and O^3 on adenine by the addition of methyl groups. The methylated moieties can remain mutated, repaired by MGMT or removed by BER by the action of a DNA glycosylase such as APNG protein. Expression of MMR causes cytotoxicity of TMZ, whereas when MGMT, APNG and BER proteins are expressed, glioma cells are resistant to TMZ.

Despite the numerous studies in order to identify the cause of GBM resistance to TMZ, multiple complex molecular pathways seem to be involved and they will not be discussed further as it is beyond the scope of this thesis. Further investigation is required to better understand the mechanisms of chemoresistance of GBM cells for the development of new effective treatment.

4.3.2 Glioma cell culture on HA-BSA hydrogels

4.3.2.1 Morphology of U87MG cells on HA-BSA hydrogels

As discussed in Chapter 2, four different crosslinking densities of HA-BSA hydrogels were prepared and their ability to promote cell adhesion was investigated. The critical experimental conditions for the preparation of HA-BSA hydrogels at different crosslinking densities are provided in Table 4.3. Briefly, hydrogels were prepared into the wells of a 96-well plate with a final volume of 50 μL in the absence or the presence of the chemoattractant UII. Stock solution of UII of concentration 10^{-4} M in DMEM in the absence of FBS was prepared. Subsequently, HA-BSA hydrogels were loaded with UII as described in section 4.2.2.3. In addition, hydrogels were prepared in the absence of UII as control condition, in order to check whether the chemoattractant affects the phenotype of GBM cells.

Table 4.3: Critical experimental conditions for the preparation of HA-BSA hydrogels at different crosslinking densities.

Sample abbreviation	HA (mg/nmole)	Sulfo-NHS (mg/μmole)	EDC (mg/μmole)	BSA (mg/nmole)	Gelation time (minutes)
HB16	6.0/3.7	0.5/2.3	2.0/10.4	3.0/45.4	2
HB17	6.0/3.7	1.25/5.86	5.0/26.1	3.0/45.4	3
HB18	6.0/3.7	2.5/11.5	10.0/52.2	3.0/45.4	6
HB19	6.0/3.7	3.75/17.2	15.0/78.2	3.0/45.4	8

U87MG cells were passaged and seeded on the surface of the hydrogels at a density of 5×10^3 cells per well. Glioma cells were seeded for 48 h in DMEM supplemented with 1 % of AA and 1 % of sodium pyruvate in the absence of serum at 37 °C. Subsequently, the morphology of U87MG cells seeded on HA-BSA hydrogels at different crosslinking densities was monitored as function of incubation time.

As presented in Figure 4.30, U87MG cells showed morphology, which was highly dependent on the stiffness of the matrix. Moreover, the presence of UII had negligible effect on the morphology of GBM cells. After 24 h of incubation, U87MG cells seeded on the standard 2D culture surface obtained their typical elongated morphology, whereas GBM cells seeded on the surface of the hydrogels at different crosslinking densities adopted rounded morphology. More specifically, in the case of HB16 and HB17 hydrogels, cells obtained rounded morphology and progressive clustering of glioma cells was observed over time. In contrast, in the case of HB18 and HB19 hydrogels, single cells were predominantly spreading on the surface of the hydrogels in contrast with the clustered neurosphere formation on HB16 and HB17 conditions after 48 h of seeding.

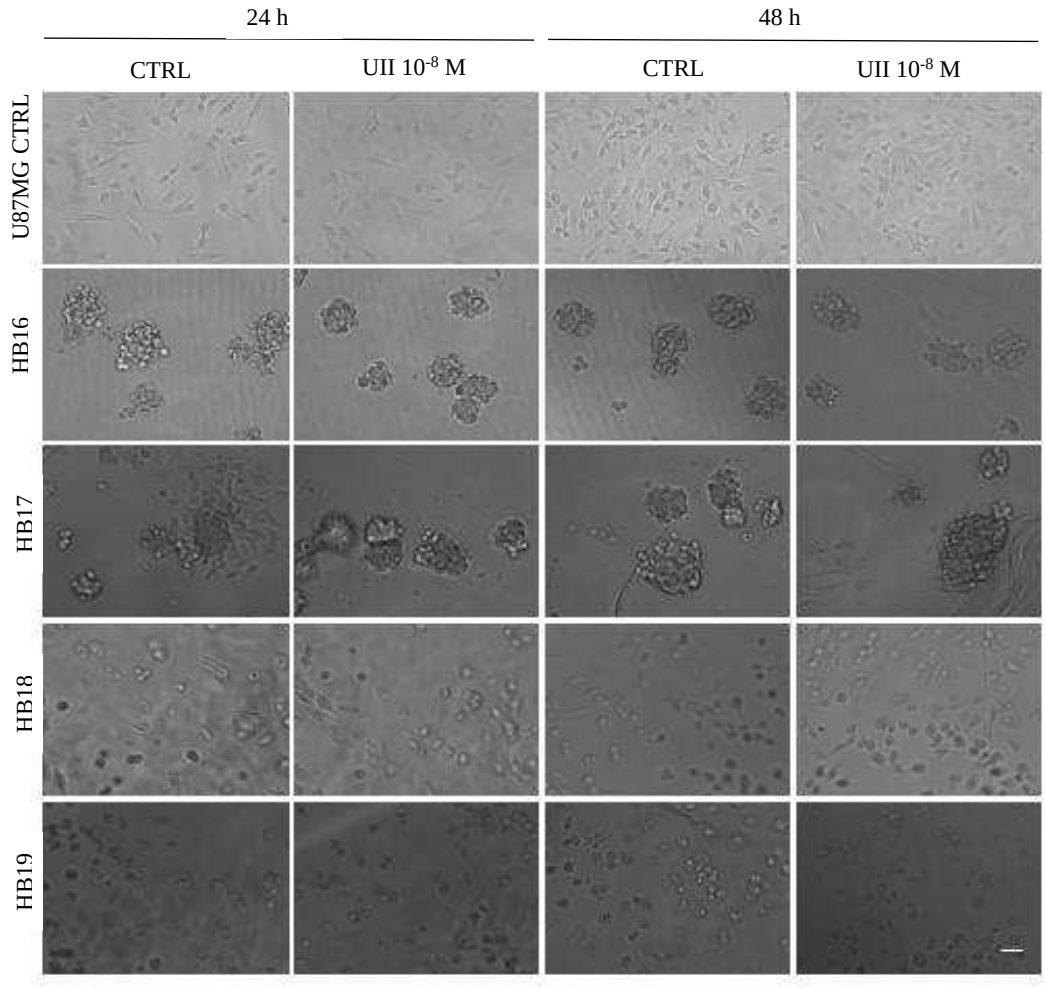

Figure 4.30: Morphology of U87MG cells cultured on different crosslinking conditions of HA-BSA hydrogels in the absence or the presence of UII (10^{-8} M). Cells were seeded on the hydrogels for 24 and 48 h in DMEM in the absence of FBS. Representative photos of cell cultures were taken using an EVOS FLoid Cell Imaging station. Magnification: 20×, Scale bar: 50 µm.

4.3.2.2 Viability of U87MG cells on HA-BSA hydrogels

The effect of crosslinking density of HA-BSA hydrogels on the viability of U87MG cells was determined quantitatively using MTS assay and qualitatively using Live/Dead assay. Briefly, hydrogels were prepared as described in section 4.2.2.3 into the wells of a 96-well plate. U87MG cells were passaged and seeded on the HA-BSA hydrogels at a density of 5×10^3 cells per well. The viability of the cells was evaluated after 24 and 48 h of seeding on the hydrogels in the absence or presence of the chemoattractant UII. As summarised in the graphs A and B in Figure 4.31, glioma cells presented viability >80 %, indicating the biocompatibility of the hydrogels. More specifically, cells seeded on the HB16 and HB17 hydrogels were slightly more metabolically active compared with those seeded on the surface of the HB18 and HB19 hydrogels. Similarly, with the seeding of glioma cells on HA-ADH hydrogels, the presence of the chemoattractant UII did not present any significant effect on the cell viability after 48 h of incubation.

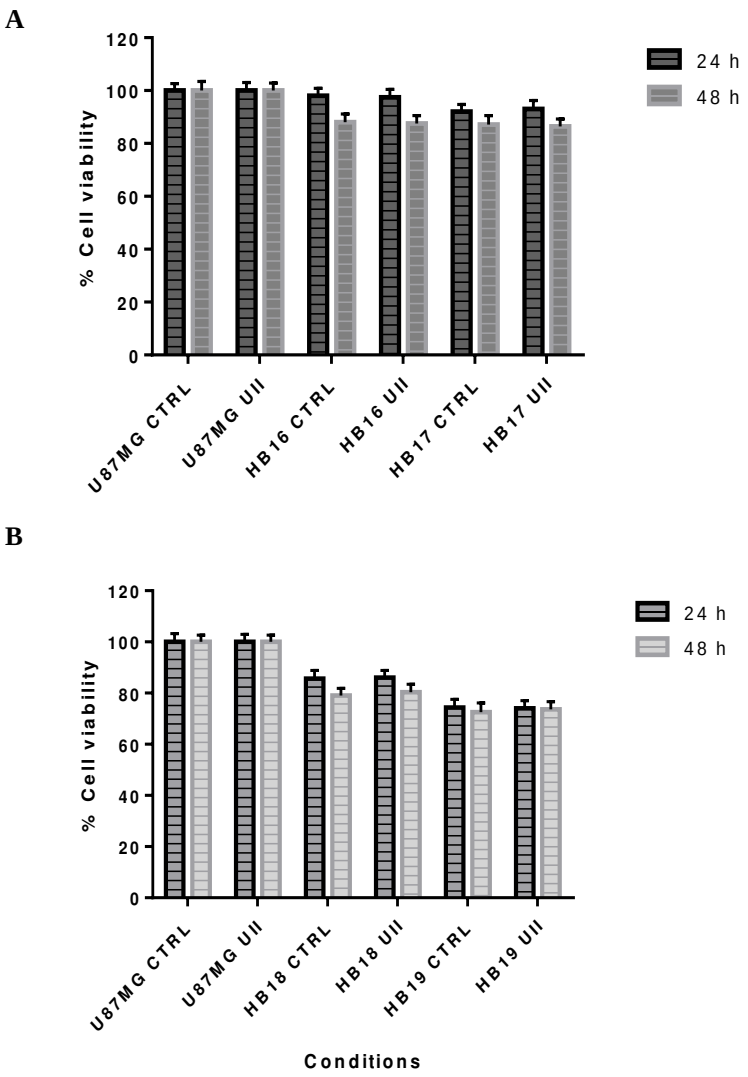

Figure 4.31: Viability of U87MG cells seeded on different crosslinking densities of HA-BSA hydrogels in absence or presence of UII (10^{-8} M). **A.** % Cell viability on HB16 and HB17 hydrogels. **B.** % Cell viability on HB18 and HB19 hydrogels. The viability of glioma cells was evaluated after 24 and 48 h of incubation. The presence of UII did not affect the viability of glioma cells. The data represent the average of n=5 with the corresponding standard deviation.

The biocompatibility of the hydrogels was also assessed by Live/Dead assay using U87MG cells. Glioma cells were seeded on HA-BSA hydrogels at four different crosslinking densities for 48 h as described above. As presented in Figure 4.32, glioma cell growth was not significantly affected at the various crosslinking densities, indicating no cytotoxicity and biocompatibility of the hydrogels. Consistent with the results from the MTS assay, the majority of cell population remained viable after seeding on the hydrogels for 48 h. As shown in Figure 4.32, cells adopted rounded morphology and formed clusters when cultured on HB16 and HB17 hydrogels, whereas on HB18 and HB19 hydrogels, cells remained single and cell spreading was predominant across the culture surface, suggesting adhesion to the matrix. These observations reporting that cells tend to obtain rounded morphology on soft surfaces and keep their elongated shape on stiffer surfaces, likely allowing guided migration.

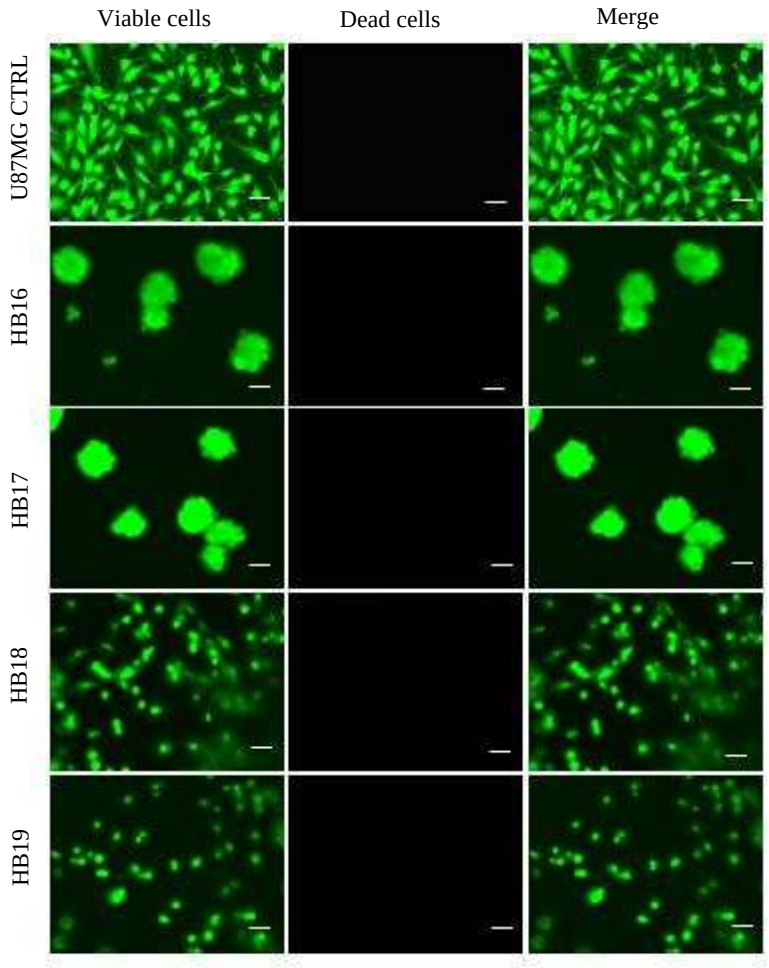

Figure 4.32: Representative Live/Dead photos of U87MG cells seeded on HA-BSA hydrogels at different crosslinking densities for 48 h. Glioma cells remained viable after seeding on hydrogels for 48 h, indicating the biocompatibility of the hydrogels. Magnification: 20×, Scale bar: 50 μm.

4.3.2.3 *In vitro* cytotoxicity of DOX-loaded HA-BSA hydrogels

The in vitro cytotoxicity of DOX-loaded hydrogels was determined using MTS and Live/Dead assay. Briefly, DOX-loaded hydrogels were prepared into the wells of a 96-well plate as described in section 4.2.2.5. U87MG cells were passaged and seeded on the drug-loaded hydrogels at a density of 5×10^3 cells per well for 24 and 48 h. After treatment, MTS solution (30 μL) was added on the hydrogels and cells were incubated for 1 h at 37 °C. The absorbance was measured at 490 nm and the % cell viability was calculated. Blank HA-BSA hydrogels were also prepared as negative control. As demonstrated in Figure 4.33, DOX-loaded HA-BSA hydrogels induced significant cytotoxicity after 24 and 48 h of incubation. Moreover, it is noteworthy that the cytotoxicity from the drug-loaded hydrogels on U87MG cells was lower than the cytotoxicity induced from the free DOX. In addition, HB16 and HB17 hydrogels loaded with DOX demonstrated higher cytotoxicity after 48 h of incubation, while the highly crosslinked hydrogels did not present significant cytotoxic effect on glioma cells.

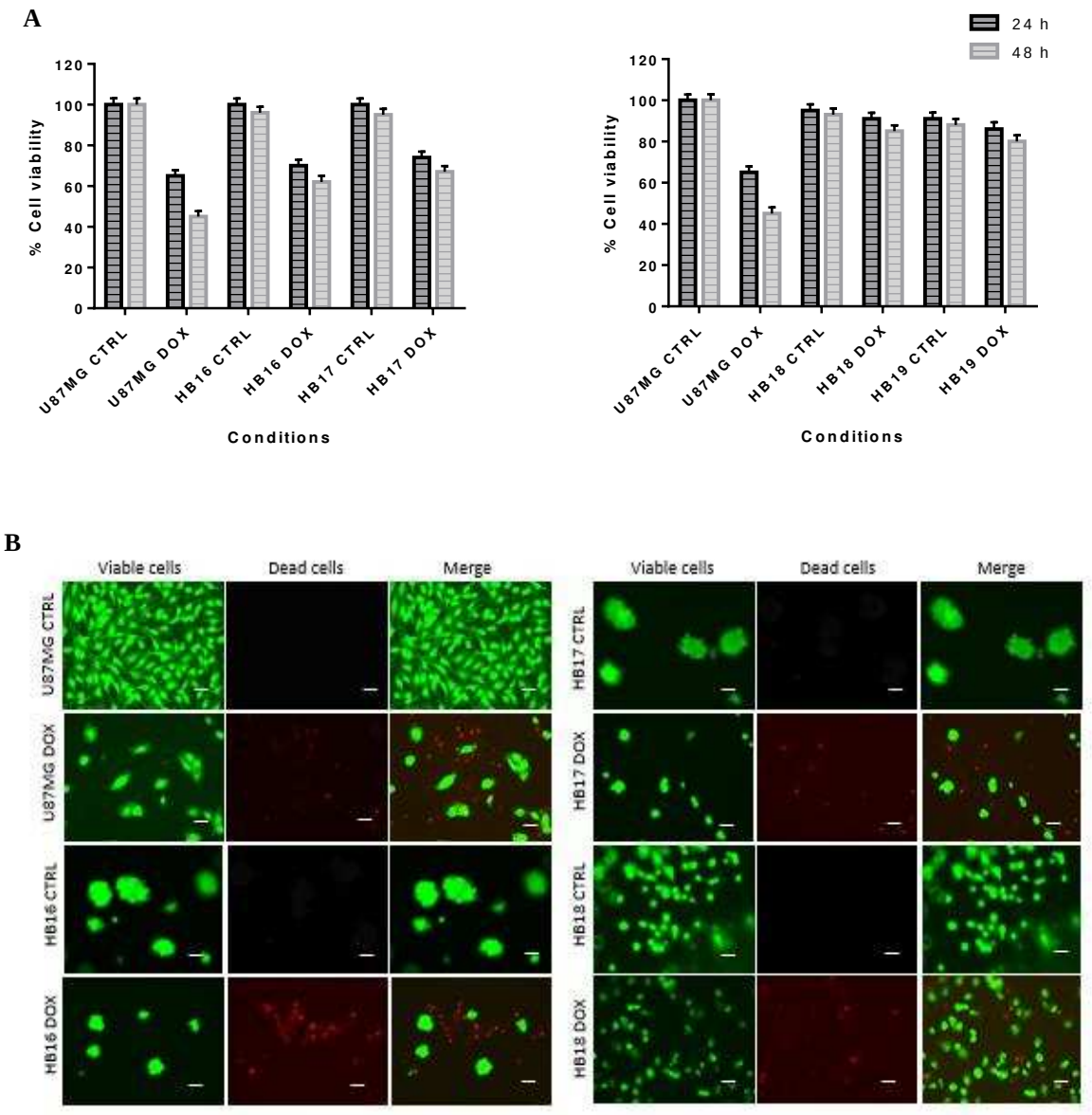

Figure 4.33: A. U87MG cell viability was measured after 24 and 48 h of seeding on DOX-loaded HA-BSA hydrogels. All the results presented are the mean of n=6 with the corresponding standard deviation. **B.** Representative Live/Dead photos of U87 MG cells seeded on DOX-loaded hydrogels for 48 h. Magnification: 20×, Scale bar: 50 μm.

These results are consistent with the data obtained from DOX release experiments discussed in Chapter 3. Higher cumulative DOX release was observed in HB16 and HB17 hydrogels compared to highly crosslinked hydrogels, resulting in high in vitro cytotoxicity on U87MG cells. Moreover, Live/Dead staining results were consistent with the MTS assay, confirming the higher cytotoxicity of the DOX-loaded HB16 and HB17 hydrogels, due to the highest DOX release from these crosslinking densities.

4.3.2.4 Modified Boyden Chamber invasion and migration assay on HA-BSA hydrogels

Herein, a modified Boyden Chamber assay was applied in order to evaluate the ability of glioma cells to invade a 3D ECM and migrate in response to the chemoattractant UII. As described previously in section 4.2.2.15, glioma cells were seeded on a thin layer of HA-BSA hydrogels at a density of 5×10^4 cells. HA-BSA hydrogels were prepared at HB16, HB17 and HB18 crosslinking densities according to the preparation protocol and a volume of hydrogel 100 μL was applied on the upper part of the polycarbonate membrane.

In this set up, cells were required to invade through the hydrogel into the lower chamber containing the chemoattractant as described in section 4.3.1.3. U87MG cells were allowed to invade the thin layer of the hydrogel for 48 h. After this incubation time, GBM cells were fixed and stained with hematoxylin solution. Quantification of the cells that invaded the hydrogel and migrated in response to UII was performed using ImageJ. The reproducibility of the invasion assay was assessed by measuring the invasive capability of glioma cells in triplicate (3 transwells). U87MG cells were previously shown to be highly invasive and migratory as demonstrated in section 4.3.1.3. Therefore, this cell line was chosen and the extent of invasion and migration on HA-BSA hydrogels was further investigated. As summarised in Figure 4.34, a higher number of GBM cells invaded and migrated in the presence of UII in the absence or presence of the layer of hydrogel. Moreover, it was noted that the crosslinking density of the hydrogels affected at some point the extent of the invasion and migration of cells. As the crosslinking density increases, lower number of cells were able to invade and migrate through the hydrogel. In overall, these results indicated that hydrogels allowed the invasion of GBM cells through its porous network.

A

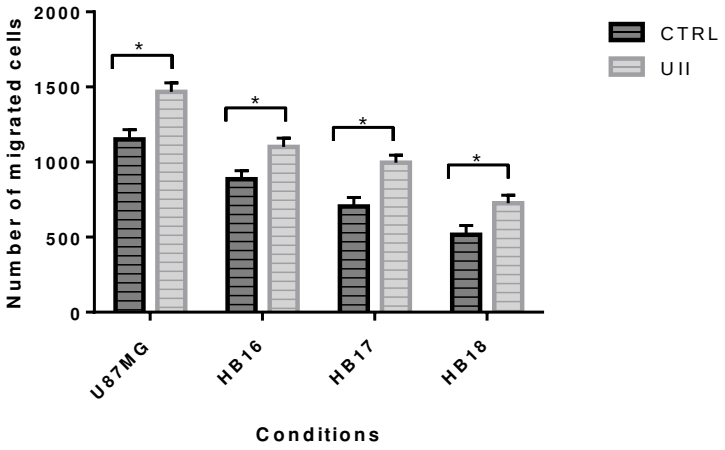

B

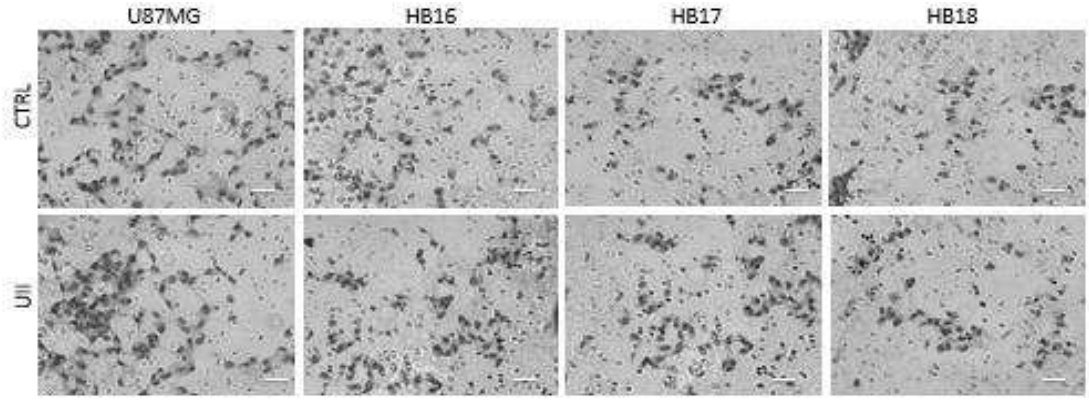

Figure 4.34: Modified Boyden Chamber invasion and migration assay on HA-BSA hydrogels **A.** Histogram shows the quantification of U87MG cells that invaded the thin layer of the hydrogel compared with the control. The data obtained from one representative experiment in triplicate with the corresponding standard deviation. Mann and Whitney test; *P < 0.05. **B.** Representative photos of the membranes after staining with hematoxylin solution. Magnification: 20×, Scale bar: 50 μm.

4.3.3 Glioma cell culture on MC-based hydrogels

4.3.3.1 *In vitro* evaluation of biocompatibility of MC-based hydrogels

MC is a polysaccharide derived from cellulose and its aqueous solutions form thermoreversible hydrogels that undergo sol-gel transition upon heating. As described in Chapter 2, the thermal gelation properties of MC solutions of various polymer and salt concentrations were investigated and their in vitro biocompatibility was evaluated. Briefly, MC solutions of various concentrations in sterile PBS were prepared according to the Table 4.4 and as described in section 2.2.2.3.

Table 4.4: Different concentrations of MC in various concentrations of PBS solution for U87MG cell culture.

MC Concentration (% w/w)	PBS Composition	Gelation Temperature (°C)
2	1×PBS	-
4	1×PBS	42
6	1×PBS	37
8	1×PBS	34
2	5×PBS	35
4	5×PBS	32
6	5×PBS	30
2	10×PBS	28
4	10×PBS	25

U87MG cells were passaged and seeded on the surface of MC-based hydrogels for 24 and 48 h. Unfortunately, glioma cells were poorly adherent to the hydrogel surface and formation of cell clusters/neurospheres was observed (data are not shown). The % cell viability on the hydrogels after 24 and 48 h of seeding was determined using MTS assay. As summarised in Figure 4.35, GBM cell viability was highly dependent on the polymer concentration. Specifically, as the MC concentration

increased, significant decrease in cell viability was observed. In addition, it can be concluded that the concentration of salts in the PBS solution induced considerable cytotoxicity on U87MG cells.

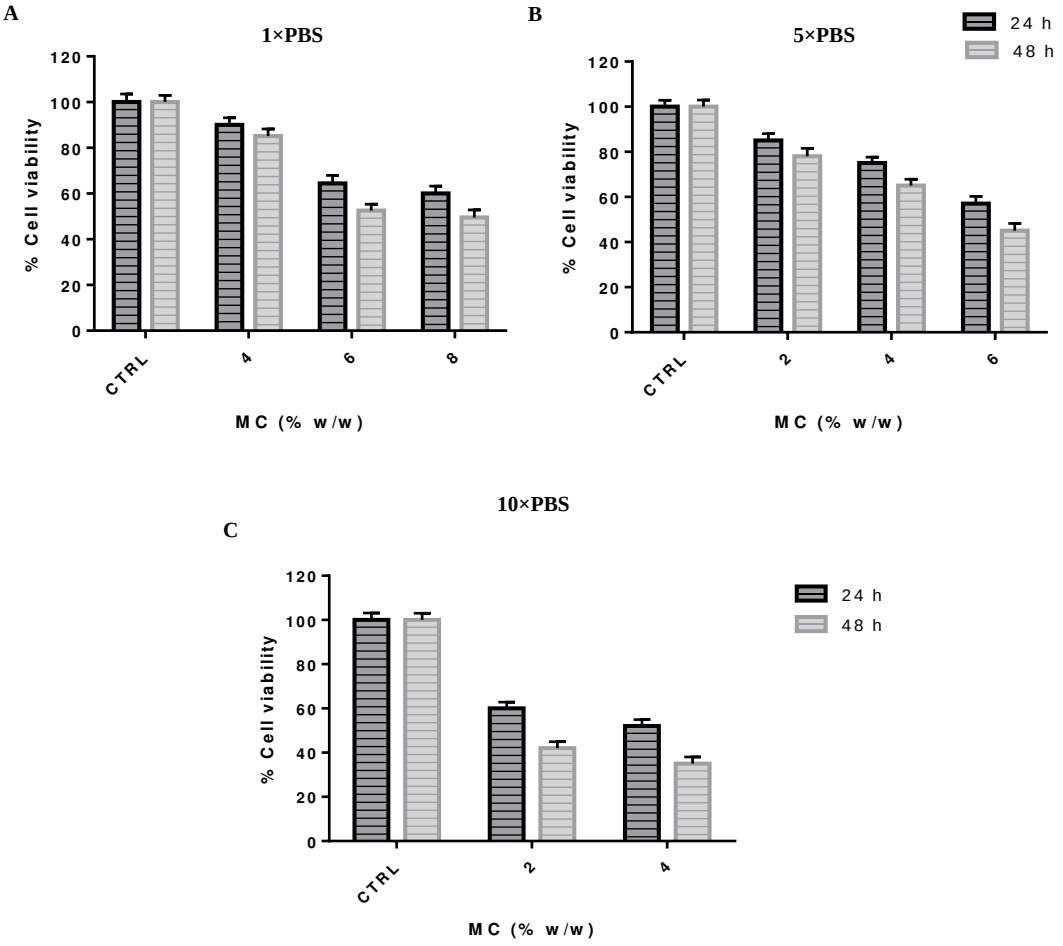

Figure 4.35: U87MG cell viability on MC-based hydrogels after 24 and 48 h of seeding. The polymer concentration and the concentration of salts in PBS showed significant effect on the viability of glioma cells. Data represent the average of n=6 with the corresponding standard deviation.

Increasing concentrations of salts that were present in the PBS solution, resulted in lower cell viability after 24 and 48 h of seeding. As discussed in Chapter 2, our goal was to develop biocompatible MC-based hydrogels that undergo gelation at body temperature. Therefore, the addition of salts to the MC solution contributed to lower gelation temperature. However, the addition of salts induced significant increase in osmolality of MC solutions and this was detrimental for glioma cell viability as shown in Figure 4.35. This observation agrees with the literature where it is reported that increase in osmolality is harmful to cell viability due to the induction of cellular dehydration [75]. MC-based hydrogels were not further studied due to their cytotoxicity on glioma cells, therefore, blend solutions of XG/MC were prepared and the biocompatibility of the formed hydrogels was further investigated.

4.3.3.2 *In vitro* evaluation of biocompatibility of blend XG/MC hydrogels

Blend hydrogels have gained a lot of attention in biomedical applications such as drug delivery, cell culture and tissue engineering [76]. Blend hydrogels combine the physicochemical and biological properties of each component. Chen et al prepared injectable hydrogels from physical blend of thiolated hyaluronic acid and collagen I for in vitro construction of engineered cartilage [77]. Furthermore, Zheng et al fabricated gelatin-based hydrogels upon blending with gellan at body temperature. These hydrogels presented a great potential as injectable wound dressing or scaffold for tissue engineering applications [78].

Herein, as described in chapter 2, injectable blend hydrogels consisted of MC and XG were prepared in an effort to improve the biocompatibility of MC-based hydrogels. XG is a non-toxic, hydrophilic, biodegradable polymer that has been used in a variety of biomedical applications demonstrating good biocompatibility [79]. Taking advantage of this, XG/MC blend solutions were prepared at different compositions in 1×PBS (pH 7.4) as summarised in Table 4.5. XG/MC hydrogels were prepared into the wells of a 96-well plate and U87MG cells were seeded on the hydrogels at a density of 5×10^3 cells per well for 24 and 48 h. Subsequently, MTS solution was added and the % cell viability was determined.

Table 4.5: XG and MC concentrations in various blend solutions of XG/MC in 1×PBS.

Sample abbreviation	XG Concentration (% w/w)	MC Concentration (% w/w)
XG1/MC0	1	0
XG1/MC3	1	3
XG1/MC6	1	6
XG1/MC8	1	8
XG2/MC1	2	1
XG2/MC6	2	6
XG3/MC1	3	1

As summarised in Figure 4.36, XG/MC hydrogels at specific ratios of XG/MC presented relatively good biocompatibility after 48 h of seeding. In addition, it is noteworthy that increasing concentration of MC in the blend hydrogels demonstrated substantial cytotoxicity on U87MG cells. On the other hand, blend solutions consisted of higher concentration of XG presented better biocompatibility. Moreover, separate solutions of MC and XG were evaluated for their cytotoxicity. Specifically, XG did not induce significant cytotoxicity, while solutions of MC at high concentrations (4-8 % w/w) demonstrated substantial cytotoxic effect on glioma cells. XG/MC hydrogels that demonstrated relatively good biocompatibility, were not studied further due to their poor mechanical properties.

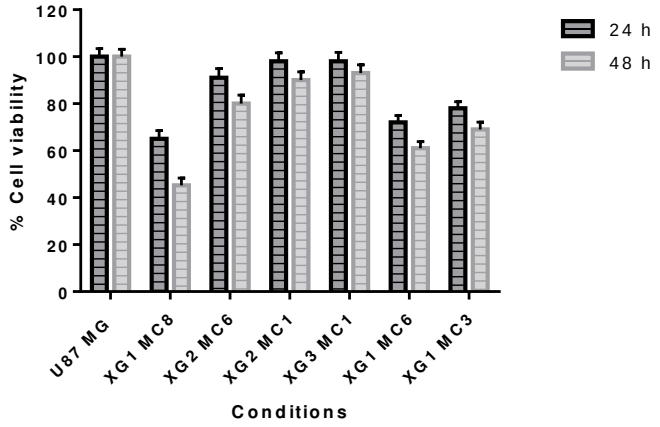

Figure 4.36: Evaluation of viability of U87MG cells seeded on blend XG/MC hydrogels for 24 and 48 h. Data represent the average of n=6 with the corresponding standard deviation.

4.4 Conclusions

GBM is one of the most devastating and incurable cancer of the last decades. Current methods of treatment lack of several limitations as extensively discussed in Chapter 1, rending treatment of GBM challenging. Therefore, a great attention has been paid on alternative strategies that focus on targeted drug delivery methods.

To date, various drug delivery systems have been investigated for the treatment of GBM including liposomes, nanoparticles and injectable hydrogels. Among them, hydrogels have demonstrated promising results due to their unique and tunable physical properties. Moreover, the majority of the studies have used hydrogels as anticancer drug delivery systems for the treatment of malignant brain tumours. However, these systems present several critical limitations, including the absence of molecules that naturally exist in the brain ECM and most importantly they lack from effective chemoattractants. Consequently, residual invasive tumour cells remain in the margins of the resection cavity, leading to inevitable tumour recurrence.

Herein, in order to overcome these limitations, we investigated the fabrication of hydrogels mainly consisted of HA. Fabricated hydrogels were loaded with human UII as chemoattractant at gradient concentration and subsequently with an anticancer drug in order to achieve attraction of GBM cells into the hydrogel matrix and cause cell death. Overall, fabricated scaffolds based on HA presented good biocompatibility and the preliminary results showed that glioma cells can invade the hydrogel matrix and migrate in response to the loaded chemoattractant UII. Hydrogels also loaded with DOX induced considerable cytotoxicity on GBM cells. The viability assays performed on GBM culture on MC-based hydrogels revealed that these scaffolds do not promote cell adhesion and growth and they were not studied further.

References

[1] Zimmermann D.R., Dours-Zimmermann M.T., Extracellular matrix of the central nervous system: from neglect to challenge, Histochem. Cell Biol., 2008, 130, 635-653.

[2] Lau L.W., Cua R., Keough M. B., Haylock-Jacobs S., Yong, V.W., Pathophysiology of the brain extracellular matrix: a new target for remyelination. Nat. Rev. Neurosci., 2013, 14, 722-729.

[3] Zhu J., Marchant R.E., Design properties of hydrogel tissue-engineering scaffolds, Expert Rev. Med. Devices, 2011, 8, 607-626.

[4] Munson J. M., Bellamkonda R.V., Swartz, M. A., Interstitial flow in a 3D microenvironment increases glioma invasion by a CXCR4-dependent mechanism, Cancer Res., 2013, 73, 1536-1546.

[5] Kearns S.M., Laywell E.D., Kukekov V.K., Steindler D.A., Extracellular matrix effects on neurosphere cell motility, Exp. Neurol., 2003, 182, 240-244.

[6] Delpech B., Maingonnat C., Girard N., Hyaluronan and hyaluronectin in the extracellular matrix of human brain tumour stroma. Eur. J. Cancer, 1993, 29A, 1012-1017.

[7] Mahesparan R., Read T.A., Lund-Johansen M., Skaftnesmo K.O., Bjerkvig R., Engebraaten O., Expression of extracellular matrix components in a highly infiltrative in vivo glioma model, Acta Neuropathol., 2003, 105, 49-57.

[8] Quirico-Santos T., Fonseca C.O., Lagrota-Candido J., Brain sweet brain: importance of sugars for the cerebral microenvironment and tumour development, Arq. Neuropsiquiatr., 2010, 68, 799-803.

[9] Yang Y.L., Sun C., Wilhelm M.E., Fox L.J., Zhu J., Kaufman L.J., Influence of chondroitin sulfate and hyaluronic acid on structure, mechanical properties, and glioma invasion of collagen I gels, Biomaterials, 2011, 32, 7932-7940.

[10] Kievit F.M., Florczyk S.J., Leung M.C., Veiseh O., Park J.O., Disis M.L., Zhang M., Chitosan-alginate 3D scaffolds as a mimic of the glioma tumour microenvironment, Biomaterials, 2010, 31, 5903-5910.

[11] Pedron S., Harley B.A., Impact of the biophysical features of a 3D gelatin microenvironment on glioblastoma malignancy, J. Biomed. Mater. Res. A., 2013, 101, 3404-3415.

[12] Khaing Z.Z., Seidlits S.K., Hyaluronic acid and neural stem cells: implications for biomaterial design, J. Mater. Chem. B., 2015, 3, 7850-7866.

[13] Bignami A., Asher R., Some observations on the localisation of hyaluronic acid in adult, newborn, and embryonal rat brain, Int. J. Devel. Neurosci., 1992, 10, 45-57.

[14] Akiyama Y., Jung S., Salhia B., Lee S., Hubbard S., Taylor M., Mainprize T., Akaishi K., van Furth W., Rutka J.T., Hyaluronate receptors mediating glioma cell migration and proliferation, J. Neuro-Oncol., 2001, 53, 115-127.

[15] Ranuncolo S.M., Ladeda V., Specterman S., Varela M., Lastiri J., Morandi A., Matos E., Bal de Kier Joffé E., Puricelli L., Pallotta M.G., CD44 expression in human gliomas, J. Surg. Oncol., 2002, 79, 30-35.

[16] Park J.B., Kwak H.J., Lee S.H., Role of hyaluronan in glioma invasion, Cell Adh. Migr., 2008, 2, 202-207.

[17] Cha J., Kang S.G., Kim P., Strategies of Mesenchymal Invasion of Patient-derived Brain Tumours: Microenvironmental Adaptation, Sci. Rep., 2016, 6, 24912-24923.

[18] Hegedus B., Marga F., Jakab K., Sharpe-Timms K.L., Forgacs G., The interplay of cell-cell and cell-matrix interactions in the invasive properties of brain tumours, Biophys. J., 2006, 91, 2708-2716.

[19] Jin S.G., Jeong Y.I., Jung S., Ryu H.H., Jin Y.H., Kim I.Y., The effect of hyaluronic Acid on the invasiveness of malignant glioma cells: comparison of invasion potential at hyaluronic Acid hydrogel and Matrigel, J. Korean Neurosurg. Soc., 2009, 46, 472-478.

[20] Rao S.S., Dejesus J., Short A.R., Otero J.J., Sarkar A., Winter J.O., Glioblastoma behaviours in three-dimensional collagen-hyaluronan composite hydrogels, ACS Appl. Mater. Interfaces, 2013, 5, 9276-9284.

[21] Ananthanarayanan B., Kim Y., Kumar S., Elucidating the mechanobiology of malignant brain tumours using a brain matrix-mimetic hyaluronic acid hydrogel platform, Biomaterials, 2011, 32, 7913-7923.

[22] Pedron S., Becka E., Harley B., Regulation of glioma cell phenotype in 3D matrices by hyaluronic acid, Biomaterials, 2013, 34, 7408-7417.

[23] Conlon J.M., O'Harte F., Smith D., Tonon M.C., Vaudry H., Isolation and primary structure of urotensin II from the brain of a tetrapod, the frog Rana ridibunda, Biochem. and biophys. Res. Comm., 1992, 188, 578-583.

[24] Douglas S.A., Dhanak D., Johns D.G., From 'gills to pills': urotensin-II as a regulator of mammalian cardiorenal function, Trends Pharmacol. Sci., 2004, 25, 76-85.

[25] Clavier T., Mutel A., Desrues L., Lefevre-Scelles A., Gastaldi G., El Amki M., Dubois M., Melot M., Wurtz V., Curey S., Gérardin E., Proust F., Compère V., Castel H., Association between

vasoactive peptide urotensin II in plasma and cerebral vasospasm after aneurysmal subarachnoid hemorrhage: potential therapeutic target, J. Neurosurg., 2018, in press.

[26] Thompson J. P., Watt P., Sanghavi S., Strupish J. W., Lambert D. G., A comparison of cerebrospinal fluid and plasma urotensin II concentrations in normotensive and hypertensive patients undergoing urological surgery during spinal anesthesia: a pilot study, Anesth. Analg., 2003, 97, 1501-1503.

[27] Douglas S.A., Tayara L., Ohlstein E.H., Halawa N., Giaid A., Congestive heart failure and expression of myocardial urotensin II, Lancet, 2002, 359, 1990-1997.

[28] Matsushita M., Shichiri M., Imai T., Iwashina M., Tanaka H., Takasu N., Co-expression of urotensin II and its receptor (GPR14) in human cardiovascular and renal tissues, J. Hypertens., 2001, 19, 2185-2190.

[29] Wu Y.Q., Song Z., Zhou C.H., Xing S.H., Pei D.S., Zheng J.N., Expression of urotensin II and its receptor in human lung adenocarcinoma A549 cells and the effect of urotensin II on lung adenocarcinoma growth in vitro and in vivo, Oncol. Rep., 2010, 24, 1179-1184.

[30] Zhou, C. H., Wan Y.Y., Chu H.H., Song Z., Xing S.H., Wu Y.Q., Yin X.X., Urotensin II contributes to the formation of lung adenocarcinoma inflammatory microenvironment through the NF-κB pathway in tumour-bearing nude mice, Oncol. Lett., 2012, 4, 1259-1263.

[31] Rempel S.A., Dudas S., Ge S., Gutiérrez J.A., Identification and localisation of the cytokine SDF1 and its receptor, CXC chemokine receptor 4, to regions of necrosis and angiogenesis in human glioblastoma, Clin. Cancer Res., 2000, 6, 102-111.

[32] Medeiros P.J., Al-Khazraji B.K., Novielli N.M., Postovit L.M., Chambers A.F., Jackson D.N., Neuropeptide Y stimulates proliferation and migration in the 4T1 breast cancer cell line, Int. J. Cancer, 2012, 131, 276-286.

[33] Lu D.Y., Leung Y.M., Huang S.M., Wong K.L., Bradykinin-induced cell migration and COX-2 production mediated by the bradykinin B1 receptor in glioma cells, J. Cell Biochem., 2010, 110, 141-150.

[34] Segain J.P., Rolli-Derkinderen M., Gervois N., Raingeard de la Blétière D., Loirand G., Pacaud P., Urotensin II is a new chemotactic factor for UT receptor-expressing monocytes, J. Immunol., 2007, 179, 901-909.

[35] Lecointre C., Desrues L., Joubert J.E., Perzo N., Guichet P.O., Le Joncour V., Brulé C., Chabbert M., Leduc R., Prézeau L., Laquerrière A., Proust F., Gandolfo P., Morin F., Castel H.,

Signaling switch of the urotensin II vasosactive peptide GPCR: prototypic chemotaxic mechanism in glioma, Oncogene, 2015, 34, 5080-5094.

[36] Coly P.M., Perzo N., Le Joncour V., Lecointre C., Schouft M.T., Desrues L., Chemotactic G protein-coupled receptors control cell migration by repressing autophagosome biogenesis, Autophagy, 2016, 12, 1-19.

[37] Jiguet J.C., Baeza-Kallee N., Denicolai E., Barets D., Metellus P., Padovani L., Chinot O., Figarella-Branger D., Fernandez C., Ex vivo cultures of glioblastoma in three-dimensional hydrogel maintain the original tumour growth behaviour and are suitable for preclinical drug and radiation sensitivity screening, Exp. Cell Research, 2014, 321, 99-108.

[38] Florczyk S., Wang K., Jana S., Wood D., Sytsma S., Sham J., Kievit F., Zhang M., Porous chitosan-hyaluronic acid scaffolds as a mimic of glioblastoma microenvironment ECM, Biomaterials, 2013, 34, 10143-10150.

[39] Kaufman L.J., Brangwynne C.P., Kasza K.E., Filippidi E., Gordon V.D., Deisboeck T.S., Weitz D.A., Glioma expansion in collagen I matrices: analysing collagen concentration-dependent growth and motility patterns, Biophys. J., 2005, 89, 635-650.

[40] Glaß M., Möller B., Zirkel A., Wächter K., Hüttelmaier S., Posch S., Cell migration analysis: Segmenting scratch assay images with level sets and support vector machines, Pattern Recogn., 2012, 45, 3154-3165.

[41] Liang C.C., Park A.Y., Guan J.L., In vitro scratch assay: a convenient and inexpensive method for analysis of cell migration in vitro, Nat. Protoc., 2007, 2, 329-333.

[42] Tibbitt M.W., Anseth K.S., Hydrogels as extracellular matrix mimics for 3D cell culture, Biotechnol. Bioen., 2009, 103, 655-663.

[43] Schwarz J. Bierbaum V., Merrin J., Frank T., Hauschild R., Bollenbach T., Tay S., Sixt M., Mehling M., A microfluidic device for measuring cell migration towards substrate-bound and soluble chemokine gradients, Sci. Rep., 2016, 6, 36440-36451.

[44] Kramer N., Walzl A., Unger C., Rosner M., Krupitza G., Hengstschlager M., Dolznig H., In vitro cell migration and invasion assays, Mut. Res., 2013, 752, 10-24.

[45] Campbell J.J., Husmann A., Hume R.D., Watson C.J., Cameron R.E., Development of three-dimensional collagen scaffolds with controlled architecture for cell migration studies using breast cancer cell lines, Biomaterials, 2017, 114, 34-43.

[46] Topman G., Shoham N., Sharabani-Yosef O., Lin F.H., Gefen A., A new technique for studying directional cell migration in a hydrogel-based three-dimensional matrix for tissue engineering model systems, Micron, 2013, 51, 9-12.

[47] Scholzen T., Gerdes J., The Ki-67 protein: from the known and the unknown, J. Cell Physiol., 2000, 182, 311-322.

[48] Lomovskaya N., Otten S.L., Doi-Katayama Y., Doxorubicin overproduction in Streptomyces peucetius: cloning and characterization of the dnrU ketoreductase and dnrV genes and the doxA cytochrome P-450 hydroxylase gene, J. Bacteriol., 1999, 181, 305-318.

[49] Thorn C.F., Oshiro C., Marsh S., Hernandez-Boussard T., McLeod H., Klein T.E., Altmana R.B., Doxorubicin pathways: pharmacodynamics and adverse effects, Pharmacogenet. Genomics, 2011, 21, 440-446.

[50] Ansari L., Shiehzadeh F., Taherzadeh Z., Nikoofal-Sahlabadi S., Momtazi-borojeni A.A., Sahebkar A., Eslami S., The most prevalent side effects of pegylated liposomal doxorubicin monotherapy in women with metastatic breast cancer: a systematic review of clinical trials, Cancer Gene Ther., 2017, 24, 189-193.

[51] Fan C., Georgiou K.R., Morris H.A., McKinnon R.A., Keefe D.M.K., Howe P.R., Xian C.J., Combination breast cancer chemotherapy with doxorubicin and cyclophosphamide damages bone and bone marrow in a female rat model, Breast Cancer Res. Treat., 2017, 165, 41-51.

[52] Stan A.C., Casares S., Radu D., Walter G.F., Brumeanu T.D., Doxorubicin-induced cell death in highly invasive human gliomas, Anticancer Res., 1999, 19, 941-950.

[53] Lesniak M.S., Upadhyay U., Goodwin R., Tyler B., Brem H., Local delivery of doxorubicin for the treatment of malignant brain tumours in rats, Anticancer Res., 2005, 25, 3825-3831.

[54] Annovazzi L., Caldera V., Mellai M., Riganti C., Battaglia L., Chirio D., Melcarne A., Schiffer D., The DNA damage/repair cascade in glioblastoma cell lines after chemotherapeutic agent treatment, Int. J. Oncol., 2015, 46, 2299-2308.

[55] Muldoon L.L., Neuwelt E.A., BR96-DOX immunoconjugate targeting of chemotherapy in brain tumour models, J. Neuro-Oncol., 2003, 65, 49-62.

[56] Steiniger S.C., Kreuter J., Khalansky A.S., Skidan I.N., Bobruskin A.I., Smirnova Z.S., Severin S.E., Uhl R., Kock M., Geiger K.D., Gelperina S.E, Chemotherapy of glioblastoma in rats using doxorubicin-loaded nanoparticles, Int. J. Cancer, 2004, 109, 759-767.

[57] Walter K.A., Tamargo R.J., Olivi A., Burger P.C., Brem H., Intratumoural chemotherapy, Neurosurgery, 1995, 37, 1128-1145.

[58] Lobo J.F.R., Castro E.S., Gouvea D.R., Fernandes C.P., de Almeida F.B., de Amorim L.M.F., Burth P., Rocha L., Santos M.G., Harmerski L., Lopes N.P., Pinto A.C., Antiproliferative activity of Eremanthus crotonoides extracts and centratherin demonstrated in brain tumour cell lines, Rev. bras. Farmacogn., 2012, 22, 1295-1300.

[59] Kadioglu O., Saeed M., Kuete V., Greten H.J., Efferth T., Oridonin Targets Multiple Drug-Resistant Tumour Cells as Determined by in Silico and in Vitro Analyses, Front Pharmacol., 2018, 9, 355-365.

[60] Zimmermann S., Dziadziuszko R., Peters S., Indications and limitations of chemotherapy and targeted agents in non-small cell lung cancer brain metastases, Cancer Treat. Rev., 2014, 40, 716-722.

[61] Hoare T.R., Kohane D.S., Hydrogels in drug delivery: Progress and challenges, Polymer, 2008, 49, 1993-2007.

[62] Moody C.L., Wheelhouse R.T., The medicinal chemistry of imidazotetrazine prodrugs, Pharmaceuticals, 2014, 7, 797-838.

[63] Friedman H.S., Kerby T., Calvert H., Temozolomide and Treatment of Malignant Glioma, Clinical Cancer Res., 2000, 6, 2585-2597.

[64] Mutter N., Stupp R., Temozolomide: a milestone in neuro-oncology and beyond?, Expert Rev. Anticancer Ther., 2006, 6, 1187-1204.

[65] De Gooijer M.C., de Vries N.A., Buckle T., Buil L.C.M., Beijnen J.H., Boogerd W., van Tellingen O., Improved Brain Penetration and Antitumour Efficacy of Temozolomide by Inhibition of ABCB1 and ABCG2, Neoplasia, 2018, 20, 710-720.

[66] Stupp R., Mason W.P., van den Bent M.J. et al, Radiotherapy plus concomitant and adjuvant temozolomide for glioblastoma, N. Engl. J. Med., 2005, 352, 987-996.

[67] Lee Y.S., Temozolomide resistance in glioblastoma multiforme, Genes and Diseases, 2016, 3, 198-210.

[68] Montaldi A.P., Godoy P.R., Sakamoto-Hojon E.T., APE1/REF-1 down-regulation enhances the cytotoxic effects of temozolomide in a resistant glioblastoma cell line, Mutat. Res. Genet. Toxicol. Environ. Mutagen, 2015, 793, 19-29.

[69] Hermisson M., Klumpp A., Wick W. et al, O^6-methylguanine DNA methyltransferase and p53 status predict temozolomide sensitivity in human malignant glioma cells, J. Neurochem., 2006, 96, 766-776.

[70] Baer J.C., Freeman A.A., Newlands E.S., Watson A.J., Rafferty J.A., Margison G.P., Depletion of O^6-alkylguanine-DNA alkyl transferase correlates with potentiation of temozolomide and CCNU toxicity in human tumour cells, Br. J. Cancer, 1993, 67, 1299-1302.

[71] Ryu C.H., Yoon W.S., Park K.Y. et al, Valproic acid downregulates the expression of MGMT and sensitises temozolomide-resistant glioma cells, J. Biomed. Biotechnol., 2012, 2012, 1-9.

[72] Happold C., Roth P., Wick W. et al, Distinct molecular mechanisms of acquired resistance to temozolomide in glioblastoma cells, J. Neurochem., 2012, 122, 444-455.

[73] Agnihotri S., Gajadhar A.S., Ternamian C. et al, Alkylpurine DNA-N-glycosylase confers resistance to temozolomide in xenograft models of glioblastoma multiforme and is associated with poor survival in patients, J. Clin. Invest., 2012, 122, 253-266.

[74] Blough M.D., Beauchamp D.C., Westgate M.R., Kelly J.J., Cairncross J.G., Effect of aberrant p53 function on temozolomide sensitivity of glioma cell lines and brain tumour initiating cells from glioblastoma, J. Neuro-Oncol., 2011, 102, 1-7.

[75] Luh E.H., Shackford S.R., Shatos M.A., Pietropaoli J.A., The effects of hyperosmolarity on the viability and function of endothelial cells, J. Surg. Res., 1996, 60, 122-128.

[76] Lv Z., Chang L., Long X., Liu J., Xiang Y., Deng H., Deng L., Dong A., Thermosensitive in situ hydrogel based on the hybrid of hyaluronic acid and modified PCL/PEG triblock copolymer, Carbohyd. Polym., 2014, 108, 26-33.

[77] Chen Y., Sui J., Wang Q., Yin Y., Liu J., Wang Q., Han X., Sun Y., Fan Y., Zhang X., Injectable self-crosslinking HA-SH/Col I blend hydrogels for in vitro construction of engineered cartilage, Carbohyd. Polym., 2018, 190, 57-66.

[78] Zheng Y., Liang Y., Zhang D., Sun X., Liang L., Li J., Liu Y.N., Gelatin-Based Hydrogels Blended with Gellan as an Injectable Wound Dressing, ACS Omega, 2018, 3, 4766-4775.

[79] Pooja D., Panyaram S., Kulhari H., Rachamalla S.S., Sistla R., Xanthan gum stabilised gold nanoparticles: Characterisation, biocompatibility, stability and cytotoxicity, Carbohyd. Polym., 2014, 110, 1-9.

Chapter 5: Conclusion

5.1 General Conclusions

In many countries, cancer ranks the second most common cause of death following cardiovascular diseases and it remains as a major health problem around the world. There are different types of cancer, the most common types include lung, breast, prostate, colorectal, bladder cancer, melanoma and leukaemia. Brain tumours are less common, but there is evidence that the incidence of these tumours has been rising. Among malignant brain tumours, GBM is the most common and deadly primary tumour, accounting for approximately 50 % of all brain tumours. As discussed in Chapter 1, brain cancer treatment presents several challenges due to the unique sanctuary situation of the brain and there is an urgent need for the development of new therapeutic strategies.

Conventional methods of treatment include surgical resection of the tumour combined with concomitant chemotherapy and radiotherapy are mainly unsuccessful and they suffer from several limitations. Residual cancer cells that have not been removed and remain in the periphery of the tumour site and the existence of brain tumour initiating cells can increase the risk for tumour recurrence. The systemic delivery of the drugs at the site of the tumour is mainly ineffective due to the presence of BBB and the repeated administration of high doses of the drugs is necessary which leads in adverse side effects. Malignant gliomas are often resistant to alkylating agents and this results in the formation of recurrences close to the resection borders. In the context of radiotherapy, increasing and repeated doses of radiation also lead to severe side effects.

For the aforementioned limitations of the current chemotherapeutic approaches, there is an urgent need to develop more efficient local drug delivery strategies that will enable the targeted drug release to the tumour site over a sustained period of time. To date, several pharmaceutical formulations including liposomes, nanoparticles and hydrogels have been used as drug delivery systems for the treatment of GBM. Among them, hydrogels have gained a lot of attention due to their unique physical properties and structural versatility which resembles the ECM of the living tissues. However, the majority of the studies have utilised these systems as injectable anticancer drug loaded carriers in the resection cavity. The introduction of this thesis outlined the current limitations of the already developed formulations and they are listed below:

1. Need for the development of relatively easy and cost-effective methods for the formation of biocompatible hydrogels

2. Lack of robust protocols for reproducible hydrogel formation

3. Lack of molecules that naturally exist in the brain ECM

4. Absence of effective chemoattractants

Each of these points were addressed and discussed throughout this thesis and it is believed that the findings presented here will accelerate the potential of these scaffolds in the treatment of GBM. Chapter 2 focused on the preparation of hydrogels mainly based on HA, proposing relatively simple, reproducible and cost-effective crosslinking methods. Hydrogels were prepared at different crosslinking densities and subsequently loaded with the chemoattractant UII in order to identify the optimal conditions that will promote invasion and migration of invasive glioma cells towards the matrix as illustrated in Figure 5.1. An optimal hydrogel for the treatment of GBM should have some critical features that are reported below.

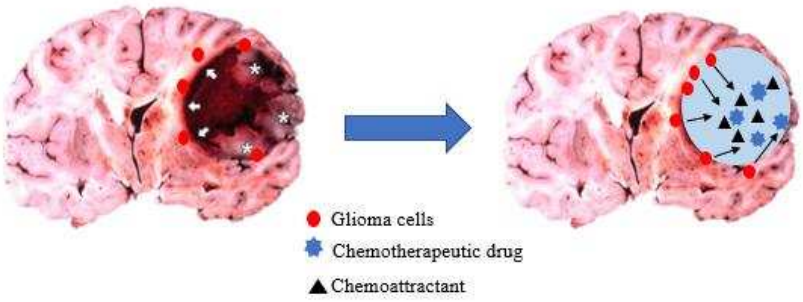

Figure 5.1: Schematic representation of the use of chemoattractant and drug loaded hydrogel for the treatment of GBM and the critical features for its successful application.

Critical features of hydrogels designed for the local treatment of GBM:

- Biocompatible and injectable in situ
- Biodegradable and non-immunogenic
- Adhesion to resection cavity border
- Mechanical properties compatible with the brain tissue
- Controlled and sustained release of the loaded drug over time
- Gradient concentration of the chemoattractant and sustained release from the hydrogel

The characterisation of the physicochemical and mechanical properties of the fabricated hydrogels was imperative in order to ensure that they possess all the aforementioned desirable characteristics. The results from the characterisation of hydrogels properties showed that the formulated scaffolds had all the desirable characteristics as summarised in Figure 5.2. Hydrogels presented an interconnected porous structure and porosity that was highly dependent on the crosslinking density. The high porosity of the hydrogels enabled them to swell and the equilibrium swelling degree was determined. The in vitro enzymatic degradation experiments revealed that hydrogels can be degraded when they are incubated with hyaluronidase. The mechanical characterisation of the hydrogels showed that their viscoelastic properties were close to those of the brain tissue, highlighting their potential as injectable scaffolds in the brain. The drug release studies performed on hydrogels showed that these crosslinked networks can promote sustained release of the drug over a specific period of

time, while the release experiments of the FITC- UII loaded hydrogels demonstrated low amount of the chemoattractant is released as most of it remains inside the gel, which is desirable for our application.

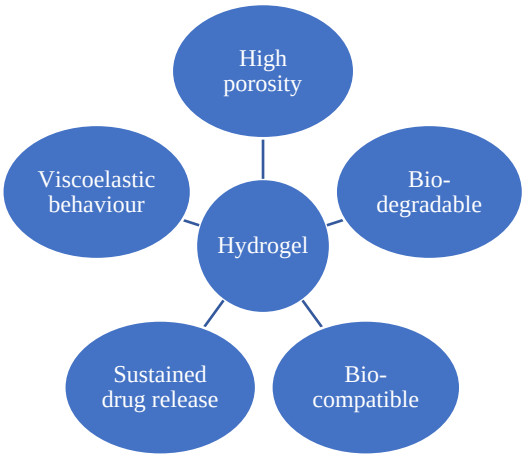

Figure 5.2: Desirable properties of the fabricated hydrogels as injectable scaffolds for the treatment of GBM.

The biocompatibility of the hydrogels was investigated in Chapter 4. GBM cells were seeded on the hydrogels in the absence or presence of the chemoattractant UII and the response of GBM cells was evaluated. The viability assays indicated that hydrogels can promote cell growth and the presence of the chemoattractant in the matrix can induce invasion and migration of the cells towards the hydrogel network.

5.2 Future work

It is hoped that this thesis has acknowledged the various limitations of the conventional methods of GBM treatment and encouraged the development of alternative strategies using hydrogels. Hydrogels have presented promising results and they need to be further investigated. Future work could focus on experiments carried out with healthy neural cells in order to ensure the biocompatibility of the scaffolds within the healthy brain tissue since the foreseen application of the hydrogel is as an injectable material in the resection cavity. Moreover, the response of the hydrogels should be tested in vivo conditions including initially mouse models and human models in the future. In vitro experiments are indicative of the hydrogel performance but not representative of the in vivo environment. Particularly, it is expected that the degradation rate of the hydrogels will be different in vivo conditions due to the variable enzymatic conditions and different aqueous environment. In cancer research, in vitro systems lack the microenvironment, physiological reactions and mainly heterogeneity and thus it is too simplistic to predict the response to biomaterials. Therefore, the performance of the chemoattractant UII and drug-loaded hydrogels injected in a cavity after tumour resection should be investigated further to ensure the functionality of the designed biomaterial.

Furthermore, future work can be focused on the optimisation of the designed formulations. As stated previously, the foreseen application of the designed hydrogel is as an injectable biomaterial in the cavity after resection of brain tumour. On this account, the injectability of the prepared scaffolds can be tested using double barrel syringes. The precursor gelator components can be loaded in the barrels and the specific set up can allow the homogeneous mixing and formation of hydrogel in situ. Another critical factor that should be studied further is the quantification of the diffusion of drug molecules or the FITC-labelled UII within the hydrogel network in order to understand better the release kinetics.

5.3 Personal perspective on the implication of hydrogels for GBM treatment

The last few years, have witnessed a great interest in the development of alternative therapeutic methods for the treatment of GBM. Conventional chemotherapeutic agents fail to present clinical relevance in the treatment of brain tumours, due to their high toxicity or chemoresistance, therefore emerged research on the design of local drug delivery systems is a good alternative. Several studies have focused on the use of hydrogels for this purpose. However, better consideration of these 3D networks is necessary to understand why the number of clinical trials performed on hydrogel-based systems for the treatment of GBM is so limited. The current chemotherapy regimen includes the administration of TMZ or BCNU. Although, BCNU has shown to be effective on GBM cells, the first line treatment of GBM is TMZ. On the other hand, GBM cells have shown chemoresistance to this drug and many researchers have focused on the administration of alternative anticancer drugs or cocktail of drugs. Another critical factor that affects the efficiency of these drug delivery systems is the sustained release of the drug from the hydrogel. The drug release is dependent on the hydrogel characteristics, structure of the drugs and most importantly on the brain tissue conditions after surgery which can influence the drug diffusion behaviour. Recently, computational simulation models have been developed to predict the drug release rate and its delivery to the tumour.

Despite the ongoing research on the development of hydrogels for the treatment of GBM, there is a medical demand for more effective therapies to treat this devastating disease. From my perspective, hydrogels offer many advantages over other pharmaceutical formulations and these systems can address most of the drug delivery challenges, but the extent of their ability to address GBM challenges requires more clinical investigation. More knowledge on the long-term stability, safety data and performance of injectable hydrogels is required in order to translate these scaffolds from the bench to clinical trials for applications in brain tumours.

*"*Important thing in science is not so much to obtain new facts as to discover new ways of thinking *about them"*.

Sir William Bragg

Appendix

Chapter 3

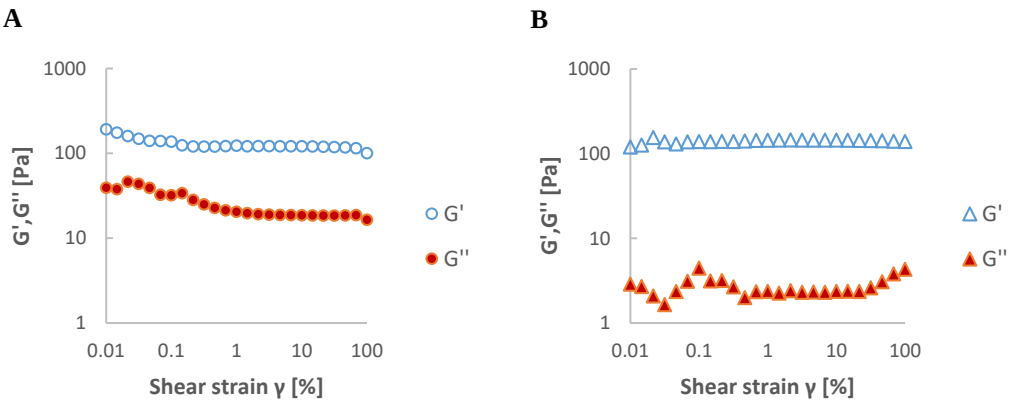

Figure 3.44: Amplitude sweep experiments performed on **A.** L1 and **B.** H2 crosslinking densities of HA-ADH hydrogels. Strain scans were performed from 0.01 to 100 % keeping constant frequency at 1 Hz.

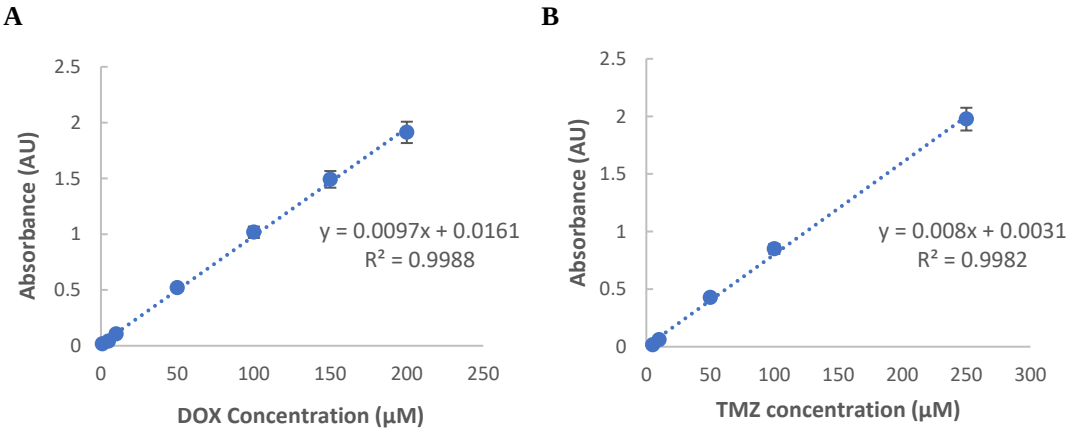

Figure 3.45: A. Calibration curve of DOX and **B.** Calibration curve of TMZ in PBS (pH 7.4).

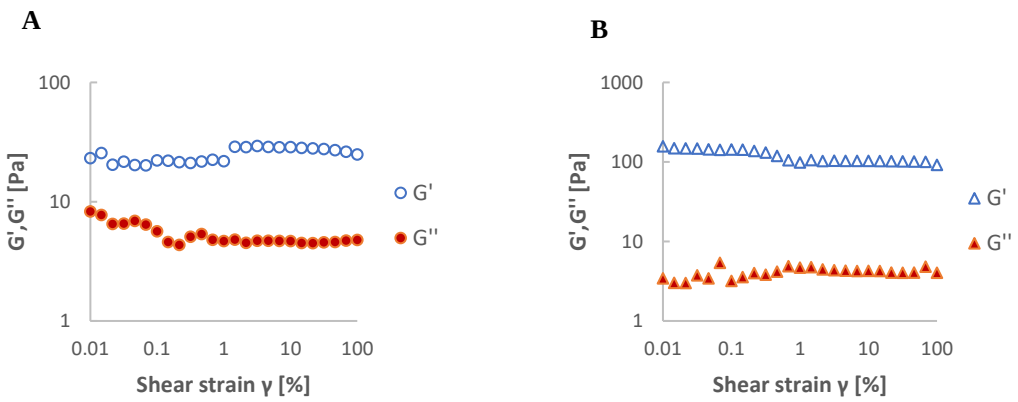

Figure 3.46: Amplitude sweep experiments performed on **A.** HB16 and **B.** HB19 crosslinking densities of HA-BSA hydrogels. Strain scans were performed within a range from 0.01 to 100 % keeping constant frequency at 1 Hz.

Chapter 4

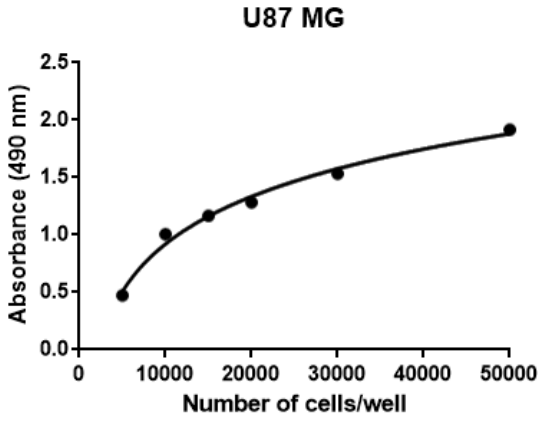

Figure 4.37: A calibration curve was obtained by plotting the semi log relationship between the different number of U87MG cells and their corresponding absorbance values. Various numbers of U87MG cells were added to the wells of a 96-well plate in fully supplemented DMEM and they were incubated for 1 h at 37 °C. Then MTS solution was added and after 1 h of incubation, the absorbance at 490 nm was measured. Each point represents the mean of 6 replicates. The background absorbance was subtracted from these data.